ANALYSING THE IMPACT OF SOIL MOISTURE ON RUNOFF FROM URBAN GREEN AREAS AND ITS APPLICATION IN FLOW MODELLING

Master Thesis
Water and Environmental Engineering
June 2025

Anna Hansen
Helene Vilsen
Maria Behnk Solnæs

DEPARTMENT OF THE BUILT ENVIRONMENT

AALBORG UNIVERSITET

AALBORG UNIVERSITY
STUDENT REPORT

Eng & Tech
Built Environment
Thomas Manns Vej 23
9220 Aalborg Ø
http://www.build.aau.dk

Title:

Analysing the Impact of Soil Moisture on Runoff from Urban Green Areas and Its Application in Flow Modelling

Project:

Master Thesis

Project period:

September 2024 - June 2025

Participants:

Anna Hansen
Helene Kirkebye Vilsen
Maria Behnk Solnæs

Supervisors:

Jesper Ellerbæk Nielsen
Søren Thorndahl

ECTS: 45
Pages: 218
Appendices: 93
Submission deadline: 04-06-2025

Abstract:

The impact of contingent runoff from urban green areas is often overlooked in runoff modelling, particularly in relation to urban drainage systems. This thesis examines how such runoff relates to soil moisture across three spatial scales: hillslope scale, urban subcatchment scale, and hydrological scale.
As part of the MUDP-project VandKant, volumetric water content (VWC) sensors were installed and flow observations conducted at representative sites. Analyses are conducted at all three spatial scales to assess the relationship between VWC and runoff generation. A relationship is identified, though it varies by scale. At the urban subcatchment scale, no statistically significant relationship is observed due to the dominance of impervious surfaces. In contrast, a clear statistical correlation is found at the hillslope scale and hydrological scale, where green areas play a more prominent role.
Lastly, the thesis assesses whether the incorporation of VWC or the DMI drought index (DI) can improve flow models. To evaluate predictive capability, flow at the hydrological scale is simulated using three simple models: Linear Regression Model, Extended Time-Area Model, and Linear Reservoir Model. Results indicate that including either VWC or DI generally enhances model accuracy, highlighting the importance of soil moisture in runoff prediction at larger scales.

Preface

This master's thesis was developed by Anna Hansen, Helene Kirkebye Vilsen, and Maria Behnk Solnæs during the academic year 2024–2025, as part of the Water and Environmental Engineering program at Aalborg University. We would like to express our sincere gratitude to Jesper Ellerbæk Nielsen and Søren Thorndahl for their valuable supervision, continuous support, and constructive feedback throughout the thesis process. Additional thanks are extended to the participants in the MUPD-project VandKant for sharing data and providing insightful feedback.

Reading guide

This thesis follows the Harvard citation style, where references are indicated by the author's name and year of publication. Tables, figures, and equations are numbered according to the chapter and their order of appearance. Various software programs were used to create figures and develop models, including QGIS, Scalgo Live, Python, MATLAB, Canva, and PowerPoint. Additionally, generative AI tools were used to support coding tasks and provide text feedback during the writing process.

Contents

Introduction 1

Weather conditions in Denmark have changed dramatically since the 1870s, with a global temperature increase of 1.5 ℃ resulting in an approximate 100 mm rise in annual precipitation. This trend is expected to continue throughout the 21st century, with the frequency of heavy rainfall events likely to increase, affecting urban stormwater management systems and increasing the risk of urban flooding [DMI, 2024]. Traditional urban stormwater management systems, such as retention basins, drainage systems, and wastewater treatment plants, are designed to handle runoff volumes mostly from the impermeable surfaces with a specific return period. It is assumed that precipitation falling on green areas will largely infiltrate directly into the soil column, and a contribution to the stormwater management systems is limited to 0-15% [Winther et al., 2011]. However, under certain conditions, such as during heavy rainfall or when the soil is fully saturated, the soil's infiltration capacity is exceeded, resulting in runoff from permeable green areas. This phenomenon will be defined as contingent runoff and describes runoff from pervious or partially pervious surfaces. Since this contribution is typically neglected in the design of the urban stormwater management system, these systems may be under-dimensioned, especially in locations with a large percentage of green areas. The additional runoff can put severe stress on the urban stormwater management system as the increased water volumes decrease the efficiency of wastewater treatment plants and increase the general water volumes in retention basins and drainage systems, thereby occupying a large portion of their storage capacity. In a worst-case scenario, this may cause these systems to exceed their capacity, ultimately leading to urban flooding [Thorndahl et al., 2024] [Nielsen et al., 2020b].

The common mechanisms that lead to contingent runoff include: rainfall intensities that exceed the infiltration capacity of the soil, high soil moisture, and a combination of the two. Therefore, contingent runoff depends on soil properties like the saturated hydraulic conductivity, volumetric water content, soil composition, topography, and weather properties such as intensity and duration of precipitation [Wong, 2011]. Especially during fall and winter, runoff increases due to lower evaporation, long periods of rainfall, and high soil moisture [Nielsen, 2019]. With the future climate, the impact of contingent runoff, and therefore the risk of flooding, is expected to increase. For this reason, the uncertainty of the contribution from contingent runoff must be decreased in the design of the future urban drainage systems [Nielsen, 2019].

To explore the contribution of contingent runoff, the MUDP-project VandKant was initiated in 2022, representing a collaborative effort between Vejle Municipality, Vejle Spildevand (Wastewater), VandCenter Syd, Novafos, Aarhus Vand (Water), Aalborg University, Scalgo, DRYP, Envidan, Wavein, and Dannozzle. The initiative was driven by the pressing need to quantify, model, and predict contingent runoff from green areas, as this phenomenon is

expected to play an increasingly significant role in urban flooding under future climate conditions. To address this challenge, VandKant is focusing on developing robust tools for monitoring, modelling, and integrating surface runoff data into urban drainage planning. The project combines a wide range of innovative methods, including advanced rainfall-runoff modelling and improved infiltration modelling. The inclusion of sensors measuring volumetric water content in the soil, pressure sensors in recipients to estimate flow via Q/h curves, and rain gauges at key locations across Denmark. Moreover, the project encompasses diverse locations varying in scale and function, providing a comprehensive dataset.

The Project VandKant emphasises the development of practical tools that enable municipalities and utilities to screen for areas where contingent runoff significantly impacts urban water systems, thereby supporting sustainable investment and planning decisions.

Problem Statement 2

With the increasing frequency of heavy precipitation events and the consequent increase in urban flooding, there is a growing need for a more comprehensive understanding of how soil moisture affects surface runoff from green areas. Simultaneously, there is an increasing demand for tools to model and predict contingent runoff, enabling a more precise evaluation of whether existing urban drainage systems have adequate capacity to manage runoff. Additionally, insights into runoff volumes can facilitate the development of early warning systems in urban areas, particularly prone to flooding caused by intense rainfall. This makes examining the correlation between precipitation intensity, duration, and volumetric water content (VWC) especially important. Furthermore, the potential of including VWC in flow modelling is relevant to explore. As VWC sensors are relatively expensive, exploring potential correlations between the VWC and the DMI drought index (DI) could offer valuable insights, which can make models more accessible and broadly applicable.

This thesis, conducted as part of Project VandKant, uses data from multiple locations across Denmark to examine these relationships. By analysing diverse locations of varying scales, the thesis aims to explore the relationship between soil moisture and contingent runoff. Based on these considerations, the following problem statement has been formulated:

To what extent does soil moisture influence surface runoff across varying spatial scales, and can incorporating volumetric water content (VWC) measurements enhance the accuracy of flow models and their application in urban flood management?

- In which situations does contingent runoff occur, and what is the effect of it?
- What is the relationship between precipitation and VWC, and is there a critical level of VWC where contingent runoff occurs?
- Can the implementation of volumetric water content improve the quality of simple runoff models
- How does VWC correlate with the DMI drought index, and can the drought index serve as an alternative to VWC sensors?

Soil Dynamics Influence on Contingent Runoff 3

When studying the effects of contingent runoff from permeable areas, it is important to consider the hydrological cycle as a whole, as it describes the movement and phase of water within nature. This cycle includes numerous parameters that directly influence the amount of contingent runoff. [Robinson and Ward, 2017a]

Precipitation is the primary driving force behind surface runoff, with factors such as the amount, intensity, and duration of rainfall playing a critical role. When precipitation reaches the ground surface, it may infiltrate the soil, evaporate, run off, or accumulate on the surface. Intense rainfall can lead to rapid and significant surface flow, while lighter precipitation is more likely to result in slower runoff or infiltration. However, the infiltration rate is highly dependent on the soil texture and its saturation level. If the soil is fully saturated, its storage capacity is reached, preventing further infiltration and causing precipitation to contribute to surface runoff. In addition, processes such as evaporation, transpiration, temperature fluctuations, and topography also influence surface runoff. Temperature impacts runoff in varying ways: during winter, low temperatures can cause precipitation to accumulate as snow or ice, which later melts and contributes to runoff when temperatures rise. Conversely, high temperatures in summer can increase evaporation rates, thereby reducing surface runoff. [Robinson and Ward, 2017a]

Understanding the various factors that influence contingent runoff, such as precipitation, soil texture, and hydrological processes, is essential in addressing its impacts.

3.1 Infiltration

During intense rainfall events or long durations of less intense rainfall events, the rate at which water infiltrates into the soil can reach its maximum limit, known as the infiltration capacity. When rainfall intensity exceeds the infiltration capacity, excess water is unable to infiltrate into the soil and instead forms contingent runoff. A conceptual figure of the dynamics between precipitation, infiltration capacity, infiltration rate, and surface runoff is illustrated in Figure 3.1.

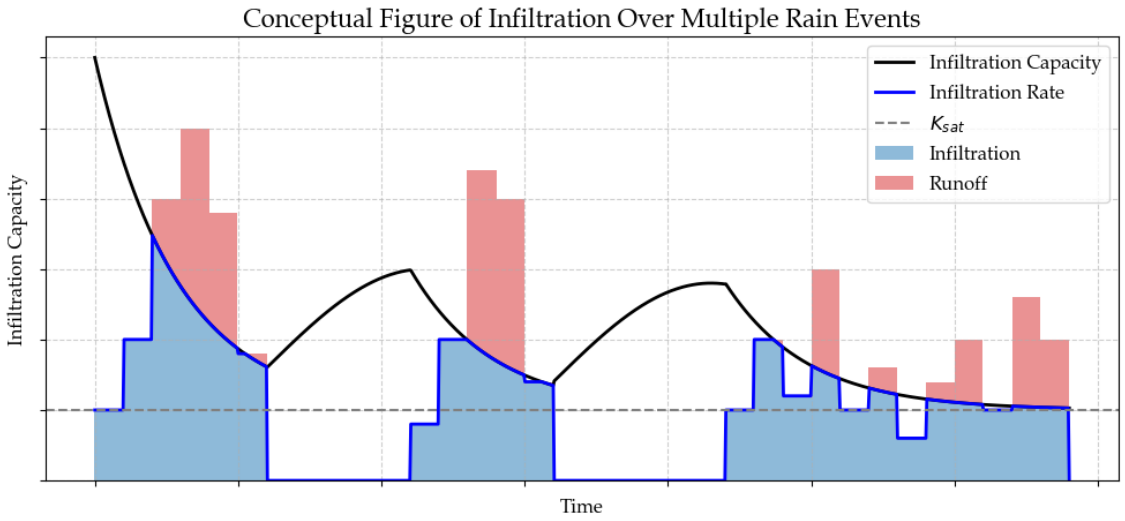

Figure 3.1. A conceptual figure of the infiltration capacity [mm/hr] and infiltration rate [mm/hr].

The infiltration capacity is influenced by soil conditions and changes throughout the rainfall event. As soil moisture levels increase and as the soil becomes increasingly saturated, the infiltration capacity decreases. Consequently, if the soil moisture is already high at the start of the rainfall, the initial infiltration capacity will be lower compared to that of drier soil. Therefore, the infiltration rate refers to the actual rate at which water enters the soil, while the infiltration capacity, as mentioned, represents the maximum rate at which water can infiltrate the soil. Thus, the infiltration rate can either equal the infiltration capacity or fall below it. When the infiltration rate is lower than the infiltration capacity, the rate is typically controlled by the rainfall intensity [Robinson and Ward, 2017b].

3.2 Soil Water Capacity

When addressing urban flooding caused by contingent runoff, it is essential to consider the soil textures within the catchment area. The infiltration of water from the surface into the soil column and the soil's storage capacity are heavily influenced by its characteristics. For instance, soils with a high content of fine particles, such as clay or organic matter, typically have slower infiltration rates than coarser soils. This is because fine particles reduce pore sizes in the soil, affecting both the infiltration and the overall storage capacity of the soil column.

A measure of how much water a soil holds is the total porosity [m^3 air/m^3 soil] [Loll and Moldrup, 2000a]. Typical total porosities of soils with different characteristics are listed in Table 3.1.

Table 3.1. Soil porosities ± standard deviation for different soil textures [Loll and Moldrup, 2000b]

Soil texture	Φ_{tot} [$\mathbf{m^3}$ **air**/$\mathbf{m^3}$ **soil**]
Sand	0.395 ±0.056
Sandy loam	0.435 ±0.086
Loam	0.451 ±0.078
Silt loam	0.485 ±0.059
Sandy clay loam	0.420 ±0.059
Clay loam	0.476 ±0.053
Silty clay loam	0.477 ±0.057
Sandy clay	0.426 ±0.057
Silty clay	0.492 ±0.064
Clay	0.482 ±0.050

In Table 3.1, it can be seen that fine-textured soils such as clay and silt tend to exhibit slightly higher total porosity due to the abundance of small pores between particles. In a systematic review *Basset et al. 2023* found a positive correlation ($R^2 = 0.46$) between the total porosity and the steady infiltration, where an increase in total porosity from 0.35 to 0.65 m^3/m^3 corresponded to an increase in infiltration from 10 up to 1000 mm/hr. This challenges the general understanding that coarse-textured soils have higher infiltration abilities. However, *Basset et al. 2023* attribute this to the enhanced structural stability of fine-textured soils. This highlights the importance of considering both soil texture and structural stability when evaluating the infiltration capacity [Basset et al., 2023].

The total porosity of a soil corresponds to VWC [m^3 H_2O/m^3 soil] when the soil is fully saturated. At this point, the soil has reached its capacity. This can occur while it is raining, if the rain volume exceeds the storage capacity of the soil. When the rain ceases, the larger soil pores will start to drain by gravitational forces, and the soil will eventually reach field capacity [Loll and Moldrup, 2000b].

Small pores, which are characteristic of fine-textured soils, retain water more effectively due to stronger capillary forces. This results in a higher water content at field capacity and an elevated capillary water table. Consequently, the soil has limited storage capacity available for additional infiltration. As a result, such soils reach saturation more quickly than coarser soils, making them more prone to surface runoff [Loll and Moldrup, 2000b] [Bleam, 2017].

As water infiltrates into the soil, it fills the pore spaces, gradually reducing the capillary forces that, in combination with gravitational forces, draw water into the soil. Once the soil becomes fully saturated, these capillary forces cease, and gravity, along with the hydraulic gradient, becomes the primary driver of infiltration. Therefore, the infiltration capacity is governed by the soil's saturated hydraulic conductivity, which describes the soil's ability to transport water under saturated conditions [Robinson and Ward, 2017b] [Loll and Moldrup, 2000a].

The table below lists the standard values for the hydraulic conductivity of various soil textures:

Table 3.2. Saturated hydraulic conductivity K_{sat} ranges in m/s for different soil types [Loll and Moldrup, 2000a]

Soil textures	$\mathbf{K}_{sat}$ [m/s]
Gravel	$3{\cdot}10^{-4}$ - $3{\cdot}10^{-2}$
Coarse sand	$9{\cdot}10^{-7}$ - $6{\cdot}10^{-3}$
Medium sand	$9{\cdot}10^{-7}$ - $5{\cdot}10^{-4}$
Fine sand	$2{\cdot}10^{-7}$ - $2{\cdot}10^{-4}$
Silt	$1{\cdot}10^{-9}$ - $2{\cdot}10^{-5}$
Clay	$1{\cdot}10^{-11}$ - $4.7{\cdot}10^{-9}$

It can be seen that the water movement is fastest in coarse soil types as gravel and sand, while it is slowest in fine particle soils like silt and clay. This can have a significant impact on the infiltration rates. However, the values listed in Table 3.2 are only guidelines and may not always be accurate, as K_{sat}, among other factors, depends on the porosity of the soil. In some cases, even a generally coarse soil can become compacted, acquiring properties similar to fine-particle soils, further reducing its infiltration rate. Additionally, soil texture can exhibit significant variability even on a very small scale, influencing surface runoff and infiltration dynamics at the local level [Loll and Moldrup, 2000c].

3.3 Terrain and Vegetation

The amount of vegetation also plays a decisive role in influencing surface runoff. This is primarily due to the ability of root systems to absorb water from the soil. Consequently, areas with dense vegetation typically contribute less to surface runoff compared to areas with bare soil surfaces or sparsely vegetated, permeable landscapes. This has been concluded in a Chinese study, which examined the infiltration rate in relation to vegetation and soil moisture. The study found a positive correlation between infiltration rate and vegetation presence while identifying a negative correlation between infiltration rate and soil moisture [Liu et al., 2019].
Moreover, the topography significantly influences both the direction and accumulation of runoff. In rural areas, runoff typically flows toward nearby streams, while in urban areas, it is directed toward the urban drainage system. In both cases, surface runoff may accumulate in depressions, forming puddles or temporary surface storage until the water either evaporates or infiltrates into the soil, depending on the local topography [Gnann et al., 2025]. In traditional drainage planning, the interplay between soil type, vegetation cover, and topography significantly influences surface runoff, but these factors are often overlooked [Li et al., 2025].
The influence of contingent runoff will be explored at multiple project locations across Denmark using the data collected as part of Project VandKant.

Presentation of Location and Data 4

With the large quantity of data available from project VandKant, it is essential to present information from each location in a clear and understandable manner. This chapter will outline the collected data and identify key selections for further analysis. Details of all measurement stations, including their locations, measurement periods, resolutions, and units of measurement, will also be presented.

The project locations included in VandKant are visible in Figure 4.1.

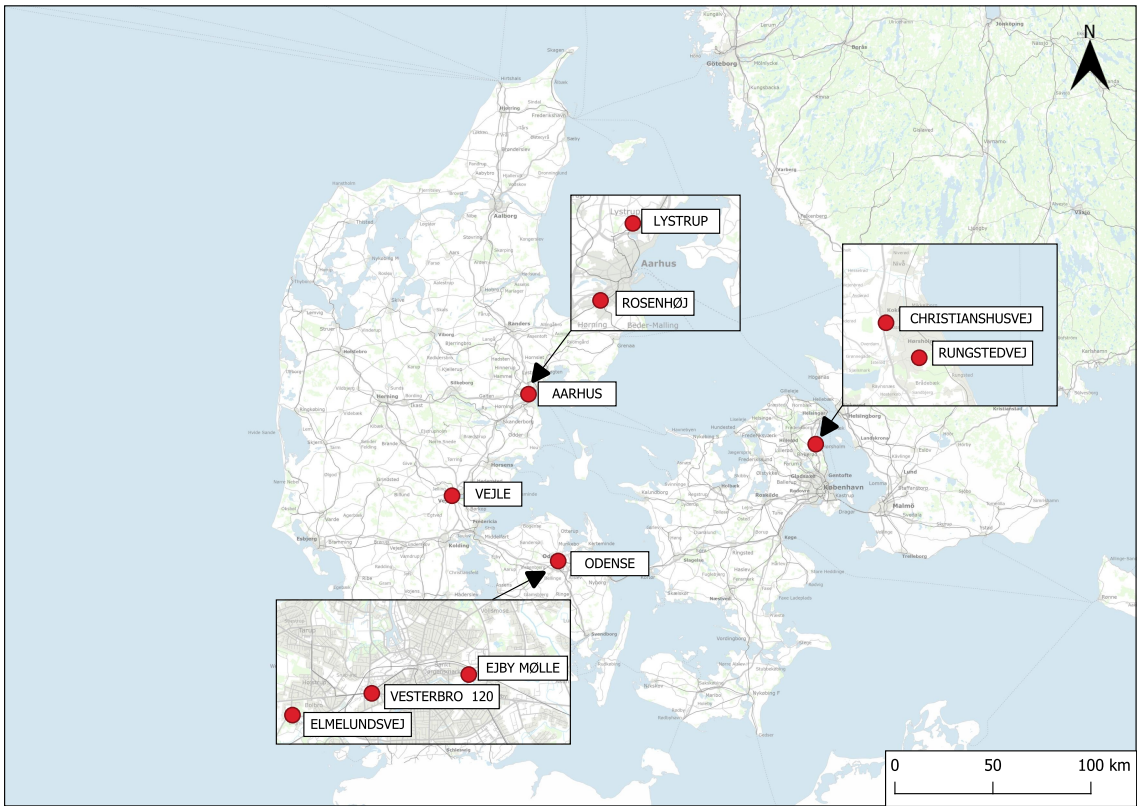

Figure 4.1. Presentation of VandKant project locations.

Common across every project location are measurements of precipitation, flow (estimated using Q/H curves, cf. Appendix F), VWC, and temperature. Data is continuously collected, however, this thesis only includes data until the 1st of May. Table 4.1 presents the type, source, resolution, and unit of the data.

Table 4.1. Overview of the data type [unit], resolution [min], and source common for all project locations.

Data type	**Resolution [min]**	**Source**
Rain [μm/s]	1	SVK
Flow [m^3/s] (Q/H estimated)	1	Dryp, Danova, Vandportalen
VWC [m^3/m^3]	10	Dryp
Temperature [°C]	10	DMI

To better understand how VWC influences contingent runoff, the phenomenon is examined at three different scales. The smallest scale is the hillslope scale, where runoff is directly measured from green areas. The three locations representing this scale are Ejby Mølle, Elmelundsvej, and Lystrup. The second scale is the urban subcatchment scale, which includes two urban areas with either separated or combined sewer systems. The two locations representing this scale are Christianshusvej and Rungstedvej. The largest of the three scales is the hydrological scale, which examines a catchment area to a stream. The location considered hydrological scale is the catchment of Grejs Å in Vejle. The data presentation and analysis will be separated into chapters based on these scales.

4.1 Hillslope Scale

The smallest scale examined is referred to as the hillslope scale. This term covers simple vegetated areas with a slope, where the only runoff expected to occur is contingent. The smallest area is 930m^2 and the largest is 4300m^2.

VandCenter Syd

As part of Project VandKant, the water company, VandCenter Syd, has selected three research areas in Odense: Elmelundsvej, Ejby Mølle, and Banegårdspladsen (Vesterbro 120), as presented in Figure 4.2. The aim for VandCenter Syd is to gain enough understanding of contingent runoff to apply this knowledge when assessing specific runoff situations.

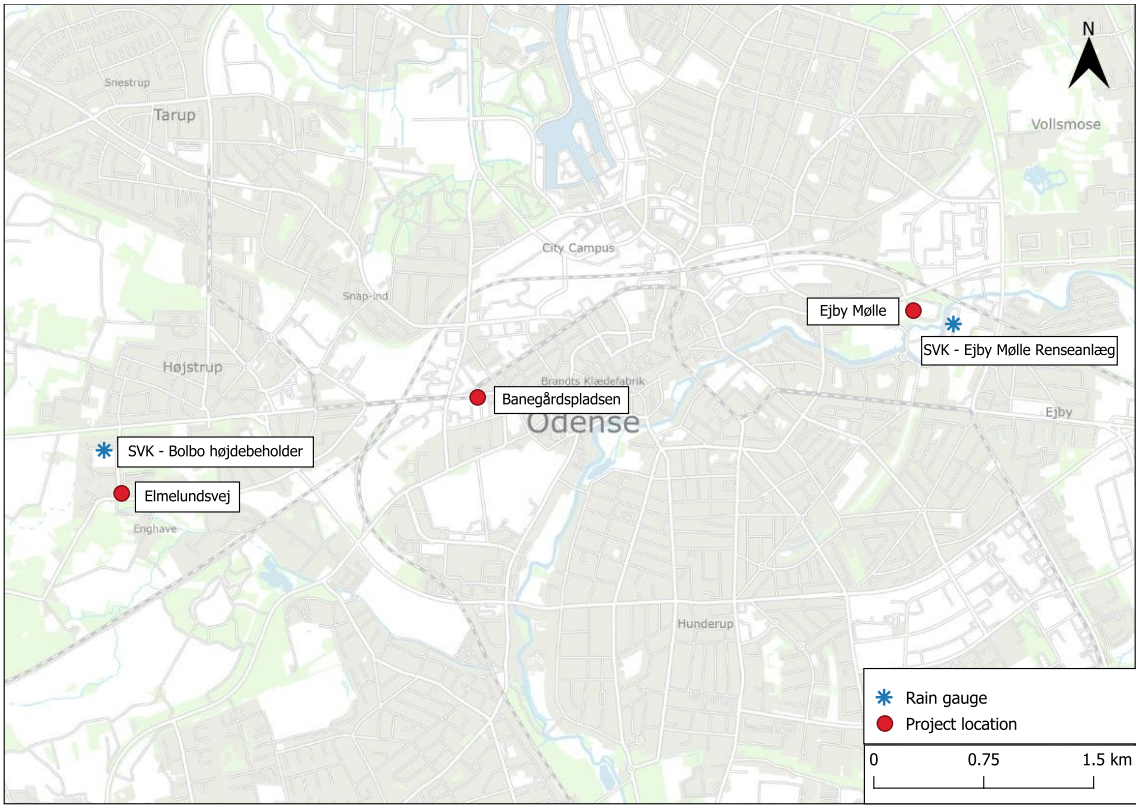

Figure 4.2. Overview of the project locations in Odense/VandCenter syd

Elmelundsvej and Ejby Mølle are green areas, while Banegårdspladsen is a semipermeable area of tiles. At each location, flow is estimated using a Q/H curve. Although the water level is measured at Banegårdspladsen, a Q/H curve has not been made. As a result, data from this location is excluded from further presentations and analysis.

Ejby Mølle

The catchment area at Ejby Mølle covers 0.093 ha (930 m^2) and consists of a sloped green area, dominated by soil texture: *fine clay with sand* (cf. Appendix A, Table A.1). An intercepting line drain is installed at the bottom of the green area. Since not all runoff from the green area is expected to reach the line drain, the catchment area has been defined based on the terrain slope. The flow is estimated using the Q/H curve shown in Appendix F Figure F.2. Three VWC sensors have been installed in the area. Distribution functions of the VWC measurements can be found in Appendix D Figure D.1. An overview of the measurement installations can be seen in Appendix A, Table A.1. The line drain, elevation, and catchment area are illustrated in Figure 4.3.

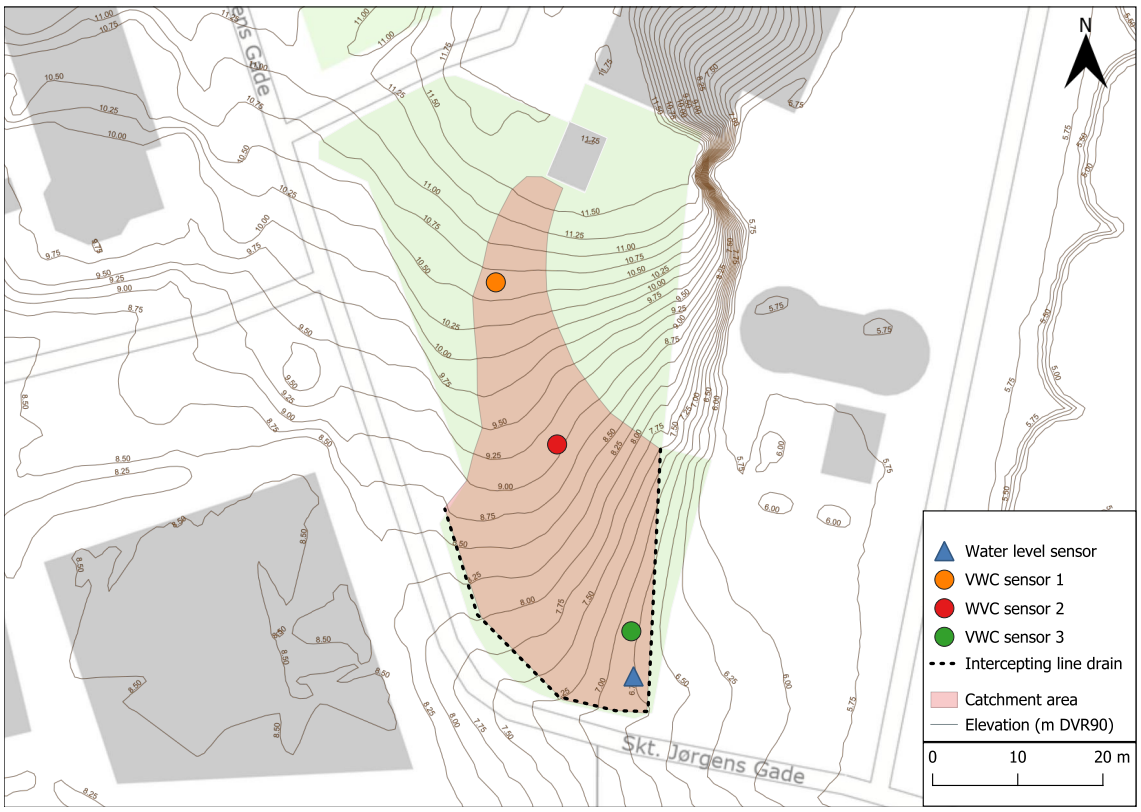

Figure 4.3. Outline of Ejby Mølle catchment with elevation lines and measurement installations.

The data collection periods vary depending on the data type. The available data from each of the measurement stations is illustrated in Appendix A Figure A.1. To assess the quality of the data from each of the VWC sensors, the individual data series are shown in Appendix A Figure A.2. The longest and most continuous data series is found in VWC sensors 1 and 3, where sensor 1 is used in further analysis. The selection of the VWC sensor is based on *statistical analysis* explained in Appendix D, section D.1. The complete data set, including precipitation, flow, and VWC measurements, used for the data analysis, is observed from 28-04-24 until 01-05-25 and presented in Figure 4.4.

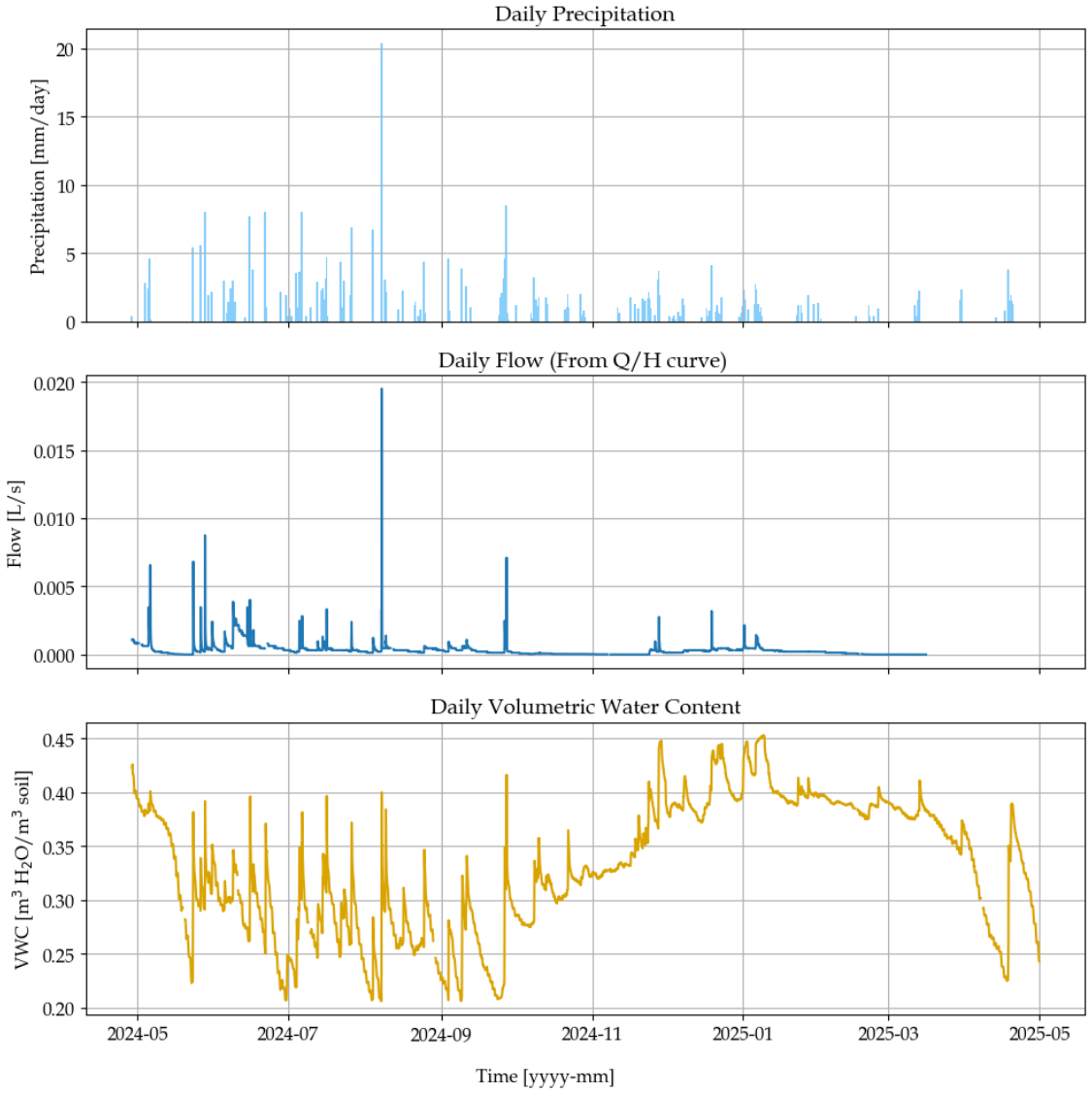

Figure 4.4. Measured precipitation [mm/day] (5417 Ejby Mølle renseanlæg), runoff [L/s] (EM tryk 1) and VWC [m^3/m^3] (Sensor 1 - 971-nord) in Ejby Mølle.

It is clear that flow only occurs under certain conditions in Ejby Mølle. This tendency will be further analysed in Part I, chapter 6.

Elmelundsvej (HHX)

The catchment area at Elmelundsvej is 0.1123 ha (1123 m^2) and consists of a sloped green area, dominated by soil texture: *coarse clay with sand* (cf. Appendix A, Table A.2). An intercepting line drain is installed at the bottom of the green area. The flow is estimated using the Q/H curve shown in Appendix F Figure F.3. Three VWC sensors have been installed in the area. Distribution functions of the VWC measurements can be found in Appendix D Figure D.2. An overview of the measurement installations can be seen in Appendix A, Table A.2. The line drain, elevation, and catchment area are illustrated in Figure 4.5.

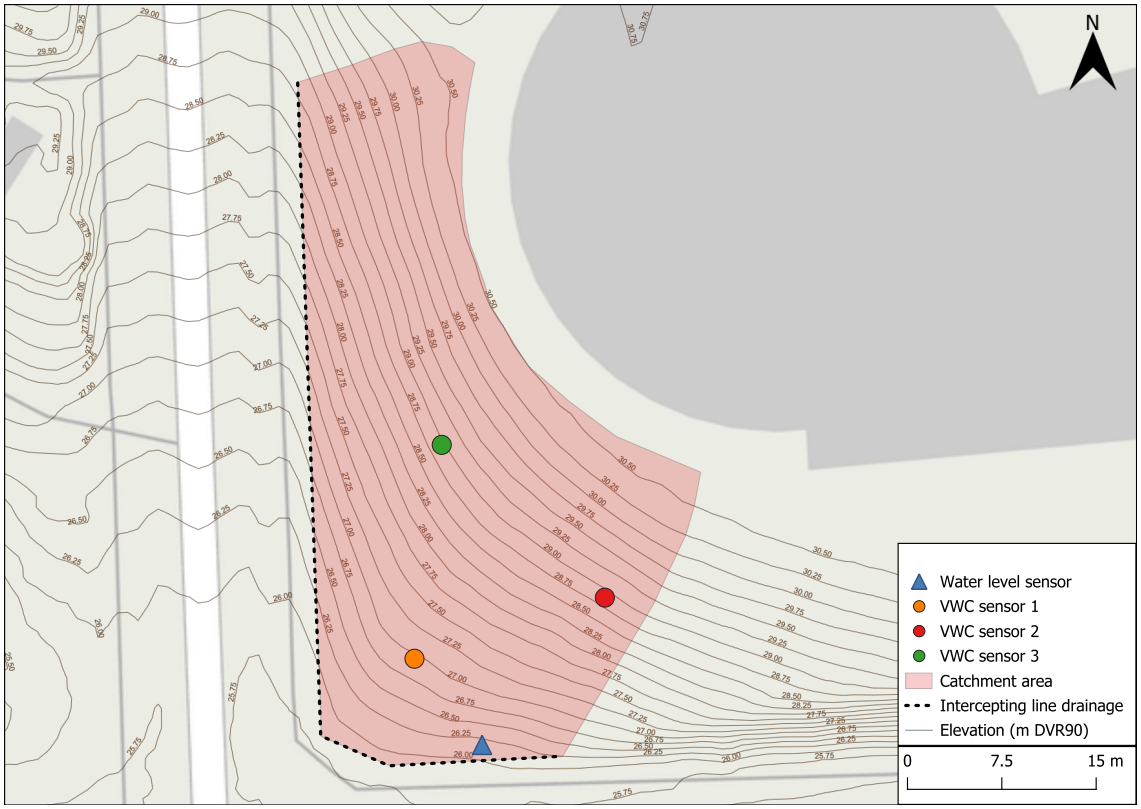

Figure 4.5. Outline of Elmelundsvej catchment with elevation lines and measurement installations.

During the measurement period, the land use of the area has changed from being a maintained lawn to a deliberately wild, natural landscape. The green area can be seen in Appendix A, Figure A.3 and Figure A.4.

The data collection periods vary depending on the data type. The available data from each of the measurement stations is illustrated in Appendix A Figure A.5. In order to assess the quality of the data from each of the VWC sensors, the individual data series are shown in Appendix A Figure A.6. The longest and most continuous data series are found in VWC sensors 2 and 3, where further analysis is based on sensor 3. The selection of the VWC sensor is based on *statistical analysis* explained in Appendix D, section D.1.

The complete set of data, including precipitation, flow, and VWC measurements, used for the data analysis, is observed from 01.05.23 until 01.05.25 and presented in Figure 4.6.

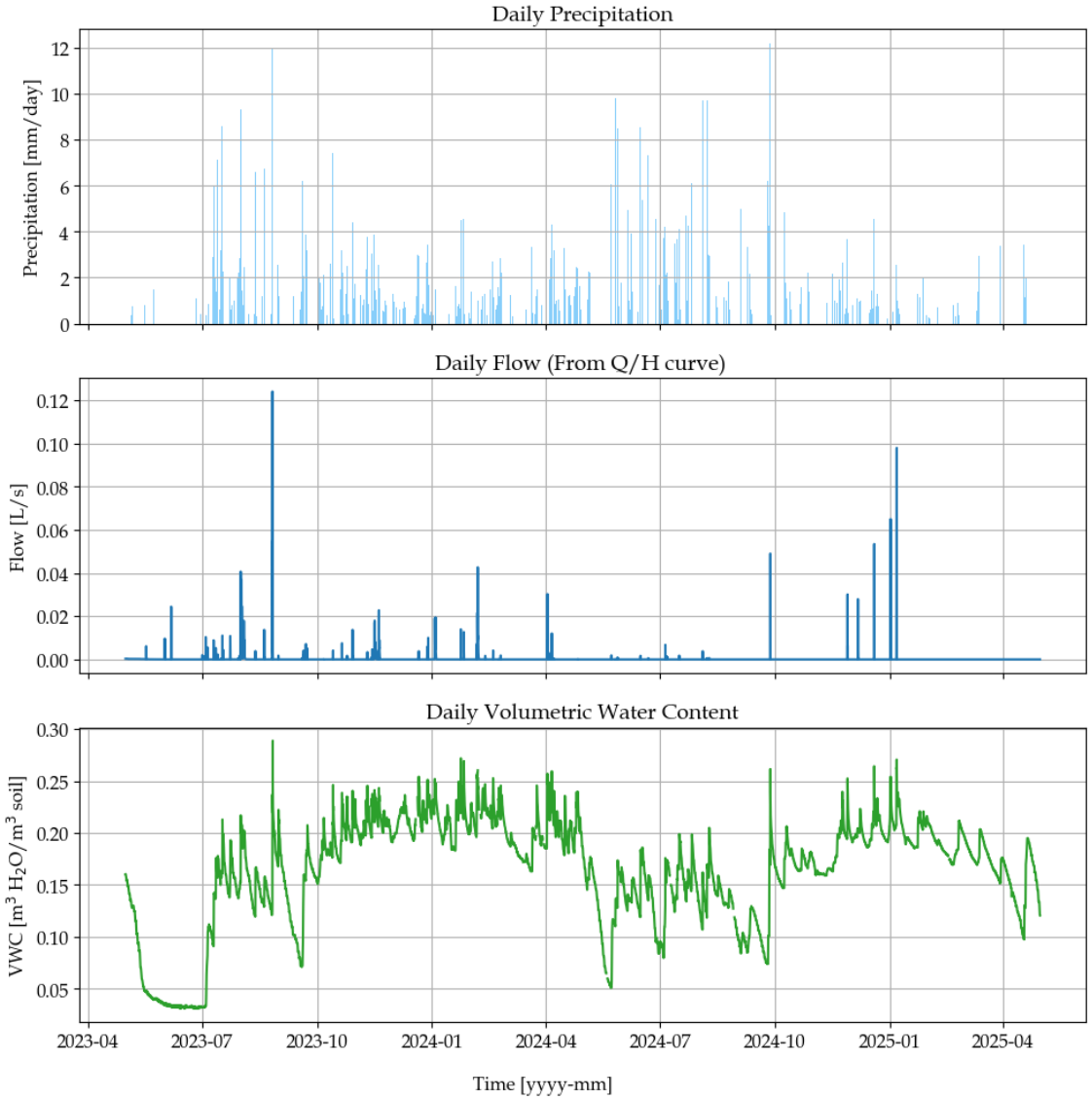

Figure 4.6. Measured precipitation [mm/day] (5422 Bolbo Højdebeholder), runoff [L/s] (Tryk 2 water level) and VWC [m^3/m^3] (Sensor 3 - 5bb-nord) at Elmelundsvej.

A tendency is observed where the flow at Elmelundsvej only occurs under specific conditions, which will be further analysed in Part I, chapter 6.

Aarhus Vand

Aarhus Vand is the water utility company covering Aarhus municipality. In collaboration with the Municipality, Envidan, and Copenhagen University, Aarhus Vand aims to implement climate adaptation measures in the city. The adaptation includes creating more time and room for water in the urban landscape, through innovative urban planning [Aarhus Kommune et al., 2017]. As part of the climate adaptation, it is important to expand the knowledge of contingent runoff, hence why Aarhus Vand is part of Project VandKant.

As part of the project, Aarhus Vand has chosen two research areas: Lystrup and Viby. Since there are no VWC measurements available in Viby, this project will only include a presentation and analysis of data from Lystrup. The purpose of the research areas in Aarhus is to measure direct runoff from green areas.

Lystrup

The Lystrup catchment is 0.43 ha (4300m^2) and is composed of a sloped green area, dominated by soil texture: *fine clay with sand* (cf. Appendix A, Table A.3), surrounded by properties (as seen in Appendix A, Figure A.7). At the bottom of the sloped terrain, an intercepting line drain is installed to measure surface runoff. The runoff is measured in a node with a V-shaped overflow, and the VWC is measured in three different VWC sensors. Distribution functions of the VWC measurements can be found in Appendix D Figure D.3.

An overview of the measurement installations in the catchment can be seen in Appendix A, Table A.3. The catchment area to the line drain and the location of the measurement installations can be seen in Figure 4.7.

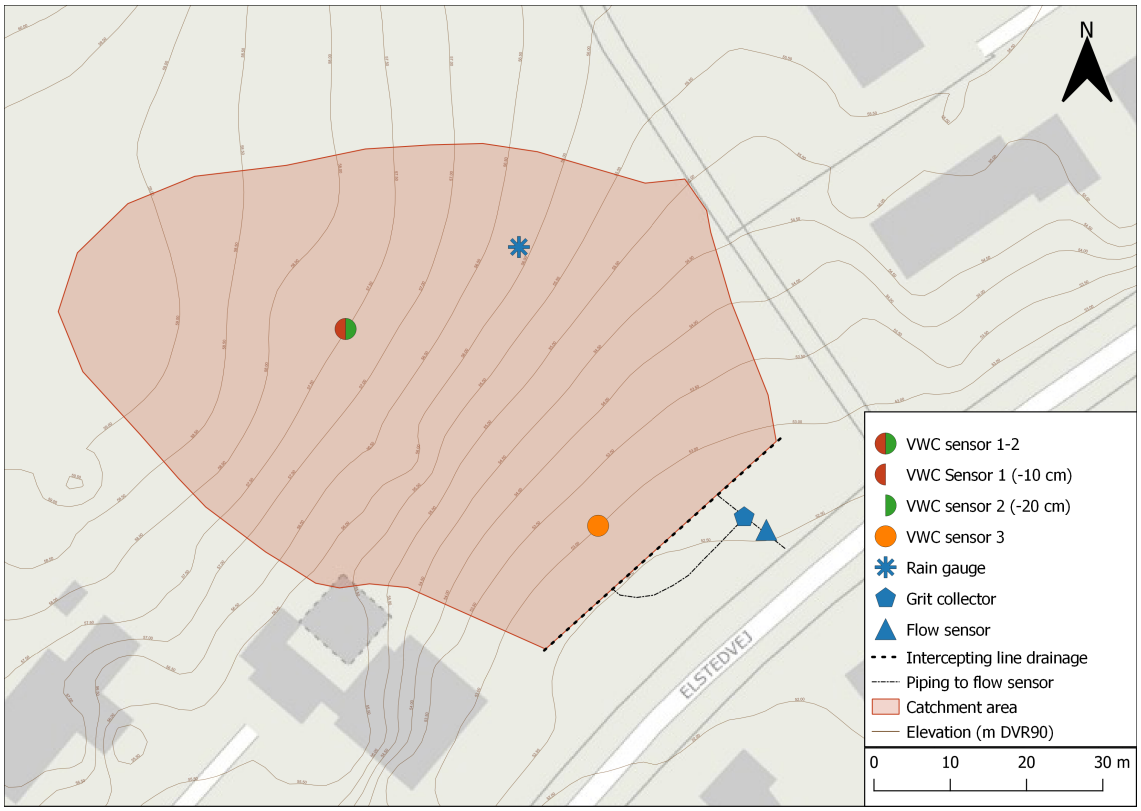

Figure 4.7. Outline of Lystrup catchment with elevation lines and measurement installations.

Nielsen, 2019 found that subsurface throughflow is the dominant runoff process in Lystrup due to a clay and silt layer at a depth of 46 cm. Additionally, it is found that the subsurface throughflow occurs when the soil reaches a VWC of 0.34 [m^3 H_2O/m^3 soil] [Nielsen, 2019] [Nielsen et al., 2020a].

The data collection periods vary depending on the data type. The available data from each of the measurement stations is illustrated in Appendix A Figure A.8. In order to assess the quality of the data from each of the VWC sensors, the individual data series are shown in Appendix A Figure A.9. The longest and most continuous data series is found in VWC sensor 3. The selection of the VWC sensor is further based on *statistical analysis* explained in Appendix D, section D.1. The complete set of data including precipitation, flow, and VWC measurements, used for the data analysis, is observed from 11-10-2022 until 01-05-2025 and presented in Figure 4.8.

Figure 4.8. Measured precipitation [mm/day] (5180 Egå renseanlæg), runoff [L/s] (V-overløb - Venstre) and VWC [m^3/m^3] (Sensor 3 - Lystrup nederst 20 cm dybde) in Lystrup.

A tendency is observed where the flow only occurs under specific conditions, which will be further analysed in Part I, chapter 6.

4.2 Urban Subcatchment Scale

The medium-sized scale is defined as the urban subcatchment scale. This scale includes areas that consist of both green (pervious) and impervious surfaces, making it more complex than the hillslope scale. Runoff in these areas is measured within the sewer system. In the following analysis, two types of urban subcatchments are presented: one with a combined sewer system and one with a separate sewer system.

Novafos

Novafos is the water utility company responsible for the water management in nine municipalities in the Capital Region of Denmark: Allerød, Ballerup, Egedal, Furesø, Frederikssund, Gentofte, Gladsaxe, Hørsholm, and Rudersdal. Novafos aims to take the lead regarding sustainable solutions for future generations [Novafos, 2025].

As part of the VandKant project, Novafos has chosen two research areas in Hørsholm Municipality. The purpose of the research areas in Hørsholm is to investigate the effect of contingent runoff in residential areas. Additionally, Novafos aims to develop screening tools in order to assess whether or not contingent runoff can be neglected in certain areas or situations. The project areas are presented in Figure 4.9.

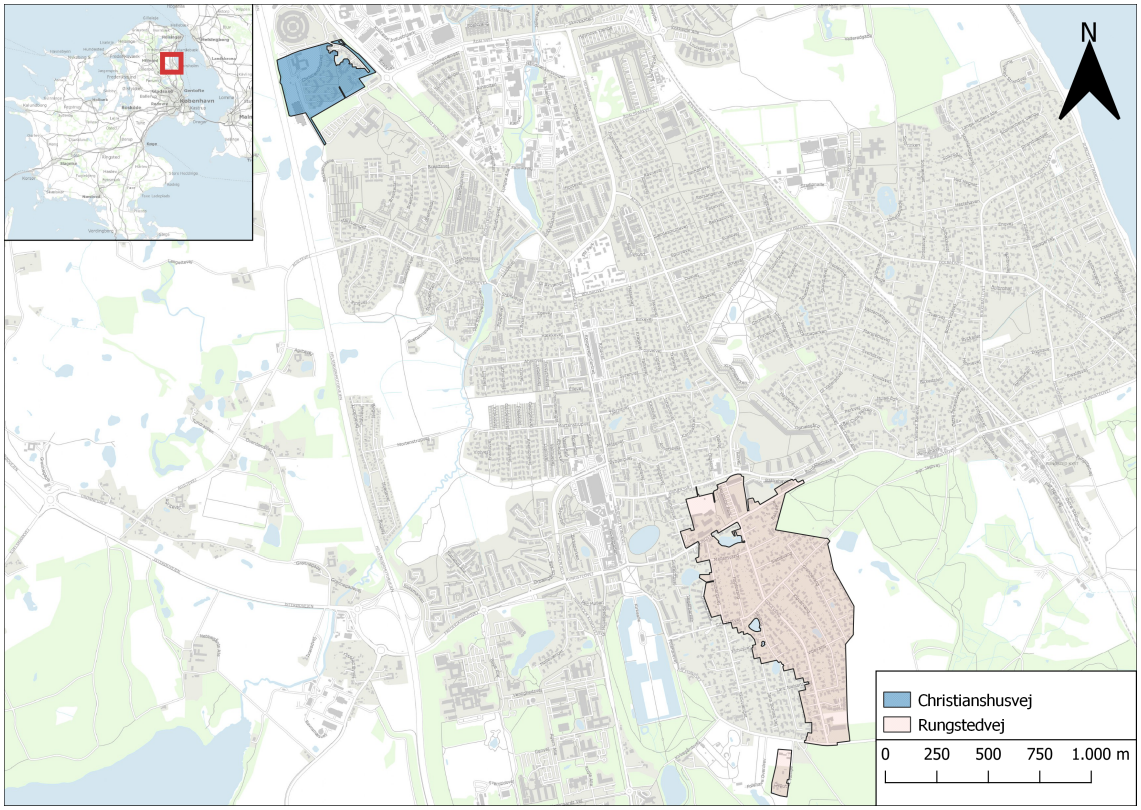

Figure 4.9. An overview of the two project areas in Hørsholm; Christianshusvej (blue) and Rungstedvej (red).

The northern area has a separate sewer system and is referred to as Christianshusvej, while the southern area has a combined sewer system and is referred to as Rungstedvej.

Christianshusvej

The Christianshusvej catchment is 10.5 ha and consists of single-story residential houses, green areas, dominated by soil texture: *fine clay with sand* (cf. Appendix B, Table B.1), and a stormwater-runoff pond with a permanent water table. Downstream from the rainwater detention pond, a flow sensor is installed in the stormwater runoff pipe (Ø150). An overview of the measurement installations can be seen in Appendix B, Table B.1. The degree of imperviousness for the area is calculated to be 37% using the Land Cover from Scalgo Live [Scalgo, 2024]. The land cover map and its corresponding areas are presented in Appendix B, Figure B.3 and Table B.2.

The VWC sensors are installed at three distinct locations within the area, positioned across varying elevations and terrains. Sensors 1, 2, 3, and 4 are situated in a garden at four different depths. Sensor 5 is located in a larger green space, whereas Sensor 6 is positioned on an artificial elevation in the southern part of the area. Distribution functions of the VWC measurements can be found in Appendix D Figure D.4. An outline of the catchment and the location of the measurement installations can be seen in Figure 4.10.

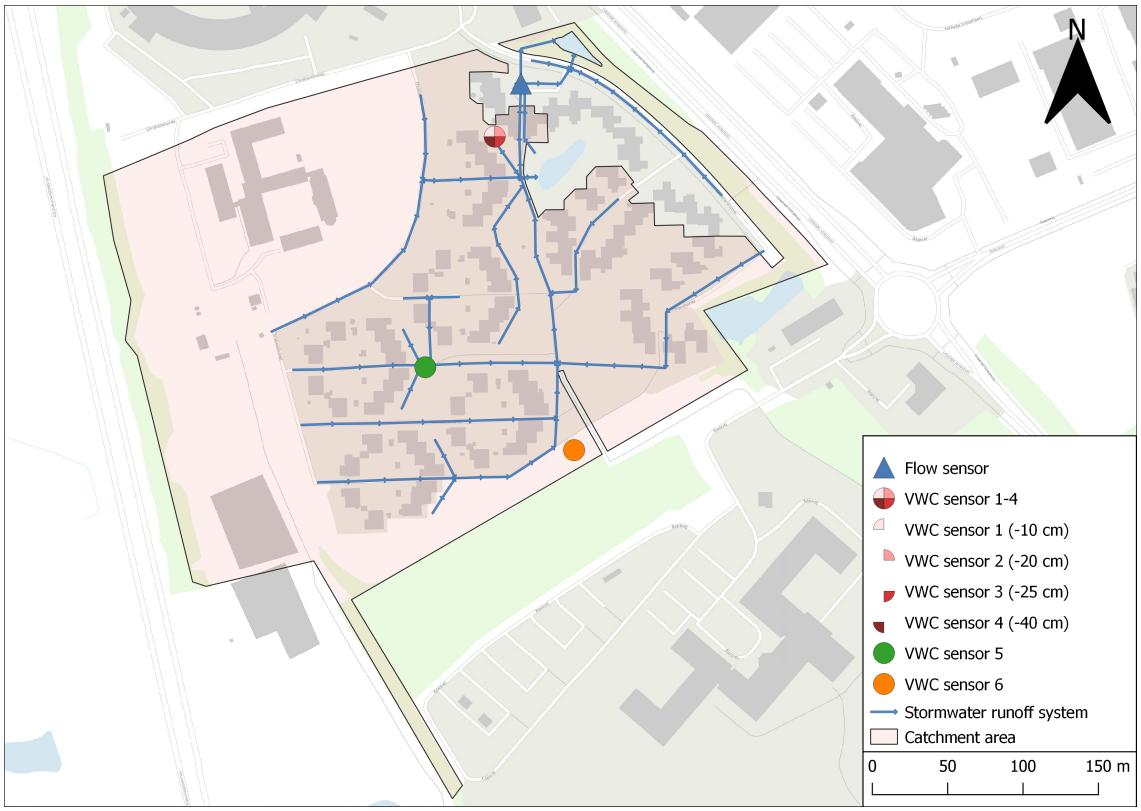

Figure 4.10. Outline of Christianshusvej catchment with stormwater pipes [Novafos, 2025] and measurement installations.

The data collection periods vary depending on the data type. The available data from each of the measurement stations is illustrated in Appendix B, Figure B.1.

In order to assess the quality of the data from each of the VWC sensors, the individual data series are shown in Appendix B, Figure B.2. The longest and most continuous data series is found in VWC Sensors 5 and 6, where Sensor 6 will be used for the data analysis. The selection of the VWC sensor is based on *statistical analysis* explained in Appendix D, section D.1. The complete set of data, including precipitation, flow, and VWC measurements, used for the data analysis, is observed from 09-09-2023 until 01-05-2025 and presented in Figure 4.11.

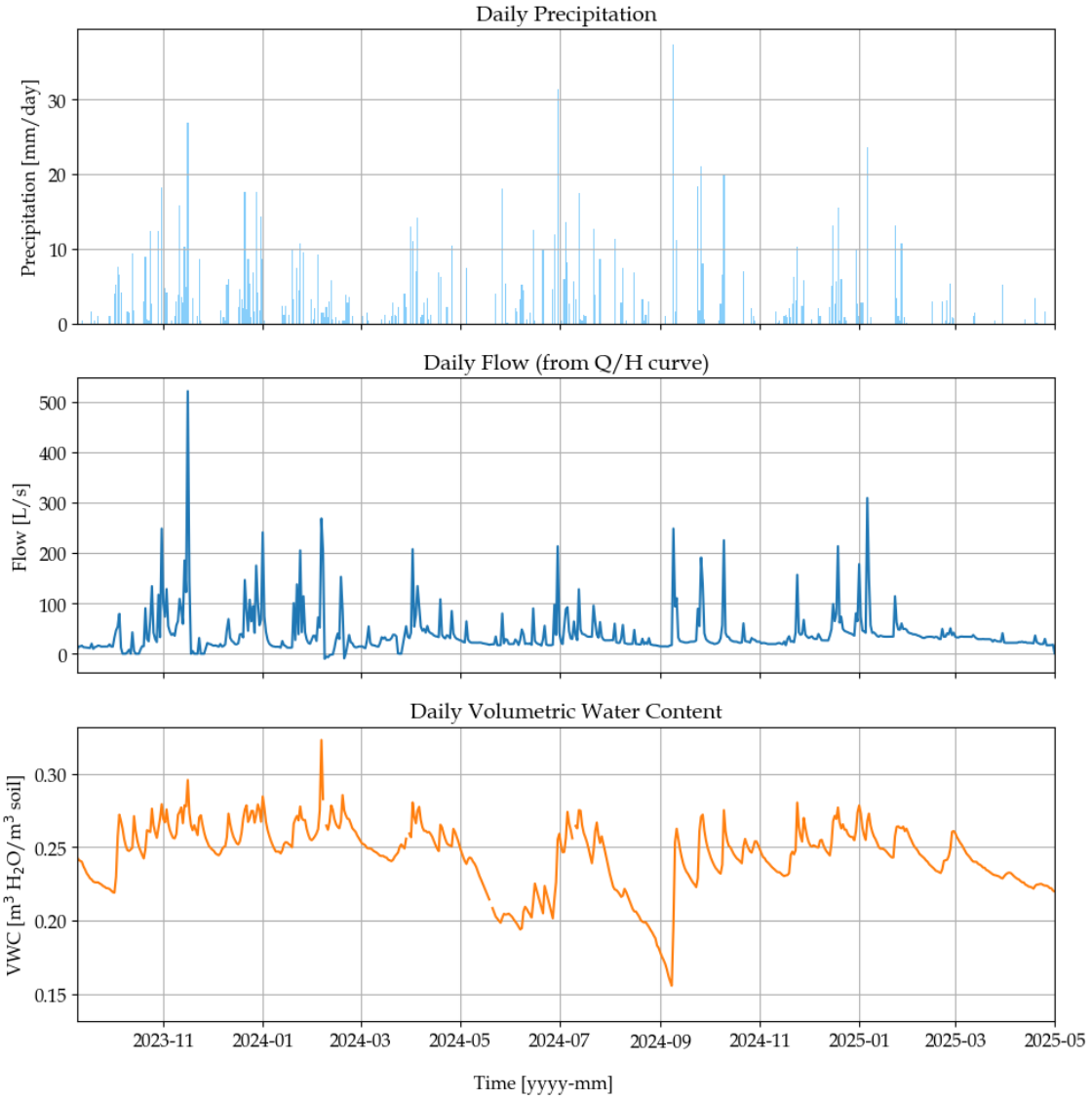

Figure 4.11. Measured precipitation [mm/day] (5622 Usserød Renseanlæg), flow [L/s] (Målebrønd - Pipeflow-est-lvl1) and VWC [m^3/m^3] (Sensor 6 - Skråning syd) at Christianshusvej.

A continuous flow above 0 L/s is observed, which suggests that water from the soil is leaking into the stormwater pipes. Additionally, A tendency is observed where the flow in the stormwater pipe increases under specific conditions, which will be further analysed in Part I, chapter 7.

Rungstedvej

The Rungstedvej catchment is 56.5 ha and consists of single-story residential houses and green areas, dominated by soil texture: *fine clay with sand* (cf. Appendix B, Table B.3). The flow sensor is installed in the combined sewer system in a 700mm conical-bottom pipe. In the southwest part of the catchment area, the sewer system has been separated. The wastewater from the separated sewer system is being directed to the combined system, and the stormwater drains into a pond in the area. An overview of the measurement installations can be seen in Appendix B, Table B.3. The degree of imperviousness for the area is calculated to be 47% using the Land Cover from Scalgo Live [Scalgo, 2024]. The land cover map and its corresponding areas are presented in Appendix B, Figure B.6 and Table B.4.

The VWC sensors are installed in private gardens at approximately 20 cm depth. Distribution functions of the VWC measurements can be found in Appendix D Figure D.5. An outline of the catchment and the location of the measurement installations can be seen in Figure 4.12.

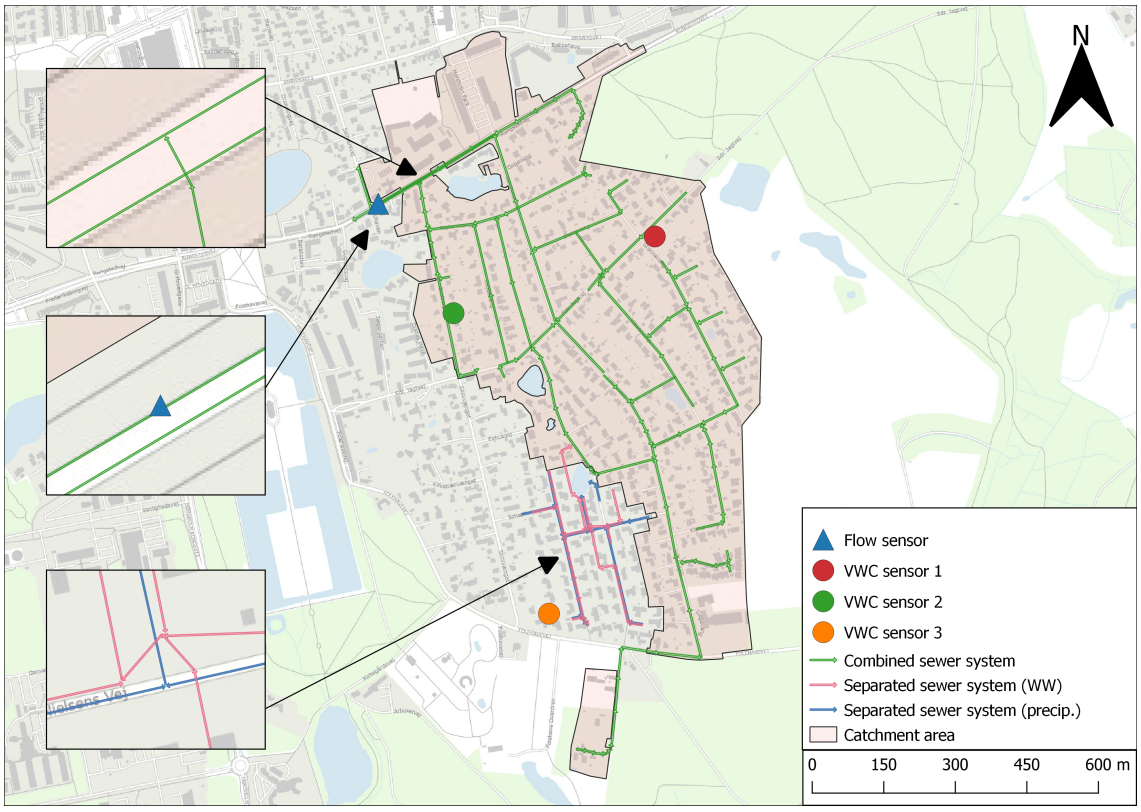

Figure 4.12. Outline of Rungstedvej catchment with sewer pipes [Novafos, 2025] and measurement installations. The flow sensor (blue triangle) is placed on the upper sewer pipe.

The data collection periods vary depending on the data type. The available data from each of the measurement stations is illustrated in Appendix B, Figure B.4. In September 2023, Novafos decided to reduce the number of project locations from two to one, and data collection at Rungstedvej was consequently discontinued.

In order to assess the quality of the data from each of the VWC sensors, the individual data series are shown in Appendix B, Figure B.5. All three data series are of good quality, however there is a small outage in the data for VWC Sensor 3. The best correlation with the flow is Sensor 2, therefore, this series will be used for the data analysis. The selection of the VWC sensor is explained in Appendix D, section D.1. The complete set of data, including precipitation, flow, and VWC measurements, used for the data analysis, is observed from 01-01-2023 until 25-01-2024 and presented in Figure 4.13.

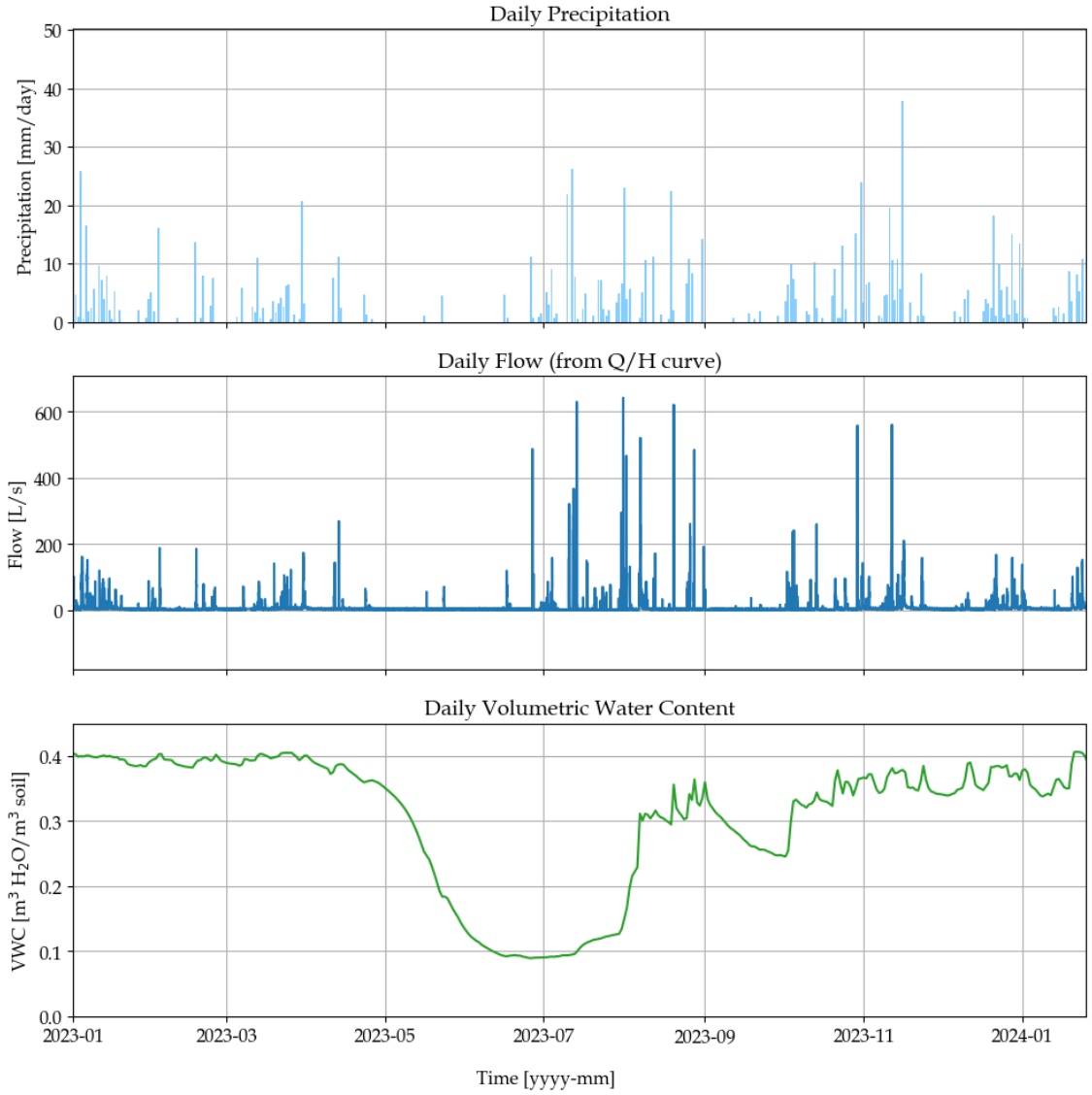

Figure 4.13. Measured precipitation [mm/day] (5623 Bukkeballevej pumpestation), flow [L/s] (2.1970000 flow) and VWC [m^3/m^3] (Sensor 2 - Ane's brors have) at Rungstedvej.

A tendency is observed where the flow in the combined sewer pipe increases under specific conditions, which will be further analysed in Part I, chapter 7.

4.3 Hydrological Scale

The largest scale is referred to as the hydrological scale, which encompasses the entire catchment area of a stream. This is the most complex scale, as it includes a wide range of soil types, textures, compaction levels, and land uses. In this study, the hydrological scale is represented by the Grejs Å catchment near Vejle.

Vejle presents a characteristic example of how urban areas can be affected by upstream hydrological processes. The city lies in a valley where three major streams, Grejs Å, Vejle Å, and Højen Å, converge and flow into Vejle Fjord, draining a combined catchment of approximately 330 km^2 (Figure 4.14). A large portion of this catchment consists of rural and natural landscapes, meaning substantial volumes of contingent runoff from upstream areas can be transported via these streams toward the urban centre.

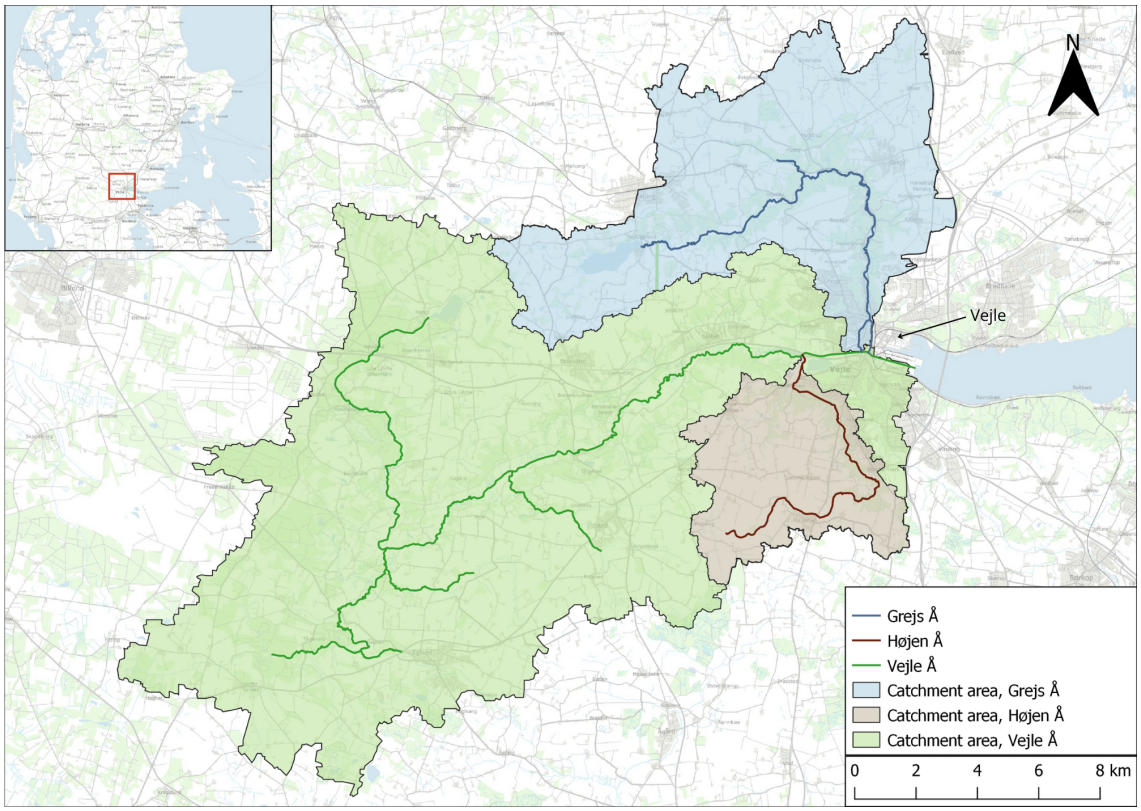

Figure 4.14. Overview of the catchment area of Vejle.

When intense or prolonged rainfall events occur, the runoff generated in the rural upstream catchment can contribute significantly to elevated water levels in the urban stream network. If this coincides with local cloudbursts or urban drainage systems operating near capacity, the risk of urban flooding increases drastically. In such scenarios, both surface runoff and streamflow exceedances can pressurise the urban infrastructure. This interaction between rural runoff and urban flooding is illustrated in the conceptual overview in Figure 4.15.

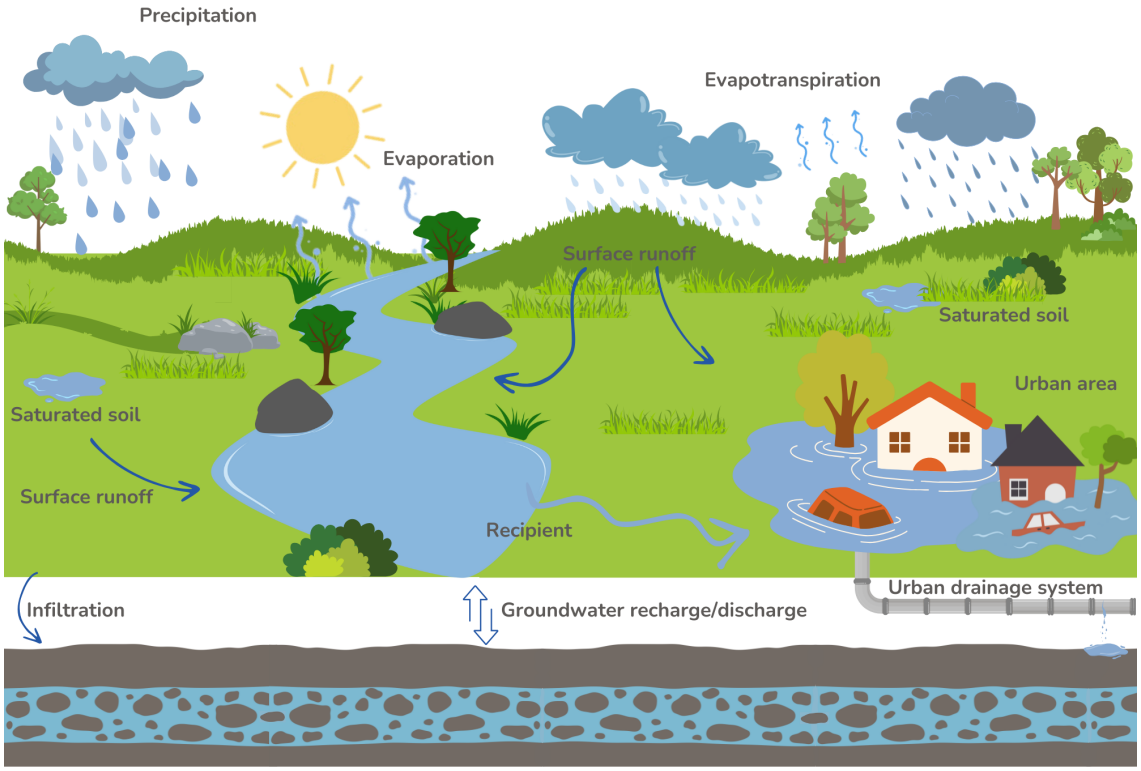

Figure 4.15. A conceptual sketch of the dynamics of surface runoff in relation to soil and hydrology.

Due to its topographical setting and large upstream catchment, Vejle is particularly vulnerable to flood events, not only from intense local precipitation but also from snowmelt, high water levels in Vejle fjord, and storm surges. These risks have led to the city being designated as one of Denmark's 10 most flood-prone areas under the EU Floods Directive. As a response, mitigation efforts such as a lock system with pumping capacity have been implemented [Miljøstyrelsen, 2025].

As part of the flood management efforts, it is important to expand the knowledge of contingent runoff. Therefore, both Vejle Municipality and Vejle Spildevand (the local utility company) are part of the VandKant project. The purpose of the research area in Vejle is to examine the effect of contingent runoff on a large scale. An additional goal for Vejle is to develop a warning system for urban flooding that incorporates contingent runoff. A special focus is placed on Grejs Å because the water contribution from the catchment is large and the water is lead directly through the city.

Grejs Å

The Grejs Å catchment covers an area of 78 km^2 and is predominantly rural, as explained in Appendix C. At the upper part of the catchment, a water level sensor (St. 32.06) has been installed, where flow is estimated using a Q-h curve. Further downstream, just before the stream enters the urban area, a combined flow and water level sensor (St. 32.22) is

located. Similarly, one rain gauge is placed at the top of the catchment (5230 Jelling) and another closer to the city (5235 Vejle Centralrenseanlæg). In addition, eight VWC sensors have been installed throughout the catchment. An overview of the sensor installations is provided in Appendix C, Table C.3.

The VWC sensors are installed at three distinct locations within the area, positioned across varying elevations and terrains. Sensor 1 is situated at the top of the catchment on steep terrain. Sensors 2, 3, and 4 are situated in the middle of the catchment in an alkaline fen and forest area. Sensors 5, 6, 7, and 8 are located further downstream of Grejs Å, close to St. 32.22. This area consists of forests and open fields. Distribution functions of the VWC measurements can be found in Appendix D Figure D.6. An outline of the catchment and the location of the measurement installations can be seen in Figure 4.16.

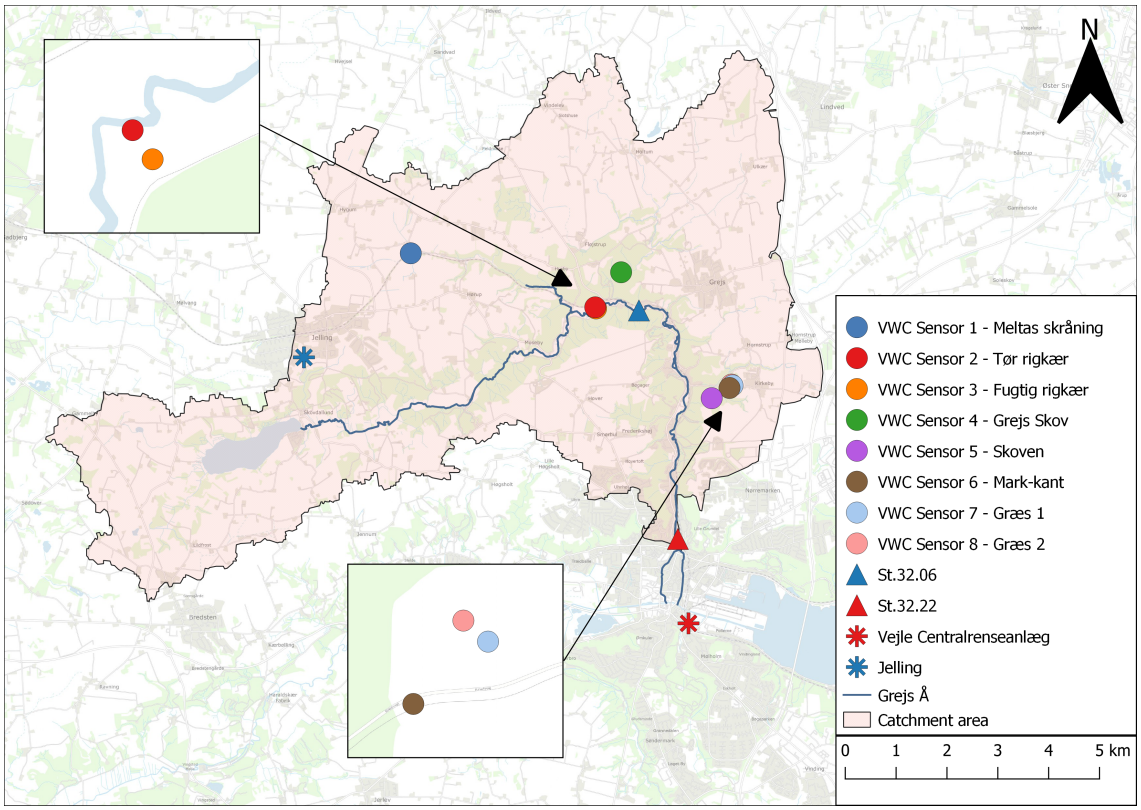

Figure 4.16. Outline of Vejle catchment with the location of measurement installations.

The data collection periods vary depending on the data type. The available data from each of the measurement stations is illustrated in Appendix C, Figure C.2. In order to assess the quality of the data from each of the VWC sensors, the individual data series are shown in Appendix C, Figure C.3 and Figure C.4. Sensor 6 will be used for further analysis based on *statistical analysis* explained in Appendix D, section D.1. The set of data, including rain, flow, and VWC measurements, used for the data analysis, is observed from 01-01-2022 until 01-05-2025 and presented in Figure 4.17.

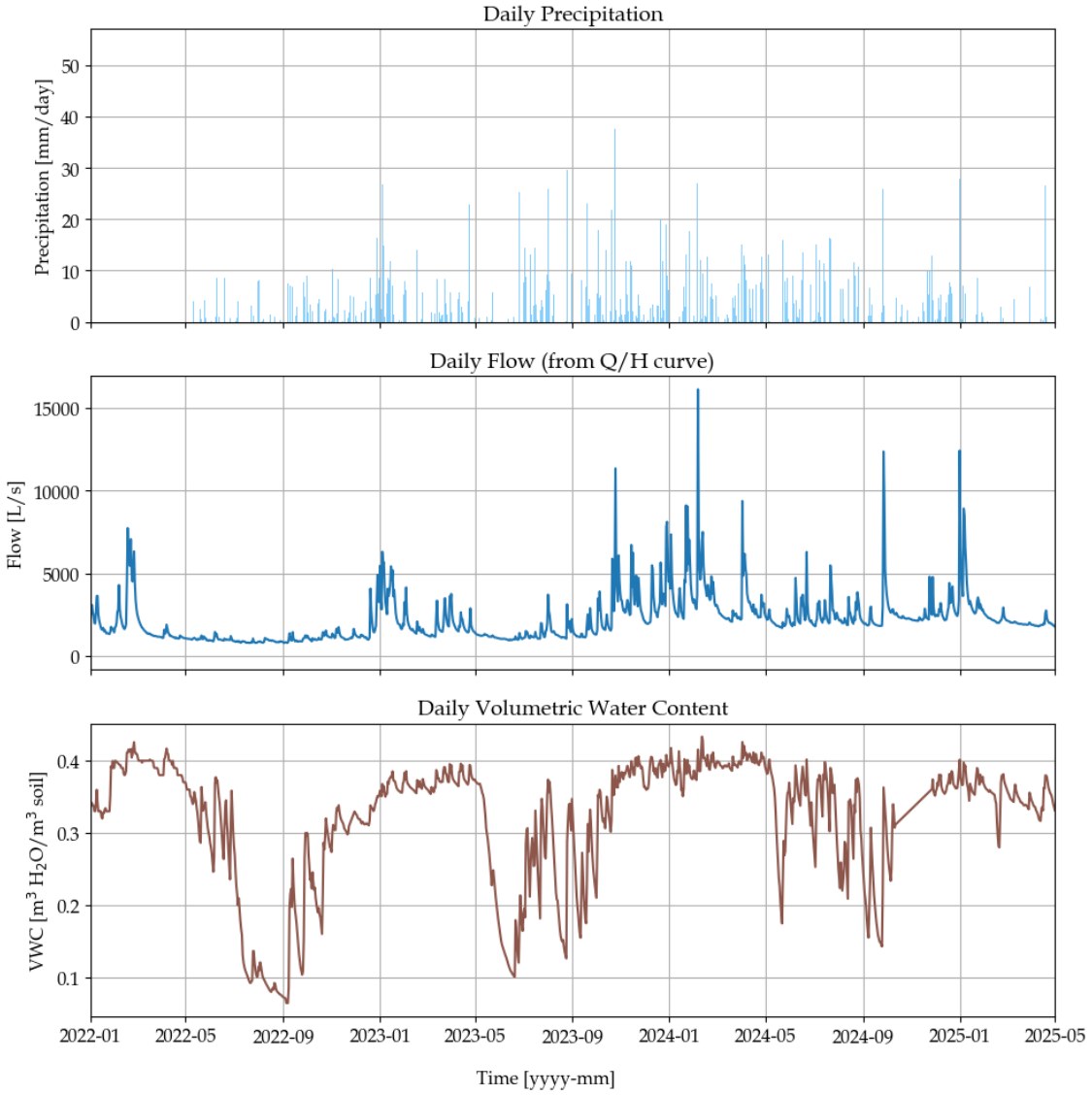

Figure 4.17. Measured precipitation [mm/day] (5235 Vejle Centralrenseanlæg and 5230 Jelling), flow [L/s] (St. 32.22) and VWC [m^3/m^3] (Sensor 6 - Mark-kant) in Vejle.

The precipitation data used in the analysis is calculated as an hourly average of the measurements from the two rain gauge stations.
A tendency is observed where the flow in Grejs Å increases under specific conditions, which will be further analysed in Part I, chapter 8.

Based on the data presented in this chapter, the impact of contingent runoff across the six project locations will be analysed in Part I.

Part I

Location Analysis of Contingent Runoff

Analysis Framework 5

The VWC-, flow-, and precipitation data are processed as uniformly as possible to evaluate the contingent runoff from project locations of different scales. This ensures consistency in the analysis and provides a common frame of reference for comparing the datasets.

An overview of the elements of the analysis is listed below and elaborated in the following sections and in the appendix:

- **Cross-Correlation Analysis** - Examines the occurrence of delay between precipitation and the corresponding flow in the system. The cross-correlation method is elaborated in section 5.1 and the results are presented in Appendix E.
- **Runoff Separation Analysis** - The flow in pipes or streams is separated into baseflow and surface runoff. The runoff separation is presented in Appendix G.
- **Event Analysis** - The events of which the largest rain and runoff volumes are shown as a time series. The figure illustrates the relationship between rain, flow, and VWC during the events.
- **VWC and Runoff Analysis** - The VWC data is classified into intervals, and the dynamics between rain, runoff and VWC are explored, including the effects of:
  - Wet/dry conditions
  - Rainfall intensity
  - Change in VWC during rainfall

  The classification of VWC is visualised in Appendix H and the runoff analysis is presented in section 5.4.
- **Runoff Ratio Analysis** - The proportion of rainfall converted into runoff is examined using two plots. The upper plot compares runoff ratio under wet/dry conditions, while the lower plot categorises VWC into bins with intervals of 0.05 m^3/m^3 to assess its influence on runoff. The *runoff ratio analysis* is elaborated in section 5.5
- **Statistical Analysis** - To support the visual analyses, several statistical analyses are conducted. These include Kolmogorov-Smirnov, Kruskal-Wallis test, Dunn's test and Spearman's correlation. The *statistical analysis* is elaborated in section 5.6, and additional results can be found in Appendix I.

5.1 Cross-Correlation Analysis

A cross-correlation between precipitation and flow is performed on the project locations to estimate the system's response time (also known as lag time). The response time corresponds to the time it takes for the flow to show a response after precipitation, as illustrated in Figure 5.1.

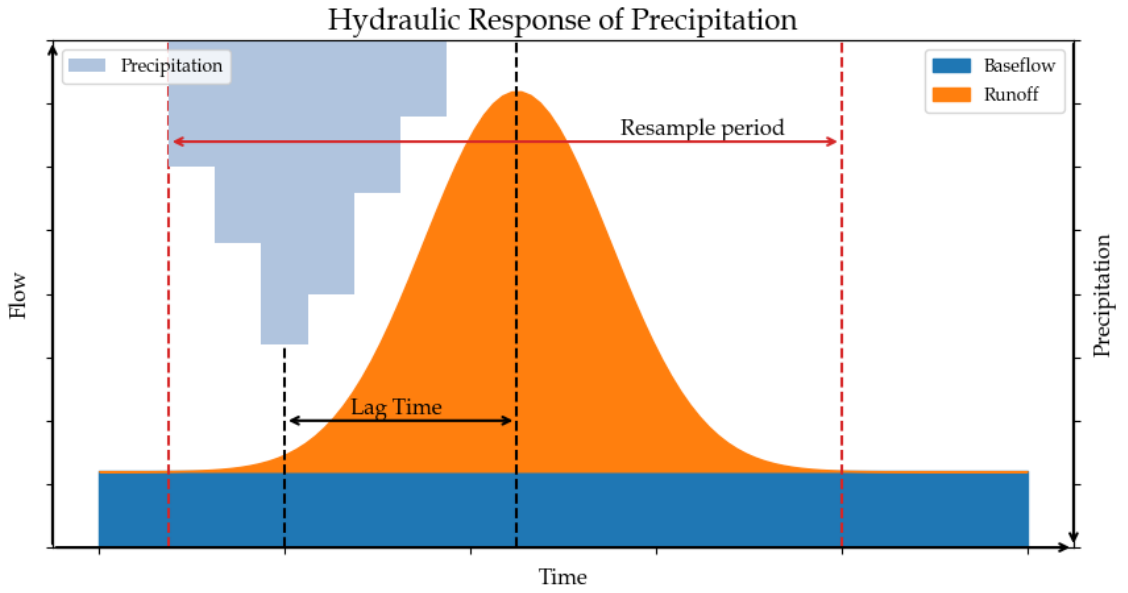

Figure 5.1. Conceptual figure of the *cross-correlation analysis* and lag time.

The cross-correlation is used to determine the resample period so that each data point in the analysis best resembles both the precipitation and flow.

The resampling is based on events, and is defined as starting at the onset of precipitation and continuing for one day in hillslope scale and urban subcatchment scale project locations, and two days for the hydrological scale project location. As illustrated by the red and black resample periods in Figure 5.2, there is a risk of including excess water if a new event begins within the duration of the initial event.

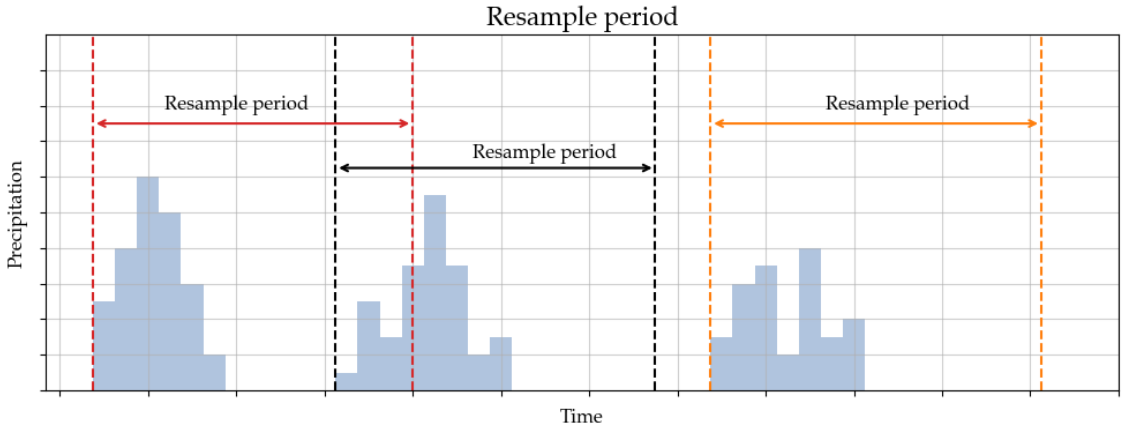

Figure 5.2. Conceptual figure of the resample period for the determined event.

5.2 Runoff Separation Analysis

A baseflow analysis is performed at those project locations within the urban subcatchment scale and the hydrological scale, where it is assumed that not all observed flow is attributed to contingent runoff. The flow at these places is considered to consist of a direct runoff and a baseflow, as illustrated on Figure 5.1. To isolate and analyse only the direct runoff, a runoff separation is performed and presented in Appendix G. The appendix includes theory, plots of the baseflow, the direct runoff, and a zoomed-in view of the separation. Additionally, a sensitivity analysis is conducted to examine the influence of the runoff separation.
At a hillslope scale, the estimated flow (based on Q/H curve, cf. Appendix F) is assumed to originate solely from the catchment area. Therefore, the analysis can be conducted directly on the flow data without performing a *runoff separation analysis*.

5.3 Event Analysis

To understand the relationship between VWC and runoff at the different project locations, rainfall events with the highest daily accumulated rainfall and runoff are selected and analysed. As shown in Figure 5.3, the *event analysis* illustrates the change in VWC during these rainfall events and how they relate to the amount of generated runoff.

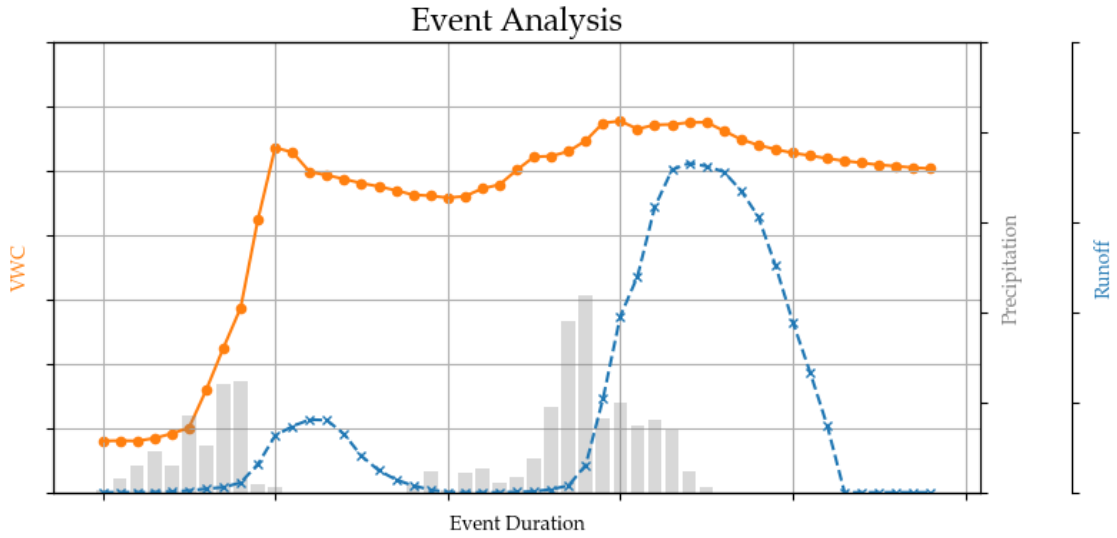

Figure 5.3. Conceptual figure of the *event analysis*

In the analysis, a figure with three to four events is presented, consisting of both the largest rainfall events and the largest flow events.

The selected events are presented in Appendix H, section H.2.

5.4 VWC and Runoff Analysis

As mentioned above, the *VWC and runoff analysis* consists of multiple parts. Firstly, the influence of soil moisture on contingent runoff is explored by classifying the VWC into three bins. The classification is based on quartiles, where the low VWC bin consists of the 25% lowest values, the high bin consists of the 25% highest values, and the medium bin consists of the 50% values in the middle. Each bin has been assigned a colour and shape which will persist throughout the thesis:

- High VWC (red, triangle)
- Mid VWC (yellow, cross)
- Low VWC (green, circle)

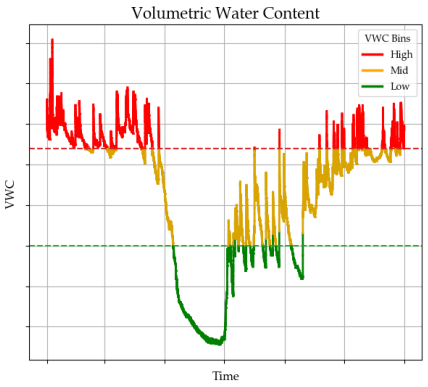

Figure 5.4. A conceptual figure of VWC classification.

Figure 5.4 illustrates how the VWC measurements are classified into the three bins. Figures of the VWC bin classification for all six project locations can be found in Appendix H, section H.1. Thereafter, the data points from periods where the air temperature, according to DMI, has dropped below 0°C, will be excluded from the analysis [DMI, 2025]. This is done as snow can delay the response between precipitation and runoff, making it difficult to predict, as described in chapter 3. This is done for all further analysis, and all precipitation is hereafter assumed to represent rainfall. The data points excluded from the analysis are illustrated in Appendix H, section H.2.

To gain a comprehensive understanding of the parameters influencing runoff, a composite plot featuring four subplots is generated for each project location. The composite plot consists of scatter plots with rainfall per event on the x-axis and runoff per event on the y-axis, and is illustrated in Figure 5.5. In the first scatter plot, the data points are coloured by the VWC bins to illustrate the influence of VWC on the amount of runoff. This scatter plot is denoted "1. Original Scatter Plot".
In the second scatter plot, the data points are coloured by wet and dry conditions to illustrate the influence of seasons on the amount of runoff. This scatter plot is denoted "2. Coloured by Season". The wet period spans 7 months (from October to April), while the dry period covers 5 months (from May to September).
In the third scatter plot, the data points are coloured by rain intensity to illustrate the influence of heavy rain events on the amount of runoff. This scatter plot is denoted "3. Coloured by Intensity". The rain event classifications are defined by WMO [World Meterological Organization, 2025] as:

- Heavy shower, $\geq$10 mm/hr (black)
- Heavy rain, $\geq$4 mm/hr (orange-red)
- Normal rain, <4 mm/hr (light blue)

In the fourth scatter plot, the data points are coloured by change in VWC to illustrate the infiltration into the soil and its influence on the amount of runoff. This scatter plot is denoted "4. Coloured by VWC Difference". This is achieved by calculating the difference between the initial and the maximum VWC values during the event. The maximum VWC value is chosen instead of the final VWC value to avoid capturing a potential drop in VWC, which may occur within the event if the rainfall ceases before the event ends. This drop can be caused by flow within the soil or evaporation. The change in VWC is classified into three bins: High increase, Low increase, and No increase. The high increase bin consists of the 25% largest changes, the low increase bin consists of the remaining data points where the VWC increases, and the No increase bin consists of data points where the VWC remains the same or drops.

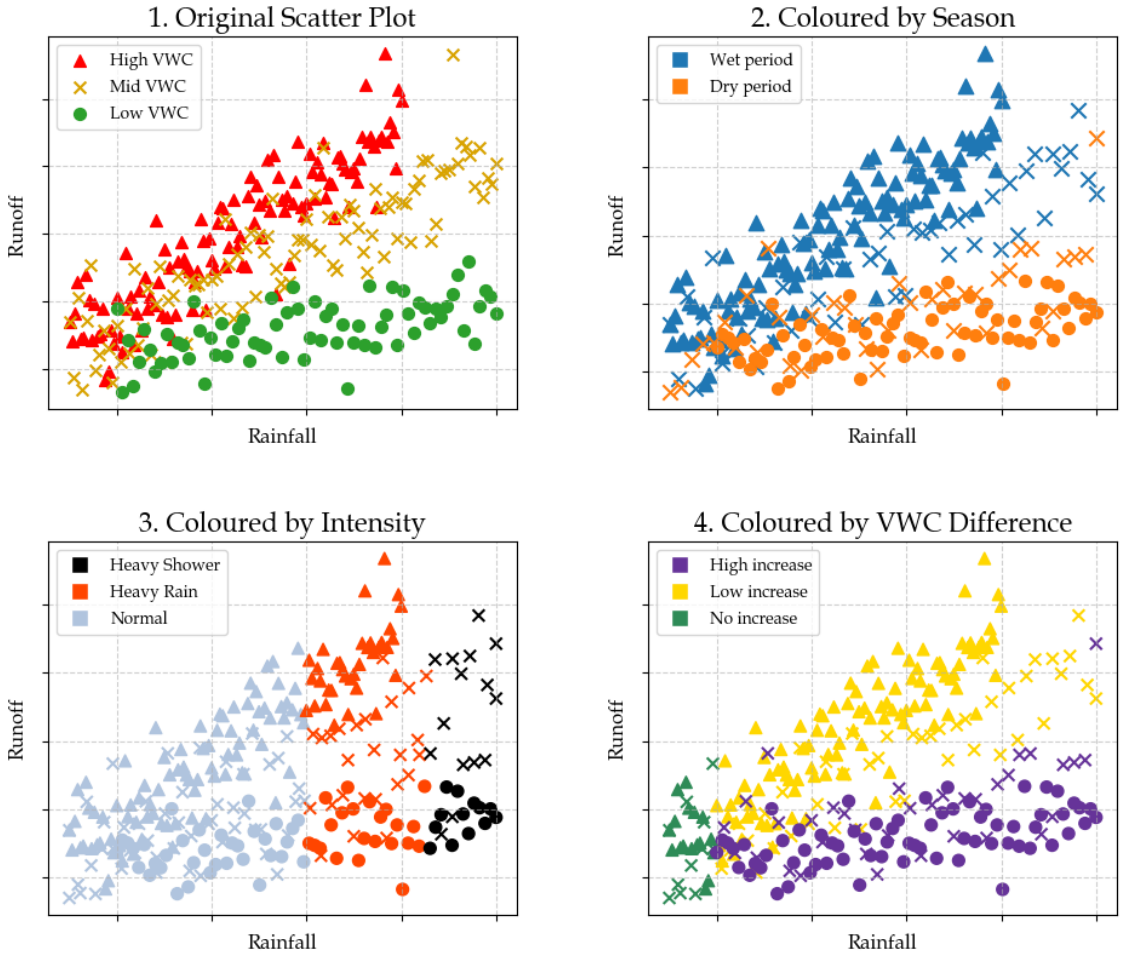

Figure 5.5. Conceptual figure of the composite plot showing the influence of VWC, season, rain intensity and change in VWC.

5.5 Runoff Ratio Analysis

The *runoff ratio analysis* consists of a plot with two subplots. The upper plot presents the runoff ratio versus VWC, distinguishing between the wet period (blue) and the dry period (orange). The lower plot illustrates the median runoff ratio binned by VWC, along with the corresponding interquartile range (IQR) for each bin. The subplots share the same x-axis representing VWC [m^3 H_2O/m^3 soil]. The fraction of rainfall converted into runoff [mm runoff/mm rainfall] is shown on the y-axis.

In some cases, a runoff ratio exceeding 1 is observed. This may be attributed to rapid snowmelt, inaccuracies in the catchment area size, or measurement errors. These values are visualised in the upper plot but will be excluded from the runoff analysis in the lower plot.

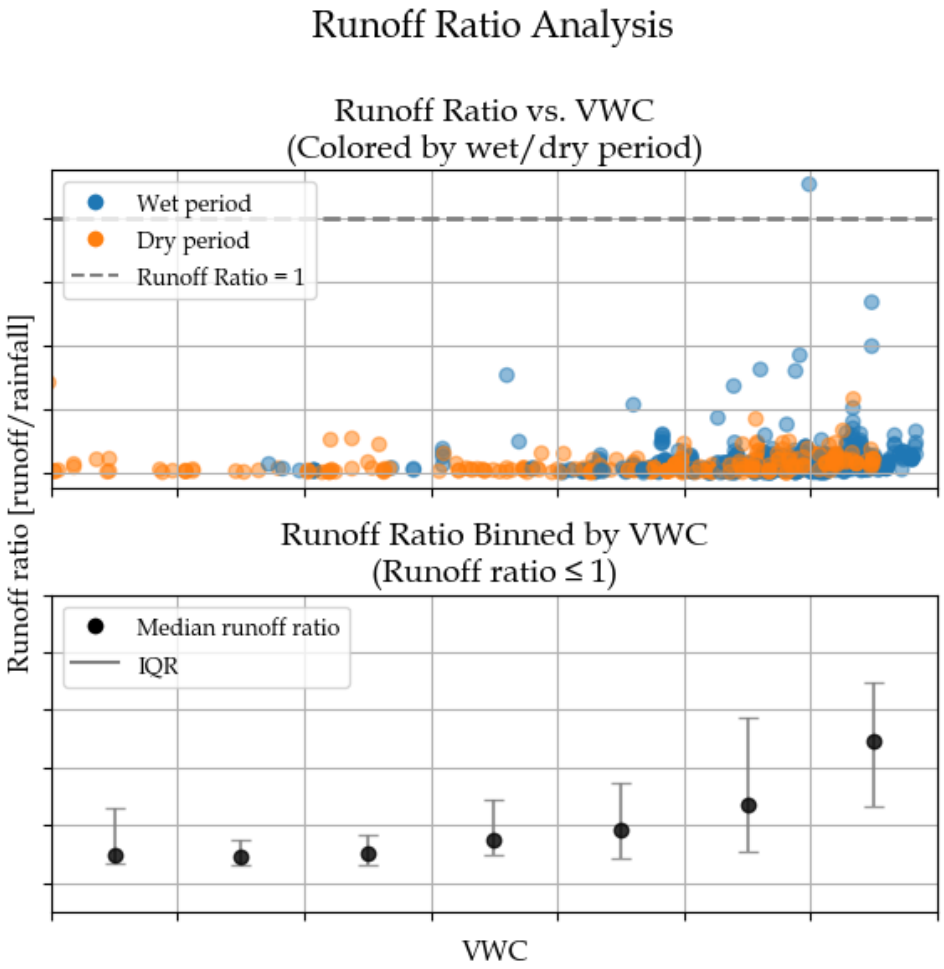

Figure 5.6. Conceptual figure of the *runoff ratio analysis*.

5.6 Statistical Analysis

In the *statistical analysis*, the distribution of runoff data is first visualised using a frequency histogram along with a p-value from a Kolmogorov-Smirnov Test to assess normality. A p-value below a significance level of 0.05 indicates that the null hypothesis of normal distribution can be rejected. A significance of 0.05 means that there is a 5% chance of making a Type I error where the null hypothesis is falsely rejected [Coolidge, 2020]. The histograms and Kolmogorov-Smirnov tests for all project locations can be found in Appendix I section I.1. The runoff data are non-normally distributed, hence, a non-parametric approach is employed in all cases.

To visualise the spread of the runoff data and to easily detect outliers within the three bins (high, mid, and low VWC), a box plot is made for each of the locations. The outliers, represented as individual data points outside the whiskers, are extreme values, which likely are results from intense or irregular rainfall events rather than measurement errors; they are considered to be reflections of natural variability rather than true statistical outliers. Therefore, they are not removed from the dataset. The boxplots are presented in Appendix I, section I.2.

A Kruskal–Wallis test is conducted on the runoff data in the high, mid and low VWC bins to determine if there is a significant difference between the median runoff amounts for different VWC conditions [Reid, 2014]. If a significant difference is detected, a Dunn's test is performed to identify which groups differ from each other. When multiple hypothesis' are tested, the probability of making a Type I error increases. Therefore, a Bonferroni correction is applied to adjust the significance level and reduce the probability of Type I errors [Dinno, 2015]. The Bonferroni correction is calculated as the significance level (α) divided by the number of comparisons (m):

$$\alpha_{adjusted} = \frac{\alpha}{m} \tag{5.1}$$

The number of comparisons depends on the number of groups (N) compared:

$$m = \frac{N(N-1)}{2} \tag{5.2}$$

Additionally, the Kruskal-Wallis test and Dunn's test are performed to examine if there is a significant difference between the median runoff values for each of the VWC bins in the Runoff ratio plot described in section 5.5.

Finally, a Spearman's correlation is used to measure the strength of monotonic relationship between runoff [mm] and rain [mm], VWC [m^3 H_2O/m^3 soil], or ΔVWC [m^3 H_2O/m^3 soil]. This is done to test which of the parameters have an effect on the runoff at each of the project locations.
The Spearman correlation test is used to identify which of the VWC sensors has the best

correlation with the flow at each of the project locations. This test is performed to help decide on the most relevant VWC sensor to use for the analysis. Lastly, Spearman's correlation test is similarly used to explore if the minimum, mean, median, or maximum VWC value during the rain event best describes the corresponding runoff amount. At all project locations, it is found that the maximum VWC has the best correlation with the flow. For this reason, the data points in the *VWC and runoff analysis*, explained in section 5.4, are coloured by the maximum VWC. The result of these two Spearman correlation tests can be found in Appendix D, section D.1 and section D.2.
The Spearman correlation coefficients (ρ) can take on values between -1 and 1, where 1 indicates a strong positive monotonic relationship, -1 indicates a strong negative monotonic relationship, and 0 indicates no monotonic relationship. To test whether a monotonic relationship, found in Spearman's correlation, is present, a significance test is performed. The null hypothesis of the test is that there is no monotonic correlation. If the p-value of the significance test is below the Bonferroni adjusted significance level, the null hypothesis can be rejected and there is significant evidence that a monotonic relationship is present [Reid, 2014].

Hillslope Scale 6

The runoff at the three hillslope-scale areas, Ejby Mølle, Elmelundsvej, and Lystrup, is first analysed individually, followed by a brief discussion of the results and at the end of this chapter, the three areas are compared. The three areas, and the data available, are presented previously in section 4.1.

6.1 Ejby Mølle

As described in section 4.1, the catchment area for Ejby Mølle consists of a lawn on a small hill. For the runoff analysis, VWC data from Sensor 1 is used.

To understand the relationship between VWC and runoff at Ejby Mølle, rainfall events with the highest daily accumulated rainfall and runoff are selected (cf. Appendix H, Figure H.7) and analysed in Figure 6.1. From the top two plots, it is evident that the VWC generally increases in response to rainfall, and that runoff tends to be generated when the VWC exceeds approximately 0.25 m^3/m^3. The first event, on 07-08-2024, exhibits the highest recorded rainfall (42.00 mm) with a corresponding runoff response of 0.14 mm (0.33 % of the rainfall becomes runoff). It is evident that the rainfall occurs primarily within the first seven hours, resulting in a significant increase in VWC from 0.2 to 0.4 m^3/m^3 during this period. The runoff response is observed four hours after the event starts, with a peak runoff (0.08 mm/hr). Moreover, a runoff peak is observed two hours after the peak rainfall intensity (approximately 21 mm/hr). This aligns with the cross-correlation results presented in Appendix E, Figure E.1, which indicates a lag time of two hours between rainfall and runoff.
The second event, on 26-09-2024, displays the second-highest daily rainfall (40.94 mm) with a corresponding runoff of 0.07 mm (0.17% of the rainfall becomes runoff). Rainfall is observed during the first seven hours and again in the final six hours of the event. In the first rainfall phase, a VWC response is seen after approximately five hours, followed by a runoff response one hour later. Between the two phases, a minor decrease in both VWC and runoff occurs, whereafter the second phase results in a VWC increase, yet no visual runoff response is observed.
From the lower two plots in Figure 6.1, the two events with the highest daily accumulated runoff are presented. It is evident that high runoff is generally generated when VWC is elevated. The event on 08-06-2024, which exhibits the highest recorded runoff (0.24 mm) and a corresponding rainfall of 7.80 mm (3.1% of the rainfall becomes runoff), shows that rainfall occurs during the first five hours and again around 20 hours after event start. In the first rainfall phase, VWC increases from 0.3 to 0.35 m^3/m^3, while a runoff response is observed approximately two hours after the start of the event, which aligns with the

cross-correlation analysis. Furthermore, no visual delay is observed between the VWC increase and the onset of runoff. However, despite the two relatively low and short rainfall phases, the runoff is observed throughout the entire event.

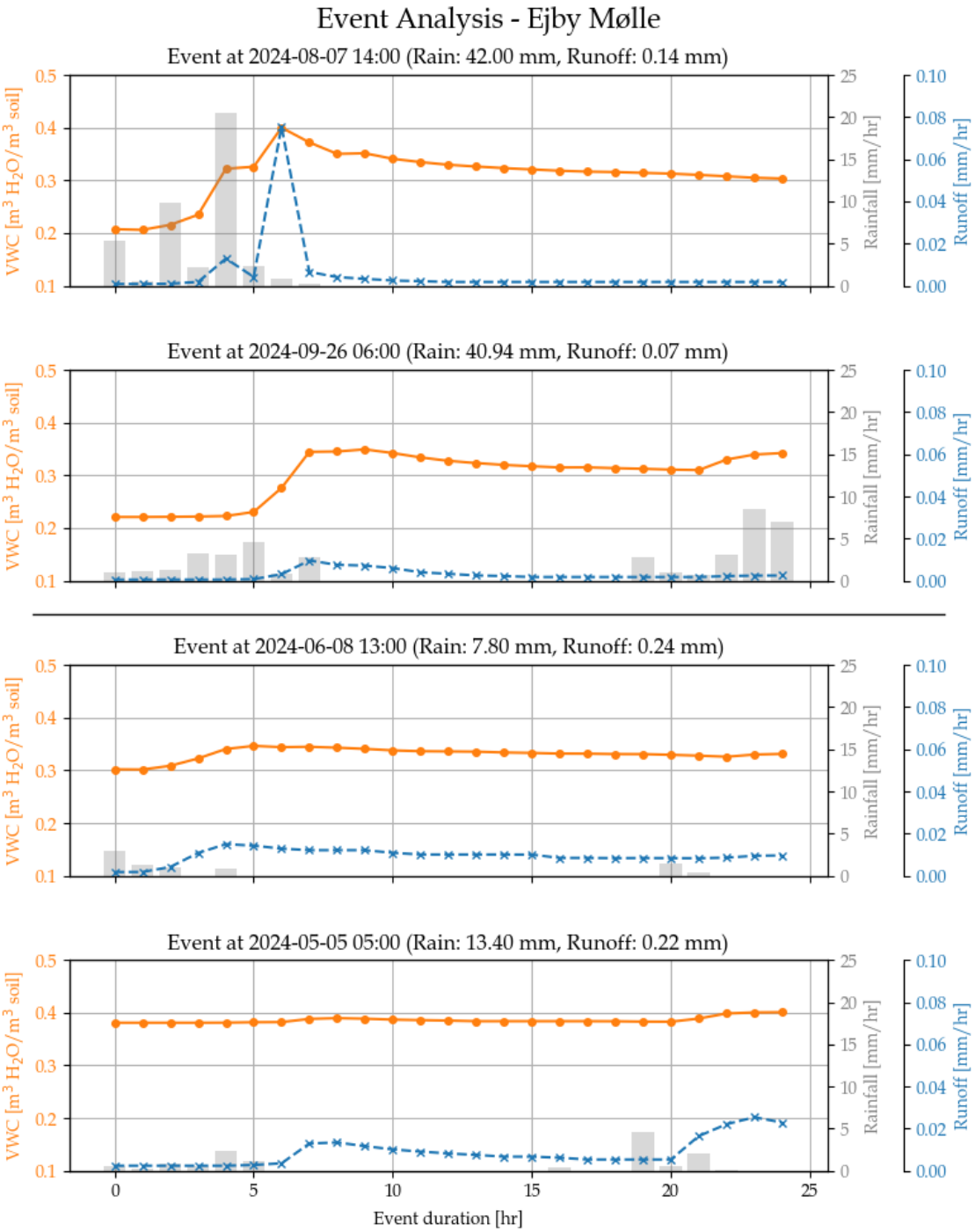

Figure 6.1. Analysis of VWC and runoff response to rainfall for selected events at Ejby Mølle, Odense.

The event on 05-05-2024 shows the second-largest daily runoff (0.22 mm) and a corresponding rainfall of 13.40 mm (1.6% of the rainfall becomes runoff). During this event, two rainfall phases are observed, however, VWC remains fairly constant at around

0.40 m^3/m^3, with a slight increase observed after 20 hours. Despite the relatively limited variation in VWC and the rainfall input, the runoff response from the first phase appears with a delay of six hours, followed by a runoff increase peaking at approximately 0.01 mm/hr. The second phase leads to a more immediate runoff response with a two-hour delay, peaking at around 0.02 mm/hr. When comparing the two events with the highest rainfall and the two events with the highest runoff at Ejby Mølle, it becomes evident that large runoff does not necessarily occur during the largest rainfall events, but rather depends heavily on the VWC level. This suggests that when VWC is already high, even moderate rainfall can trigger runoff with minimal delay. Therefore, it is necessary to further examine the relationship between daily rainfall, daily runoff, and daily VWC for Ejby Mølle, as visualised in Figure 6.2. The *VWC and runoff analysis* is conducted for each of the defined high, mid, and low VWC classifications (presented in Appendix H, Figure H.1), and is further subdivided into three subcategories within the high, mid, and low VWC.

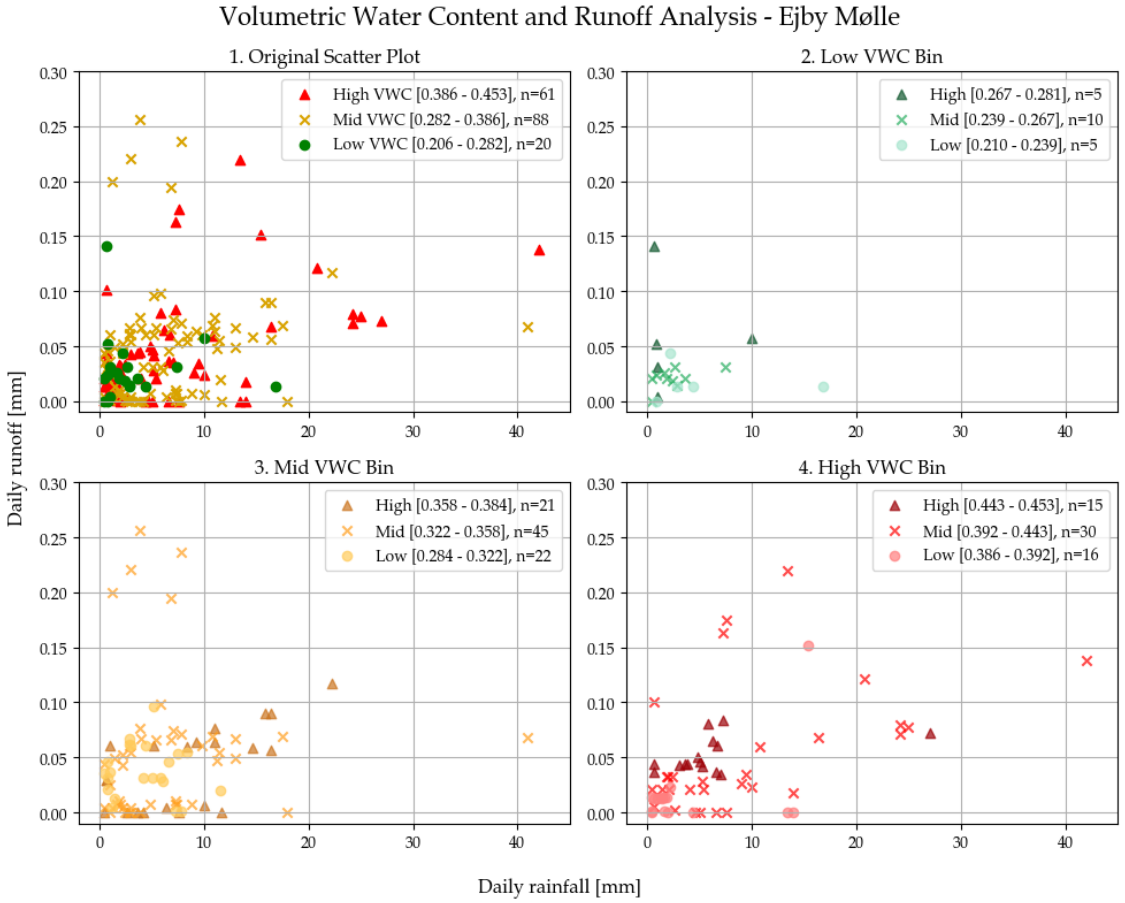

Figure 6.2. The *VWC and runoff analysis* for Ejby Mølle, Odense, consisting of (1) daily runoff/rainfall coloured by VWC, (2) daily runoff/rainfall in the low bin divided into three sub intervals, (3) daily runoff/rainfall in the mid bin divided into three sub intervals, and (4) daily runoff/rainfall in the high bin divided into three sub intervals.

As shown in Figure 6.2, the runoff at Ejby Mølle exhibits a generally low response to rainfall with daily runoff values between 0.00 to 0.25 mm. Subplot "2. Low VWC Bin" exhibit the lowest runoff values from 0.00-0.15 mm, while subplots "3. Mid VWC Bin" and "4. High VWC Bin" suggest a stronger correlation between daily rainfall and daily

runoff. Yet, mid and high VWC both exhibit scattered and spread out runoff responses, whereas the response is more linear at high VWC. This indicates that the runoff response at mid VWC is more unpredictable compared to the runoff response at high VWC. Moreover, it is evident that the largest rainfall events do not align with the largest amount of runoff, as observed in the *event analysis*. Consequently, it is necessary to examine the runoff data in more detail by identifying their seasonal grouping, rainfall intensity, and the change in VWC during the rainfall event. This is explored in Figure 6.3.

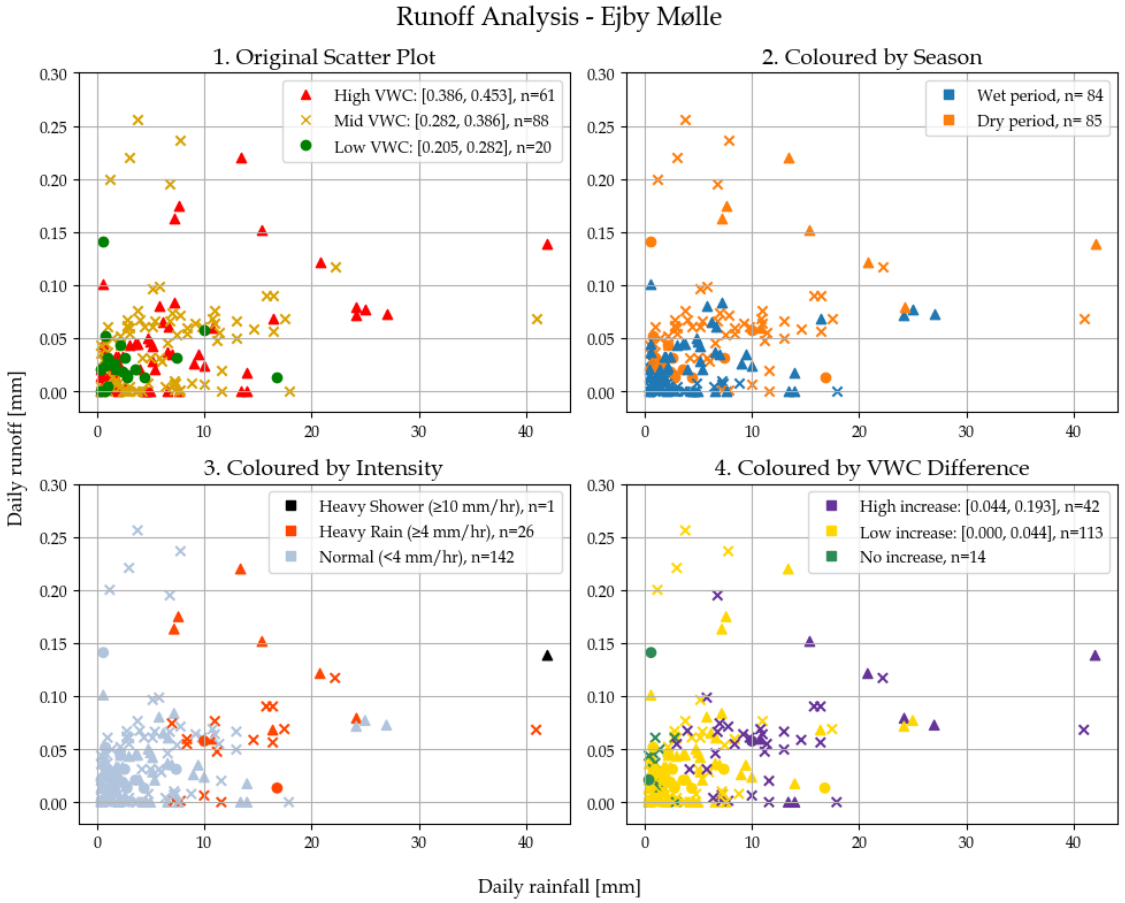

Figure 6.3. The runoff analysis for Ejby Mølle, Odense, consisting of daily runoff/rainfall coloured by (1) VWC, (2) wet/dry period, (3) rainfall intensity, and (4) change in VWC during the rainfall event.

Figure 6.3 shows that most data points fall within the dry period, as illustrated in subplot "2. Coloured by Season" (for a clearer wet/dry periodical segregation of the runoff-rainfall relationship coloured by VWC, see Appendix H, Figure H.13). The majority of rainfall events are classified as normal intensity, a few as heavy rain, and only one as heavy shower (cf. subplot "3. Coloured by Intensity"). Notably, the highest runoff amounts occur during the normal-intensity events. Subplot "4. Coloured by VWC Difference" indicates that this is because little to no increase in VWC occurs for most data points within this classification. By contrast, data points with higher daily rainfall are generally classified as either heavy rain or heavy shower, and show substantial increases in VWC, which explains why some of these events exhibit lower runoff than expected. As an example, during the heavy shower event, the daily rainfall is approximately 40 mm, yet less than 0.15 mm of

runoff is generated. Subplot 4 shows a relatively clear trend in the generated daily runoff depending on the change in VWC. When no VWC increase is present, the trend has an almost vertical slope, indicating that even a small increase in daily rainfall generates a simultaneous runoff response. By contrast, the data points with a high VWC increase exhibit a more gradual slope, suggesting that a larger portion of the rainfall is absorbed by the soil and less runoff is generated. Moreover, it is evident that the data points within the wet period mainly show no to low increase in VWC at rainfall, yet very little runoff is generated (0.00-0.10) despite daily rainfall amounts of up to approximately 30 mm.

By conducting a Kruskal-Wallis test ($p = 0.27$), no statistically significant difference between the median daily runoff of the VWC categories in Ejby Mølle is found, which is also evident from the boxplot presented in Appendix I, section I.2. This is likely due to the infiltration rate remaining the dominant factor, independent of the VWC.

To further examine the rainfall-generated runoff, a *runoff ratio analysis* is performed and presented in Figure 6.4. Most values lie near a runoff ratio of zero, indicating that infiltration is more prominent than runoff at Ejby Mølle.
In the lower plot, the median runoff ratio across all VWC bins is close to 0.01 mm/mm or lower, while IQR remains narrow, with the widest IQR of approximately 0.05 mm/mm found in Bins 1-3 covering VWC ranging from 0.20 to 0.35 m^3/m^3. In contrast, Bins 4-6 show a much narrower IQR, suggesting less variation in runoff ratio under higher VWC conditions. Overall, the *runoff ratio analysis* supports the observation that runoff response remains low and relatively consistent, even as VWC increases.

The visual indication of differences among the bins, a Kruskal–Wallis test ($p = 0.02$), confirms a statistically significant difference between their medians. To identify which specific medians differ, a Dunn's test is performed, indicating a statistically significant difference between the medians of Bin 3 and Bin 4. A visualisation of these results is presented in Appendix I, Figure I.13.

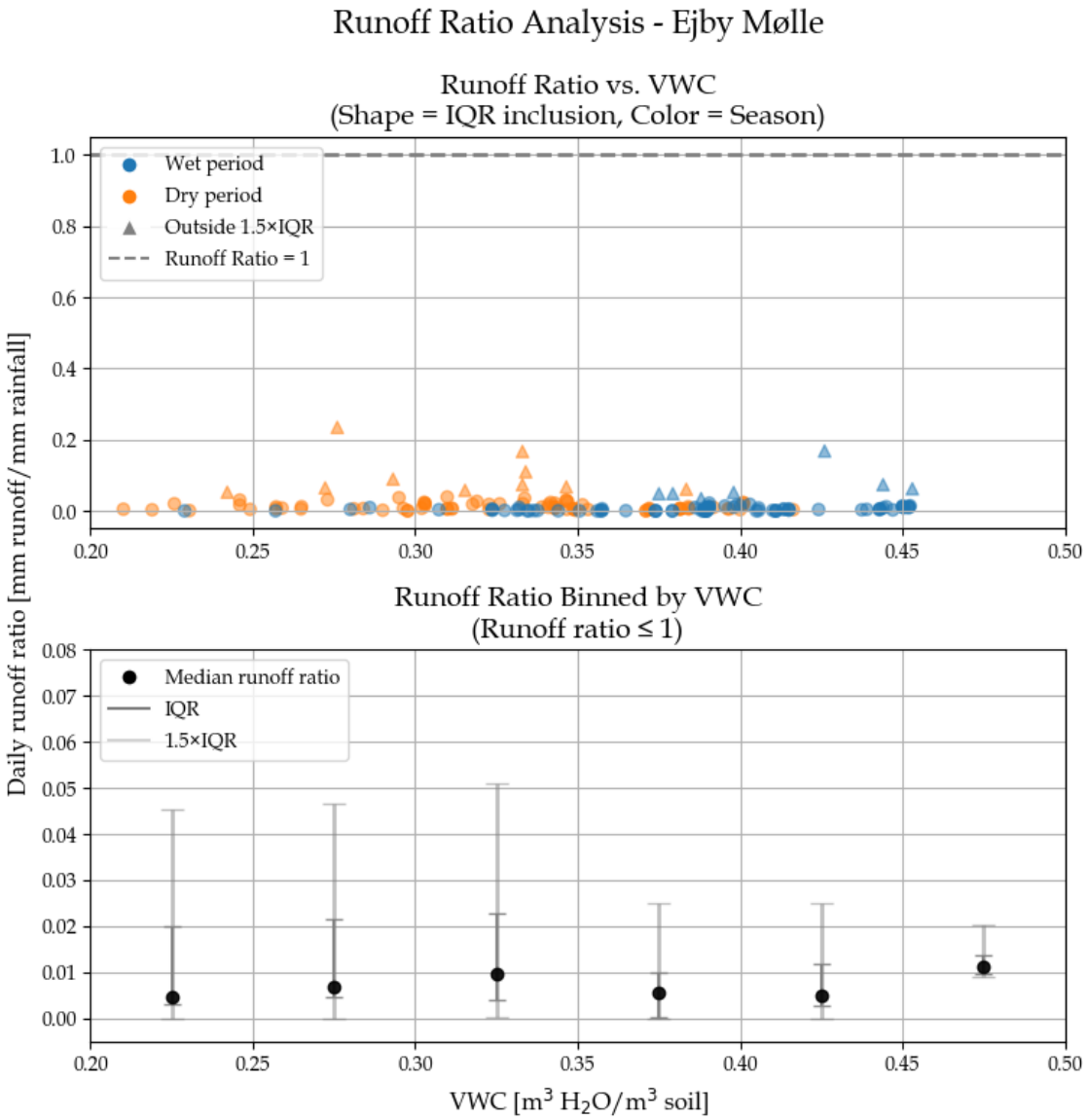

Figure 6.4. Ratio between the runoff and rainfall at different VWC levels for Ejby Mølle, Odense. Data points are coloured by wet (blue) and dry (orange) periods, and their shapes indicate whether they lie within or outside 1.5×IQR. Data points with a runoff ratio larger than 1 are removed from the lower plot. The median runoff ratio, the IQR and the 1.5×IQR for each of the intervals are shown.

To examine whether a more general monotonic relationship exists between runoff and VWC, alongside rain, and change in VWC, a Spearman's correlation analysis is performed for the area, and visualised in Table 6.1.

Table 6.1. Spearman's correlation (ρ) for Ejby Mølle, Odense ($\alpha_{adjusted} = 0.0166$).

	Rain [mm]	**VWC** [m^3 H_2O/m^3 soil]	**ΔVWC** [m^3 H_2O/m^3 soil]
ρ	0.351	0.110	0.223
p-value	$2.897 \cdot 10^{-6}$	$1.54 \cdot 10^{-1}$	$3.53 \cdot 10^{-3}$

The Spearman correlation analysis shows a significant monotonic relationship between rain and runoff, suggesting that higher rainfall generally leads to increased runoff. This aligns with expectations, as precipitation is the primary driver of surface runoff. Moreover, a significant monotonic relationship between change in VWC and runoff is evident, indicating that changes in VWC influence variations in runoff, likely due to the soil's infiltration capacity. However, no significant correlation is found between runoff and VWC.

Main Findings
The runoff analysis and the corresponding statistical evaluation of parameters affecting runoff at Ejby Mølle overall indicate that runoff from the lawn is limited, as a maximum runoff of 0.25 mm is observed, suggesting that infiltration is quite high. Generally, the runoff analysis implies that VWC alone does not exert a strong influence on the runoff ratio, while rainfall and change in VWC remain the key determinants of runoff at the site. However, the limited number of data points recorded in this project location introduces uncertainties, making it challenging to fully assess the impact of runoff.

6.2 Elmelundsvej

As described in section 4.1, the catchment area consists of a lawn on a small hill with a line drainage at the bottom. For the runoff analysis VWC data from Sensor 3 is used.

To understand the relationship between VWC and runoff at Elmelundsvej, rainfall events with the highest daily accumulated rainfall and runoff are selected (cf. Appendix H, Figure H.8) and analysed in Figure 6.5.
From the top three plots, it is evident that VWC generally increases in response to rainfall. The first event, on 26-09-2024, which exhibits the highest recorded rainfall (39.56 mm), results in no measurable runoff (0.00 mm). The rainfall consists of two distinct phases: the first during the initial seven hours and the second phase during the last six hours. In the first phase, a VWC increase from approximately 0.23 to 0.30 m^3/m^3 is observed after approximately two hours, while the second phase results in a similar increase from approximately 0.26 to 0.30 m^3/m^3. The lack of runoff may be due to a combination of high infiltration capacity, limitations from the resample period method and the measurement technology.
The second event, on 25-08-2023, displays the second-highest daily rainfall (35.40) with a corresponding runoff of 0.57 mm (1.6% of the rainfall becomes runoff). The event consists of three rainfall phases. A VWC increase and subsequent runoff response are observed one and two hours, respectively, after the second phase (characterised by high-intensity rainfall), with VWC increasing from 0.12 to 0.25 m^3/m^3 and runoff peaking at 0.36 mm/hr. During a pause in rainfall, both VWC and runoff decrease before increasing again during the third phase. This event illustrates that no runoff is observed at low VWC.

The lower two plots at Figure 6.5, present the two events with the highest daily runoff. It is evident that significant runoff is generally generated when VWC is elevated. The event on 31-07-2023 exhibits the highest recorded runoff (1.09 mm) and a rainfall of 22.20 mm (4.9% of the rainfall becomes runoff). The event consists of three rainfall phases, whereas the first phase results in a VWC increase from 0.17 to 0.26 m^3/m^3, with a simultaneous runoff response peaking at approximately 0.12 mm/hr. No clear delay is observed between the VWC increase and the runoff onset, while a two-hour delay occurs between peak rainfall and peak runoff. During the lower-intensity second and third rainfall phases, only minimal VWC increases are observed, yet a notable runoff response occurs, with peak values of approximately 0.13 mm/hr and 0.10 mm/hr, respectively, and a delay of three hours. These findings align with the *cross-correlation analysis* for Elmelundsvej (cf. section 5.1, Figure E.2). The variation in runoff delay likely reflects differences in rainfall intensity.
The event on 01-08-2023 shows the second-largest runoff (0.92 mm) and a rainfall of 6.20 mm (14.8% becomes runoff). During this event, VWC remains relatively constant around 0.22 m^3/m^3. Rainfall occurs during the first five hours and again 10 hours after the event starts. A larger runoff response is observed during the first phase, which exhibits lower-intensity but continuous rainfall. In contrast, the second phase, characterised by more intense and short-duration rainfall, results in a smaller runoff response.

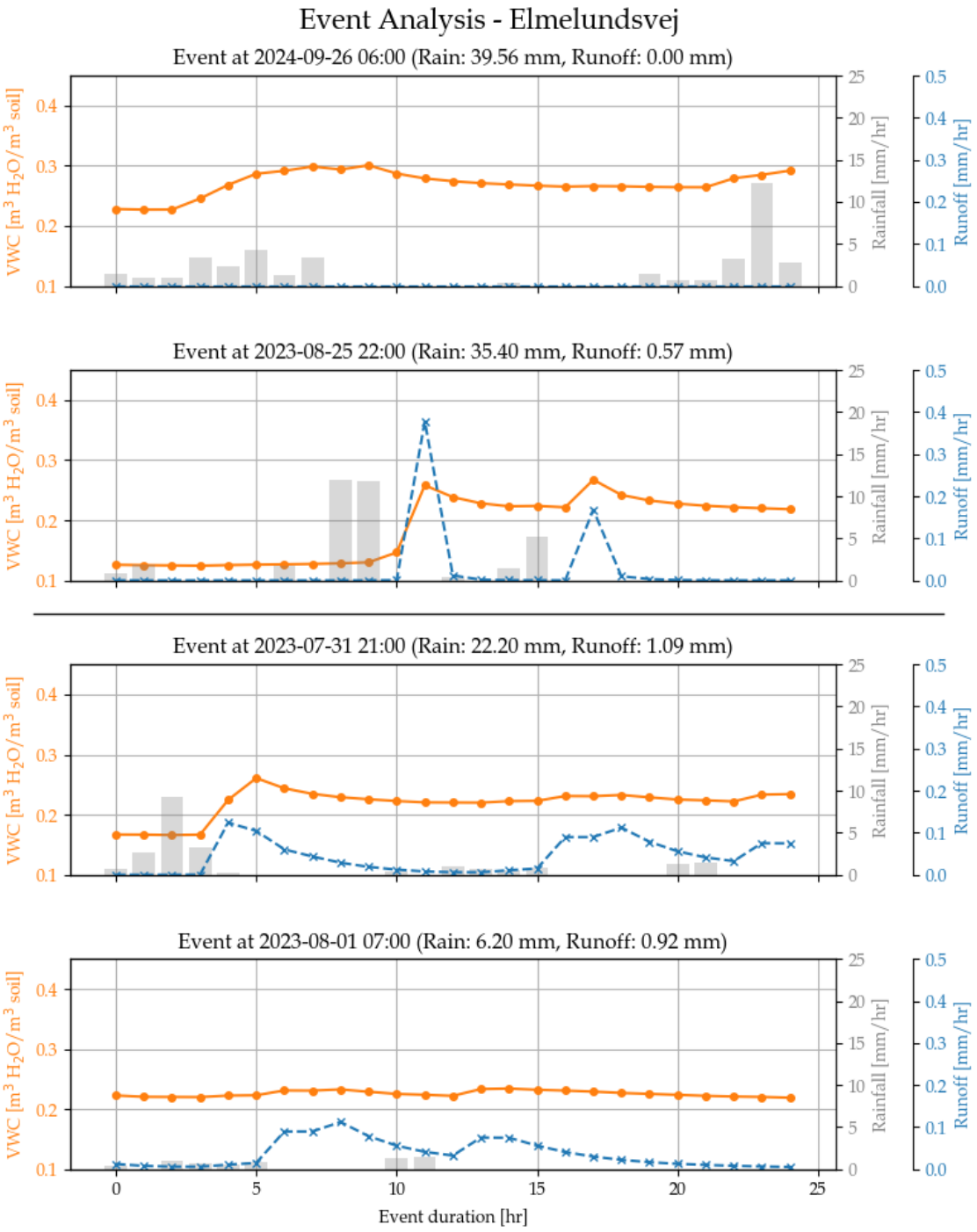

Figure 6.5. Analysis of VWC and runoff response to rainfall for selected events at Elmelundsvej, Odense.

When comparing the two events with the highest rainfall and the highest runoff at Elmelundsvej, it becomes evident that the response time of runoff depends on both the VWC and rainfall intensity. Generally, a delay of approximately three hours between rainfall and runoff is observed across the events. Thus, large runoff does not necessarily occur during the most intense rainfall events but depends more strongly on the VWC conditions. This is evident in three out of the four highlighted events, whereas the event

on 26-09-2024 deviates from this trend. However, since all four events occur during the dry period, it is possible that the runoff behaviour may differ under wet period conditions. Therefore, it is necessary to further examine the relationship between daily rainfall, daily runoff, and daily VWC at Elmelundsvej, as visualised in Figure 6.6. The analysis is conducted for each of the defined high, mid, and low VWC classifications (presented in Appendix H, Figure H.2), and is further subdivided into three subcategories within the high, mid, and low VWC.

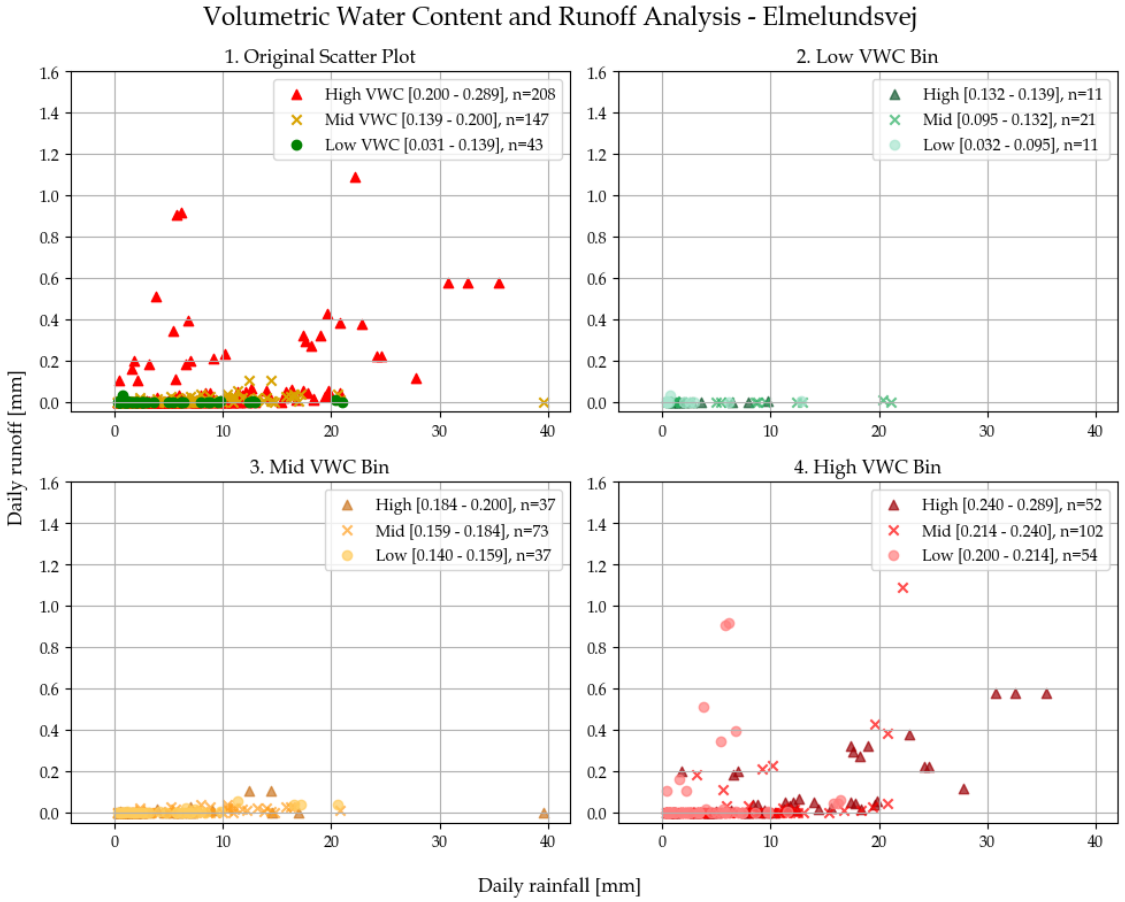

Figure 6.6. The *VWC and runoff analysis* for Elmelundsvej, Odense consisting of (1) total runoff/rainfall coloured by VWC, (2) runoff/rainfall in the low bin divided into three sub intervals, (3) runoff/rainfall in the mid bin divided into three sub intervals, and (4) runoff/rainfall in the high bin divided into three sub intervals.

As shown in Figure 6.6, the runoff at Elmelundsvej generally exhibits a low response to rainfall with daily runoff values between 0.00-1.10 mm. This is particularly evident at the low and mid VWC categories (cf. subplots "2. Low VWC Bin" and "3. Mid VWC Bin"), which show a narrow distribution of runoff values, approximately ranging from 0.00 to 0.05 mm and 0.00 to 0.10 mm, respectively. A slight increasing trend in runoff is observed with rising daily rainfall in the mid category.

The high VWC category exhibits a wide spread in runoff, ranging from 0.00 to 1.10 mm, with the largest generated runoff observed at a daily rainfall of approximately 22 mm. It is evident that the largest rainfall events do not align with the largest amount of runoff, as observed in the *event analysis* for Elmelundsvej. Moreover, it is evident that runoff events

primarily can occur when VWC exceeds 0.20 m^3/m^3.

Consequently, Figure 6.6 suggests that a higher VWC may lead to larger runoff volumes; however, it also indicates that infiltration in this area is generally quite high. Therefore, it is necessary to examine the runoff data in more detail by identifying their seasonal grouping, rainfall intensity, and the change in VWC during the rainfall event. This is explored in Figure 6.7.

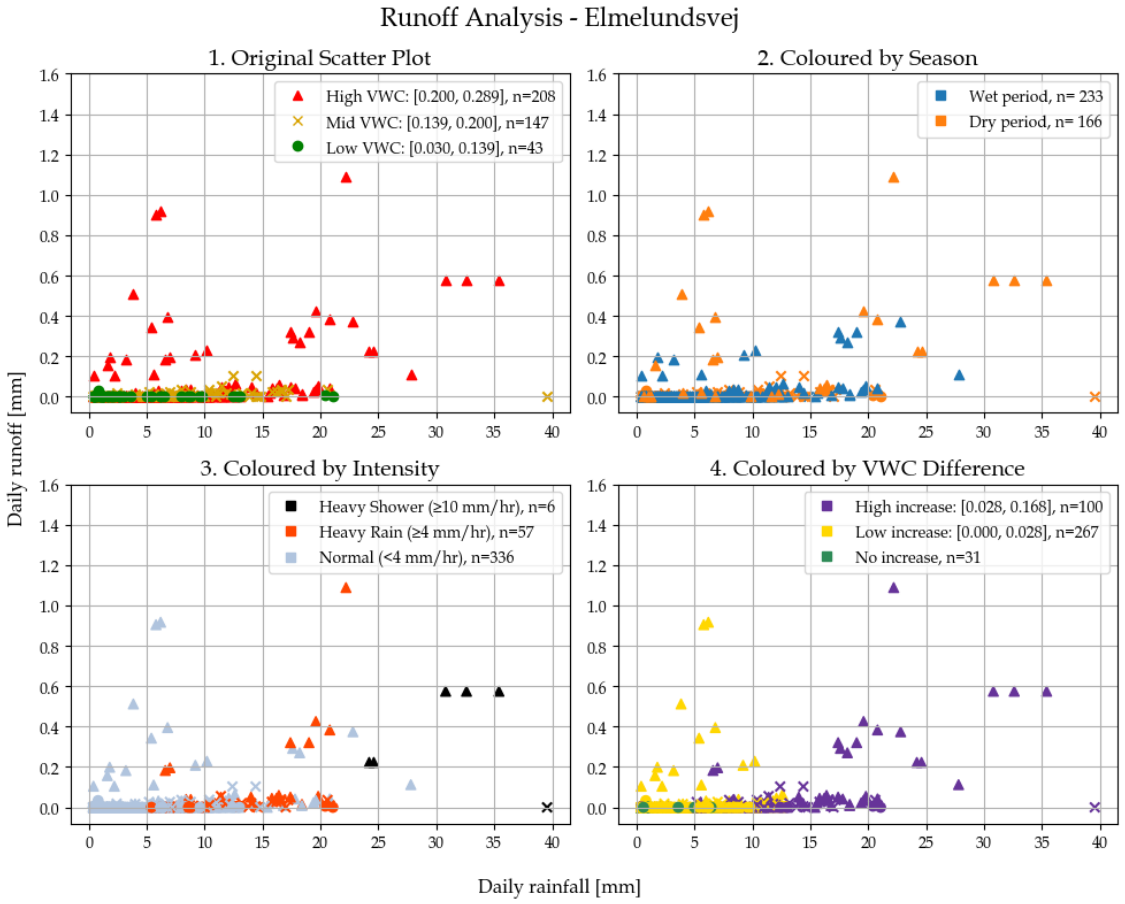

Figure 6.7. The runoff analysis for Elmelundsvej, Odense, consisting of runoff/rainfall coloured by (1) VWC, (2) wet/dry period, (3) rainfall intensity, and (4) change in VWC during the rainfall event.

Figure 6.7 shows that most data points fall within the wet period, as illustrated in subplot "2. Coloured by Season". The majority of rainfall events are classified as normal intensity, some categorised as heavy rain, and only six as heavy showers (cf. subplot "3. Coloured by Intensity"). Notably, the highest runoff amounts are generally generated during normal-intensity events, where the change in VWC is low, as illustrated by Subplot "4. Coloured by VWC Difference". This suggests that a portion of the rainwater is converted directly into runoff. In contrast, data points with high daily rainfall are mainly classified as either heavy rain or heavy showers, yet they generally generate relatively low runoff (except one data point with a maximum of 1.10 mm). This is likely due to the substantial increase in VWC, as illustrated by subplot 4. During one of the heavy shower events (first event on 26-09-2024 highlighted in the *event analysis*), the daily rainfall reached approximately

40 mm; however, no runoff was generated, while the change in VWC is marked as a high increase. Contrarily, the largest runoff generation is observed during a heavy rain event, where the change in VWC is likewise marked as a high increase.
Generally, subplot 4 shows a clear relationship between daily runoff and change in VWC. When no or only a slight increase in VWC is observed, the trend appears relatively steep, indicating that even a small increase in daily rainfall results in an immediate runoff response. In contrast, the data points with a high VWC increase display a more gradual slope, suggesting that a larger portion of the rainfall infiltrates the soil, thereby reducing runoff generation. Furthermore, most data points within the wet period are classified as high VWC (see Appendix H, Figure H.14 for a more detailed overview of the wet/dry periodical segregation of the runoff-rainfall relationship coloured by VWC) and exhibit little to no increase in VWC during rainfall events.
Moreover, it is evident that despite a general daily rainfall amounting to approximately 20 mm, runoff generation remains minimal (0.00-0.10 mm) for most of the events.

The observed differences in runoff variability align with the Kruskal-Wallis test ($p = 5.00 \cdot 10^{-4}$), where a statistically significant difference among the medians of the three VWC groups at Elmelundsvej is found. This is also evident from the boxplot presented in Appendix I, section I.2. A Dunn's test is performed (cf. Appendix I, Table I.1) to identify which specific medians differ ($\alpha_{adjusted}$=0.0166). A significant difference can be determined between both the high VWC group and the low VWC groups ($p = 1.52 \cdot 10^{-4}$) and the mid VWC group and the low VWC groups ($p = 1.26 \cdot 10^{-2}$), whereas no significant difference is found between the high and mid ($p = 6.97 \cdot 10^{-2}$) VWC groups.

To further examine the rainfall-generated runoff, a *runoff ratio analysis* is performed and presented in Figure 6.8. From the upper plot, it is evident that most data points cluster near a runoff ratio of zero, indicating that infiltration generally dominates the runoff generation at Elmelundsvej.
In the lower plot, the runoff ratio is divided into six VWC bins. The median runoff ratio is below 0.005 mm/mm in all of the six bins, with the widest range observed at a VWC of 0.25-0.30, where the upper IQR reaches approximately 0.018 mm/mm. It is evident that when VWC is below 0.25 m^3/m^3, infiltration dominates. Thus, a difference in runoff ratio is visible between Bin 6 and the remaining bins.
A Kruskal–Wallis test ($p = 2.68 \cdot 10^{-10}$) reveals a statistically significant difference among their medians. To identify which specific medians differ, a Dunn's test is performed, indicating a statistically significant difference between the medians of Bin 6 and the remaining five bins. A visualisation of these results is presented in Appendix I, Figure I.14.

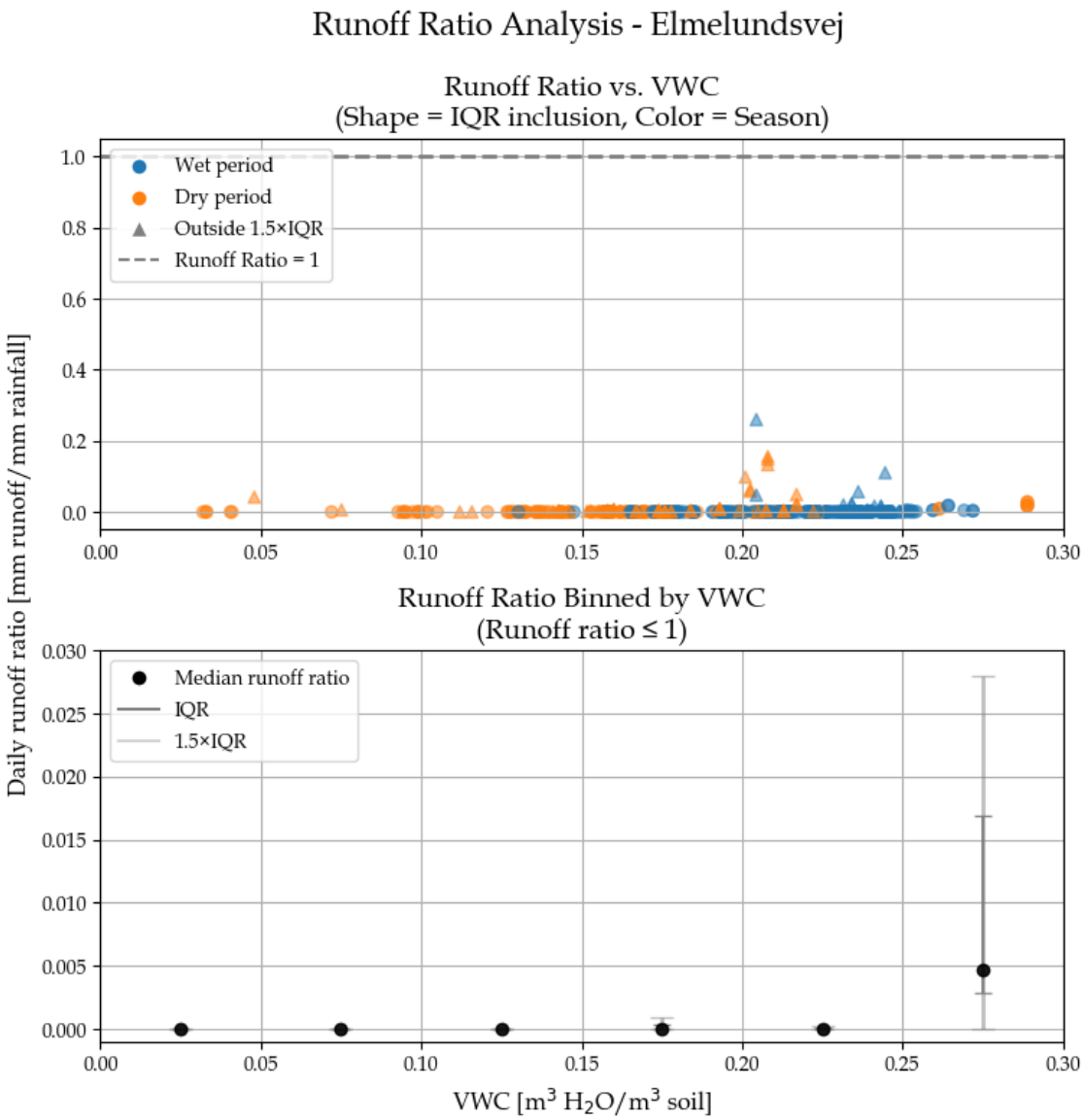

Figure 6.8. Ratio between the runoff and rainfall at different VWC levels for Elmelundsvej, Odense. Data points are coloured by wet (blue) and dry (orange) periods, and their shapes indicate whether they lie within or outside 1.5×IQR. Data points with a runoff ratio larger than 1 are removed from the lower plot. The median runoff ratio, the IQR and the 1.5×IQR for each of the intervals are shown.

When comparing predefined VWC bins, an overall effect of VWC on runoff ratio is visual. However, as the Kruskal–Wallis test and Dunn's test only assess differences among discrete groups, it does not capture broader monotonic trends in the data. Thus, to examine whether a more general monotonic relationship exists between runoff and VWC, alongside rain, and change in VWC, a Spearman's correlation analysis is performed for the area, and visualised in Table 6.2.

Table 6.2. Spearman's correlation (ρ) for Elmelundsvej, Odense ($\alpha_{adjusted} = 0.0166$).

	Rain [mm]	**VWC** [m^3 H_2O/m^3 soil]	**ΔVWC** [m^3 H_2O/m^3 soil]
ρ	0.595	0.251	0.485
p-value	$2.35 \cdot 10^{-38}$	$5.796 \cdot 10^{-7}$	$3.18 \cdot 10^{-24}$

The Spearman's correlation analysis shows a significant monotonic relationship between rain and runoff, suggesting that higher rainfall generally leads to increased runoff. This aligns with expectations, as precipitation is the primary driver of surface runoff. Moreover, a significant monotonic relationship between both VWC and runoff and the change in VWC and runoff is evident. However, as the Spearman correlation coefficient is higher for change in VWC compared to the one for absolute VWC, the initial VWC affects runoff more than the absolute VWC.

Main Findings

The runoff analysis and corresponding statistical evaluation of runoff at Elmelundsvej overall indicate that runoff from the lawn is limited. This finding implies that, within the observed range of soil moisture, VWC alone does not exert a strong influence on the runoff ratio, while rainfall and change in VWC remain the key determinants of runoff at the site.

A comparison between the *VWC and runoff analysis* and the *runoff ratio analysis* reveals a discrepancy in the threshold of runoff generation. In the *VWC and runoff analysis*, runoff appears to occur at a VWC threshold of 0.20 m^3/m^3, while the *runoff ratio analysis* suggests a slightly higher threshold of 0.25 m^3/m^3. This difference is due to several data points in the *runoff ratio analysis* being excluded as outliers (i.e., exceeding 1.5 times the interquartile range). When these outliers are included, as shown in the upper plot in the *runoff ratio analysis*, the threshold aligns with the 0.20 m^3/m^3 value observed in the *VWC and runoff analysis*.

It is important to note that, during the measurement period, VandCenter Syd changed the land use of the project area from a low-cut lawn to a lawn managed under the principle *deliberately wild*. Consequently, uncertainties in the runoff variations are present, as these variations reflect not only rainfall responses but also the effects of land use change. This complicates the full assessment of the runoff impact in this area.

6.3 Lystrup

As described in section 4.1, the catchment area consists of a sloped lawn with a line drainage system at the bottom. For the runoff analysis, VWC data from Sensor 3 is used.

To understand the relationship between VWC and runoff in Lystrup, rainfall events with the highest daily accumulated rainfall and runoff are selected (cf. Appendix H, Figure H.9) and analysed in Figure 6.9.
From the top two plots, it is evident that VWC generally increases in response to rainfall. The first event, on 02-10-2023, exhibits the highest recorded rainfall (62.00 mm) and a corresponding runoff of 2.93 mm (equivalent to 4.7% of rainfall becoming runoff). Rainfall occurs during the first 12 hours (with a peak of ≈23 mm/hr), resulting in a VWC increase from approximately 0.24 to 0.39 m^3/m^3 during this period. The VWC increase is observed approximately eight hours into the event, while the runoff response is recorded 10 hours after event start, when VWC reaches approximately 0.30 m^3/m^3. The runoff pattern mirrors the rainfall distribution, but with a delay of approximately six hours, which corresponds to the delay found in the *cross-correlation analysis* (cf. Appendix E, Figure E.3).
The second event, on 24-10-2023, displays the second-highest daily rainfall (39.20 mm) and a runoff of 3.89 mm (9.9% of rainfall becomes runoff). Rainfall is observed during the first 16 hours, with peak intensities of 5 mm/hr. A VWC response is observed seven hours into the event, increasing from 0.28 to 0.37 m^3/m^3. Runoff occurs 10 hours into the event, at a VWC of 0.30 m^3/m^3, reaching a peak runoff rate of 0.5 mm/hr. The runoff continues beyond the event duration, meaning the full runoff response is not captured due to the resampling period method, leading to an underestimation of the total runoff.
The lower two plots, showing the two events with the highest runoff volumes, illustrate generally elevated and constant VWC levels. The event on 21-01-2024, which exhibits the highest recorded runoff (8.79 mm), shows that the rainfall (9.20 mm) occurs during the first six hours (95.5% of the rainfall becomes runoff), which causes an immediate runoff response from 0.2 mm/hr to 1.0 mm/hr. The lack of delay is likely due to the consistently high VWC of 0.38 m^3/m^3 throughout the event. Furthermore, runoff is occurring at event start, possibly representing tail flow from a prior rainfall event. Additionally, the runoff tail is cut off at the end of the event, meaning that the runoff response of the event could be underestimated.

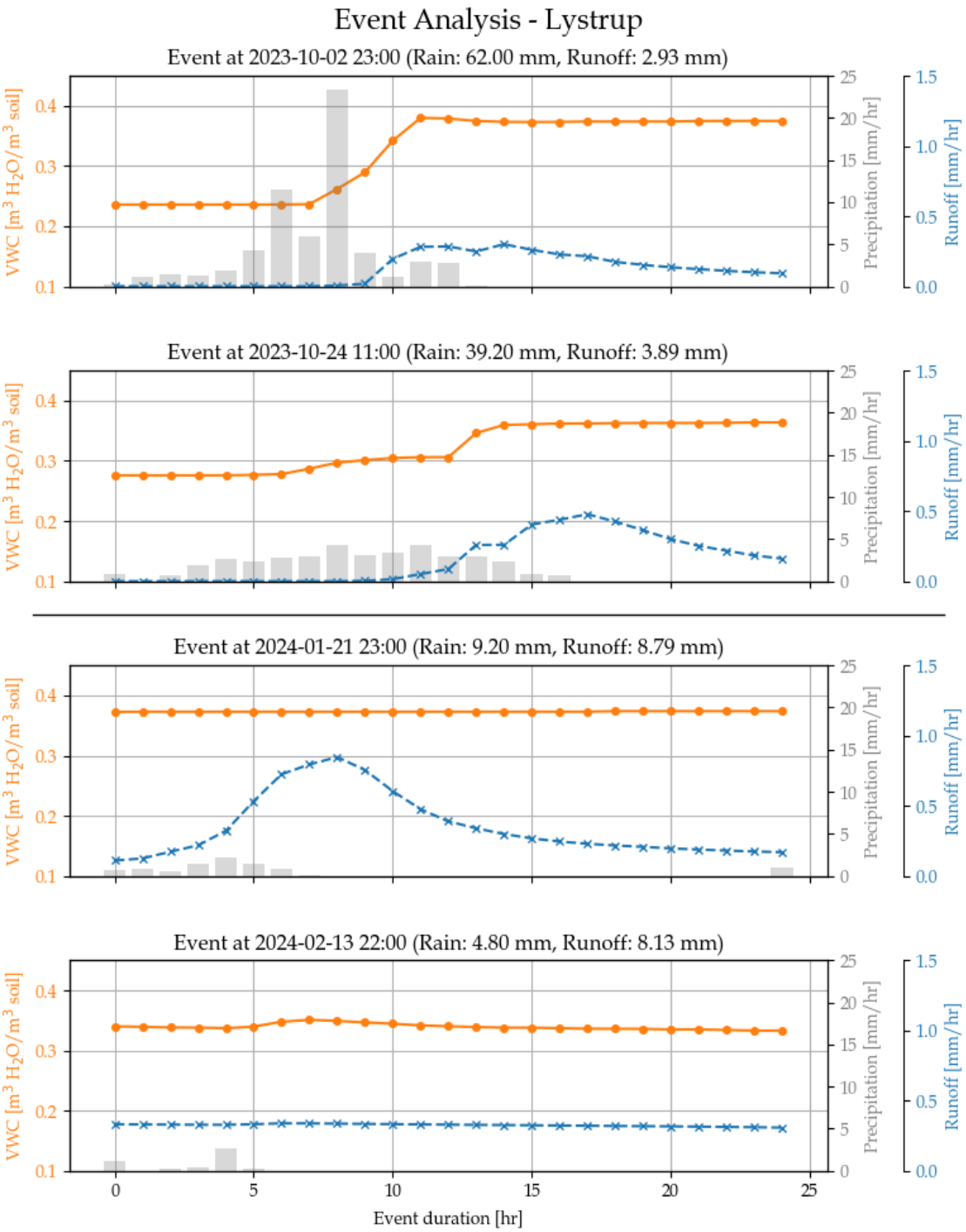

Figure 6.9. Analysis of VWC and runoff response to rainfall for selected events in Lystrup

The event on 13-02-2024 shows the second-highest runoff (8.13 mm) with an associated rainfall of 4.80 mm, yielding an extreme runoff ratio of 169.4%. During this event, both VWC and runoff remain fairly constant at around 0.35 m^3/m^3 and 0.30 mm, respectively. This suggests that runoff is already onset prior to the event, which is likely due to snow accumulated during previous events, contributing to the high runoff volumes or measurement inaccuracy.

When comparing the two events with the highest rainfall and runoff in Lystrup, it becomes clear that large runoff volumes do not necessarily result from the largest rainfall events, but rather appear to depend heavily on VWC levels. This suggests that when VWC is already high, even moderate rainfall can generate significant runoff with minimal delay. Therefore, it is necessary to further examine the relationship between daily rainfall, daily runoff, and VWC for Lystrup, as visualised in Figure 6.10. The analysis is conducted using the defined high, mid, and low VWC classifications (presented in Appendix H, Figure H.3), and is further subdivided into three subcategories within the high, mid, and low VWC.

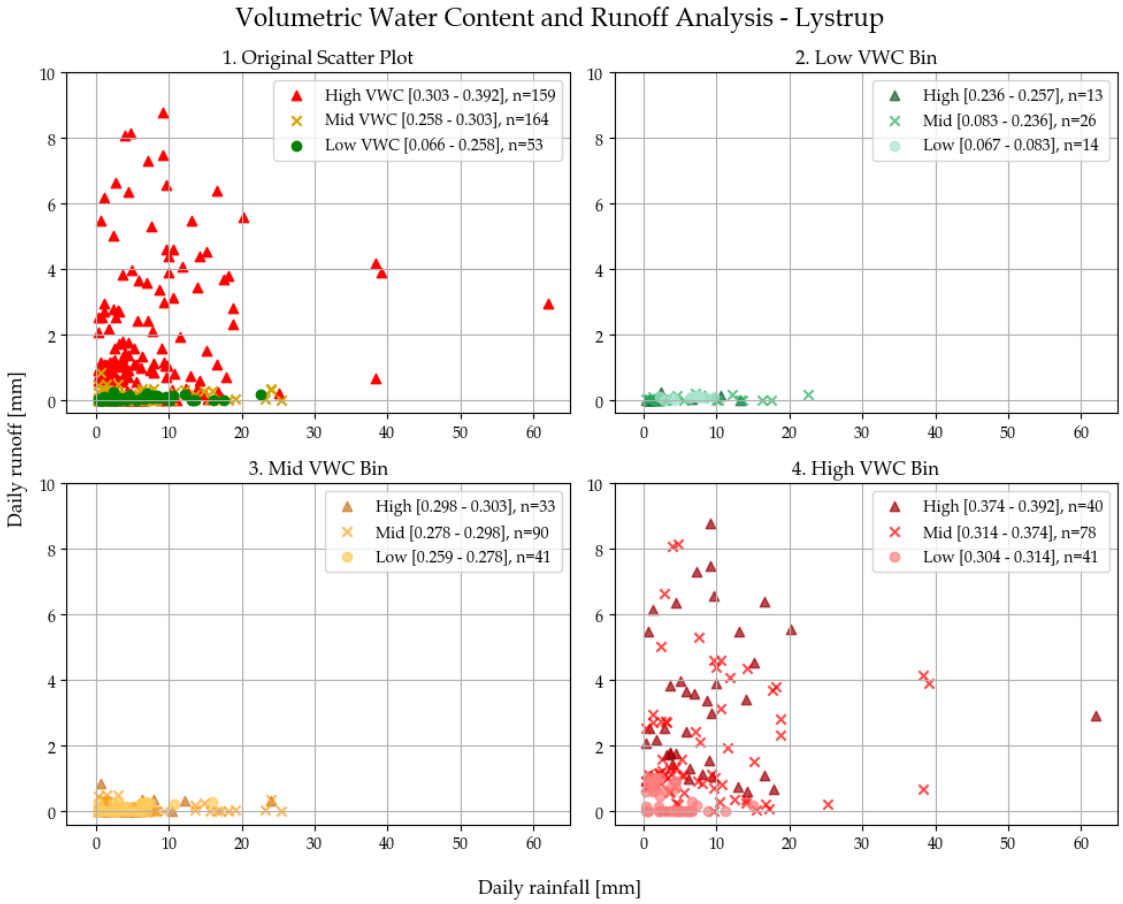

Figure 6.10. The *VWC and runoff analysis* for Lystrup consisting of (1) total runoff/rainfall coloured by VWC, (2) runoff/rainfall in the low bin divided into three sub intervals, (3) runoff/rainfall in the mid bin divided into three sub intervals, and (4) runoff/rainfall in the high bin divided into three sub intervals.

As shown in Figure 6.10, runoff in Lystrup generally exhibit a high response to VWC, with daily runoff values ranging from 0.00 to 9.00 mm. This is particularly evident in the high VWC category (cf. subplot "4. High VWC Bin"), which displays a broad distribution of runoff values (0.00-9.00 mm). Within its three sub-groups, a clear trend is visible; the high subcategory shows that runoff >1 mm occurs when VWC exceed 0.314 m^3/m^3. Notably, in the high subcategory, one data point exhibits relatively low runoff responses (approximately 3 mm) despite a high rainfall event (60 mm).
In contrast, the low and mid VWC categories (Subplot "2. low VWC Bin" and "3. Mid VWC Bin") exhibit a much narrower range of runoff values, from 0.00 to approximately

0.50 mm in the low bin and 0.00 to approximately 1.00 mm in the mid bin. Neither of these groups shows a clear increasing trend as rainfall increases.

Consequently, Figure 6.10 suggests that infiltration in Lystrup remains generally high under low and mid VWC conditions, whereas runoff primarily occurs when the soil has a high VWC. The runoff data are further analysed in terms of seasonal grouping, rainfall intensity, and the change in VWC during the rainfall event, as shown in Figure 6.11.

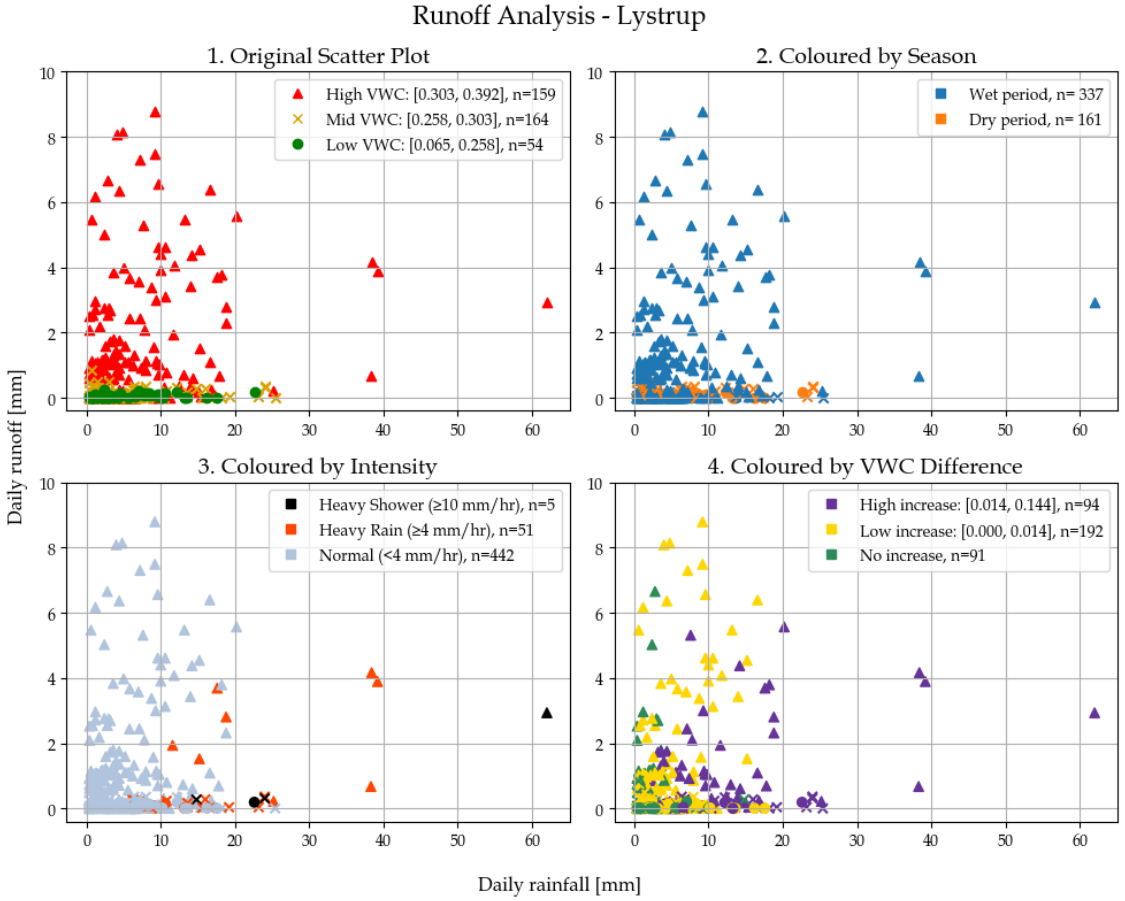

Figure 6.11. The runoff analysis for Lystrup consisting of runoff/rainfall coloured by (1) VWC, (2) wet/dry period, (3) rainfall intensity, and (4) change in VWC during the rainfall event.

Figure 6.11 shows that most data points fall within the wet period, where the soil generally exhibits high VWC levels, as illustrated in subplots "1. Original Scatter Plot" and "2. Coloured by Season" (see section H.3, Figure H.15 for a more detailed overview of the wet/dry periodical segregation of the runoff-rainfall relationship coloured by VWC). Moreover, it is evident that significant runoff is only generated during the wet period. The majority of rainfall events are classified as normal intensity, some as heavy rain, and only five as heavy showers (cf. subplot "3. Coloured by Intensity"). Notably, the highest runoff amounts occur during normal-intensity events, where mainly no or low increase in VWC occurs, as illustrated by subplot "4. Coloured by VWC Difference". This suggests that a portion of the rainwater is converted directly into runoff. In contrast, data points with daily rainfall >20 mm are mainly classified as either heavy rain or heavy showers, yet they generate relatively low runoff (maximum 4 mm). This is likely due to the substantial

increase in VWC, where a large part of the rainwater infiltrates into the soil, explaining the lower runoff compared to events with lower rainfall intensities. Furthermore, it is possible that the low runoff response may be a result of the method used for the resample period, which may cause some of the slow runoff of an event to be neglected. This can explain the aforementioned heavy shower event, where daily rainfall reached approximately 60 mm, yet only generated 3 mm of runoff.
Generally, subplot 4 shows a relatively clear relationship between daily runoff and change in VWC. When no or only a slight increase in VWC is observed, the trend appears relatively steep, indicating that even a small increase in daily rainfall results in an immediate runoff response. In contrast, the data points with a high VWC increase display a more gradual slope, suggesting that a large portion of the rainfall is absorbed by the soil, thereby reducing runoff generation.

The observed differences in runoff responses are supported by a Kruskal-Wallis test ($p = 6.17 \cdot 10^{-39}$), which indicates a significant difference among the medians of the three VWC groups. This is also evident from the boxplot presented in Appendix I, section I.2. A Dunn's test is performed (cf. Appendix I, Table I.2) to identify which specific medians differ ($\alpha_{adjusted}$=0.0166). A significant difference can be determined between the high VWC group and both the mid ($p = 6.68 \cdot 10^{-38}$) and low ($p = 2.57 \cdot 10^{-14}$) VWC groups, whereas no significant difference is found between the mid and low ($p = 0.14$) VWC groups. To further examine the rainfall-generated runoff, a *runoff ratio analysis* is performed and presented in Figure 6.12.

The upper plot visualises the distribution of the runoff ratio as a function of VWC, coloured by wet and dry periods. Most data points during the dry period cluster near a runoff ratio of zero, indicating that infiltration dominates runoff generation in Lystrup under dry conditions. In contrast, the wet period displays a broader range, reaching up to approximately 9.00 mm runoff/mm rainfall. However, as explained in chapter 5, all runoff ratio values above 1.00 are removed from the *runoff ratio analysis*.
In the lower plot, the runoff ratio is grouped into six VWC bins. The median runoff ratio is approximately 0.00 mm/mm in five of the six bins, with minimal variation in four of them. This indicates high infiltration and minimal runoff when VWC is below 0.30 m^3/m^3. However, when VWC exceeds this threshold, the runoff ratio increases significantly. The widest spread is observed in the wet period at a VWC of 0.35-0.40 m^3/m^3, where the upper whisker approaches 1.00 mm/mm, suggesting that under near-saturated conditions, nearly all rainfall can become runoff.
Thus, the *runoff ratio analysis* suggests that the soil in Lystrup generally exhibits high infiltration capacity, but when VWC exceed 0.30 m^3/m^3, runoff generation increases drastically.

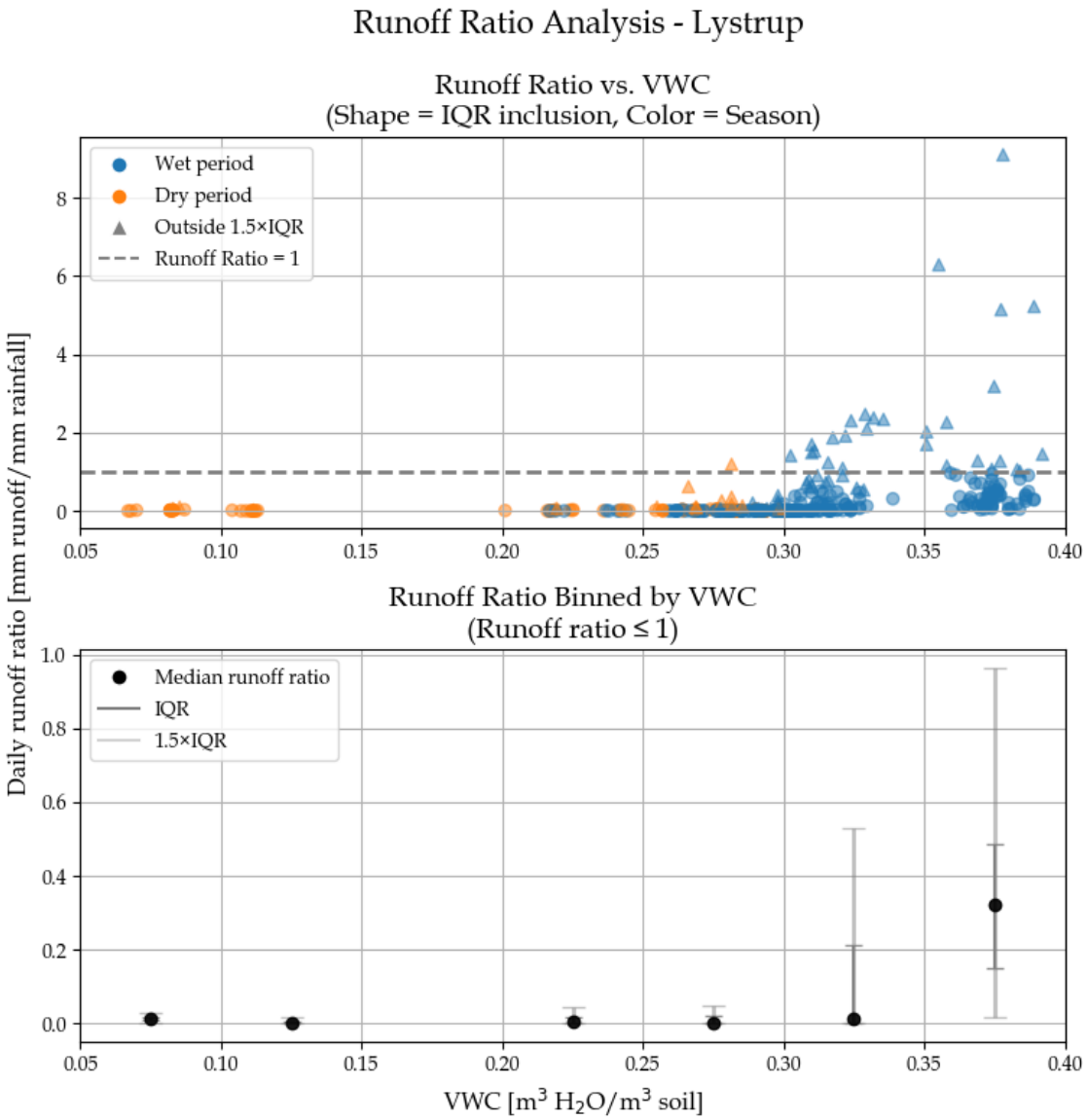

Figure 6.12. Ratio between the runoff and rainfall at different VWC levels for Lystrup. Data points are coloured by wet (blue) and dry (orange) periods, and their shapes indicate whether they lie within or outside 1.5×IQR. Data points with a runoff ratio larger than 1 are removed from the lower plot. The median runoff ratio, the IQR and the 1.5×IQR for each of the intervals are shown.

The differences among the bins are supported by a Kruskal–Wallis test ($p = 3.40 \cdot 10^{-26}$), which reveals a statistically significant difference among their medians. To identify which specific medians differ, a Dunn's test is performed and presented in Appendix I, Figure I.15. The Dunn's test reveals that the median value of Bin 6 differs significantly from those of Bin 1, 2, 3, 4, and 5, while Bin 5 also differs from Bin 4. Consequently, when comparing predefined VWC bins, an overall effect of VWC on runoff ratio appears. However, as the Dunn's test only assesses differences among discrete groups, it does not capture broader monotonic trends in the data. Thus, to examine whether a more general monotonic relationship exists between runoff and VWC, alongside rain, and change in VWC, a Spearman's correlation analysis is performed for the area, and visualised in Table 6.3.

Table 6.3. Spearman's correlation for Lystrup ($\alpha_{adjusted} = 0.0166$).

	Rain [mm]	**VWC** [m^3 H_2O/m^3 soil]	**ΔVWC** [m^3 H_2O/m^3 soil]
ρ	0.226	0.671	0.110
p-value	$9.14 \cdot 10^{-6}$	$1.11 \cdot 10^{-50}$	$3.32 \cdot 10^{-2}$

The Spearman's correlation analysis shows a statistically significant monotonic relationship between rain and runoff, suggesting that higher rainfall generally leads to increased runoff. This aligns with expectations, as precipitation is the primary driver of surface runoff. Moreover, a statistically significant monotonic relationship between runoff and VWC is evident, while no statistically significant monotonic relationship between change in VWC and runoff is observed.

Main Findings
Thus, the runoff analysis and corresponding statistical evaluation for Lystrup overall indicate that the key factor affecting runoff from the lawn is VWC. However, the runoff is also influenced by rainfall. It is clear that runoff >1 mm occurs when the VWC exceeds 0.31 m^3/m^3.
Moreover, as shown in Figure 6.12, multiple runoff ratio values exceed 1, meaning that the volume of runoff entering the drainage system is greater than the recorded rainfall during the given event. Notably, all runoff ratio values above 1 occur during the wet period, suggesting that snowmelt could be contributing to this trend. However, this could also be an effect of subsurface interflow in the topsoil, causing a delay in runoff, meaning that runoff from prior events may be registered in the following events. Additionally, it is possible that the contributing catchment area is larger in reality than estimated in section 4.1.

6.4 Comparison of the Three Hillslope-scale Project Locations

To get a better understanding of contingent runoff from green areas and to what extent location-specific conditions affect the runoff response mechanisms, and thereby the potential for surface runoff, the interplay variations between VWC, precipitation and runoff across the three hillslope scales are examined. This is done by discussing the results of the runoff analysis' for the three areas (Ejby Mølle, Elmelundsvej, and Lystrup), focusing on similarities and differences in the observed runoff dynamics.

Firstly, a comparison of the runoff-rainfall relationship is presented in Figure 6.13. A clear difference in rainfall-generated runoff at the three hillslope-scale areas is evident. The runoff generation at Lystrup is notably the largest (maximum of 9.00 mm), while the smallest (with a maximum of 0.25 mm) is observed at Ejby Mølle, at which both the

highest VWC level of 0.45 m^3/m^3 and the smallest variations in runoff ratio at high VWC are also observed.

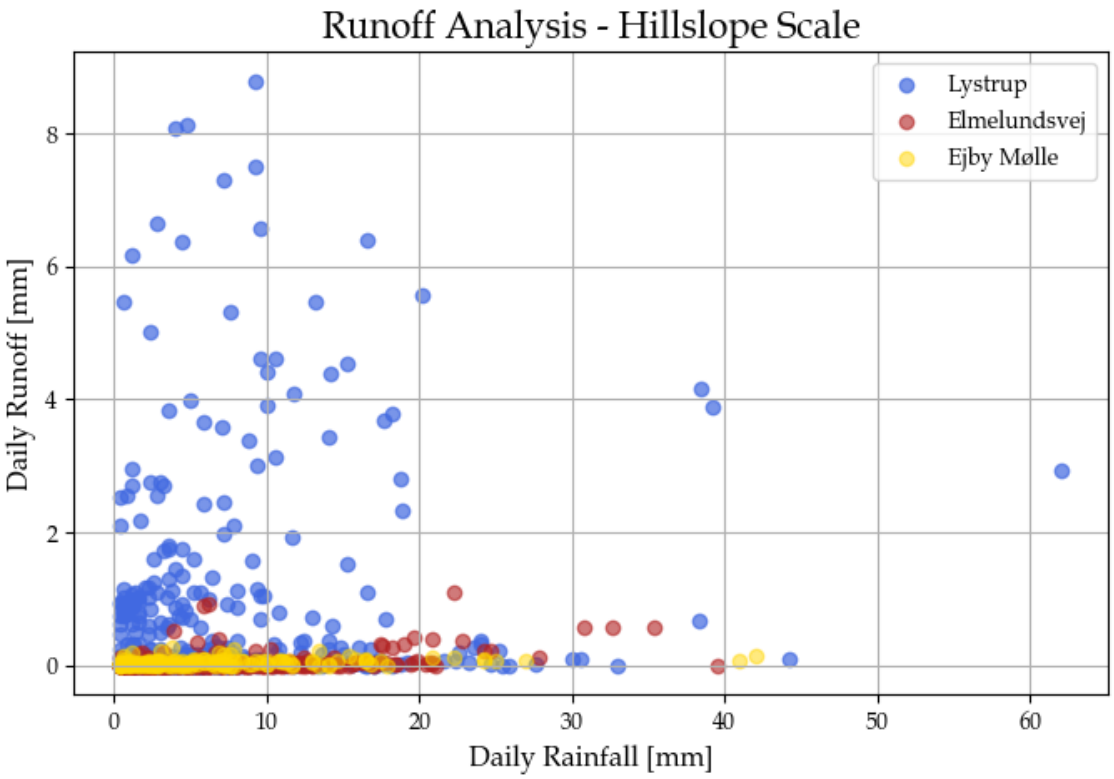

Figure 6.13. Comparison of the daily runoff and daily rainfall for the three Hillslope scales.

In contrast, the highest VWC level in Lystrup is 0.39 m^3/m^3, and 0.29 m^3/m^3 at Elmelundsvej. Furthermore, at Elmelundsvej, a threshold for significant runoff generation is found when VWC exceed 0.20 m^3/m^3, while Lystrup exhibit similar, however, more distinct patterns, as a threshold for significant runoff generation is found when VWC exceed 0.30 m^3/m^3. Additionally, according to *Nielsen, 2019*, the VWC threshold of runoff generation in Lystrup is found to be 0.34 m^3/m^3 [Nielsen, 2019]. The small difference can be explained by the runoff analysis being made on discrete groups containing a larger VWC interval.

Thus, all three areas exhibit relatively similar low runoff ratios and high infiltration capacities at low VWC conditions. However, at high VWC conditions, Lystrup exhibit the largest observed runoff ratios (close to 1 mm/mm), indicating a potential risk of all rainfall becoming runoff, when the soil is fully saturated. Additionally, Lystrup also show the highest median runoff ratio of 0.32, as presented in Table 6.4. In contrast, Ejby Mølle and Elmelundsvej generally exhibit very low runoff ratios (below 0.1 mm/mm) and a maximum median runoff ratio of 0.011 and 0.005 mm/mm, respectively. Furthermore, it is apparent in Figure 6.13 that the generated runoff at each location varies even though the rainfall remains the same. This suggests that the runoff response at all three areas depends on both rainfall intensity and duration, and not just the total rainfall amount, since the largest

runoff generation is generally observed during normal-intensity rainfall events. Moreover, the effect of seasonal variations is seen in especially Lystrup, as significant runoff only occurs during the wet period. At Ejby Mølle and Elmelundsvej, the largest runoff responses are seen in the dry period.

Several factors, such as differences in topography, surface characteristics, soil properties, vegetation cover, and land use, may explain these variations and similarities. Therefore, to provide deeper insight into the processes governing runoff variability, the effect of location- and soil-specific parameters on contingent runoff is examined and presented in Table 6.4.

Table 6.4. Comparison of sample size (n) and site-specific parameters at the hillslope-scale project locations, Ejby Mølle (Odense), Elmelundsvej (Odense), and Lystrup.

	Ejby Mølle	**Elmelundsvej**	**Lystrup**
Sample size ($n_{total\ events}$)	169	389	498
Dry period [%]	50.30	42.67	32.33
Wet period [%]	49.70	57.33	67.67
Catchment size	0.093 ha	0.112 ha	0.430 ha
Mean slope ± SD [%]	11.50 ± 10.12	17.60 ± 4.56	9.18 ± 4.97
Dominating soil type	Fine clay with sand	Coarse clay with sand	Fine clay with sand
Dominating land use	Low vegetation	Low vegetation	Low vegetation
Median runoff [mm]	0.031	0.000	0.018
Maximum runoff [mm]	0.256	1.088	8.79
Maximum median runoff ratio [mm/mm]	0.011	0.005	0.322
Delay [hr]	2	3	6

When comparing the site-specific factors such as soil composition and vegetation cover, the three areas exhibit similar characteristics. Land use at all locations is dominated by low vegetation, and the soil texture is also largely similar. The dominant soil type is *fine clay with sand* at Ejby Mølle and Lystrup, whereas at Elmelundsvej, it consists of *coarse clay with sand*.

These general similarities may explain why the median runoff at the three sites is fairly similar, with the highest median runoff observed at Ejby Mølle (0.04 mm) and the lowest at Elmelundsvej (0.00 mm). The small differences in median runoff value suggest that under typical conditions, the sites exhibit relatively low runoff generation, with limited variations in baseline hydrological response. However, median values alone do not capture the full range of runoff dynamics, as the maximum runoff differs significantly between the three locations. This suggests that additional site-specific factors may influence the observed differences in maximum runoff generation. The main explanation is likely a more compact layer of soil, which is located in the topsoil approximately 40-50 cm below the surface in Lystrup. This layer can lead to subsurface interflow, which may explain the large differences in maximum runoff between Lystrup and the two other hillslope scale project locations [Nielsen, 2019]. This phenomenon can also explain the differences in both the maximum median runoff ratio and the delay estimated by the cross-correlation, which

in Lystrup is six hours, while it in Ejby Mølle and Elmelundsvej are two and three hours, respectively.
The differences in maximum runoff between Ejby Mølle and Elmelundsvej are likely explainable by one potential factor: the slope. Elmelundsvej has a mean slope of 17.60% and maximum runoff of 1.09 mm, while Ejby Mølle has a mean slope of 11.50 % and maximum runoff of 0.26 mm, as presented in Table 6.4.

However, it can be difficult to compare the three areas due to the large difference in runoff responses. In Ejby Mølle and Elmelundsvej, the runoff responses are relatively low, why it can be discussed whether they represent actual runoff values or, to a higher degree, measurement uncertainties. Thus, it is challenging to attribute runoff variation between the three hillslope scale locations solely to soil type, land use, or slope. Instead, the differences may be primarily driven by variations in infiltration capacity and sensor uncertainties due to low runoff volumes. Moreover, it is important to note that the dataset at Ejby Mølle (n = 169) is significantly smaller than at Elmelundsvej (n = 389) and Lystrup (n = 498), which may introduce uncertainties in the analysis.

Urban Subcatchment Scale 7

Runoff at the two medium-scale areas, Christianshusvej and Rungstedvej in Hørsholm, is analysed, followed by a brief discussion of the results. The runoff is assumed to originate from the catchment area composed of both green and impervious surfaces. A runoff separation is performed to separate baseflow and surface runoff. This approach is elaborated in Appendix G.

7.1 Christianshusvej

As described in section 4.2, the catchment in Christianshusvej consists of a residential area with a separated sewer system. For the runoff analysis, VWC data from Sensor 6 is used.

To understand the relationship between VWC and runoff at Christianshusvej, rainfall events with the highest daily accumulated rainfall and runoff are selected (cf. Appendix H, Figure H.10) and analysed in Figure 7.1. From the two upper plots, it is evident that VWC generally increases in response to rainfall, while all three plots indicate a runoff response time of approximately two hours, which corresponds to the *cross-correlation analysis*, presented in section 5.1, Figure E.4. The first event, on 09-09-2024, shows the highest recorded rainfall (37.40 mm) and the second highest recorded runoff (5.38 mm), causing a runoff generation of 14.4% of the rainfall. Rainfall occurs within the first 12 hours, leading to a significant VWC increase from 0.15 to 0.26 m^3/m^3. Moreover, it is clear that runoff follows the rainfall patterns, likely due to the high imperviousness in the area. The second event, on 30-06-2024, displays the second-highest daily rainfall (31.40 mm) and a corresponding runoff of 3.79 mm (12.1% of the rainfall becomes runoff). Rainfall is observed mainly during the first nine hours, resulting in a VWC increase from 0.23 m^3/m^3 to 0.30 m^3/m^3. Furthermore, the runoff in the second event exhibits similar patterns to the rainfall.
The third event on 15-11-2023, which exhibits the second highest recorded rainfall of 31.4 mm and the highest recorded runoff of 7.19 mm (22.9% of the rainfall becomes runoff), shows an almost constantly high VWC of approximately 0.27-0.31 m^3/m^3 during the event, and a relatively constant rainfall during the first 16 hours. The constant VWC denotes an almost saturated soil, which during the event reaches full saturation. This results in a faster runoff response (of approximately one hour), as the soil's infiltration capacity is exceeded. The runoff increases gradually and peaks after eight hours, which corresponds to the rainfall distribution.

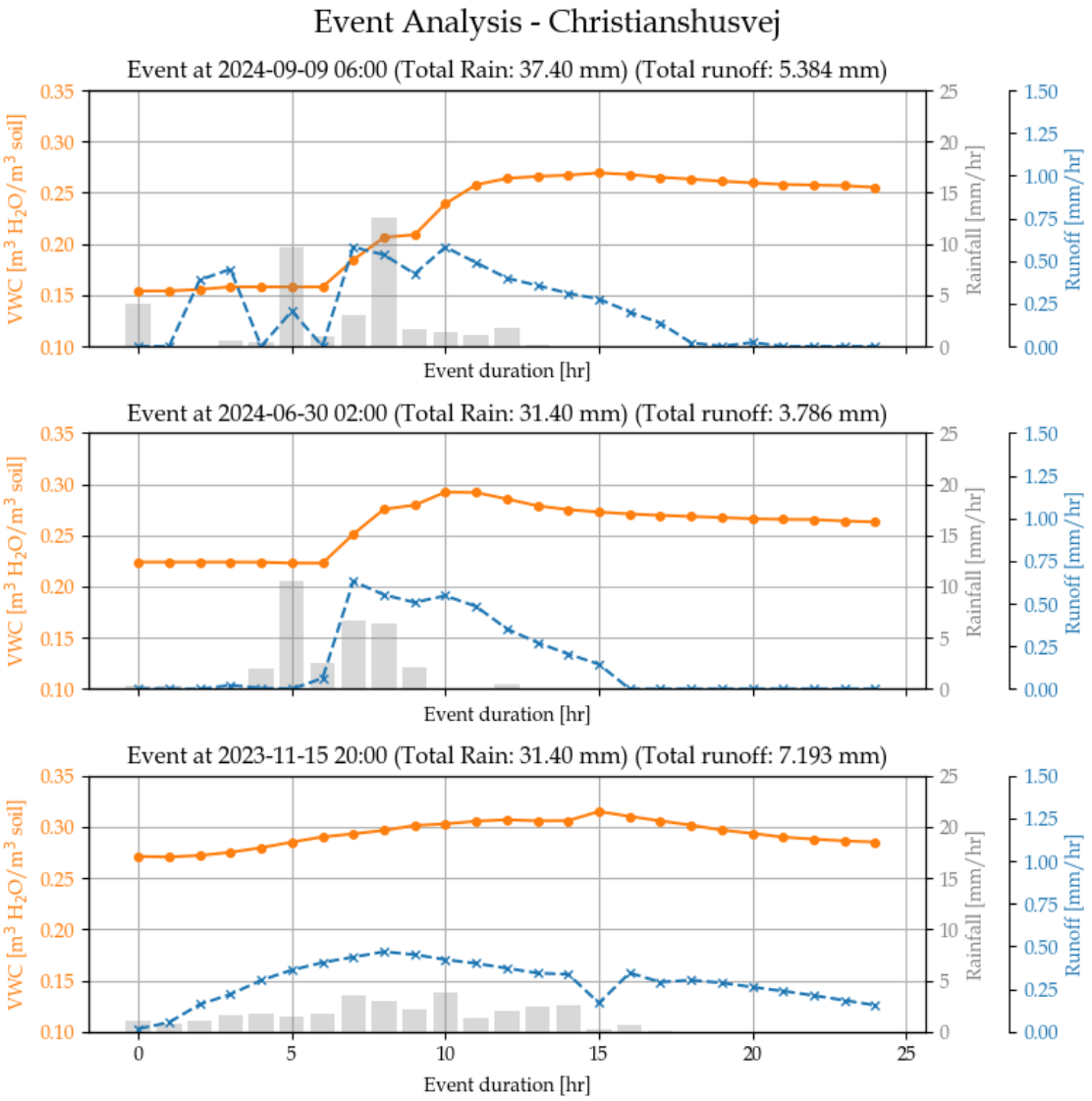

Figure 7.1. Analysis of VWC and runoff response to rainfall for selected events at Christianshusvej, Hørsholm

When comparing the three events, the runoff pattern generally aligns closely with the rainfall pattern, most likely due to the high degree of impervious surfaces in the area. This may also explain the high proportion of rainfall converted to runoff, ranging from 12-23% across the events. Moreover, it becomes evident that substantial runoff primarily occurs during events with large rainfall volumes, while the delay in runoff response is strongly influenced by the VWC levels. This suggests that when VWC is already high, even moderate rainfall can trigger runoff with minimal delay.

To gain a deeper understanding of the relationship between daily rainfall, runoff, and VWC at Christianshusvej, the analysis presented in Figure 7.2 is performed for each of the defined high, mid, and low VWC classifications (presented in Appendix H, Figure H.4), each further subdivided into three subcategories.

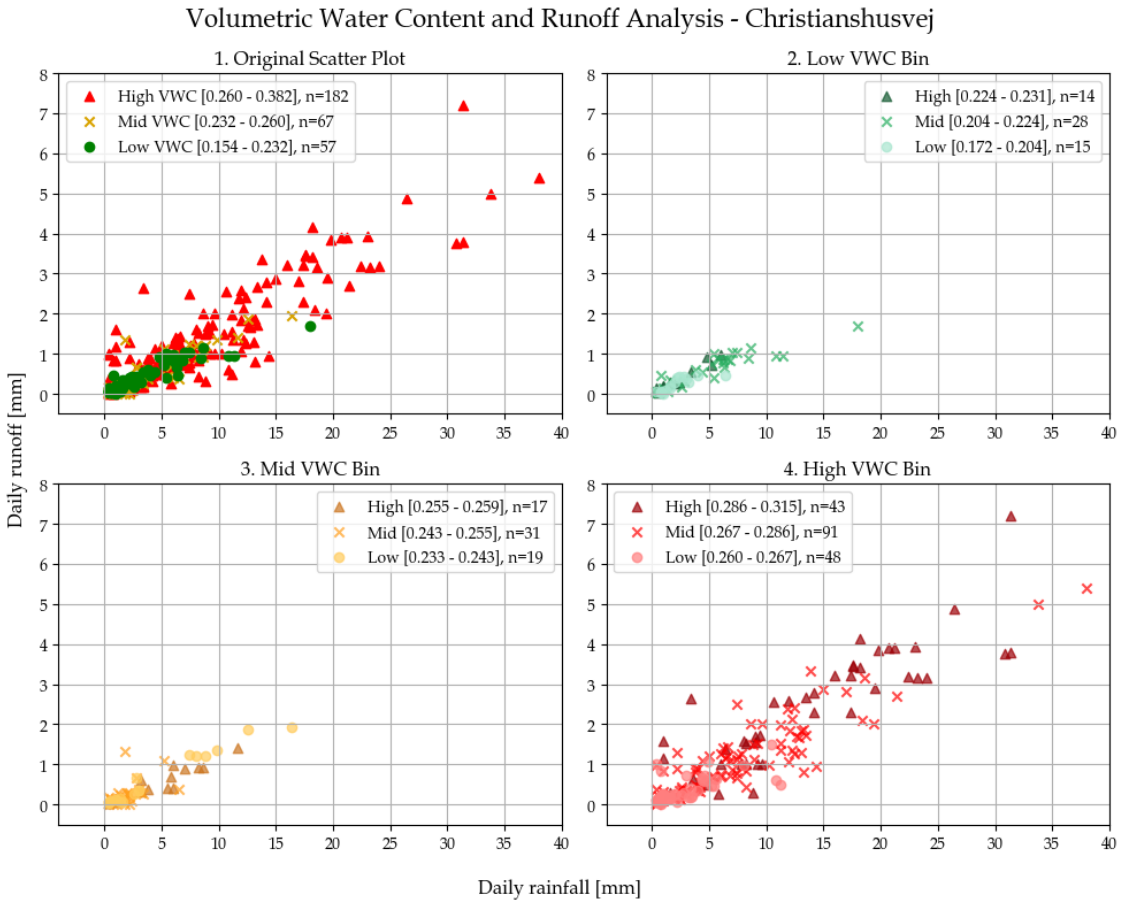

Figure 7.2. The *VWC and runoff analysis* for Christianshusvej, Hørsholm, consisting of (1) total runoff/rainfall coloured by VWC, (2) runoff/rainfall in the low bin divided into three sub intervals, (3) runoff/rainfall in the mid bin divided into three sub intervals, and (4) runoff/rainfall in the high bin divided into three subintervals.

As shown in Figure 7.2, runoff at Christianshusvej exhibits a high response to rainfall, with daily runoff values ranging from 0.00 to approximately 7.20 mm, with the largest generated runoff observed within the high VWC category (cf. subplot "4. High VWC Bin"). In contrast, the low and mid VWC categories (Subplot "2. low VWC Bin" and "3. Mid VWC Bin") exhibit a much narrower range of runoff values, from 0.00 to 1.80 mm and 0.00 to 2.00 mm, respectively. Notably, the high VWC category exhibits the greatest spread in runoff values, indicating greater variability in the rainfall-runoff response compared to the mid and low categories. However, this may partly be explained by the high proportion of observations (58.82%) that fall within this category.
No notable difference between the slope of the high, mid, and low VWC bins is present, indicating that VWC contributes minimally to runoff generation.

A further examination of the runoff data is analysed in terms of seasonal grouping, rainfall intensity, and the change in VWC during the rainfall event, as shown in Figure 7.3. It is clear that most data points falls within the wet period, where the soil generally has a high VWC, as visualised in subplot "1. Original Scatter Plot" and "2. Coloured by Season" (see Figure H.16, section H.3 for a more detailed overview of the wet/dry periodical segregation of the runoff-rainfall relationship coloured by VWC).

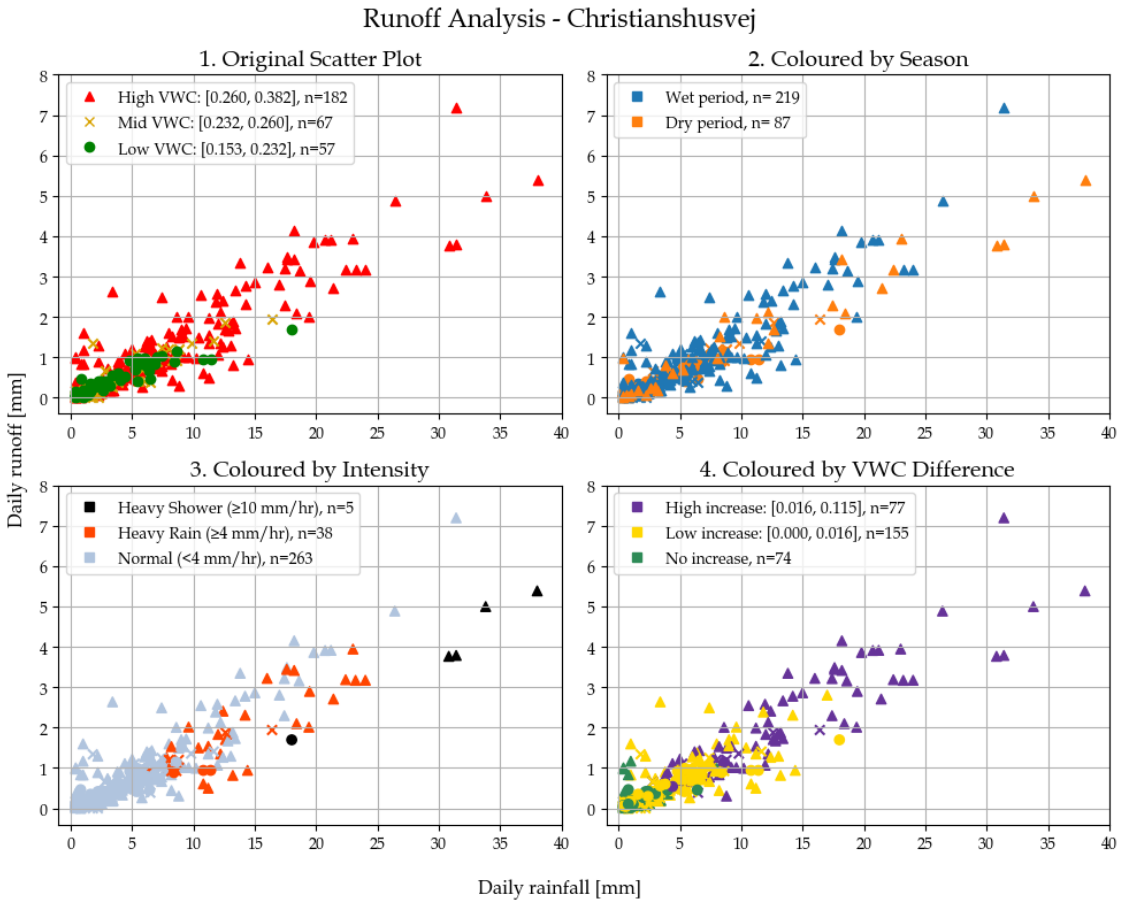

Figure 7.3. The runoff analysis for Christianshusvej, Hørsholm, consisting of runoff/rainfall coloured by (1) VWC, (2) wet/dry period, (3) rainfall intensity, and (4) change in VWC during the rainfall event.

The majority of rainfall events are classified as normal intensity, with a few categorised as heavy rain, and five as heavy showers (cf. subplot "3. Coloured by Intensity"). The heavy shower events all fall within the dry period, where a high increase in VWC occurs in four of five, while a low increase occurs in the last one (cf. subplot "4. Coloured by VWC Difference"). Furthermore, the events with daily rainfall $\geq$ 25 mm suggest that normal-intensity rainfall events during the wet period generally generates a larger proportion of runoff compared to heavy-shower intensity events during the dry period (all experiencing a high increase in VWC).
Thus, the runoff analysis generally suggests that the amount of rain converted directly into runoff generally depends on rainfall volumes and duration rather than intensity. Furthermore, a minor indication of initial VWC affecting the runoff is visible, as a few points with low or no VWC increase deviate a bit from the linear tendency, resulting in a larger proportion of the rainfall becoming runoff. However, the category high increase in subplot 4 covers a large interval, which may neglect some of the nuances in the analysis.

The observed differences in runoff viability are supported by a Kruskal-Wallis test ($p = 3.37 \cdot 10^{-11}$), which indicates a significant difference among the medians of the three VWC groups. A Dunn's test is performed to identify which specific medians differ

($\alpha_{adjusted}$=0.0166). A statistically significant difference can be determined between both the high and low VWC group (p = $2.62 \cdot 10^{-6}$), and the high and mid VWC group (p = $8.4 \cdot 10^{-10}$), whereas no statistically significant difference is found between the mid and low VWC group (p = 0.36) (cf. Appendix I, Table I.3).

To further examine the rainfall-generated runoff, a *runoff ratio analysis* is performed and presented in Figure 7.4. From the upper plot it is evident that most data points fall within the range of 0.0-0.4 mm/mm, some points near 1.0 mm/mm, and a few points above 1 mm/mm. This aligns with the observations made in the previous runoff analysis, where the runoff-rainfall relationship primarily remains the same, independent of rainfall amount and VWC. In the lower plot, the runoff ratio is divided into three VWC bins, with median runoff ratios of 0.12-0.17 mm/mm, and nearly equal whiskers. The largest median runoff ratio is observed in Bin 3 at a VWC of 0.275-0.325, where the upper whisker reaches approximately 0.32 mm/mm. Thus, a minor difference in runoff ratio is visible between Bin 3 and the remaining bins.

A Kruskal–Wallis test (p = $8.6 \cdot 10^{-7}$) indicates that statistically significant differences are present between the runoff ratio medians. This is also evident from the boxplot presented in Appendix I, section I.2. A Dunn's test reveals that the difference is between Bin 3 and the remaining two bins.

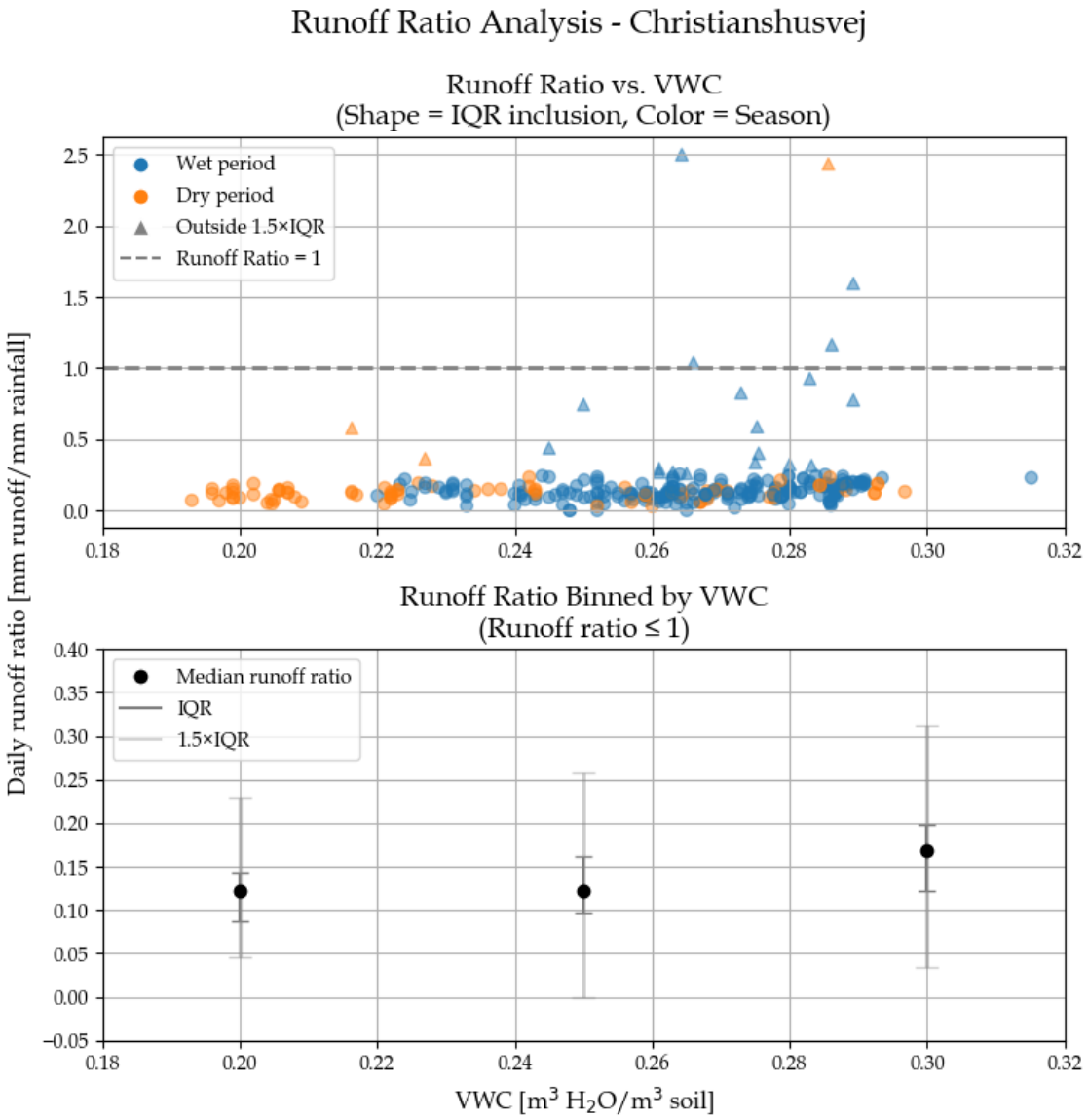

Figure 7.4. Ratio between the runoff and rainfall at different VWC levels at Christianhusvej. Data points are coloured by wet (blue) and dry (orange) periods, and their shapes indicate whether they lie within or outside 1.5×IQR. Data points with a runoff ratio larger than 1 are removed from the lower plot. The median runoff ratio, the IQR and the 1.5×IQR for each of the intervals are shown.

As the Kruskal–Wallis test and Dunn's test only assess differences among discrete groups, it does not capture broader monotonic trends in the data. Thus, to examine whether a more general monotonic relationship exists between runoff and VWC, alongside rain and change in VWC, a Spearman's correlation analysis is performed for the area, and visualised in Table 7.1.

Table 7.1. Spearman's correlation for Christianshusvej, Hørsholm ($\alpha_{adjusted} = 0.0166$).

	Rain [mm]	**VWC** [m^3 H_2O/m^3 soil]	**ΔVWC** [m^3 H_2O/m^3 soil]
ρ	0.885	0.552	0.747
p-value	$4.01 \cdot 10^{-103}$	$7.76 \cdot 10^{-26}$	$7.43 \cdot 10^{-56}$

The Spearman correlation analysis reveals a statistically significant monotonic relationship between rainfall and runoff, suggesting that higher rainfall generally leads to increased runoff. Additionally, significant correlations are found between runoff and both the VWC and the change in VWC. However, rainfall exhibits the strongest Spearman's correlation coefficient ($\rho = 0.885$), suggesting that rainfall is the dominant factor influencing runoff at Christianshusvej, as also illustrated in Figure 7.3. This finding is consistent with expectations, as precipitation is typically the primary driver of surface runoff in areas with high imperviousness.

Main Findings

The runoff analysis and the corresponding statistical evaluation of parameters affecting runoff generally suggest a linear relationship between rainfall and runoff at Christianshusvej, with rainfall being the primary driver of runoff. This is likely due to the area's land use, which is predominantly residential with a high proportion of impervious surfaces. As a result, contributions from the green areas, despite covering 63% of the total catchment area, are limited compared to those from impervious surfaces. Nevertheless, variations in VWC also influence runoff generation, both in terms of VWC and the change in VWC during events. Low initial VWC promotes greater infiltration and reduces runoff, whereas when initial VWC is already high and only a minor increase in VWC occurs, the delay between rainfall and runoff shortens. Once the VWC approaches approximately 0.30 m^3/m^3, the soil is near saturation, and both a larger and faster runoff response becomes more likely. Moreover, the runoff analysis shows that although the highest rainfall volumes occur during heavy shower events in the dry period, the largest runoff is generated during normal-intensity events in the wet period. Thus, the analysis suggests that consistent, low-intensity winter rainfall has a greater impact on runoff generation at Christianshusvej than short, high-intensity summer rainfall.

7.2 Rungstedvej

As described in section 4.2, the catchment area for Rungstedvej consists of a residential area with a combined sewer system. For the runoff analysis VWC data from Sensor 2 is used.

To understand the relationship between VWC and runoff at Rungstedvej, rainfall events with the highest daily accumulated rainfall and runoff are selected (cf. Appendix H, Figure H.11) and analysed in Figure 7.5.

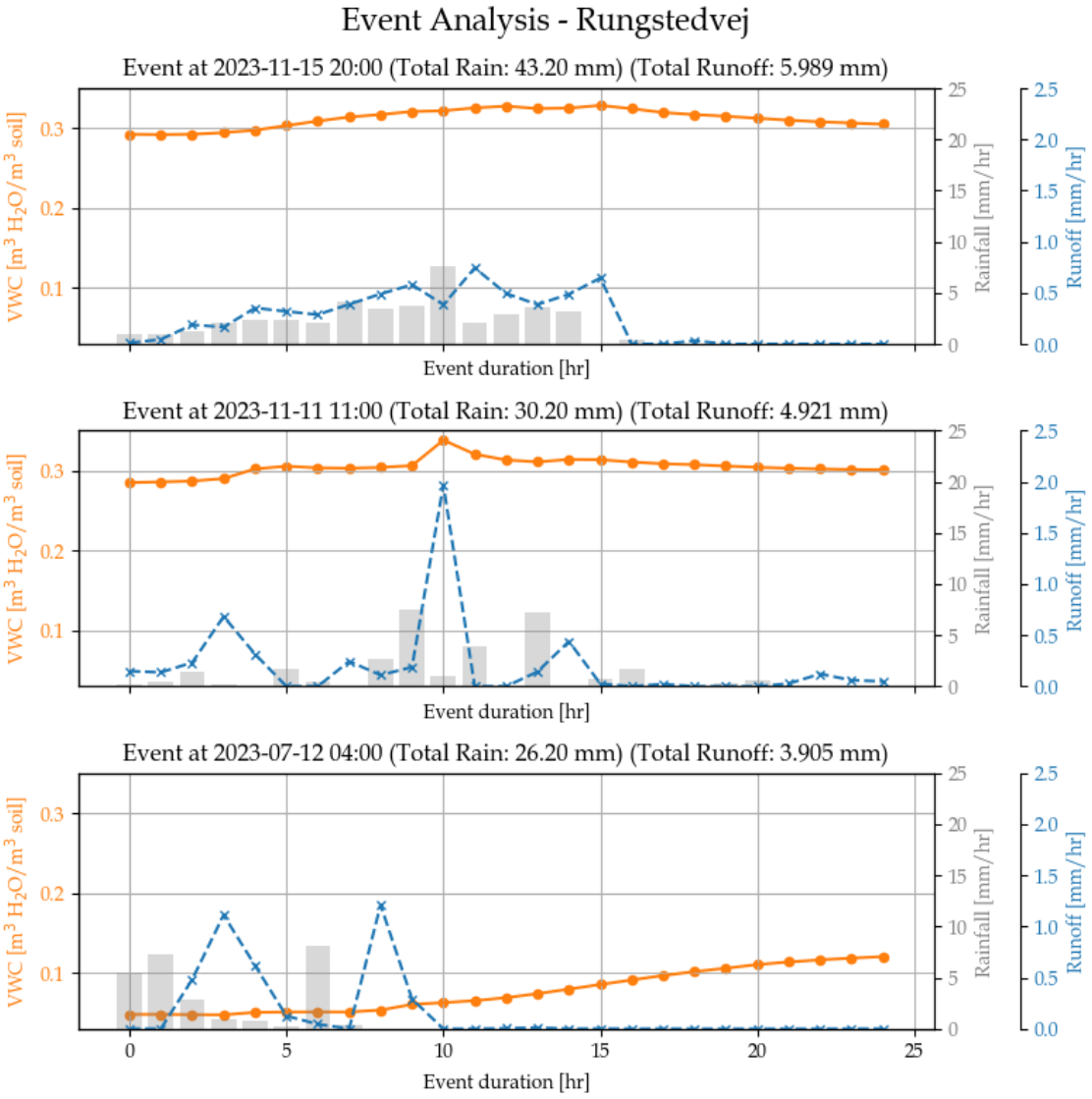

Figure 7.5. Analysis of VWC and runoff response to rainfall for selected events at Rungstedvej, Hørsholm.

The first event, on 15-11-2023, exhibits both the highest recorded rainfall (43.20 mm) and the highest recorded runoff (5.99 mm). Rainfall occurs during the first 14 hours of the event, while VWC remains relatively stable between 0.30-0.32 m^3/m^3. The runoff response

follows the rainfall patterns closely, with a one-hour delay in response. In total, 13.9% of the rainfall is converted into runoff during the event.
The second event, on 11-11-2023, shows the second-highest daily rainfall (30.20 mm) and the second-highest recorded runoff (4.92 mm). Rainfall occurs sporadically throughout the event, while VWC remains fairly constant at approximately 0.30 m^3/m^3. As in the first event, runoff closely follows the rainfall with a one-hour delay. Here, 16.3% of the rainfall becomes runoff.
The third event, on 12-07-2023, features the third-highest rainfall (26.20 mm) and the third-highest runoff (3.91 mm). Unlike the previous events, VWC increases steadily from 0.02 to 0.12 m^3/m^3 during the event. Rainfall is recorded during the first seven hours, and a two-hour delay in runoff response is observed, which aligns with the *cross-correlation analysis* presented in section 5.1, Figure E.5. As seen in the other events, runoff follows the rainfall pattern, further underlining the impact of the high impervious surface coverage in the area. During the event, 14.9% of the rainfall becomes runoff.

When comparing the three events, it is generally observed that the runoff pattern closely follows the rainfall pattern, which is likely because of the high degree of impervious surfaces in the area, limiting the general infiltration. Furthermore, it is evident that high VWC conditions, besides promoting greater runoff responses, also minimise the delay between rainfall and runoff. This may explain why the largest runoff occurs during the events containing the largest rainfall volumes, when the VWC level is high. This may also explain the high percentage of rainfall generated runoff, ranging from 14-16% in the three events.

To further examine the relationship between daily rainfall, daily runoff, and VWC for Rungstedvej, the analysis visualised in Figure 7.6 is conducted for each of the defined high, mid, and low VWC classifications (presented in Appendix H, Figure H.5), and is further subdivided into three subcategories.
It is evident that runoff at Rungstedvej responds strongly to rainfall, with daily runoff values ranging from 0.00 to approximately 5.50 mm. The highest runoff values are observed within the high VWC category (cf. subplot "4. High VWC Bin"). In comparison, the low and mid VWC categories (subplot "2. low VWC Bin" and "3. Mid VWC Bin") exhibit slightly narrower runoff ranges, from 0.00 to 3.70 mm and 0.00 to 4.00 mm, respectively. Overall, no notable difference between the slope of the high, mid, and low VWC bins is observed, indicating that VWC has a limited influence on runoff generation at Rungstedvej. The largest spread in runoff values is found within the low VWC category, likely due to increased infiltration capacity of dry soil, resulting in reduced runoff. However, the high VWC group accounts for 52.05% of all observations from Rungstedvej. This uneven distribution may introduce some uncertainties when studying the influence of VWC on runoff behaviour.

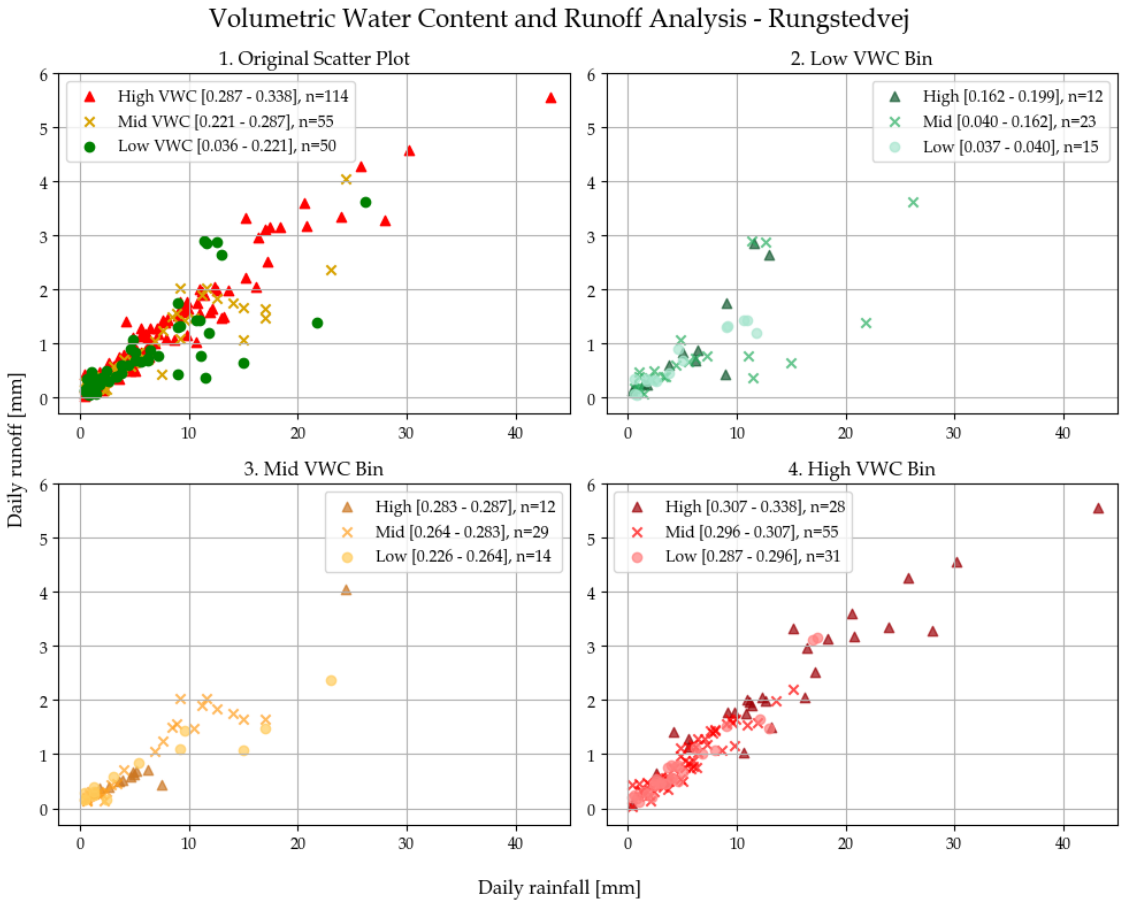

Figure 7.6. The *VWC and runoff analysis* for Rungstedvej consisting of (1) total runoff/rainfall coloured by VWC, (2) runoff/rainfall in the low bin divided into three sub-intervals, (3) runoff/rainfall in the mid bin divided into three sub-intervals, and (4) runoff/rainfall in the high bin divided into three subintervals.

A further examination of the runoff data is analysed in terms of seasonal grouping, rainfall intensity, and the change in VWC during the rainfall event, as shown in Figure 7.7. It is evident that most data points fall within the wet period, where the soil generally has a high VWC, as visualised in subplot "1. Original Scatter Plot" and "2. Coloured by Season" (see Appendix H, Figure H.17 for a more detailed overview of the wet/dry periodical segregation of the runoff-rainfall relationship coloured by VWC). The majority of rainfall events are classified as normal intensity, with some categorised as heavy rain, and only four as heavy showers (cf. subplot "3. Coloured by Intensity"). The heavy shower events fall within the dry period, where a high increase in VWC occurs in all four (cf. subplot "4. Coloured by VWC Difference"). Furthermore, subplot 4 indicates no difference in slope between high, low, and no increase in VWC. However, when the runoff generation exceeds approximately 2 mm, all events are classified as high increase, meaning that a segregation between the categories is visible.

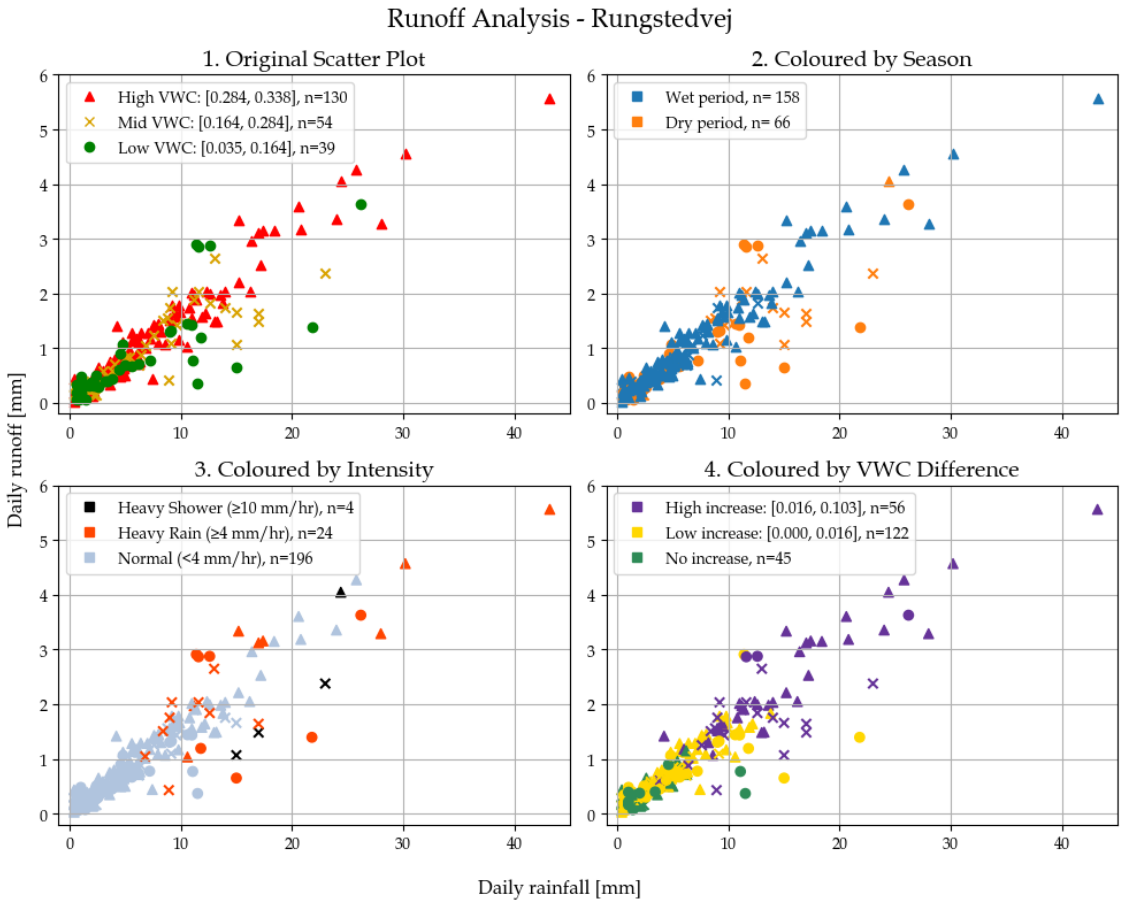

Figure 7.7. The runoff analysis for Rungstedvej, Hørsholm, consisting of runoff/rainfall coloured by (1) VWC, (2) wet/dry period, (3) rainfall intensity, and (4) change in VWC during the rainfall event.

The four heavy shower-intensity events are all marked as exhibiting a high increase in VWC, but as seen by subplot 3, three of the points are located below the general slope. This can be explained by the VWC for the three events being classified as mid VWC (cf. subplot 1), meaning that the initial VWC is likely lower for these events, resulting in a higher infiltration capacity in the soil, compared to the heavy-shower event with a higher runoff response. Generally, it is seen by subplot 3 that normal-intensity events exhibit the narrowest spread, whereas heavy rain and heavy showers deviate slightly from the runoff-rainfall trend.
The runoff analysis generally suggests that the amount of rainwater converted directly into runoff to a higher degree depends on rain intensity rather than the VWC, as indicated by the linear trend observed between rainfall and runoff. However, the analysis does reveal a minor influence of VWC, as a few points with low or no increase deviate from the overall pattern. This is further supported in the previously discussed *event analysis*, which shows that runoff response can vary slightly depending on soil moisture conditions prior to the rainfall event.

The observed differences in runoff responses are supported by a Kruskal-Wallis test ($p = 6.25 \cdot 10^{-3}$), which indicates a significant difference among the medians of the three VWC

groups. This is also evident from the boxplot presented in Appendix I, section I.2. A Dunn's test is performed to identify which specific medians differ ($\alpha_{adjusted}$=0.0166). A statistically significant difference can be determined between the high VWC group and the mid VWC group ($p = 5.34 \cdot 10^{-3}$), whereas no statistically significant difference is found between the low VWC group and both the high ($p = 2.65 \cdot 10^{-2}$) and mid ($p = 0.83$) VWC groups (cf. Appendix I, Table I.4).

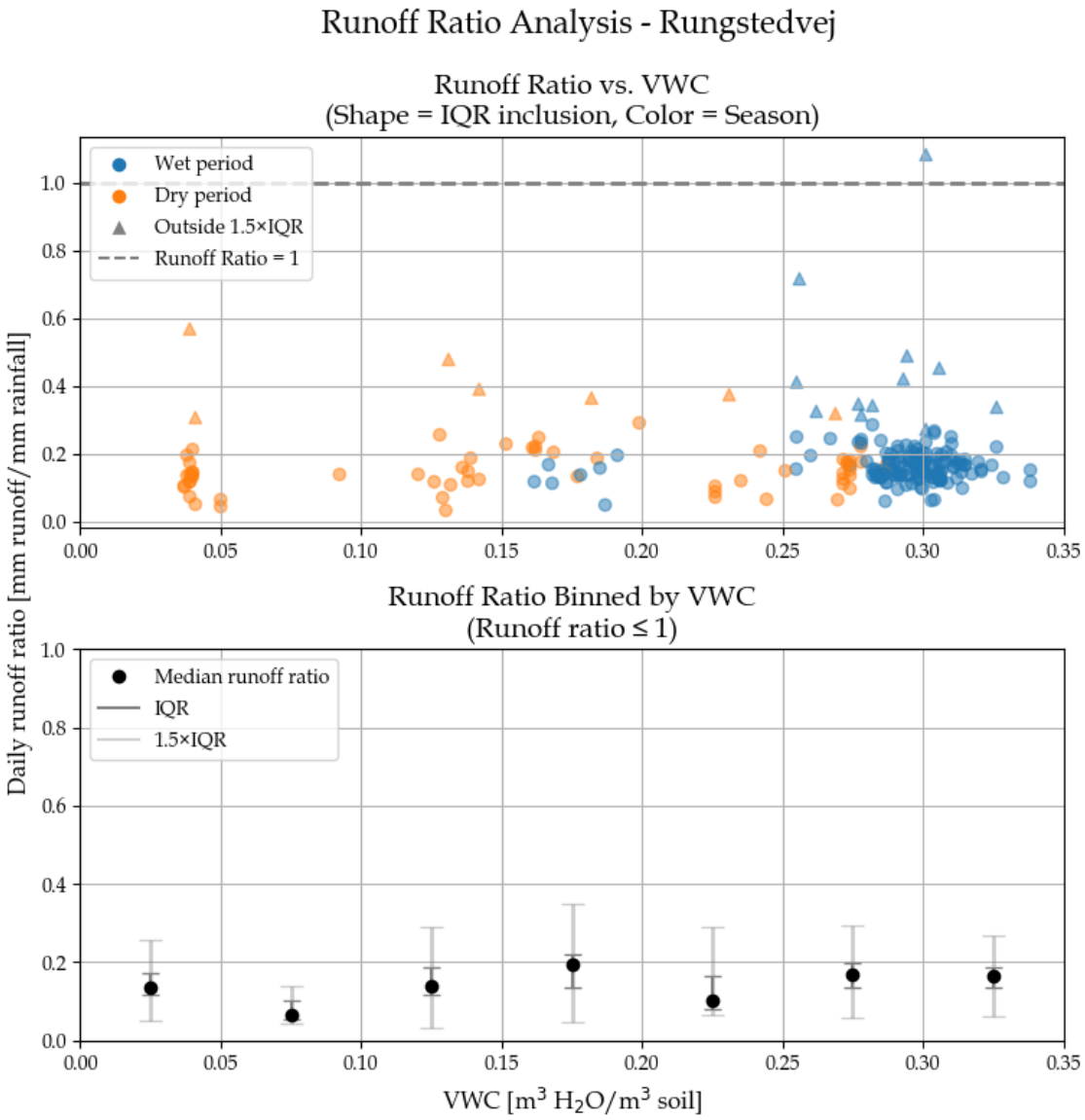

Figure 7.8. Ratio between the runoff and rainfall at different VWC levels at Rungstedvej. Data points are coloured by wet (blue) and dry (orange) periods, and their shapes indicate whether they lie within or outside 1.5×IQR. Data points with a runoff ratio larger than 1 are removed from the lower plot. The median runoff ratio, the IQR and the 1.5×IQR for each of the intervals are shown.

To further examine the rainfall-generated runoff, a *runoff ratio analysis* is performed and presented in Figure 7.8. From the upper plot, it is evident that most data points cluster within the range of 0.05-0.25 mm/mm, while a few points exceed this range. This aligns with the observations made in the previous runoff analysis, where the runoff-rainfall

relationship primarily remains the same, independent of rainfall amount and VWC.
In the lower plot, the runoff ratio is divided into seven VWC bins, with median runoff ratios of 0.08-0.2 mm/mm, and nearly equal IQR. The largest median runoff ratio is observed in Bin 4 at a VWC of 0.175, where the upper IQR reaches 0.21 mm/mm. Thus, a minor difference in runoff ratio is visible between Bin 4 and the remaining bins.
A Kruskal–Wallis test (p = 0.02) confirms that a statistically significant difference is present between the medians of the seven bins, however, a subsequent Dunn's test reveals no statistically significant difference between the bins. This may be due to the Dunn's test using more conservative significance level.

When comparing predefined VWC bins, the overall effect of VWC on runoff ratio appears limited. As the Kruskal–Wallis test and Dunn's test only assess differences among discrete groups, it does not capture broader monotonic trends in the data. Thus, to examine whether a more general monotonic relationship exists between runoff and VWC, alongside rain and change in VWC, a Spearman's correlation analysis is performed for the area, and visualised in Table 7.2.

Table 7.2. Spearman's correlation for Rungstedvej, Hørsholm ($\alpha_{adjusted} = 0.0166$).

	Rain [mm]	**VWC** [m^3 H_2O/m^3 soil]	**ΔVWC** [m^3 H_2O/m^3 soil]
ρ	0.935	0.318	0.795
p-value	$2.196 \cdot 10^{-101}$	$1.24 \cdot 10^{-6}$	$6.56 \cdot 10^{-50}$

The Spearman's correlation analysis shows a significant monotonic relationship between all three parameters and runoff, with the highest Spearman's correlation coefficient being between rain and runoff ($\rho = 0.935$), suggesting that higher rainfall generally leads to increased runoff. The second highest Spearman's correlation coefficient is observed between change in VWC and runoff ($\rho = 0.795$), indicating a significant monotonic relationship between them, while the VWC and runoff have the lowest Spearman's correlation coefficient ($\rho = 0.318$). As the coefficient for rain is highest, the rain has a larger effect on runoff than the change in VWC, while VWC has the lowest impact on runoff.

Main Findings

The runoff analysis and the corresponding statistical evaluation of parameters affecting runoff generally suggest a linear relationship between rainfall and runoff at Rungstedvej, with rainfall being the primary driver of runoff. This is likely due to the area's land use, which is predominantly residential with a high proportion of impervious surfaces. As a result, contributions from the green areas, despite covering 53% of the total catchment area, are limited compared to those from impervious surfaces.

Nevertheless, VWC also influence runoff generation, both in terms of maximum VWC and the change in VWC during events. Low initial VWC promotes greater infiltration and reduces runoff, whereas when initial VWC is already high and only a minor increase in VWC occurs, the delay between rainfall and runoff shortens. Once the maximum VWC approaches approximately 0.30 m^3/m^3, the soil is near saturation, and both a larger and faster runoff response becomes more likely.

Moreover, the analysis suggests that normal intensity rainfall during the wet period has a greater and more predictable impact on runoff generation at Rungstedvej, compared to events occurring during the dry period, where a more variable runoff response is observed.

7.3 Comparison of the Two Urban Subcatchment-Scale Project Locations

Variations in VWC, rainfall, and runoff at the two urban subcatchment-scale locations (Christianshusvej and Rungstedvej) are compared to better understand how both contingent runoff from urban green areas (with a high degree of impervious surfaces) and site-specific factors influence runoff response mechanisms. In the following, the results of the runoff analyses for both sites are discussed, highlighting key similarities and differences in the runoff responses.

Firstly, a comparison of the daily runoff-rainfall relationship at the two sites is presented in Figure 7.9. Although the highest runoff ($\approx$ 7.00 mm) is observed at Christianshusvej, both locations exhibit identical linear trends and slopes. This likely reflects their similar land use: predominantly residential areas with a high percentage of impervious cover, where surface runoff generation is primarily driven by rainfall volume rather than infiltration capacity.

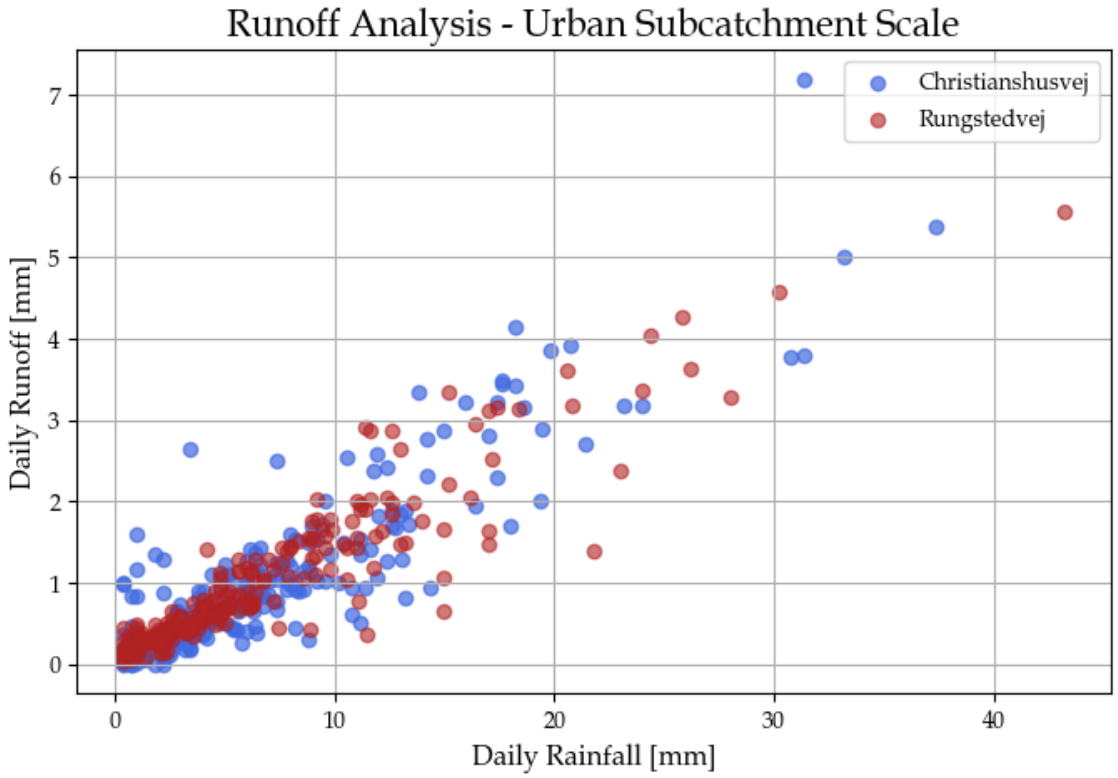

Figure 7.9. Comparison of the daily runoff and daily rainfall for the two urban subcathment scales.

However, since the runoff responses include contributions from both impervious and pervious surfaces, it is difficult to isolate fast runoff originating specifically from the green surfaces. This limits the ability to accurately assess the extent of runoff generated solely by green areas.

Although rainfall is the dominant driver of runoff at both sites, due to the high degree of imperviousness (supported by the limited variations in runoff ratio), it is also evident that VWC, to some extent, influences runoff generation. Both locations exhibit similar maximum VWC levels (0.38 and 0.34 m^3/m^3). As shown in Table 7.3, several factors, such as differences in topography, surface characteristics, soil properties, vegetation cover, and land use, may further explain the runoff dynamics and highlight the influence of site-specific conditions on contingent runoff.

Table 7.3. Comparison of sample size (n) and site-specific parameters at the urban subcatchment project locations, Christianshusvej and Rungstedvej.

	Christianshusvej	**Rungstedvej**
Sample size ($n_{total\ events}$)	306	224
Dry period [%]	28.43	29.46
Wet period [%]	71.57	70.54
Catchment size	10.5 ha	62.5 ha
Degree of imperviousness [%]	37	47
Mean slope [%]	13.76	11.42
Dominating soil type	Fine clay with sand	Fine clay with sand
Dominating land use	High vegetation	High vegetation
Runoff delay [hr]	2	2
Median runoff [mm]	0.448	0.692
Maximum runoff [mm]	7.192	5.559
Maximum median runoff ratio [mm/mm]	0.168	0.195

From Table 7.3, it appears that Christanshusvej and Rungstedvej share similar site-specific characteristics, such as soil composition and vegetation cover. Land use at both locations is dominated by green areas, comprising 63% and 53% of the catchments, respectively. This could contribute to slightly higher infiltration and reduced runoff at Christianshusvej, which aligns with the observed minor difference in both median runoff and maximum median runoff ratio. Conversely, the steeper average slope at Christanshusvej may promote increased surface runoff and reduced infiltration, partially counterbalancing the effects of the higher green area coverage. The soil texture at both sites is predominantly fine clay with sand, which likely explains the similar runoff delay times ($\approx$ 2 hours).
As green areas are generally expected to contribute only 0-15% to surface runoff, compared to up to 80% from impervious surfaces [Winther et al., 2011, p. 271], the visual differences in runoff from green areas may still appear limited, despite more than half of each catchment consisting of green areas. This is likely due to the dominant hydrological influence of the impervious surfaces.

Moreover, both Christianshusvej and Rungstedvej show increased runoff generation under wet conditions. However, Rungstedvej exhibits a more predictable runoff response pattern, while Christianshusvej shows greater variability. It is important to note that the available measurement data predominantly represent wet-period observations, which may bias the comparison between wet and dry period runoff behaviour.
Lastly, the runoff separation method applied in this thesis (cf. Appendix G) is designed

to isolate fast surface runoff, and therefore excludes a substantial proportion of the total flow by classifying it as baseflow. This introduces a level of uncertainty, particularly if some fast runoff is inadvertently filtered out. However, a sensitivity analysis of the alpha parameter, used to control the separation, suggests that changes in alpha primarily affect the magnitude of calculated runoff, while the overall pattern remains stable. Thus, to evaluate the influence of the runoff separation, the runoff analysis is performed both including and excluding the baseflow, as presented in section G.1. Here, it is found that baseflow does have a slight influence, but not one that interferes with the overall results and findings. Therefore, the runoff separation method is considered sufficiently robust for the purpose of this analysis.

Hydrological Scale 8

The runoff at the hydrological scale is first analysed, followed by a brief discussion of the results. As described in section 4.3, the catchment area mainly consists of rural land in a landscape dominated by hills. For the runoff analysis, VWC data from Sensor 6 is used.

To understand the relationship between VWC and runoff to Grejs Å, rainfall events with the highest daily accumulated rainfall and runoff are selected and analysed in Figure 8.1.

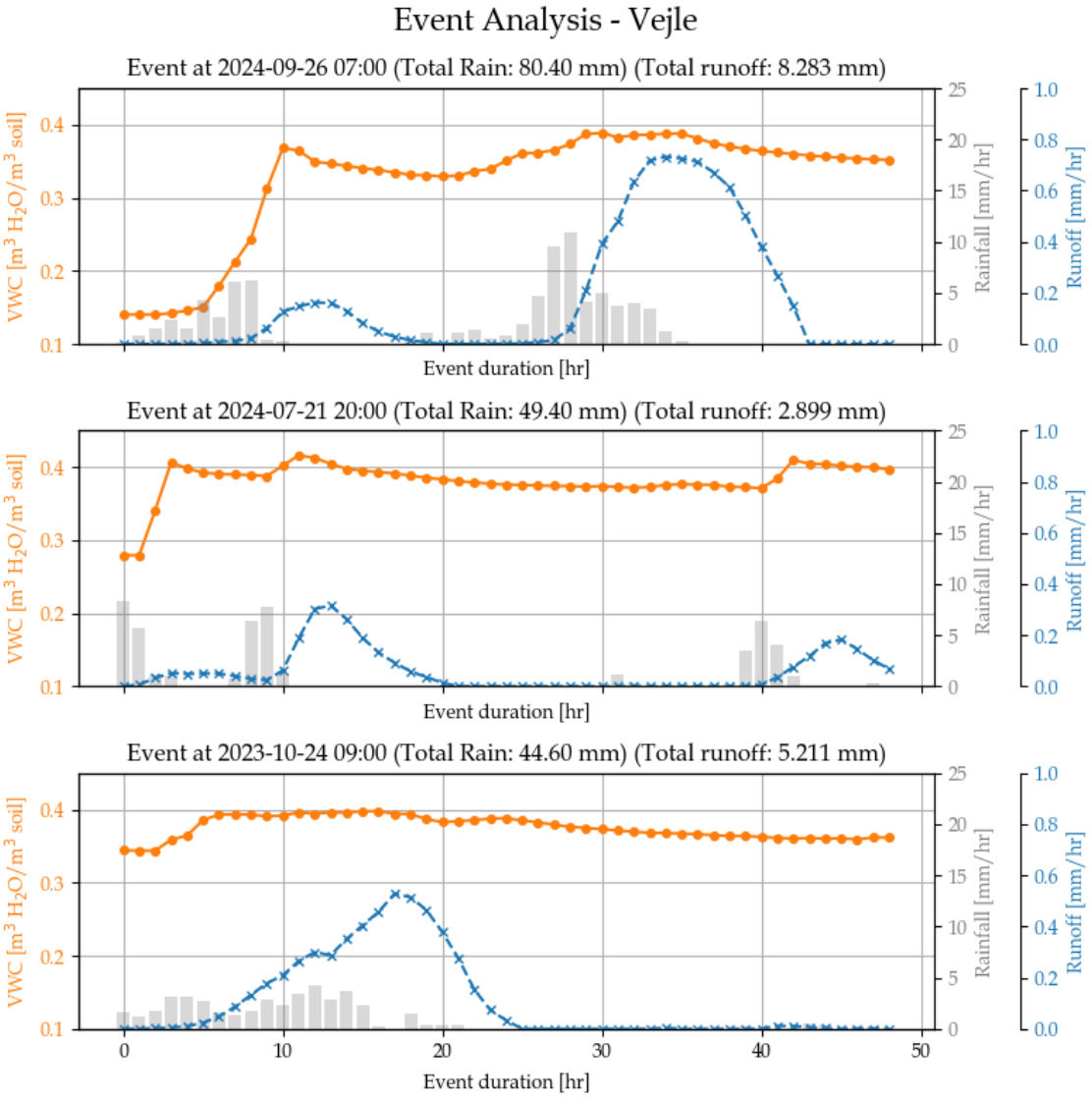

Figure 8.1. Analysis of VWC and runoff response to rainfall for selected events at Vejle.

From Figure 8.1, it is evident that VWC generally increases in response to rainfall. The

first event, on 26-09-2024, which exhibits the highest recorded rainfall (80.40 mm) and the highest observed runoff (8.28 mm), includes two distinct rainfall phases, the first during the initial 10 hours and the second from approximately hours 20 to 35. During the first phase, VWC increases from 0.15 to 0.37 m^3/m^3, while a runoff response (with a peak of $\approx$ 0.20 mm/hr) is observed around seven hours after the onset of the event. This aligns with the results of the *cross-correlation analysis* presented in section 5.1, Figure E.6. During the second rainfall phase, a smaller increase in VWC is observed (from 0.33 to 0.39 m^3/m^3); however, a significantly higher runoff response (with a peak of $\approx$ 0.70 mm/hr) occurs approximately seven hours later. This discrepancy in runoff responses between the two phases is likely due to both the difference in initial VWC and rainfall intensity: the soil is more saturated in the second phase, reducing its capacity to absorb water, thus producing a greater proportion of runoff. Overall, 10.30% of the total rainfall results in runoff during this event.
The second event, on 21-07-2024, shows the second-highest daily rainfall (49.40 mm) and a daily runoff of 2.90 mm (5.89% of rainfall). Three shorter rainfall phases (each of approximately four hours) occur throughout the event. During the first phase, VWC increases from 0.28 to 0.41 m^3/m^3 (whereafter VWC remains fairly stable), with only a minor runoff response ($\approx$ 0.05 mm). In contrast, larger runoff responses are observed during the two following phases (with peaks of 0.35 mm and 0.20 mm). This tendency aligns with the pattern seen in the first event. However, the delay between rainfall and runoff does not fully align with the *cross-correlation analysis*, as a delay of only approximately two hours is observed. This discrepancy may be explained by the generally high VWC during the event, combined with relatively short and high-intensity rainfall phases. Furthermore, the cross-correlation reflects the average delay across multiple events, which individual events do not necessarily correspond to.
The third event, on 24-10-2023, exhibited the third-highest daily rainfall (44.60 mm) and the second-highest runoff (5.21 mm), equivalent to 11.68% of the rainfall becoming runoff. Initial VWC is already high at the beginning of the event, and increases slightly from 0.35 to 0.40 $^3/m^3$ during the initial hours. A runoff response is observed five hours after event start, continuing to increase until reaching a peak runoff at approximately 0.55 mm/hr. A delay of approximately five hours between runoff and rainfall is observed, which deviates from the *cross-correlation analysis*, though to a lesser extent than in the second event. Although the third event exhibits a higher initial VWC compared to the second event, the longer delay can likely be attributed to the lower-intensity rainfall that characterises the third event.

When comparing the events at Vejle, it becomes evident that large runoff does not necessarily occur during the largest rainfall events, but rather depends heavily on the VWC level. This suggests that when the initial VWC is already high, even moderate rainfall can trigger runoff with minimal delay. Moreover, rainfall intensity plays a significant role, as high-intensity rainfall can generate substantial runoff even under lower VWC conditions, if the soil's infiltration capacity is exceeded, which was the case in the third event. Therefore, it is necessary to further examine the relationship between daily rainfall, daily runoff, and VWC for Vejle, as visualised in Figure 8.2. The analysis is conducted for each of the defined high, mid, and low VWC classifications (presented in Appendix H, Figure H.6), and is further subdivided into three subcategories.

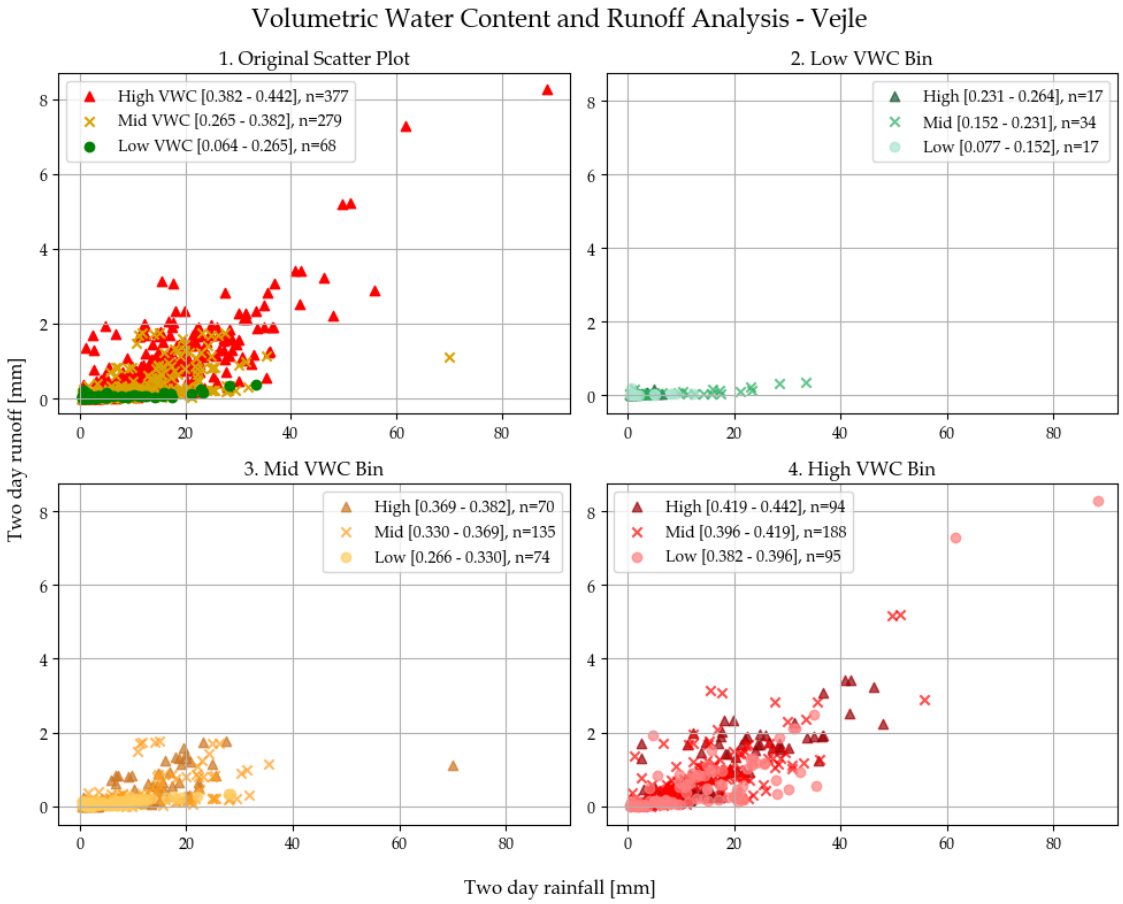

Figure 8.2. The *VWC and runoff analysis* for Vejle consisting of (1) total runoff/rainfall coloured by VWC, (2) runoff/rainfall in the low bin divided into three sub-intervals, (3) runoff/rainfall in the mid bin divided into three sub-intervals, and (4) runoff/rainfall in the high bin divided into three subintervals.

As shown in Figure 8.2, runoff in Vejle generally exhibit a strong response to rainfall, with two-day runoff values ranging from 0.00 to 8.20 mm. This is particularly pronounced in the high VWC category (cf. subplot "4. High VWC Bin"), which displays the broadest distribution of runoff values. Notably, the two highest runoff responses are found in the low subcategory within the high bin.
In contrast, the low and mid VWC categories (subplots "2. low VWC Bin" and "3. Mid VWC Bin") exhibit much narrower runoff ranges of 0.00 to approximately 0.50 mm in the low bin and up to 2.00 mm in the mid bin. In the low bin, a slight increase in runoff is visible when rainfall exceed 20 mm, while the increasing trend is more distinct in the mid bin. However, one data point deviates from the general trend, as a total rainfall of 70 mm only generates 1 mm runoff, which may be attributed to the resampling method.

Overall, Figure 8.2 indicates that under low VWC conditions, infiltration in Vejle remains dominant, while significant runoff tends to occur when VWC exceed approximately 0.33 m^3/m^3 (cf. subplot "3. Mid VWC Bin"). The runoff dynamics are further examined in terms of seasonal grouping, rainfall intensity, and VWC change during events in Figure 8.3.

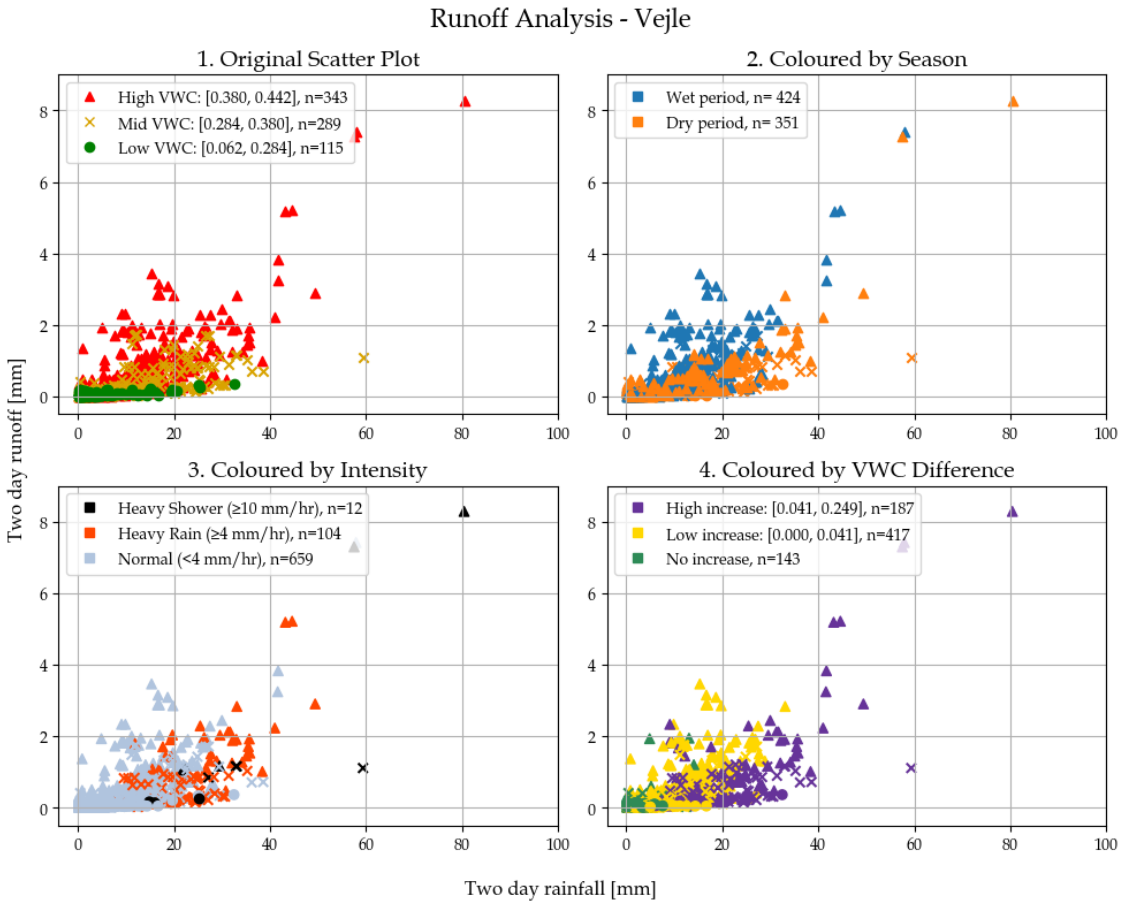

Figure 8.3. The runoff analysis for Vejle consists of runoff/rainfall coloured by (1) VWC, (2) wet/dry period, (3) rainfall intensity, and (4) change in VWC during the rainfall event.

Figure 8.3 shows that most data points fall within the wet period, during which the soil generally exhibits high VWC. This is evident from subplot "1. Original Scatter Plot" and "2. Coloured by Season" (see also section H.3, Figure H.18 for a more detailed overview of the seasonal runoff-rainfall relationship coloured by VWC). The majority of rainfall events are classified as normal intensity, with some categorised as heavy rain, and 12 as heavy showers (cf. subplot "3. Coloured by Intensity"). Notably, the highest runoff amounts occur during heavy shower events in the dry period (cf. subplot "2. Coloured by Season"), where both the VWC and the change in VWC are high, as seen in subplot "1. Original Scatter Plot", and "4. Coloured by VWC Difference". Generally, subplot 4 indicates a relatively clear relationship between two-day runoff and change in VWC. When no significant increase in VWC is observed, the trend appears relatively steep, indicating that even a small increase in two-day rainfall leads to immediate runoff. In contrast, data points with a high VWC increase show a more gradual slope, suggesting that a larger proportion of rainfall infiltrates the soil, thereby reducing runoff.

The observed differences in runoff are statistically supported by a Kruskal-Wallis test ($p = 6.2 \cdot 10^{-48}$), confirming statistically significant differences between the medians of the three VWC groups, which is also evident from the boxplot presented in Appendix I, section I.2. A Dunn's test ($\alpha_{adjusted}$=0.0166) identifies statistically significant differences between all

group pairs: high VWC vs. mid VWC ($p = 1.26 \cdot 10^{-24}$), high VWC vs. low VWC ($p = 3.14 \cdot 10^{-41}$), and mid VWC vs. low VWC ($p = 1.03 \cdot 10^{-8}$) VWC groups (cf. Appendix I, Table I.5).

To further evaluate rainfall-generated runoff at different VWC conditions, a *runoff ratio analysis* is performed and presented in Figure 8.4.

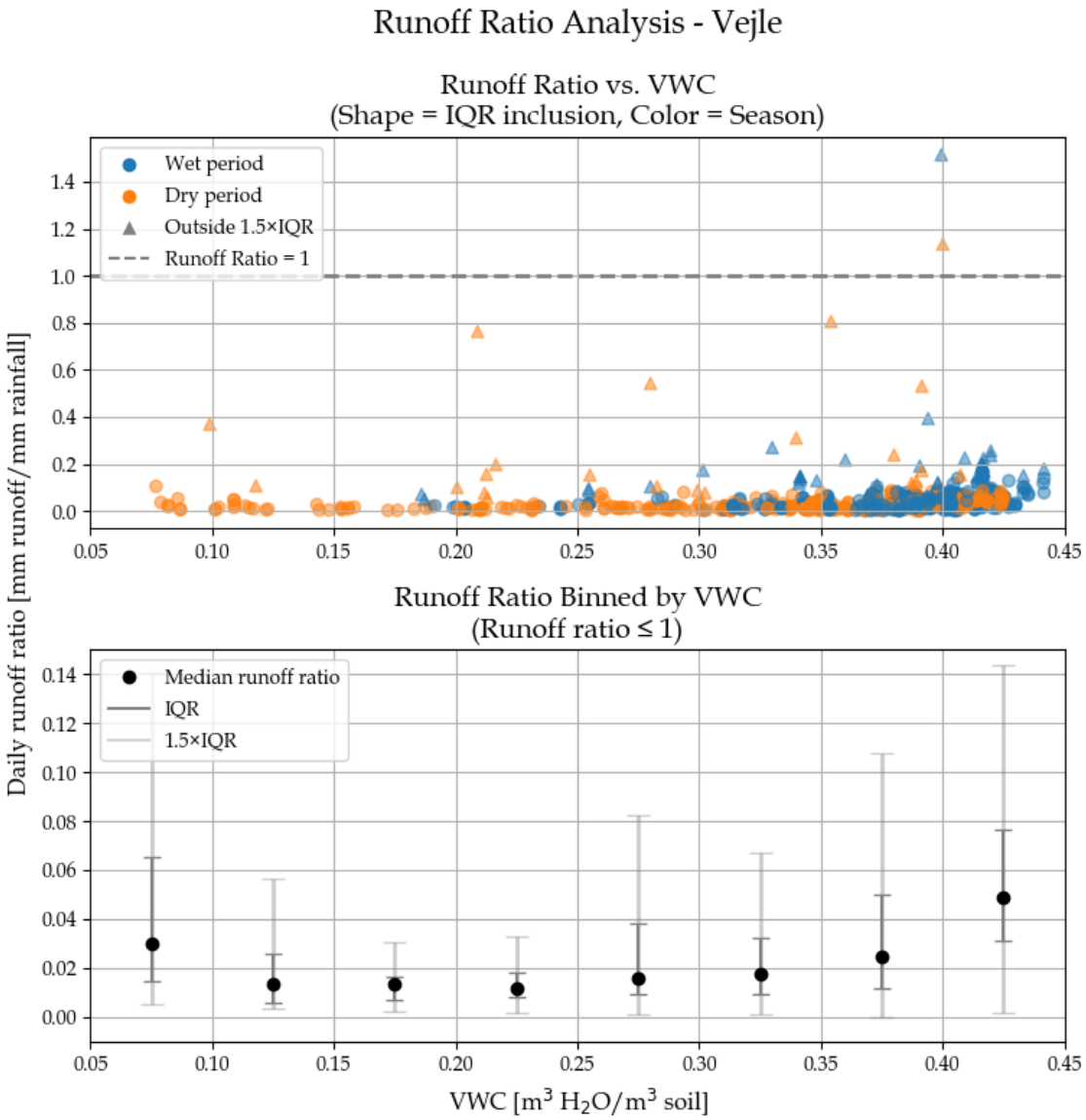

Figure 8.4. Ratio between the runoff and rainfall at different VWC levels in Vejle. Data points are coloured by wet (blue) and dry (orange) periods, and their shapes indicate whether they lie within or outside 1.5×IQR. Data points with a runoff ratio larger than 1 are removed from the lower plot. The median runoff ratio, the IQR and the 1.5×IQR for each of the intervals are shown.

From the upper plot in Figure 8.4, most data points exhibit a runoff ratio of 0.00-0.20 mm/mm. The lowest VWC conditions occur during the dry period, while the wet period primarily consists of higher VWC levels, although the dry period covers the entire range of VWC conditions. Within the wet period, a larger spread of runoff ratios is observed, including one data point with a runoff ratio of approximately 1.5 mm/mm.

In the lower plot, the runoff ratio is divided into eight VWC bins. The median runoff ratio ranges from approximately 0.01-0.05 mm/mm, with the largest variation observed in the bins representing the lowest and highest VWC levels. This indicates high infiltration and minimal runoff ratio when VWC is 0.15-0.25 m^3/m^3. In contrast, the runoff ratio increases significantly when VWC is either very low, suggesting that dry soils may exhibit hydrophobic behaviour, or exceeds 0.35 m^3/m^3, both resulting in minimal infiltration and thus increased runoff ratio. The widest range and highest median in runoff ratio are observed during the wet period at a VWC of 0.40-0.45 m^3/m^3, where the upper whisker extends above 0.14 mm/mm. This is likely due to the soil reaching saturation, which promotes increased surface runoff. Conversely, a large range is also observed at a low VWC of 0.05-0.10 m^3/m^3, which may be attributed to an interplay between the potential for hydrophobic soil conditions and the occurrence of high-intensity rainfall events.

The differences among the bins are supported by a Kruskal–Wallis test ($p = 1.73 \cdot 10^{-23}$), which reveals statistically significant differences among their medians. To determine which specific pairs differ, a Dunn's test is performed, revealing statistically significant differences between Bin 8 and Bins 2, 3, 4, 5, 6, and 7, respectively. Additionally, a statistically significant difference is observed between Bin 7 and Bin 4 (cf. Appendix I, Figure I.17). Furthermore, to examine whether a general monotonic relationship exists between runoff and VWC, as well as rain, and change in VWC, a Spearman's correlation analysis is performed and visualised in Table 8.1.

Table 8.1. Spearman's correlation for Vejle ($\alpha_{adjusted} = 0.0166$).

	Rain [mm]	**VWC** [m^3 H_2O/m^3 soil]	**ΔVWC** [m^3 H_2O/m^3 soil]
ρ	0.788	0.604	0.557
p-value	$2.6 \cdot 10^{-159}$	$2.40 \cdot 10^{-75}$	$3.83 \cdot 10^{-62}$

The Spearman's correlation analysis reveals a statistically significant monotonic relationship between rain and runoff, suggesting that higher rainfall generally leads to increased runoff. This aligns with expectations, as precipitation is the primary driver of surface runoff. Furthermore, statistically significant monotonic relationships are observed between runoff and VWC and between change in VWC and runoff. These findings suggest that both absolute VWC and changes in VWC influence runoff variations, likely due to their effect on the soil's infiltration capacity.

Main Findings

The runoff analysis and the corresponding statistical evaluation of parameters affecting runoff generally suggest that VWC is a key factor influencing runoff generation in the catchment, as large runoff responses do not necessarily coincide with the highest rainfall amounts, but rather occur when VWC is high, leading to both faster and greater runoff. Additionally, significant runoff tends to occur in Vejle when the VWC exceed approximately 0.33 m^3/m^3, while the *runoff ratio analysis* suggests that very dry conditions may also enhance runoff generation due to potential hydrophobic soil behaviour. Furthermore, runoff in Vejle is influenced not only by VWC but also by rainfall intensity and change in VWC, highlighting the importance of both antecedent and current soil VWC.

Thus, the analysis suggests that the soil in Vejle generally has a high capacity for rainwater infiltration but becomes saturated during prolonged rainfall events, promoting runoff.

However, it should be noted that the runoff separation method used in the analysis may carry a risk of underestimating actual runoff volumes, as it is designed to isolate only fast surface runoff. This may entail that a significant proportion of delayed or moderate quick surface runoff may be incorrectly classified as baseflow and therefore excluded from the runoff analysis. A sensitivity analysis of the alpha parameter in the separation algorithm is conducted and shows that adjustments primarily affect the magnitude rather than the pattern of runoff events (cf. section G.1), why the applied method is considered appropriate for the purpose of isolating rapid runoff dynamics.

Scale-Dependent Runoff Responses 9

This chapter examines how spatial scales affect the runoff response from an area, based on the runoff analysis conducted at hillslope scale (chapter 6), urban subcatchment scale (chapter 7) and hydrological scale (chapter 8). By comparing runoff responses under varying VWC conditions, rainfall intensities, and land use characteristics, the aim is to understand how scale influences both the magnitude and timing of runoff.
Accurately detecting runoff from the smallest monitored area, Ejby Mølle, is challenging due to the limited runoff volumes and the sensitivity of the installed water level sensors. Therefore, runoff from Ejby Mølle, and to some extent also from Elmelundsvej, may be underestimated or even lost in the analysis. In contrast, Lystrup, being a larger catchment, generates more runoff, which enhances the accuracy of the flow estimations from a measurement-technical perspective. Therefore, only Lystrup is included in the subsequent scale comparison. For the urban subcatchment scale, Christianshusvej is selected, as this area has the most comprehensive dataset.
Overall, different runoff dynamics are observed across the three scales, as illustrated by Figure 9.1. At both the hillslope and hydrological scales, runoff generation tends to be triggered under high VWC conditions, while the occurrence of outliers across all VWC groups underscores the complexity of runoff generation, which depends not only on soil moisture but also on rainfall intensity, duration and other environmental factors.

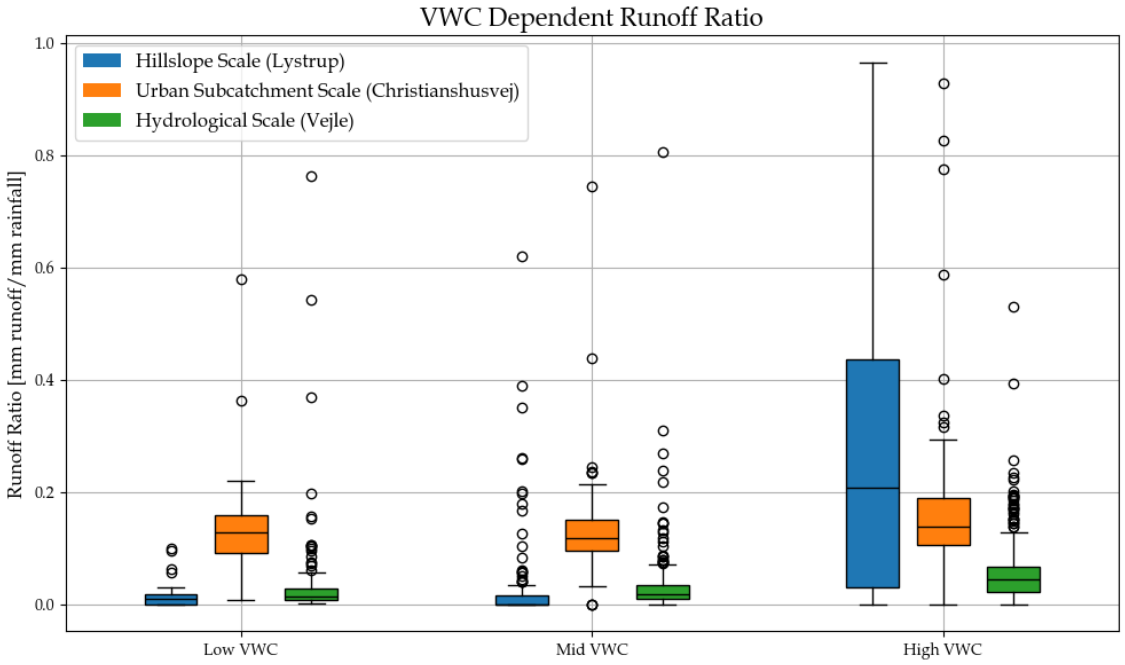

Figure 9.1. Boxplot of VWC dependent runoff ratio

Based on the runoff ratio analysis at the hillslope scale, it is evident that green urban areas can contribute notable amounts of runoff under certain conditions. Since the urban subcatchment runoff includes runoff from both impervious and pervious areas, masking the full effect of runoff from the green areas, it can be assumed that similar tendencies may apply to the green areas within these catchments. Thus, in an urban context, there is a risk that runoff from green areas may exceed the expected 10% contribution to the drainage system, potentially adding unexpected pressure to the system. However, runoff from green areas tends to occur with a delay compared to runoff from impervious surfaces. This time lag may result in staggered runoff peaks, which could help mitigate the momentary hydraulic pressure on the system.
This is supported by the *cross-correlation analysis*, which estimates a maximum delay between rainfall and runoff of 2 hours for both urban subcatchments, compared to 6 hours at the hillslope scale.

The runoff ratio analysis for the hydrological scale site (Vejle, Figure 8.4) indicates that up to 80% of rainfall can be converted into runoff in certain conditions. However, since this is a natural system with a large catchment, this finding cannot be directly translated to urban-scale systems.
Although hydrological and hillslope scales show similar delays (7 and 6 hours, respectively), the underlying causes differ due to the disparity in catchment size. At the hydrological scale, the delay is mainly driven by a long travel distance from both the outer edges of the catchment area to the stream and from the upstream part of the catchment to the measuring point in the stream. At hillslope scale, the delay is more strongly influenced by subsurface interflow processes, as discussed in chapter 6, section 6.4. Furthermore, due to the larger spatial extent of the hydrological-scale catchment, there is a greater possibility for water to evaporate or be intercepted by vegetation before it reaches the stream as surface runoff. This difference is also reflected in the *VWC and runoff analysis*. At the hydrological scale, the response curve is more gradual, and generally higher runoff amounts are observed under saturated conditions. At hillslope scale, however, substantial runoff is only generated when VWC exceeds 0.315 m^3/m^3, largely independent on daily rainfall amount. Moreover, the hydrological scale typically exhibits a greater hydrological memory compared to smaller scales. Hillslope-scale catchments tend to dry out and saturate more rapidly due to their limited spatial extent. In contrast, urban subcatchments are dominated by impervious surfaces, meaning soil processes are often less dominant in runoff generation, as discussed in chapter 7, section 7.3.
It is also observed at both hillslope and hydrological scales that moderate rainfall events can result in higher runoff ratios than intense rainfall events, particularly during wet periods when VWC is already elevated.

When comparing runoff across the three scales, it is important to acknowledge that even though the term contingent runoff is used consistently, the nature of the runoff may not be entirely the same across all scales.
At the hillslope and urban subcatchment scales, runoff is considered to be contingent in the sense that water flows over or just beneath the soil surface before entering the drain. In contrast, at the hydrological catchment scale in Vejle, the system is more complex. Here, runoff may include contributions from deeper flow paths, and it is not clear whether

increased flow is a result of rising groundwater levels or other subsurface processes. Water may move through a larger soil column before contributing to streamflow, meaning the mechanism behind the observed flow can differ significantly from the more direct surface or near-surface flows seen at smaller scales. Therefore, while the term contingent runoff is applied across all three scales, a direct one-to-one comparison may not be entirely accurate due to differences in the system's complexity and the runoff generation mechanisms. Furthermore, it is important to note that the runoff analysis at the hydrological scale is based on two-day accumulations of rainfall and runoff, whereas a one-day resolution is applied for the hillslope and urban subcatchment scale. This methodological difference may influence the comparability of the results.

The analysis is based on classifying the VWC into three bins, defined by quantiles rather than fixed threshold values. While an alternative approach could involve using specific, physically meaningful thresholds, such as field capacity or typical saturation levels during steady rainfall, this would require a site-specific assessment of each sensor due to variations in soil properties. The quantile-based approach is chosen as it does not rely on detailed knowledge of local soil characteristics. Furthermore, although some sensors may not provide accurate absolute VWC measurements, they reliably reflect relative changes over time, making quantiles a practical and robust classification method. A general limitation of using the quantile method is that, e.g. during very dry or wet periods, the bins may reflect unrealistic VWC classifications. An alternative strategy could be to use fixed VWC ranges or more than three bins, allowing for a more nuanced analysis. However, maintaining three consistent bins throughout the thesis enhances comparability and simplifies interpretation.

Furthermore, the resample method used in the runoff analysis can introduce some uncertainty in the relationship between the amount of precipitation and the associated runoff. Specifically, it may result in underestimations of runoff. Additionally, the method can cause "repetition" of data points, as the same event may be included multiple times in the plot. However, this approach is considered more accurate than using fixed time intervals, as fixed intervals risk "cutting off" events, thereby excluding either the onset or the end of precipitation. This omission could also introduce errors in the analysis.
An alternative could be a fully dynamic resample method, based on actual rainfall duration combined with the system's response delay. However, this too introduces uncertainty, as the delay times derived from *cross-correlation analysis* represent average behaviour and may not accurately reflect the lag during individual events.
Thus, by applying a semi-dynamic event definition, the method aims to capture entire rainfall-runoff responses more reliable, reducing the risk of missing delayed runoff responses in the sensors.

Finally, the comparative analysis shows that each spatial scale offers distinct insights, yet only the hydrological-scale site at Vejle combines the data quality, measurement reliability, and hydrological representativeness required for robust, process-based modelling. The hillslope sites are constrained by very small runoff volumes, while the urban subcatchments mix runoff from impervious and pervious areas, which makes it difficult to isolate and analyse the influence of soil moisture, which is a key focus of this thesis. By contrast, the Vejle catchment, containing large upstream areas which may generate substantial

runoff and contributes to the city's flooding issues (as discussed in section 4.3), provides continuous discharge records, clear VWC–runoff signals, and a spatial extent that can be linked meaningfully to regional forecasting. These factors, together with the need to improve early warning systems for flood-risk assessments, justify focusing all subsequent modelling efforts exclusively on the hydrological scale in Vejle.

Part II

Implementation of VWC and DI in Flow Modelling

Modelling Framework 10

As discussed in chapter 9, the analysis of contingent runoff at the hydrological scale showed a relationship between VWC and runoff. This finding can be essential in addressing the severe flooding issues in Vejle city centre, which are often driven by elevated water levels in Grejs Å. As mentioned in section 4.3, this issue is the primary motivation behind Vejle Municipality's and Vejle Spildevand's involvement in the Vandkant project.

In this part, it is examined whether it is possible to develop simple flow models for Grejs Å and whether incorporating VWC can improve model performance. Additionally, the potential of using the DMI Drought Index (DI) as an alternative to direct VWC measurements is explored. The potential of using the DI is explored due to its free access and nationwide availability. Accurate flow modelling in Grejs Å can, for example, be valuable for flood risk management or early warning systems in Vejle. The focus is deliberately placed on simple flow models, as they are easy to implement and fast to simulate. Moreover, this makes the implementation of VWC and DI more straightforward, making them particularly suitable for practical applications such as flood management, where rapid model calibration with new live data may be required. The models examined in this thesis include:

- **Linear Regression Model** - chapter 11
- **Extended Time-Area Model** - chapter 12
- **Linear Reservoir Model** - chapter 13

The Linear Regression Model is a simple statistical model that uses data sampling methods and VWC classifications from the Location Analysis (see Part I) to fit a linear relationship between rainfall and runoff. It is chosen for its simplicity, accessibility, and direct linkage to the prior analysis. Like the analysis, the model operates on a two-day resolution and aims to predict runoff as a function of rainfall.

The Extended Time-Area Model is a more area-specific but still relatively simple model. Here, the Vejle catchment is divided into 26 subcatchments using the commercial tool Scalgo Live. Based on the Time-Area method, each subcatchment contributes to the flow at different times, depending on its distance and travel time to the outlet. This model uses a slightly finer resolution, with a daily time step.

The Linear Reservoir Model is a classic conceptual hydrological model that does not require external commercial tools like Scalgo Live. It represents the catchment as a series of reservoirs that store and release water, simulating the delayed response of runoff. With an hourly time step, this model is particularly suitable for flood forecasting, aligning with the needs of Vejle Municipality and Vejle Spildevand.

10.1 Model Inputs

All three models are based on rainfall, catchment area, and flow data specific to the Grejs Å catchment. The rainfall input, consistent with the approach used in the analysis, is represented by the average intensity recorded at the two rain gauges 5230 Jelling and 5235 Vejle Centralrenseanlæg, assuming each gauge represents 50% of the catchment area. The catchment area, also consistent with the analysis, is estimated to be 78 km^2, based on delineation using Scalgo Live. In the Extended Time-Area Model, Scalgo Live is additionally used to divide the catchment into multiple subcatchments, each assigned a corresponding flow path length [Scalgo, 2024]. All models are calibrated and validated against the Q/H-derived flow data at Station 32.22. This station is selected due to its strategic location just upstream of Vejle city centre, making it especially relevant for flood forecasting. Furthermore, real-time flow measurements from a flow sensor are available at the same location, allowing for model evaluation using both estimated and measured flow data.

Rainfall and flow data are standard inputs in hydrological modelling and are widely available across Denmark. However, through the VandKant project, several VWC sensors have been installed, enabling investigation of this parameter's applicability in flow modelling. In the models, the focus is on incorporating VWC and DI and exploring their impact on flow modelling. The impact of other model inputs, such as rainfall and catchment area, is not examined.

10.2 Incorporating VWC in the Models

This section describes how VWC is incorporated into the Extended Time-Area Model and the Linear Reservoir Model. The incorporation of VWC in the Linear Regression Model is explained in chapter 11.

In both the Extended Time-Area Model and the Linear Reservoir Model, the rainfall input (P) is multiplied by the catchment area (A). However, not all of the catchment is expected to contribute to runoff due to factors such as infiltration, evaporation, and urban water management. To account for this, an area regulation factor (C_x) is introduced. This calibration parameter scales the contributing area and can range between 0 (no contribution) and 1 (full contribution).

The effect of the VWC is introduced by adding multiple area regulation factors (C_1, C_2 and C_3), which will regulate the contributing area based on the VWC measurement. The VWC is classified into three intervals, as defined in the analysis in section 5.4:

- C_0 = Baseline
- C_1 = Low VWC: $VWC < 0.28$ m^3/m^3
- C_2 = Mid VWC: $0.28 < VWC < 0.38$ m^3/m^3

- C_3 = High VWC: $VWC > 0.38$ m^3/m^3

The constants C_1, C_2, and C_3 are also calibration parameters, each representing the proportion of the catchment area contributing under different soil moisture conditions.

10.3 Incorporating DI in the Models

The Drought Index (DI) is a nationwide model, developed by the Danish Meteorological Institute (DMI), which is used to estimate the water content in the topsoil. In the model, the soil reservoir size is assumed to be 100 mm, representing an average value for all of Denmark. The DI ranges from 0 to 10, where 0 indicates the soil is saturated and 10 indicates completely dry soil [DMI, 2025]. The DI is converted into a water content percentage (WC), representing the relative water content in the soil. The conversion is performed using Equation 10.1:

$$WC = \frac{10 - DI}{10} \tag{10.1}$$

Now, the WC ranges from 0 to 1, where 0 indicates completely dry soil and 1 indicates the soil is saturated. The converted drought index WC will be utilised in the flow models but will be referred to as DI.

To assess whether the DI can serve as an alternative to the VWC measurements, a Pearson correlation analysis is performed, as shown in Figure 10.1.

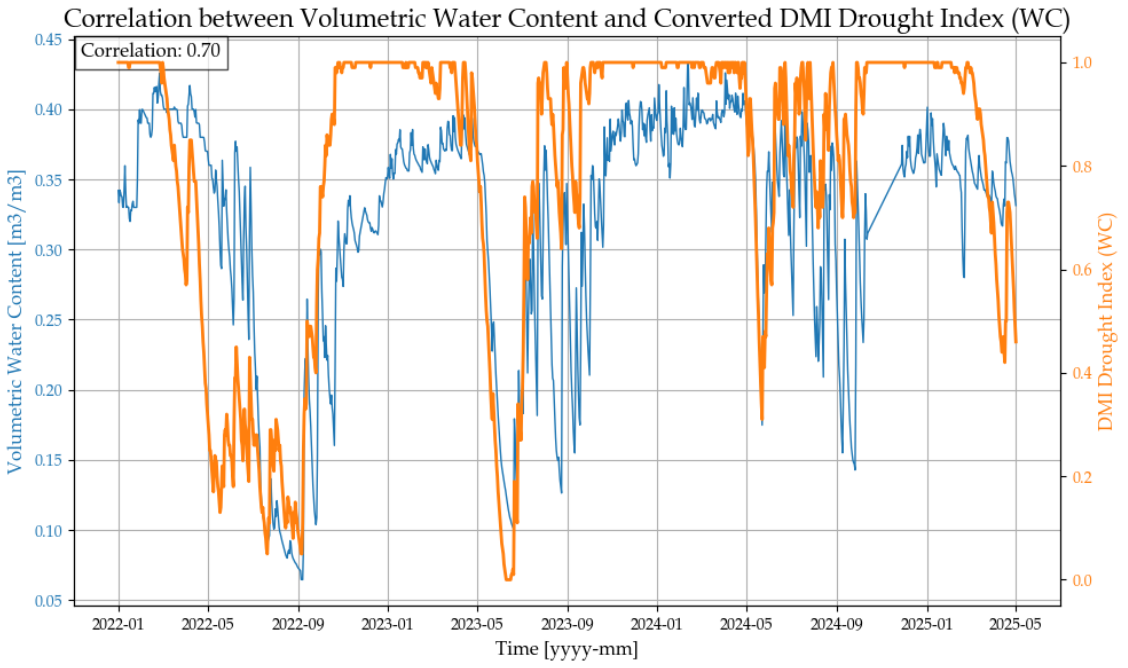

Figure 10.1. Pearson correlation between volumetric water content measurements from sensor 6 Mark-kant (Blue) and the converted DMI drought index (WC) from Vejle (Orange).

The VWC measurements and the DI exhibit a reasonably strong positive correlation, with a correlation coefficient of 0.70. Based on this, it is logical to explore whether DI is applicable in flow modelling.

The WC values are used similarly to the VWC measurements by classifying them into three bins: low, mid, and high. The low threshold is defined as the 25th percentile of DI. The high threshold is set at 1, corresponding to a saturated soil, and the 65th percentile and the mid bin include the values between the lower and upper threshold (40% of the data). The area regulation factors (C_x) will regulate the contributing area based on the DI:

- C_0 = Baseline
- C_1 = Low DI: $DI < 0.7725$
- C_2 = Mid DI: $0.7725 < DI < 1$
- C_3 = High DI: $DI = 1$

10.4 Calibration and Validation

To ensure that the runoff models are both robust and comparable, they are calibrated against two years of observations from 01-05-2022 to 01-05-2024, based on the following four data sets:

- Q/H-estimated flow data at Station 32.32
- Precipitation data (gauge 5235 Vejle Centralrenseanlæg and gauge 5230 Jelling)
- VWC data measured by Sensor 6
- DMI Drought Index data for the Vejle area

A two-year calibration period is applied to minimise the risk of overfitting. The Linear Reservoir Model and the Extended Time-Area Model are calibrated using the 'L-BFGS-B' auto-calibration method, which minimises the RMSE performance metric. The Linear Regression Model is not auto-calibrated; instead, the linear regression is fitted on the data from the calibration period and subsequently applied to the validation period.

The models are validated using flow data from St. 32.22 covering the period 01-05-2024 to 01-05-2025 (one year). A full year is selected for validation to ensure that the models can accurately predict flow under both dry and wet conditions. The model performance is assessed both visually and through performance metrics such as RMSE and NSE, as described below.

Model Performance Metrics

To quantify the model's fit to the observed flow, and to enable comparison between the models, the Root Mean Square Error (RMSE) and the Nash–Sutcliffe Model Efficiency

(NSE) Coefficient are calculated.

The RMSE describes the magnitude of the difference between observed and modelled values, and the metric is particularly sensitive to large errors, which can occur during the peak flow events. The RMSE is calculated as described in Equation 10.2.

$$RMSE = \sqrt{\frac{\sum_{i=1}^{n}(O_i - M_i)^2}{N}} \tag{10.2}$$

Where:

O_i	Observed
M_i	Modelled
N	Sample size

The RMSE ranges from 0 to ∞, where lower values indicate a better fit and RMSE = 0 represents a perfect match between model and observation [Ritter and Muñoz-Carpena, 2013].

The Nash–Sutcliffe Efficiency (NSE) describes how well the model captures the variability of the observed data. It is particularly sensitive to differences between the observed and modelled time series in both the timing (x-direction) and magnitude (y-direction) of flow. This means that even small shifts in time or flow volume can significantly impact the NSE. The NSE is calculated as described in Equation 10.3.

$$NSE = 1 - \frac{\sum_{i=1}^{N}(O_i - P_i)^2}{\sum_{i=1}^{N}(O_i - \overline{O})^2} = 1 - \left(\frac{RMSE}{SD}\right)^2 \tag{10.3}$$

Where:

$\overline{O}$	Mean of observed data
SD	Standard deviation

The NSE ranges from $-\infty$ to 1, where higher values indicate a better model fit, and NSE = 1 corresponds to a perfect fit. If NSE $\leq$ 0, the mean of the observed data provides a better prediction than the model [Ritter and Muñoz-Carpena, 2013].

Linear Regression Model

11

The Linear Regression Model is based on the runoff analysis presented in Part I, and the resampling method, described in Part I, is applied on the data.

11.1 Model Setup of the Linear Regression Model

A linear regression line is fitted to the data to describe the two-day runoff as a function of rainfall. The resulting linear regression and corresponding R^2 value can be seen in Figure 11.1.

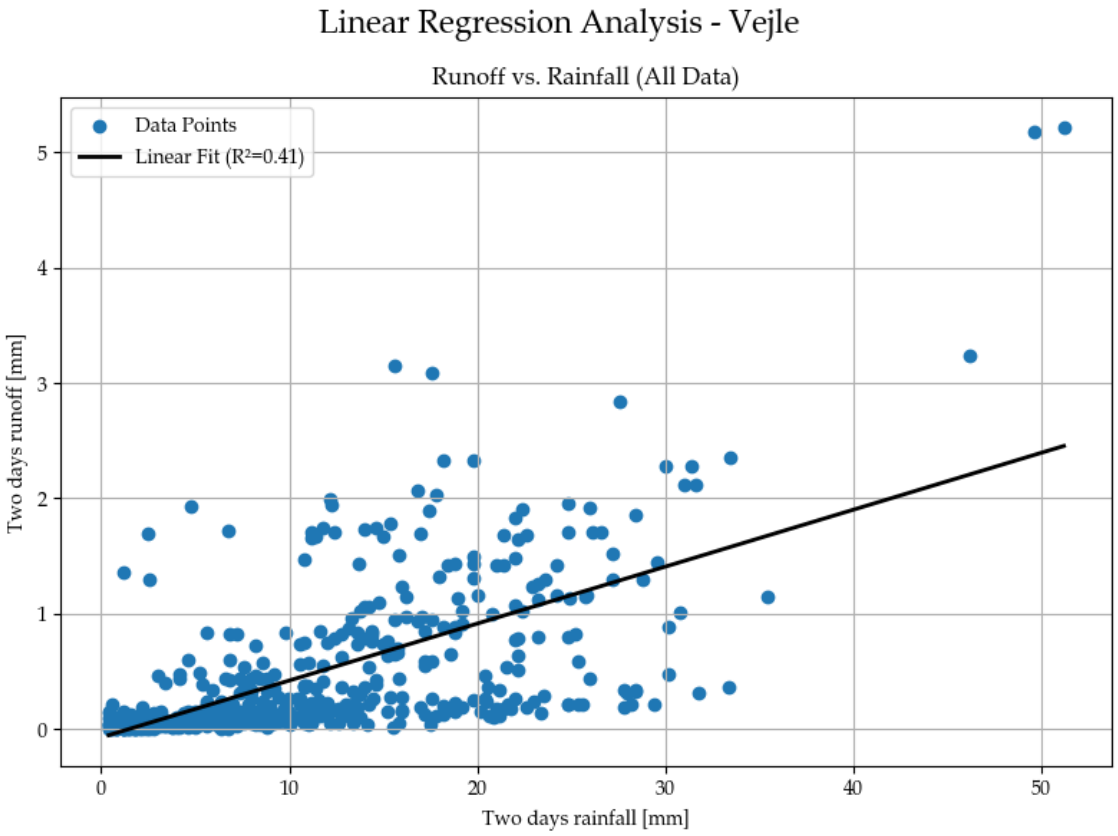

Figure 11.1. Linear Regression Model for the runoff analysis of Vejle

The data points exhibit a reasonably linear trend, with a R^2 value of 0.41. The

corresponding regression equation is:

$$y = 0.0551x - 0.1411 \tag{11.1}$$

Incorporating VWC into the Linear Regression Model

To assess the impact of VWC, a separate linear regression is applied to each of the VWC bins defined in the runoff analysis. The regression lines and their respective R^2 values for each VWC bin are shown in Figure 11.2.

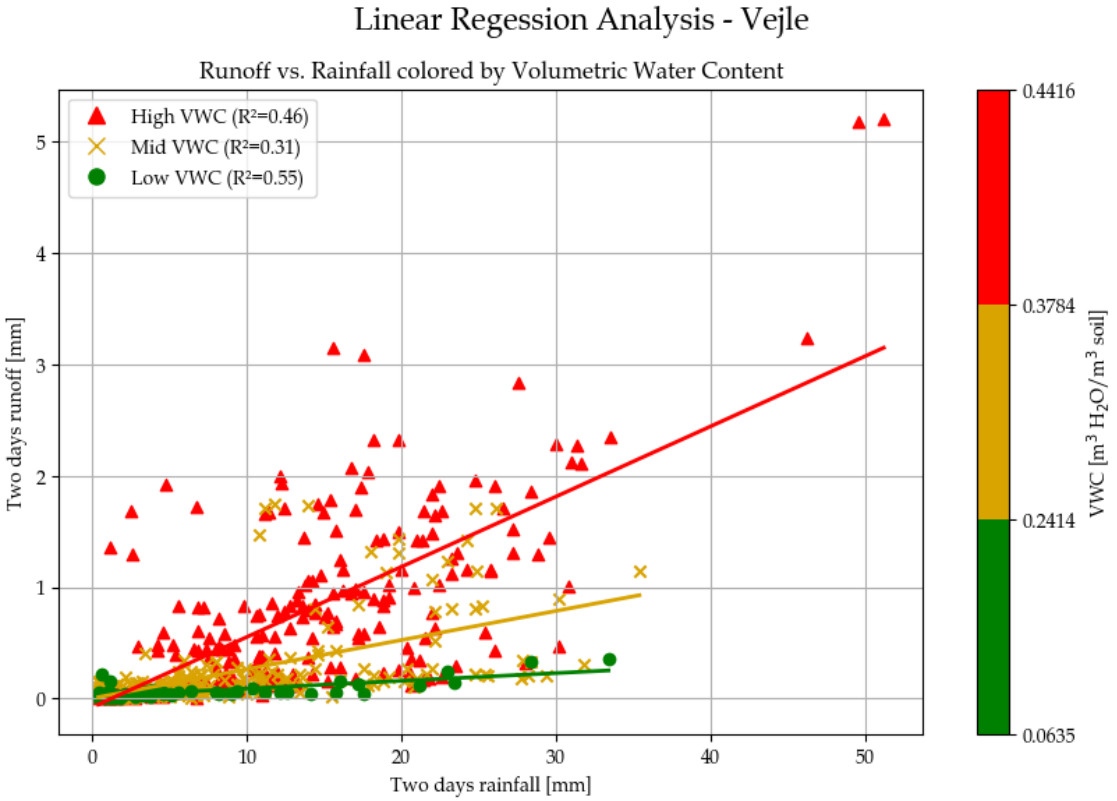

Figure 11.2. Linear Regression Model of runoff as a function of rainfall, coloured by VWC.

It is seen that the high and low VWC bins follow a reasonably linear trend, with R^2 values of 0.46 and 0.55, respectively. In contrast, the mid VWC bin is less well described by a linear trend ($R^2 = 0.31$), likely due to the large spread of scattered data points. The corresponding regression equations for the three VWC bins are:

- High VWC: $y = 0.0700x - 0.1026$
- Mid VWC: $y = 0.0283x - 0.0162$
- Low VWC: $y = 0.0078x + 0.0168$

Using both the overall regression equation and the bin-specific equations, the two-day runoff (y) is estimated based on the two-day rainfall (x).

Incorporating DI into the Linear Regression Model

As presented in section 10.3, DI is explored as an alternative to the VWC measurements. The linear regressions for each of the DI bins are illustrated in Figure 11.3.

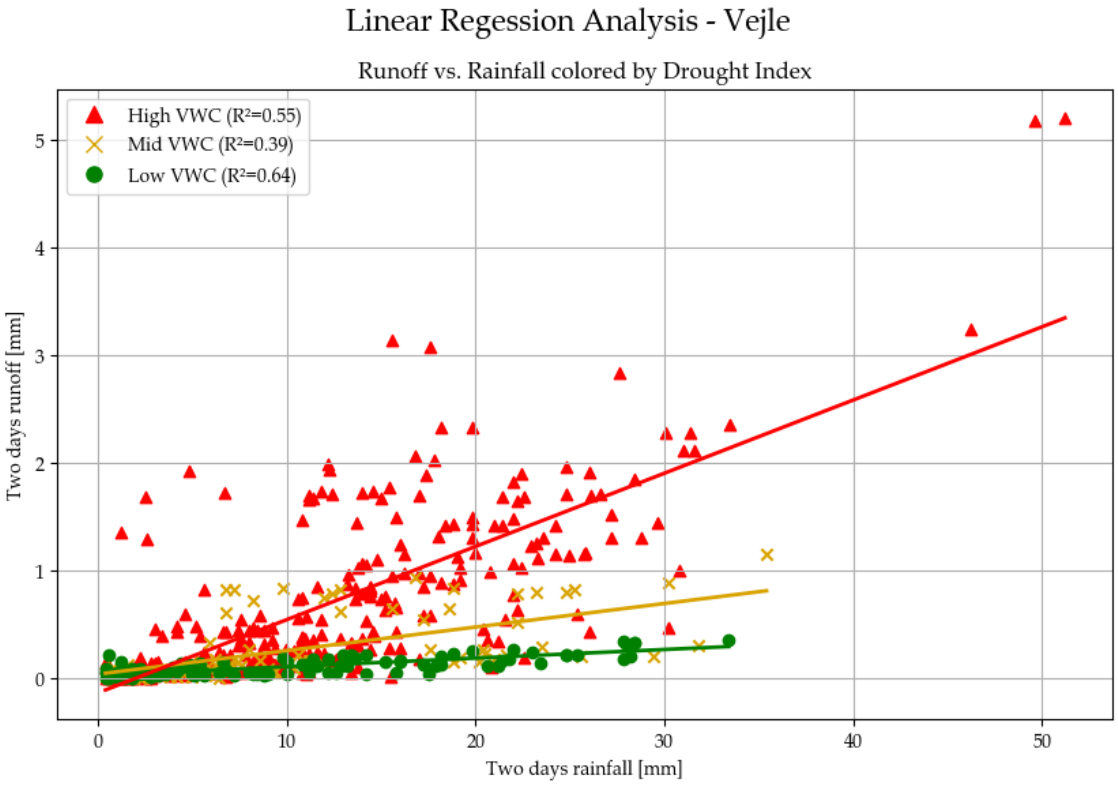

Figure 11.3. Linear Regression Model of runoff as a function of rainfall, coloured by DI.

It is seen that the high and low DI bins show a relatively strong linear trend, with R^2 values of 0.55 and 0.64, respectively. In contrast, the mid bin is less well described by a linear trend ($R^2 = 0.39$), primarily due to a high spread of data points within this range. The corresponding regression equations for the three DI bins are:

- High DI: $y = 0.0767x - 0.1744$
- Mid DI: $y = 0.0228x + 0.0084$
- Low DI: $y = 0.0086x + 0.0267$

11.2 Runoff Predictions from the Linear Regression Model

The Linear Regression Models: baseline, including VWC, and including DI are compared to the estimated runoff to Grejs Å during the validation period, as presented in Figure 11.4. The lower plot illustrates the difference between modelled and estimated runoff, where positive values indicate overestimation by the model and negative values

indicate underestimation. For all models, the NSE and RMSE values have been calculated to assess performance.

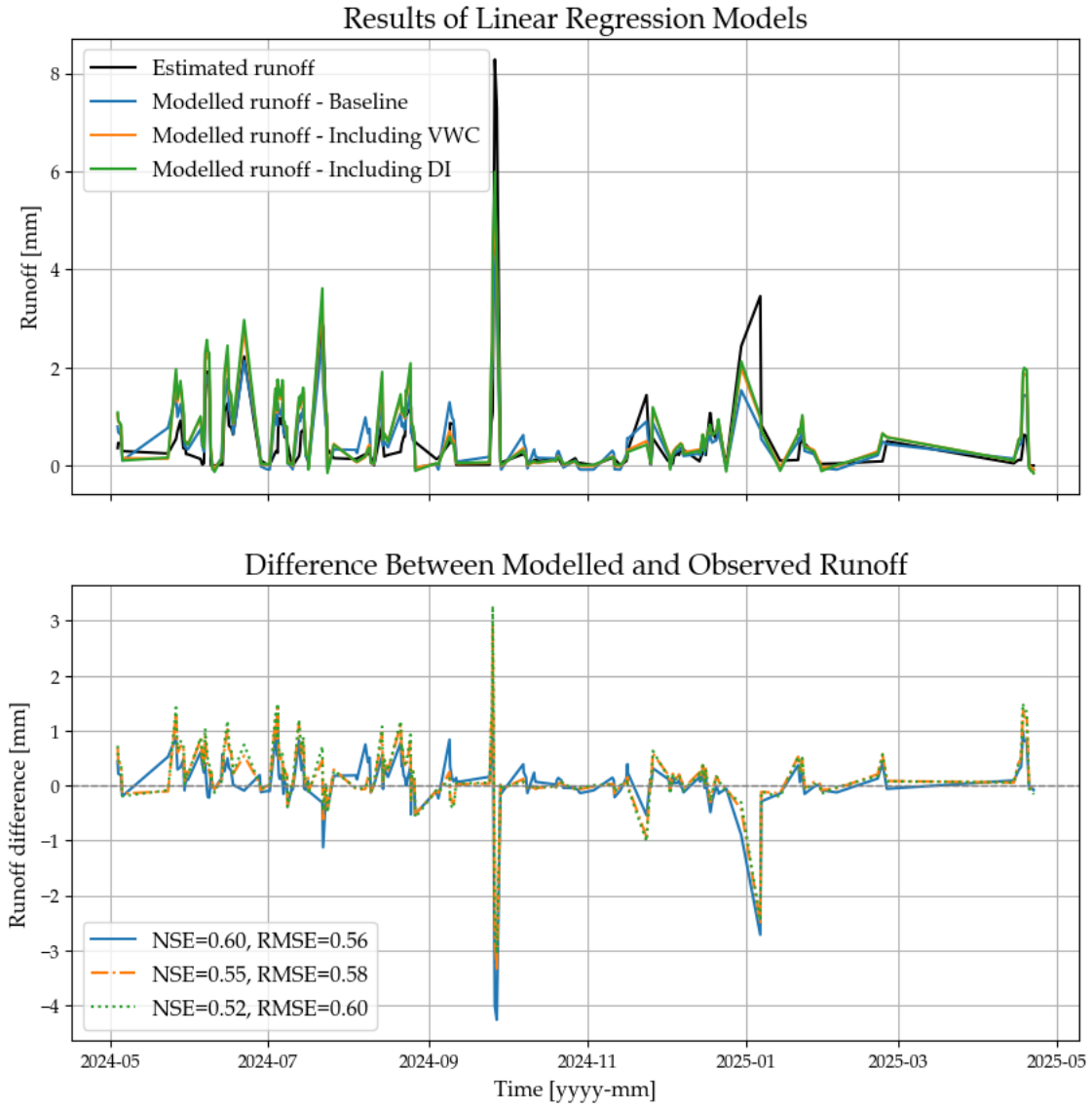

Figure 11.4. Observed flow compared with Linear Regression Models: baseline, including VWC, and including DI (upper plot), and corresponding differences (lower plot). The NSE and RMSE are shown for all models.

From Figure 11.4, it is evident that all models follow the overall pattern of the estimated runoff reasonably well. Furthermore, the NSE and RMSE values are very similar, with the baseline model exhibiting the best performance, while the model including DI exhibits the worst performance, however, only slightly worse (cf. Table 11.1). This suggests that including VWC or DI does not necessarily improve the overall model accuracy:

Table 11.1. Overview of the NSE and RMSE values for the validation period for the Linear Regression Models.

Parameter	Baseline	Including VWC	Including DI
NSE	0.60	0.55	0.52
RMSE	0.56	0.56	0.60

All models tend to overestimate runoff during the dry period, especially the model including VWC and DI, while runoff is generally underestimated during the wet period, especially during peak runoff, mostly by the baseline model. Most deviations between modelled and estimated runoff range from -1 to 1 mm of runoff. However, larger discrepancies occur during high-runoff events, with differences reaching and underestimation of up to 4 mm, as clearly seen in the lower plot. Additionally, it is important to notice that the observed peak error of approximately 3 mm in September 2024 is caused by a time lag between modelled and estimated runoff. Thus, although the baseline model provides a slightly better overall fit, the model including DI provides slightly better estimates at peak runoff. Furthermore, it is important to notice that the observed peak error of approximately 3 mm in September 2024 is caused by a time lag between modelled and estimated runoff.

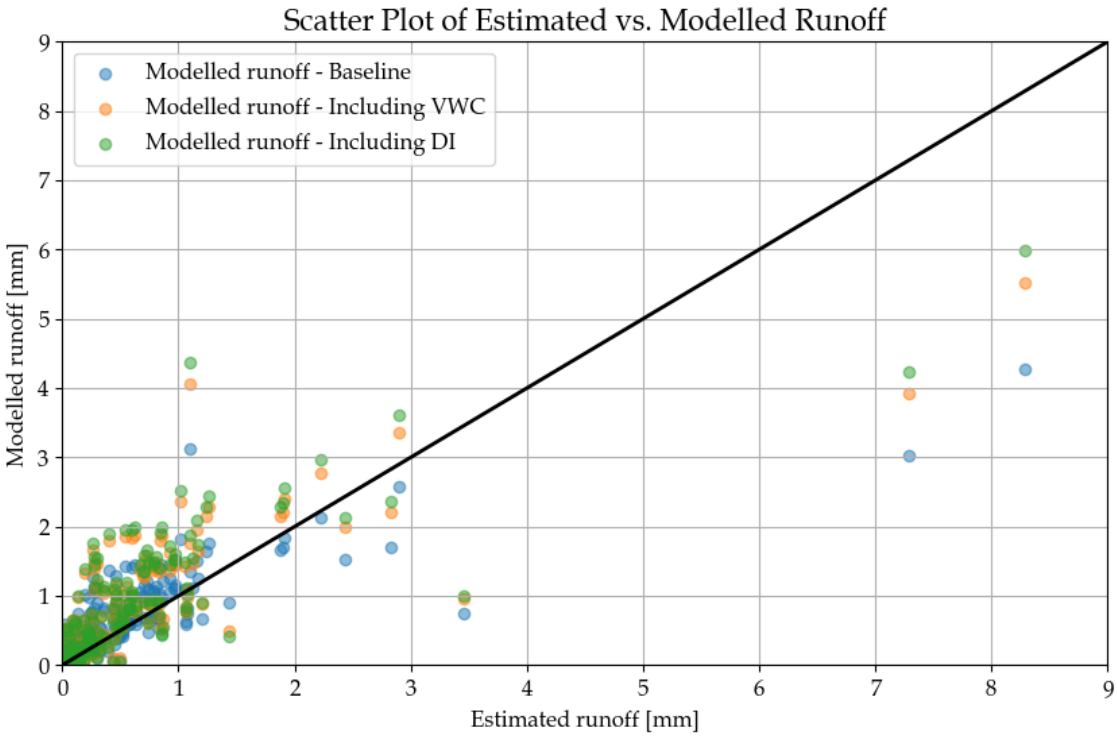

Figure 11.5. Scatter plot comparing observed flow with modelled flow from the Linear Regression Models for baseline, including VWC, and including DI. The 1:1 line indicates a perfect match between observed and modelled values. Points above the line represent overestimation, while points below indicates underestimation.

To further assess the performance of the Linear Regression Model, a scatter plot comparing estimated and modelled runoff for all three models is presented in Figure 11.5. This

visualisation supports a more detailed analysis of the model accuracy and reveals potential systematic deviations.
It is evident that models generally follow the 1:1 line for lower runoff values, with some degree of overestimation (especially when VWC and DI are included, with DI generally exhibiting the greatest overestimations), indicating a good fit for smaller events. However, for higher runoff values, all models tend to underestimate the modelled runoff, as seen by the clustering of points below the 1:1 line. This underestimation is more distinct for the model excluding VWC, while DI exhibit the "lowest" underestimation.
Thus, the scatter plot in Figure 11.5 suggests that including both VWC and DI does not consistently improve performance across all event magnitudes. The inclusion of DI slightly improves performance when estimating peak runoff, whereas the baseline model demonstrates a better overall performance. These observations support the findings from Figure 11.4 and the associated NSE and RMSE values.

Main Findings
Although VWC is expected to enhance runoff modelling, based on the slightly better fit of the linear regressions, the Linear Regression Model shows a minor decrease in performance when VWC is included, compared to the baseline model using only precipitation. This may be attributed to the simplified model structure of the linear regression approach, which may not fully utilise the added information from VWC. Furthermore, the model including DI exhibits the overall weakest performance, however, it performs slightly better during high flow events. This suggests that DI may serve as a viable alternative to local VWC sensors in simple runoff models, especially if the objective is to capture peak runoff events. Overall, the difference in performance between the three model setups is so minor that it is debatable whether a true difference exists in practice.

Extended Time-Area Model 12

The Time-Area concept is used to build an Extended Time-Area Model that uses the effective precipitation (precipitation ($P(t)$) - potential evaporation ($E(t)$)) to predict the flow (Q_{total}) in Grejs Å, Vejle.

12.1 Model Setup of the Extended Time-Area Model

The Time-Area method can be described as an extended rational method where the contributing area is divided into a number (n) of subcatchments. By dividing the area into subcatchment areas (A), the method can reveal not only the peak design flow but also a hydrograph of flow against time. A conceptual understanding of the Extended Time-Area Model is illustrated in Figure 12.1. For simplicity, the conceptual figure is based on only three subcatchments.

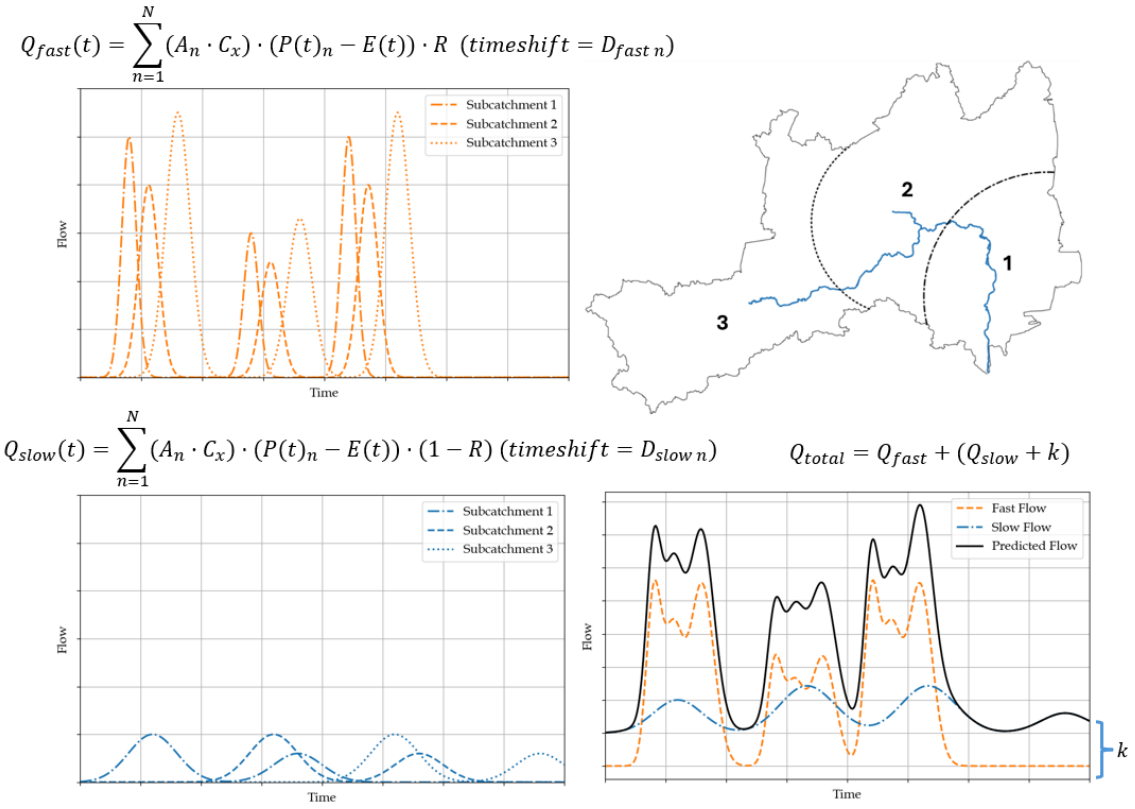

Figure 12.1. Conceptual figure of the Extended Time-Area Model setup simplified to three subcatchments as an example.

Where:

$Q_{fast}(t)$	Fast flow	[m^3/d]
$Q_{slow}(t)$	Slow flow	[m^3/d]
$Q_{total}(t)$	Total flow	[m^3/d]
R	Regulation constant separating Q_{fast} and Q_{slow}	[-]
C_x	Area regulation factor	[-]
n	Number of subcatchments	[-]
$P(t)_n$	Measured precipitation n	[m^3/d/m^2]
$E(t)$	Calculated potential evapotranspiration	[m^3/d/m^2]
A_n	Contributing area for subcatchment n	[m^2]
$D_{fast\,n}$	Time delay for fast flow for subcatchment n	[d]
$D_{slow\,n}$	Time delay for slow flow for subcatchment n	[d]
L_n	Flow path length for subcatchment n	[m]
V_{fast}	Time of concentration for $Q_{fast}(t)$	[m/d]
V_{slow}	Time of concentration for $Q_{slow}(t)$	[m/d]

In the Extended Time-Area Model, the flow from each subcatchment is divided into a fast component (Q_{fast}) and a slow component (Q_{slow}). This division is governed by the constant R, a calibration parameter ranging between 0 and 1. The main difference between the fast flow (runoff) and slow flow (baseflow) is the time of concentration, denoted as V_{fast} and V_{slow}, which are also subject to calibration. The time delays (D) for flow contributions from the various subcatchments are calculated based on flow path lengths (L) and the times of concentration, as shown in Equation 12.1 and Equation 12.2.

$$D_{fastflow\,n} = \frac{L_n}{V_{fast}} \tag{12.1}$$

$$D_{baseflow\,n} = \frac{L_n}{V_{slow}} \tag{12.2}$$

The predicted flow in the model is the sum of the fast and slow flow components, with an added constant k to account for baseflow generated prior to the modelling period. The model operates with a daily time step, as it becomes overly sensitive when a finer temporal resolution is applied. The catchment is divided into 26 subcatchments based on flow path lengths derived from the Length/Area Histogram in SCALGO Live [Scalgo, 2024]. These subcatchments and their associated flow path lengths are illustrated in Figure 12.2.

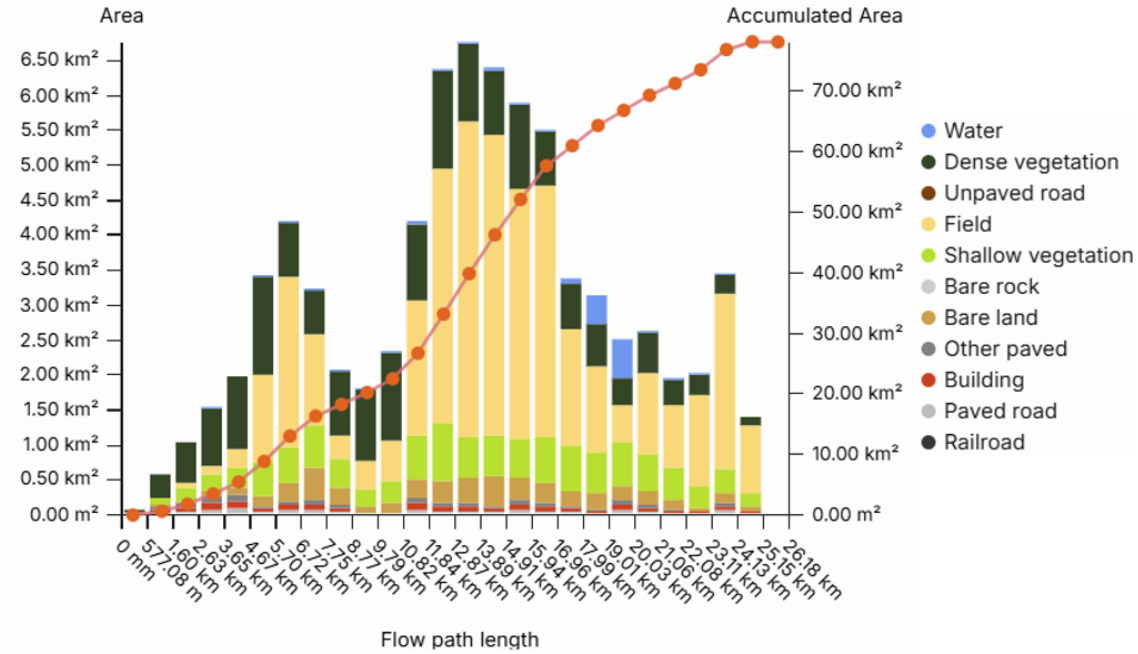

Figure 12.2. Land use distribution along the flow path of Grejs Å catchment area. Bars show the area (km^2) and land use type of each catchment area, while the red line indicates the accumulated contributing area. [Scalgo Live, 2025].

To illustrate the subdivision of the catchment, the 14 subcatchments with flow path lengths shorter than 13.89 km are shown in Figure 12.3.

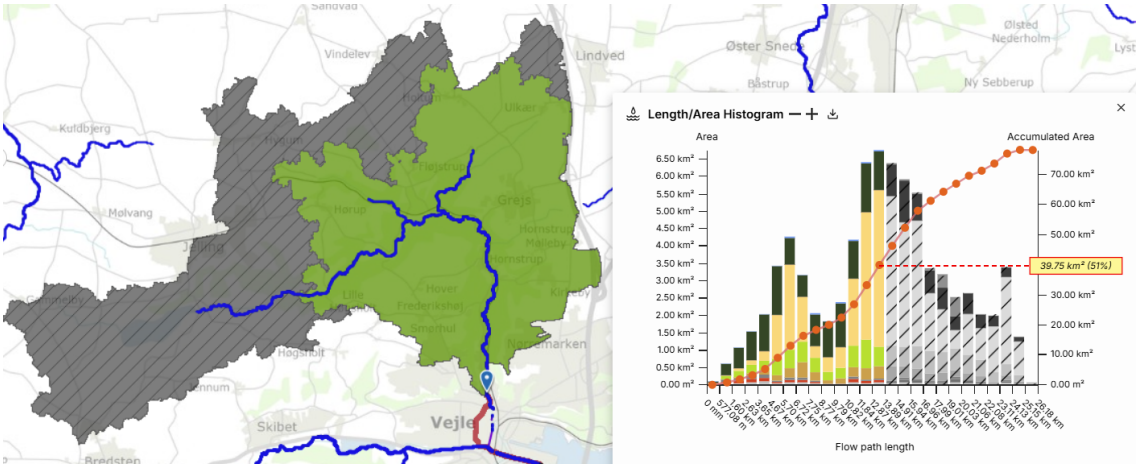

Figure 12.3. Illustration of the catchment division in Scalgo live. The green area represents 14 subcatchments, where the 14th subcatchment has a flow path length of 13.89 km to the measurement station 32.22.

In this way, each of the 26 subcatchments is divided. Within each subcatchment, precipitation and flow behaviour are assumed to be identical, despite differences in land use, soil type, and composition. An area regulation factor (C_x) is applied to each subcatchment, as it is assumed that not all precipitation contributes to flow. Additionally, the potential evaporation (E_t) is assumed to be uniform across the entire hydrological catchment. The calculation of the potential evaporation is described in Appendix K.

Calibration of the Extended Time-Area Models

Three Extended Time-Area Models are developed: a baseline model, a model including VWC, and a model including DI. All models are auto-calibrated to minimise the RMSE value. The calibration parameters and the calibration results are described and illustrated in Appendix L, section L.1.

Table 12.1. Calibration parameters of the Extended Time-Area Model.

Parameter	Baseline	Including VWC	Including DI
V_{fast}	8850.00	8850.00	8850.00
V_{slow}	995.00	995.00	995.00
X	0.36	0.46	0.49
c_0	0.91	-	-
c_1	-	0.02	0.01
c_2	-	0.53	0.18
c_3	-	0.87	0.78

A cross-correlation analysis between the modelled and observed flow reveals a lag time of zero days (cf. section L.1, Figure L.3). Therefore, no recalibration of the Extended Time-Area Model is performed.
The RMSE and the NSE values from the calibration of the three Extended Time-Area Models are presented in Table 12.2 below.

Table 12.2. Overview of the NSE and RMSE values for the calibration period for the Extended Time-Area Models.

Parameter	Baseline	Including VWC	Including DI
NSE	0.55	0.71	0.73
RMSE	1.02	0.81	0.79

From the calibration process, it is evident that both the model using the VWC and the model using the DI yield better NSE and RMSE values.

12.2 Flow Predictions from the Extended Time-Area Model

The Extended Time-Area Model is applied in the three configurations: the baseline model, the model including VWC, and the model including DI. Their performance is compared to observed flow in Grejs Å during the validation period, as shown in Figure 12.4. The lower plot of the figure presents the difference between the modelled and observed flow, where positive values indicate overestimations and negative values indicate underestimations. The NSE and RMSE values for each model are presented in Table 12.3 below.

Table 12.3. Overview of the NSE and RMSE values for the validation period for the Extended Time-Area Models.

Parameter	Baseline	Including VWC	Including DI
NSE	0.29	0.44	0.67
RMSE	1.01	0.90	0.69

It is evident from Figure 12.4, that both the VWC and DI models capture the general pattern of the observed flow more accurately than the baseline model, which shows the greatest deviation. The model including DI provides the best overall performance based on both NSE and RMSE, while the baseline model provides the weakest performance.

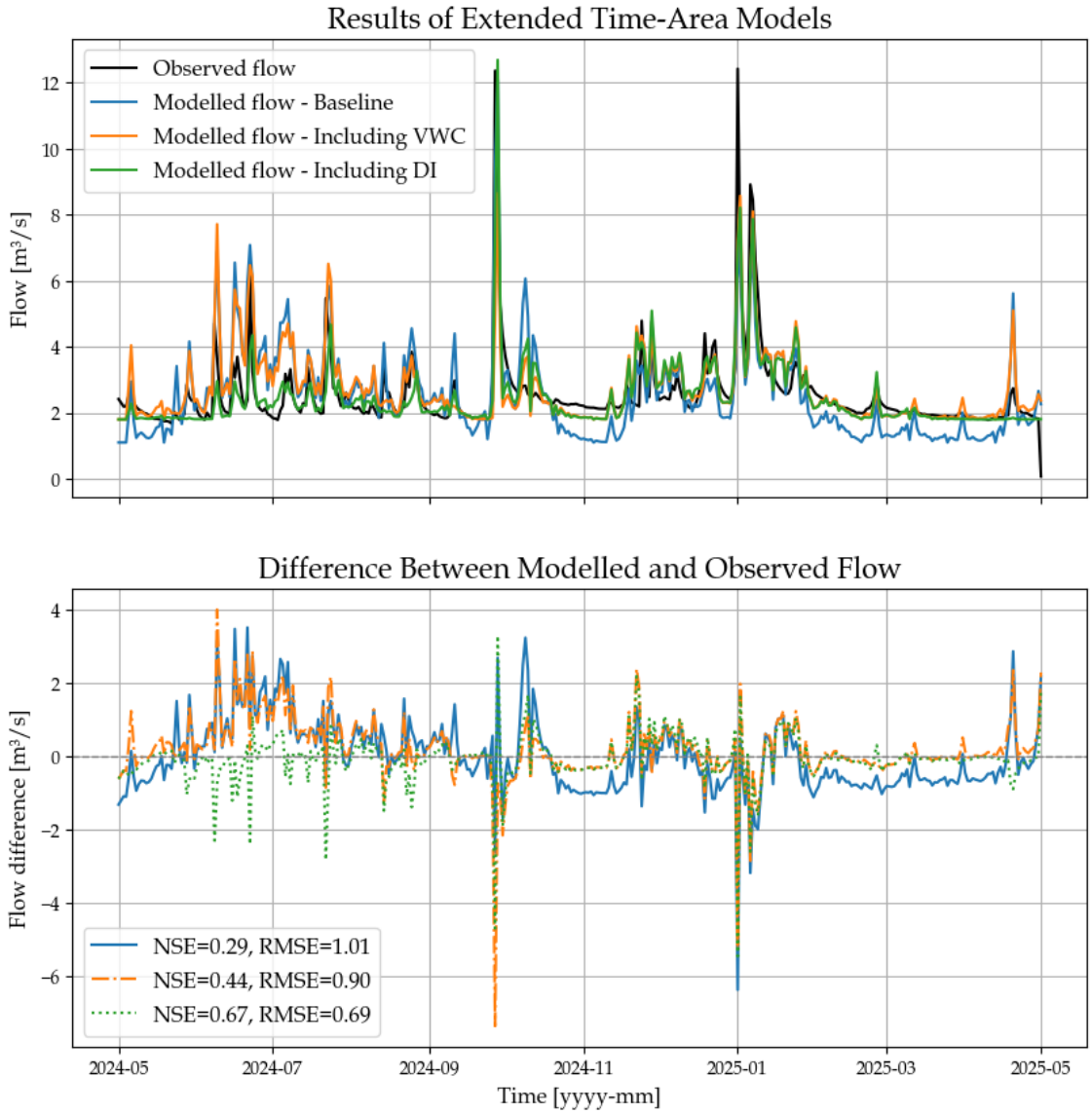

Figure 12.4. Observed flow compared with Extended Time-Area Models of baseline, including VWC, and including DI (upper plot), and corresponding differences (lower plot). The NSE and RMSE are shown for all models.

During dry periods, the baseline and VWC models tend to overestimate the flow, while the DI model aligns well with observations. In contrast, during the wet period, both the VWC and DI models capture the observed flow, while the baseline model tends to underestimate it. The largest deviations are observed during two high-flow events, with differences ranging from -7 to 4 m^3/s, as clearly seen in the lower plot. However, it is important to notice that the observed peak error of approximately -7 m^3/s in September 2024 is attributed to a time lag between modelled and estimated flow.
By including VWC, better model performances are achieved compared to the baseline. However, both the overall best fit and the best capture of peaks are found when the model including DI is applied. This aligns with the performance of the calibration period.

To further evaluate the performance of the Extended Time-Area Model, a scatter plot comparing estimated and modelled flow for all three models is presented in Figure 12.5. This visualisation supports a more detailed analysis of the model accuracy and reveals potential systematic deviations.

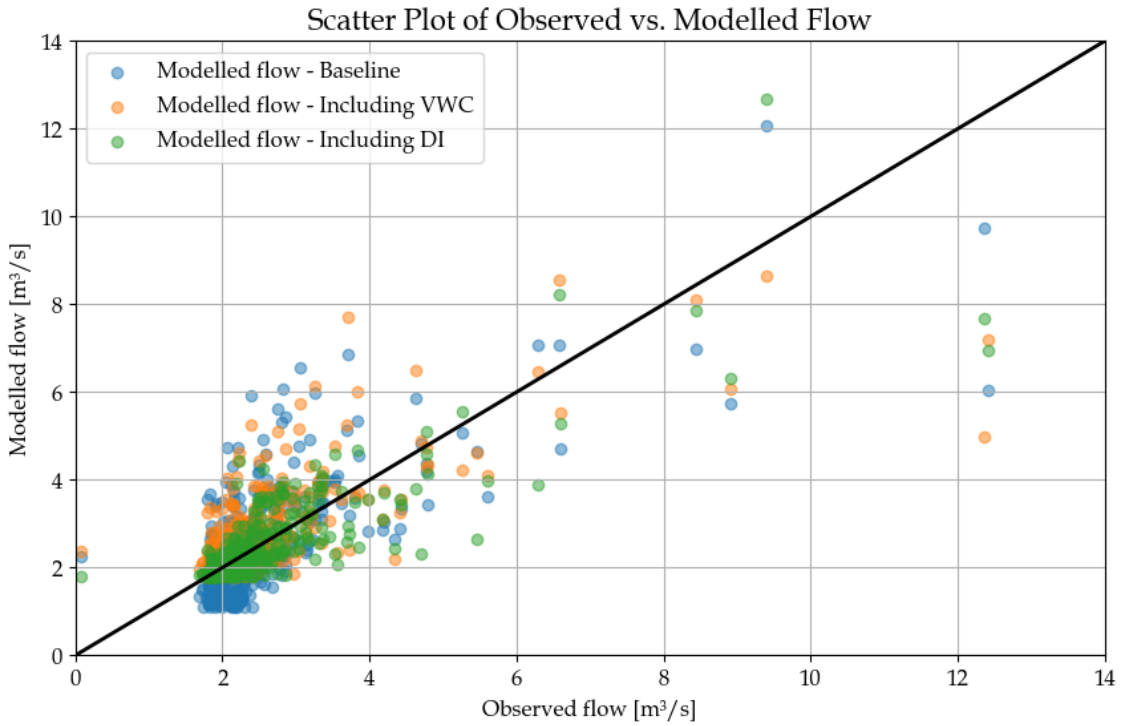

Figure 12.5. Scatter plot comparing observed flow with modelled flow from the Extended Time-Area Models for baseline, including VWC, and including DI. The 1:1 line indicates a perfect match between observed and modelled values. Points above the line represent overestimation, while points below indicate underestimation.

It is evident that the baseline model generally deviates most from the 1:1 line, while the model including DI follows it most closely. For higher flow values, all models tend to underestimate the observed flow. The model including VWC typically performs in between the two.
Thus, the scatter plot in Figure 11.5 suggests that including either VWC or DI improves model performance, with DI exhibiting the most consistent improvements. These observa-

tions support the findings from Figure 11.4 and the associated NSE and RMSE values.

Main Findings
Including VWC in flow modelling using the Extended Time-Area Model clearly enhances the accuracy of the flow estimation compared to the baseline model, which is based solely on precipitation and potential evaporation. Furthermore, substituting VWC measurements with the DI results in an additional improvement, suggesting that the DI can serve as a viable alternative to local VWC sensors when using the Extended Time-Area Model, especially during dry periods.
Overall, a distinct difference in performance is observed between the three models, highlighting the importance of incorporating an additional input variable, such as VWC, when estimating flow contribution from green areas.

Linear Reservoir Model 13

A Linear Reservoir Model is a simple hydrological model used to estimate flow (Q) from precipitation (P).

13.1 Model Setup of the Linear Reservoir Model

The model simplifies the response from the catchment area by assuming a linear proportional relationship between the storage in the system and the outflow at any given time [Schaarup-Jensen, 1985]. A conceptual understanding of a linear reservoir model is illustrated in Figure 13.1

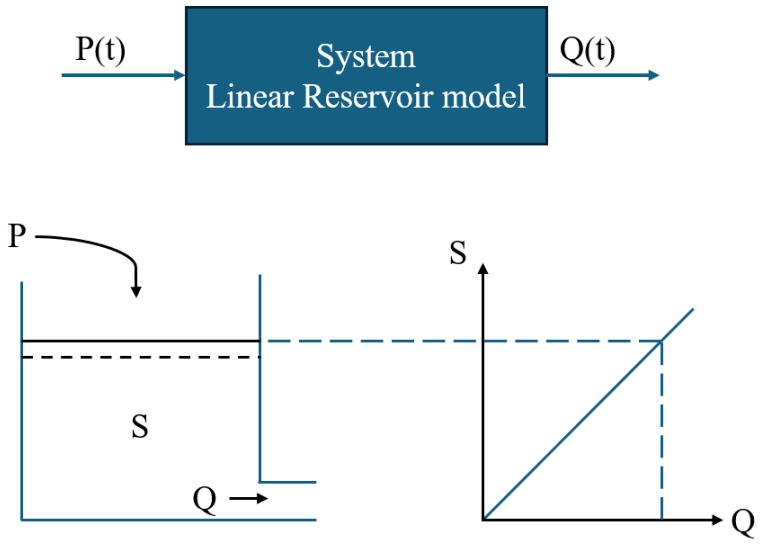

Figure 13.1. Conceptual understanding of the relationship between the precipitation (P), soil storage (S), and flow (Q).

By assuming mass conservation, the change in storage over time can be described as the difference in input vs. output [Schaarup-Jensen, 1985]:

$$P - Q = \frac{dS}{dt} \tag{13.1}$$

The storage is calculated using a reservoir constant k, which reflects how quickly water is discharged from the storage. A higher reservoir constant indicates a faster response, meaning the reservoir empties more rapidly.

Hence:

$$Q(t) = \frac{1}{k} \cdot S(t) \tag{13.2}$$

The flow in Grejs Å is estimated by a numerical Linear Reservoir Model with two reservoirs and an hourly resolution ($\Delta t = 1$ hour). The two-reservoir setup enables the separation of direct runoff and baseflow. Initial water volumes are assumed in both reservoirs ($S_1(0)$ and $S_2(0)$) before calibration and validation. Under certain conditions, such as high evaporation combined with limited precipitation, the inflow (P_1) may become negative. This is corrected in the model by adjusting the inflow to 0, preventing negative inflow values.

The inflow to reservoir 1 ($P_1(t)$) is calculated as the precipitation ($P(t)$) minus potential evaporation ($E_t(t)$) multiplied by the catchment area (A). The inflow to reservoir 2 ($P_2(t)$) is determined as a fraction of the outflow from reservoir 1 ($Q_1(t)$), represented by a regulation constant (R). The total modelled flow in Grejs Å ($Q(t)$) is the sum of the outflow from reservoir 2 ($Q_2(t)$) and the remaining outflow from reservoir 1. The system setup is illustrated in Figure 13.2.

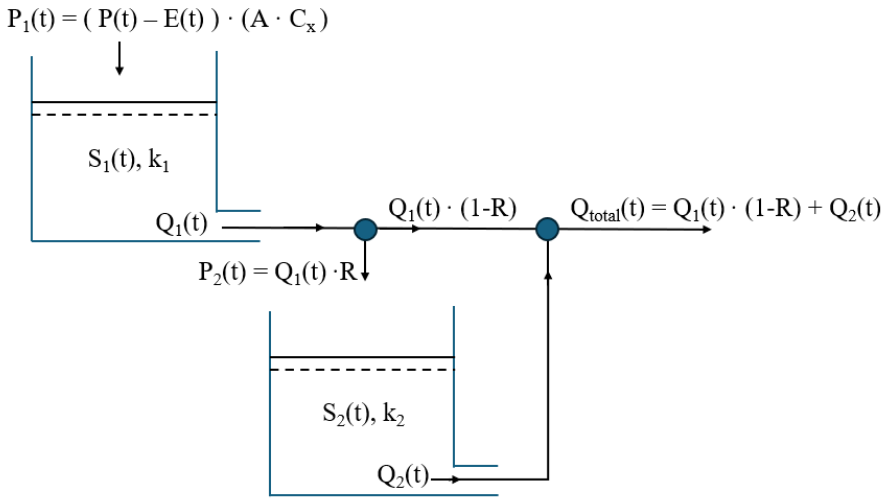

Figure 13.2. Two-reservoir model structure used for flow simulation, illustrating separation of direct runoff and baseflow.

Where:

$Q_x(t)$	Qutflow from reservoir x	$[m^3/s]$
$Q_{total}(t)$	Total flow	$[m^3/s]$
R	Regulation constant separating runoff and baseflow	$[-]$
A	Contributing area	$[m^2]$
C_x	Area regulation factor	$[-]$
$P_x(t)$	Water input to reservoir x	$[m^3/s]$
$S_x(t)$	Stored water volume in reservoir x	$[m^3]$
k_x	Reservoir constant for reservoir x	[s]
$P(t)$	Measured precipitation	$[m^3/s/m^2]$
$E(t)$	Calculated potential evaporation	$[m^3/s/m^2]$

The numerical model is based on Equation 13.1 and Equation 13.2, presented below.

Reservoir 1

$$S_1(t+\Delta t) = S_1(t) + ((P(t) - E(t)) \cdot (A \cdot C_x) - Q_1(t)) \cdot \Delta t \tag{13.3}$$

$$Q_1(t+\Delta t) = \frac{1}{k_1} \cdot S_1(t) \tag{13.4}$$

Reservoir 2

$$S_2(t+\Delta t) = S_2(t) + (Q_1(t) \cdot R - Q_2(t)) \cdot \Delta t \tag{13.5}$$

$$Q_2(t+\Delta t) = \frac{1}{k_2} \cdot S_2(t) \tag{13.6}$$

Total outflow

$$Q_{total}(t) = Q_1(t) \cdot (1 - R) + Q_2(t) \tag{13.7}$$

In the Linear Reservoir Model, the regulation constant (R) defines the proportion of water directly discharged as outflow from reservoir 1, representing the direct runoff, while the remaining portion is routed from reservoir 1 into reservoir 2. The outflow from Reservoir 2 is assumed to represent the baseflow component.
Evaporation (E) is estimated by calculating the potential evaporation rate, as described in Appendix K. This approach assumes an unlimited water supply, meaning that potential evaporation represents an upper limit and typically overestimates the actual evaporation [Linacre, 1977].

Calibration of the Linear Reservoir Models

The calibration parameters in the Linear Reservoir Model are: the area regulation factors (c_x), the reservoir constants (k_x), and the regulator constant (R). Table 13.1 presents all calibration parameters for the three models.

Table 13.1. Calibration parameters of the Linear Reservoir Model.

Parameter	Baseline	Including VWC	Including DI
k_1	30.30	23.25	30.68
k_2	2000.00	500.00	2091.54
R	0.72	0.63	0.57
c_0	0.90	-	-
c_1	-	0.07	0.09
c_2	-	0.49	0.18
c_3	-	1.00	1.00

For each model, the regulator constant (R) exceeds 0.5, indicating that the majority of the flow is routed as baseflow. Post-calibration, the area regulation factors align with the initial assumptions: $c_1 < c_2 < c_3$, where c_1, associated with low VWC conditions, is smaller

than c_2, representing moderate soil moisture, and c_3 representing high soil moisture levels. In the model incorporating DI, a smaller contributing area is observed for the mid and low bins compared to the VWC-based model. This can be attributed to a larger proportion of DI values falling within the high bin, where 100% of the area contributes to flow.

Based on a *cross-correlation analysis* between the modelled and observed flow, which reveals a lag time of two hours (cf. section M.1, Figure M.3), the Linear Reservoir Models are recalibrated by shifting the modelled flow data two hours forward. This adjustment ensures optimal average alignment between the modelled and observed flows.

Table 13.2 presents the NSE and RMSE values obtained during the calibration of the three Linear Reservoir Models. The models using VWC and DI both achieve improved performance during the calibration period, as seen by higher NSE values and lower RMSE values.

Table 13.2. Overview of the NSE and RMSE values for the calibration period for the Linear Reservoir Models.

Parameter	Baseline	Including VWC	Including DI
NSE	0.645	0.832	0.829
RMSE	0.951	0.655	0.660

13.2 Flow Predictions from the Linear Reservoir Models

The three Linear Reservoir Models (baseline, including VWC, and including DI) are compared to the observed flow in Grejs Å during the validation period, to evaluate the performance of each model, as shown in Figure 13.3. The lower plot of the figure presents the difference between the modelled and observed flow, where positive values indicate overestimations and negative values indicate underestimations. The NSE and RMSE values for each model are presented Table 13.3 below.

Table 13.3. Overview of the NSE and RMSE values for the validation period for the Linear Reservoir Models.

Parameter	Baseline	Including VWC	Including DI
NSE	0.40	0.51	0.63
RMSE	1.08	0.97	0.84

It is evident from Figure 13.3, that both the VWC and DI models capture the overall pattern of the observed flow more accurately than the baseline model. This is seen by the NSE and RMSE values, with the DI model achieving the best overall performance, while the baseline model performed the weakest.
During the dry period, the VWC model generally overestimates flow, whereas the DI model tends to underestimate it. In contrast, the baseline model both over- and underestimates.

During the wet period, all three models tend to underestimate the flow, with the VWC model providing the best representation.

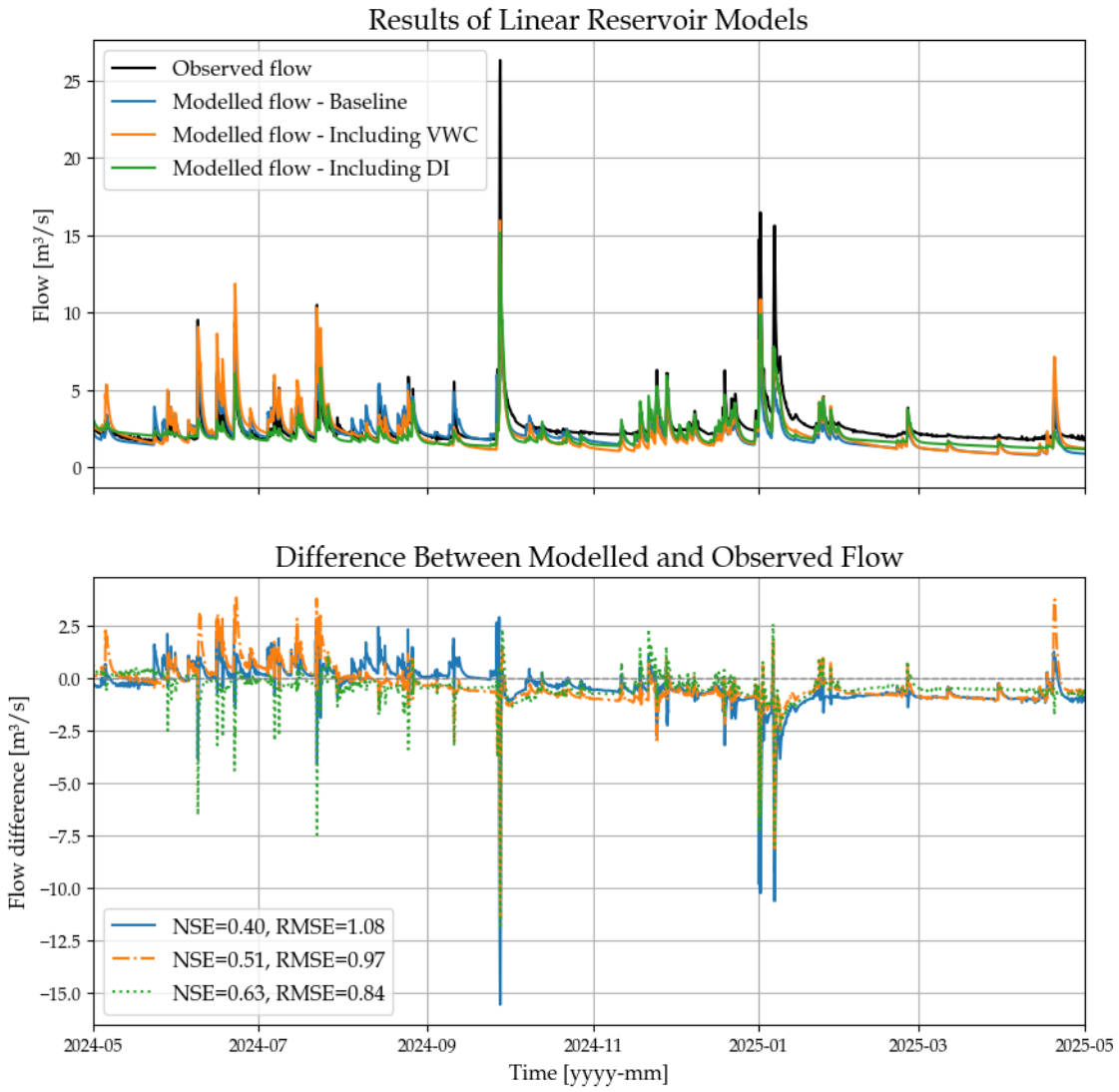

Figure 13.3. Observed flow compared with Linear Reservoir Models of baseline, including VWC, and including DI (upper plot), and corresponding differences (lower plot). The NSE and RMSE are shown for all models.

Furthermore, none of the models fully capture the peak-flow events in September 2024 and January 2025, with the deviations during the September event ranging from -15 to 2.5 mm. The model incorporating VWC provides the best representation of both peak events. Thus, including VWC improves model performance compared to the baseline. However, the model incorporating DI provides the best overall fit. In contrast, the VWC model generally performs better at capturing high and peak flow events.

To further evaluate the performance of the Linear Reservoir Model, a scatter plot comparing estimated and modelled flow for all three models is presented in Figure 13.4. This visualisation supports a more detailed analysis of the model accuracy and reveals potential systematic deviations.

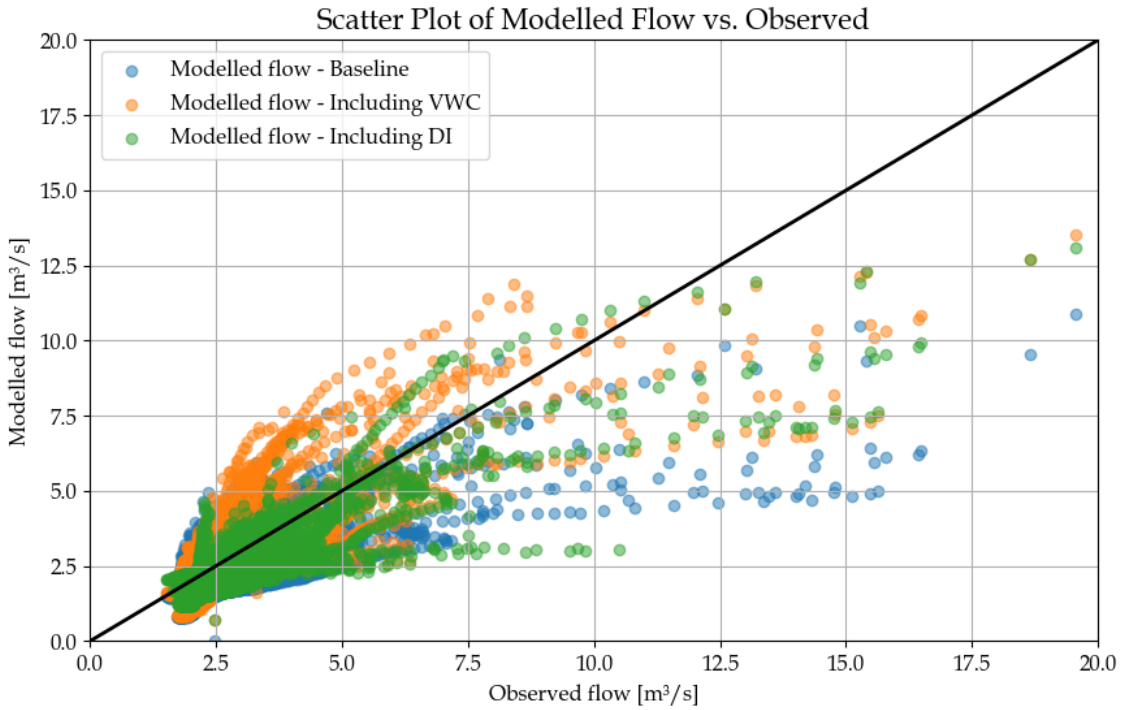

Figure 13.4. Scatter plot comparing observed flow with modelled flow from the Linear Reservoir Models for baseline, including VWC, and including DI. The 1:1 line indicates a perfect match between observed and modelled values. Points above the line represent overestimation, while points below indicate an underestimation.

It is evident that the baseline model consistently underestimates flow, particularly at higher magnitudes. The model including VWC performs better, showing a wider spread around the 1:1 line and capturing more of the higher flow values. However, it also tends to overestimate in the low-to-mid range. The model including DI provides the closest overall fit to observed values, with points more symmetrically distributed around the 1:1 line, indicating a more balanced performance across flow magnitudes.
This further supports the conclusion that incorporating DI leads to improved model accuracy, particularly in representing both moderate and high flow conditions. These observations support the findings from Figure 11.4 and the associated NSE and RMSE values.

Main Findings
Including VWC in the Linear Reservoir Model improves the accuracy of simulated flow compared to the baseline model, which relies solely on precipitation and potential evaporation. Replacing VWC with the DI leads to a further improvement in performance, indicating that the DI is a suitable substitution for VWC in this modelling context.
Overall, the results reveal clear differences in performance between the three model setups, underscoring the value of integrating additional hydrological information, such as VWC or DI, when modelling runoff from green catchments.

Evaluation of Hydrological Model Performance

14

As described in chapter 10, the purpose of developing the three models is to examine if simple models, used for predicting flow in Grejs Å can be improved when parameters such as VWC and DI are incorporated.
Firstly, the two parameters, VWC and DI, are discussed, whereafter the performance of the Extended Time-Area Model and the Linear Reservoir Model is compared. An alternative method for capturing peak flows is then presented, and finally, the potential of using the model for flood risk forecasting is evaluated.

14.1 Effect of Incorporating VWC and DI in Flow Modelling

When incorporating VWC and DI into the three models, different performance responses are observed, where the Linear Regression Model exhibits weaker performance when incorporating both parameters. However, it should be noted that the decrease in performance is almost negligible. In contrast, both the Extended Time-Area Model and the Linear Reservoir Model exhibit improved model performance when incorporating VWC and DI, as seen in Table 14.1. This aligns well with the findings in the *runoff analysis* in Part I, where a relationship is observed between high VWC and increased runoff volumes.

Table 14.1. Overview of the model performance parameters for the Linear Regression Model, the Extended Time-Area Model, and the Linear Reservoir Model

	Baseline		**Including VWC**		**Including DI**	
	NSE	RMSE	NSE	RMSE	NSE	RMSE
Linear Regression Model	0.60	0.56	0.55	0.56	0.52	0.60
Extended Time-Area Model	0.29	1.01	0.44	0.90	0.67	0.69
Linear Reservoir Model	0.40	1.08	0.51	0.97	0.63	0.84

It is important to note that the VWC data input used in all three models is based solely on data from one sensor (Sensor 6), which introduces uncertainties to the representation of VWC conditions. This approach assumes that measurements from Sensor 6 are representative of VWC conditions across the entire Grejs Å catchment, which does not

reflect reality. With eight VWC sensors distributed throughout the catchment, a more accurate representation would involve incorporating data from the remaining sensors. This is particularly relevant for the Extended Time-Area Model, which allows for the assignment of specific sensors to individual subcatchments. Incorporating spatially distributed VWC data in this way could improve the model's ability to capture the variability in flow generation across the catchment.
Therefore, to maintain a streamlined modelling framework and ensure comparability across the different model setups, Sensor 6 has been used as the sole VWC input in this analysis.

For both the Extended Time-Area Model and the Linear Reservoir Model, a further improvement in model performance is observed when DI is incorporated. This enhancement is primarily due to the DI's ability to better regulate flow during dry periods. This aligns well with expectations, as the DI is specifically designed to capture the dry conditions, and is therefore less accurate during very wet conditions.

14.2 Comparison of Extended Time-Area Model and Linear Reservoir Model

The comparison is limited to the Extended Time-Area Model and the Linear Reservoir Model, as the Linear Regression model differs significantly in both temporal resolution and structure. Specifically, it is based on baseflow-separated data and developed from the location analysis, making it unsuitable for direct comparison with the other two models.
To facilitate the comparison, the output from the Linear Reservoir Model is resampled to match the daily resolution of the Extended Time-Area Model. It is important to note that the Linear Reservoir Model is not restructured or recalibrated for daily simulations; only the hourly output is resampled to daily values. Figure 14.1 presents the observed and modelled flow for both models.

It is evident that the Linear Reservoir Model exhibits the best overall model performance. However, following the summer period of 2024, the model contains an insufficient amount of water, leading to a consistent underestimation of the flow during the remaining validation period. Despite this general underestimation, the Linear Reservoir Model provides the most accurate representation of the peak events in September 2024 and January 2025. While the Extended Time-Area Model generally performs better in capturing the overall flow patterns, its performance metrics are negatively affected by its underestimation during these two peak events. Nevertheless, as shown in the lower plot illustrating the differences, the NSE and RMSE values for the two models are very similar.
However, both models show a general difficulty in accurately capturing peak flow values, which may be attributed to the precipitation input. The input used in the models is a modified dataset combining precipitation measurements from both Vejle and Jelling. While this combined input generally improves the overall fit, it introduces certain limitations. For instance, if a heavy rain event occurs in Jelling but not in Vejle, the average precipitation may underestimate the true intensity, potentially leading to an underestimation of peak flows in the model. Although it is possible to calibrate the model to more accurately

reproduce peak flows, this often results in an overestimation of smaller peaks. Consequently, if the model were to be used for applications such as flood risk management, it can produce too many overestimations. An alternative approach to improve peak flow prediction can be to develop a custom performance metric that is specifically sensitive to peak values, or to introduce an uncertainty band within which the flow is expected to fall.

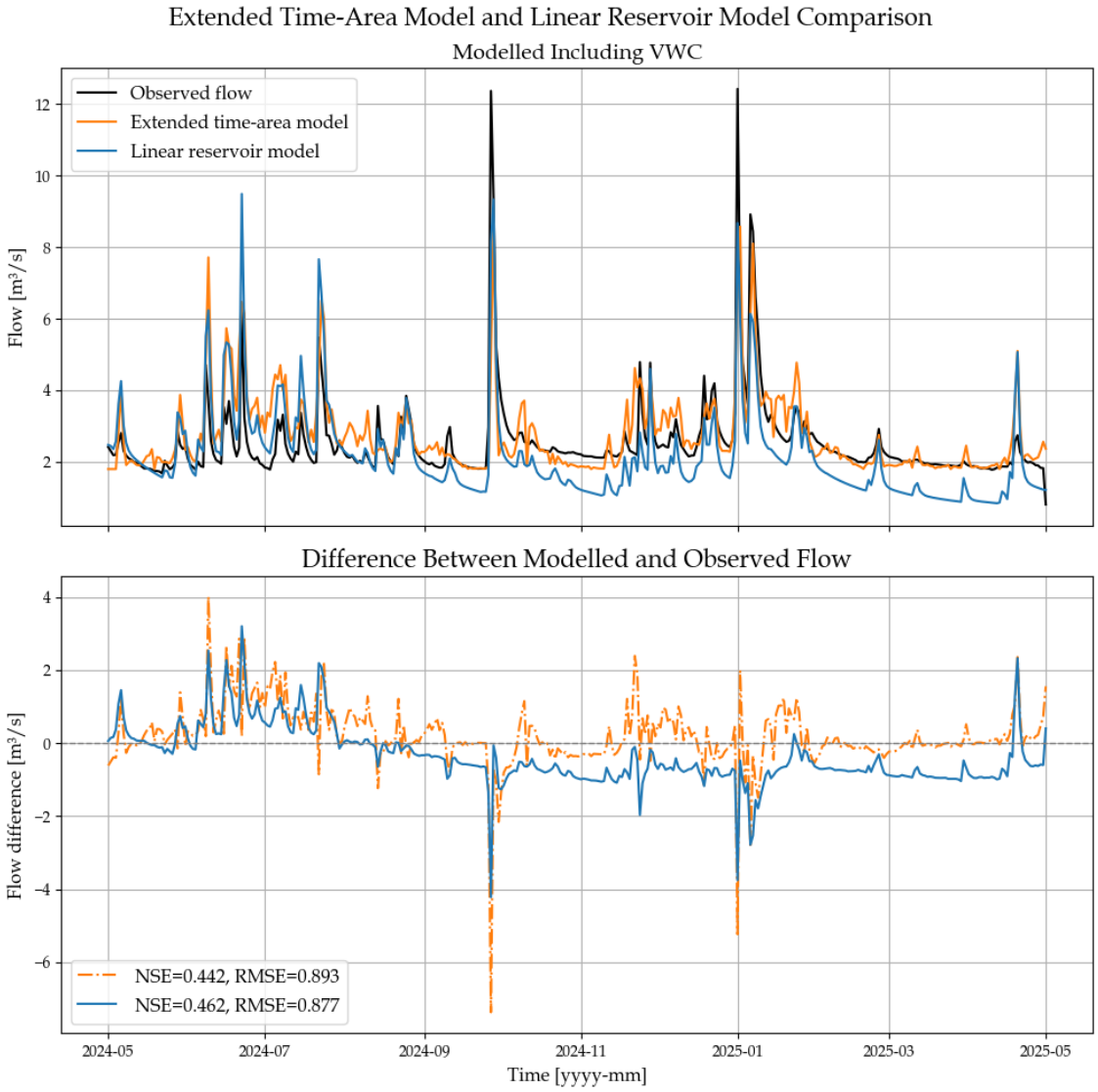

Figure 14.1. Comparison of the Extended Time-Area Model and the Linear Reservoir Model. Both models have a resolution of one day.

Since the Linear Reservoir Model exhibits both the best overall performance and the most accurate peak estimations, and is a widely used flow model, the following examination of practical applicability focuses solely on this model.

14.3 Capturing Peak Flow Through Rainfall Range Modelling

To explore the practical applicability of the Linear Reservoir Model in a real-time context, two peak flow events have been selected (cf. Appendix M, section M.3). For each event, the modelled flow is used to generate flow bands based on minimum, mean, and maximum precipitation, which are then compared to the observed flow. This allows for an assessment of the models' predictive capabilities during critical high-flow situations, that may lead to flooding in Vejle.
This is done only for the model including VWC, despite the DI model exhibiting the best performance. However, as VWC represents actual, local measurements, unlike the DI, which is a modelled parameter. Additionally, since the ultimate aim is to explore real-time flood prediction, incorporating dynamic soil conditions through VWC is considered more physically meaningful and potentially more robust for operational use.

The envelope used in rainfall range modelling is created by modifying the rainfall input. For the upper bound, the rainfall is calculated by identifying the maximum 10-minute intensity within each hour and assuming this intensity persists throughout the entire hour. This approach typically results in an overestimation of the total rainfall, which helps capture the peak flows. The lower bound is generated by using the minimum 10-minute intensity within each hour, which generally leads to an underestimation of the flow. Together, these bounds aim to enclose the range of observed flows. Figure 14.2 shows the model predictions of two critical flow events in Vejle (the minimum, mean, and maximum band for the entire validation period is presented in Appendix M, Figure M.9).

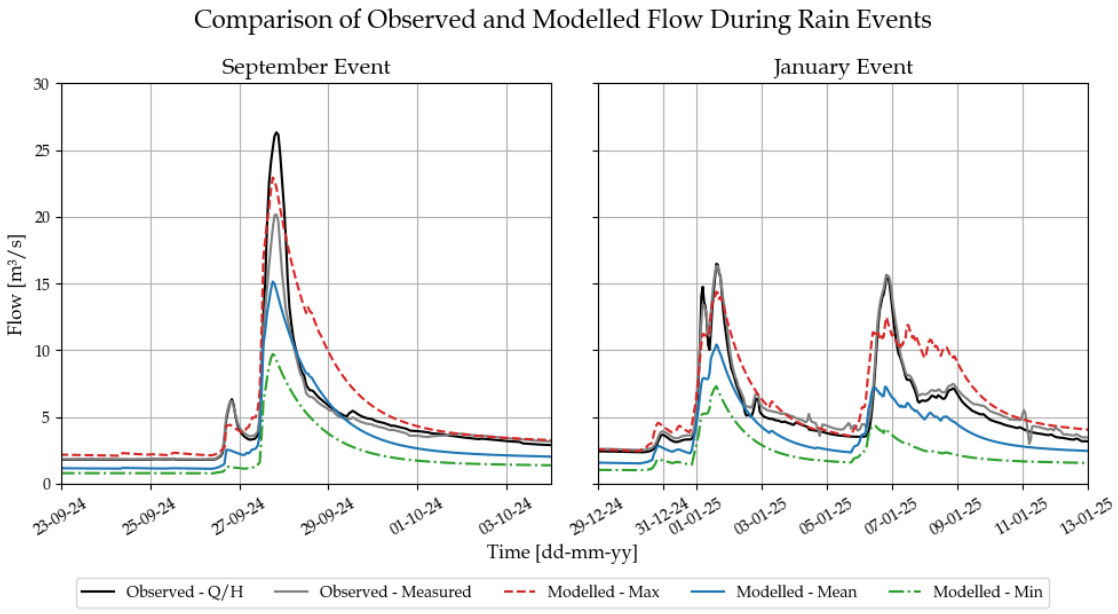

Figure 14.2. Two events with the highest peak flows. Comparison of the observed flow and the modelled flow band.

Figure 14.2 shows that the maximum rainfall input does not overestimate either of the two observed flows (one derived from the Q/H relationship and one from direct measurements), but it comes significantly closer than the mean rainfall input. It is particularly evident during the September rainfall event, where the directly measured flow is noticeably lower than the flow estimated using the Q/H relationship. It is assumed that the direct measurement is more accurate than the Q/H-based estimate.
The flow bands can, for example, be used if the model is applied in a flood risk management context. In such cases, the model can be run with forecasted precipitation, and the flow band will ensure that the risk assessment accounts for the worst-case scenario represented by the maximum modelled flow.

14.4 Predicting Peak Flow Using Different Calibration Periods

To evaluate the Linear Reservoir Model's potential for peak flow prediction, it is assessed whether the model's performance improves when different calibration period lengths are used prior to the peak flow.

The model is calibrated using two years of data from a period characterised by highly variable conditions, with 2022 being relatively normal, while 2023 marked the wettest year in Danish weather history, followed by 2024 as the second wettest [DMI, 2025], resulting in an average annual precipitation of 1099.8 mm in the calibration period. In contrast, the subsequent validation year is generally drier, with an annual precipitation of 844.4 mm [DMI, 2025]. This may partly explain the better performance observed during the calibration period compared to the validation period. To explore whether more targeted calibration improves the accuracy of peak flow prediction, the model is recalibrated using shorter time windows leading up to each prediction. Three calibration period lengths are tested: 6 months prior to the peak flow event, one year prior, and the full available dataset preceding each peak flow.
In addition to recalibrating model parameters for each calibration period, the initial conditions ($S_1(0)$ and $S_2(0)$) for each prediction are also adjusted. These are adjusted to ensure that the modelled flow on the day before the peak flow aligns with the observed flow, providing a realistic and consistent starting point.

The peak flow prediction analysis is applied to the two peak flow events in September 2024 and January 2025, respectively, as shown in Figure 14.3.
From the first peak flow event in September 2024, the model calibrated using data from one year prior to the event provides the best performance. The model calibrated with data from only six months before the event underestimates the first peak but performs better on the second. In contrast, the model calibrated using all available data prior to the event results in the largest underestimation of the peak flow.
A similar trend is observed for the January 2025 event. Once again, the model calibrated on data from the preceding year yields the best agreement with the observed flow. In this case, the model based on the most recent six months performs the worst. One explanation

for this is that the 6-month calibration period corresponds to a different season, meaning the model is better tuned to conditions such as low VWC or low flow.
For both peak flow prediction and general model calibration, using data from the full year preceding the prediction appears to perform the best. Although incorporating a larger dataset for calibration is possible, it does not necessarily improve model performance.

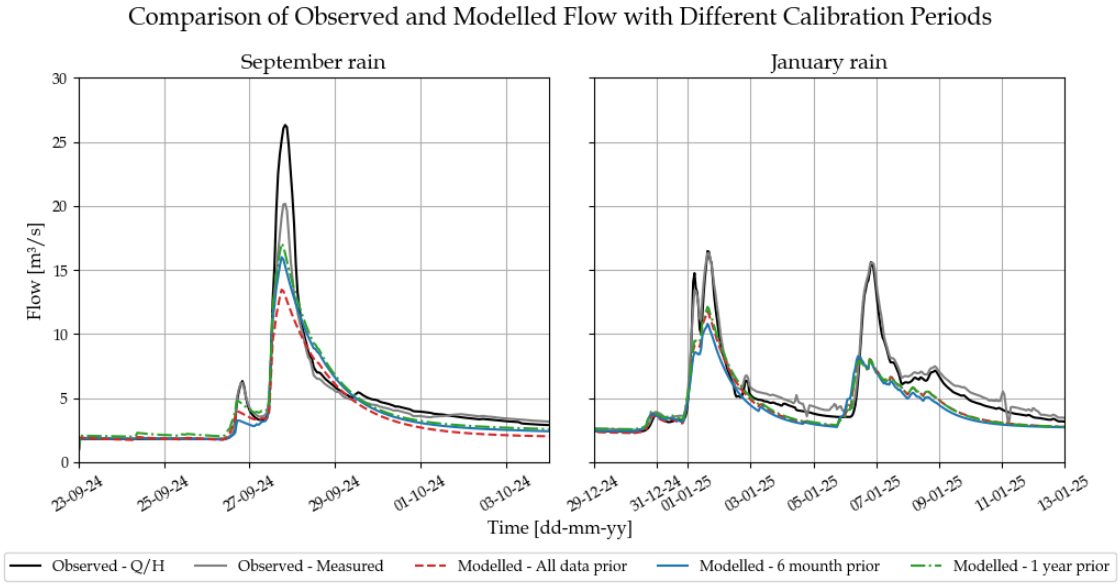

Figure 14.3. Comparison of the observed and modelled flow during the September and January events using different calibration periods.

It should be noted that the input data used in these peak flow predictions consists of actual measured rainfall during the events. By incorporating forecasted rainfall together with forecasted DI, the peak flow prediction method could be applied as a tool in a flood warning system, particularly in combination with flow bands. However, in this thesis, the use of actual rainfall data is chosen to eliminate uncertainties associated with rainfall forecasting and to focus solely on evaluating the model's ability to simulate flow based on VWC conditions.

14.5 Summary and Final Reflections

It is evident that incorporating soil-moisture information, either as VWC or DI, improves flow simulations for Grejs Å. Both the Extended Time-Area Model and the Linear Reservoir Model exhibit better model performance when including these additional inputs, while the Linear Regression Model shows only marginal change. Between the two process-based models, the Linear Reservoir Model delivers the strongest overall fit and the most reliable peak-flow estimates, although it tends to underestimate flows late in the validation period. Using flow bands and shorter, event-specific calibration windows further enhances its peak-flow representation, and calibrating on the year immediately preceding a peak flow prediction event yields the best predictive skills.

However, a limitation of all three models is their inability to account for significant snowmelt events. For example, the second peak observed during the January event is attributed to additional water from melting snow. Future improvements to be able to capture such dynamics, variables such as air and soil temperature, could be incorporated into the model.

Conclusion 15

This thesis examines the influence of volumetric water content (VWC) on contingent runoff by exploring the following problem statement:

To what extent does soil moisture influence surface runoff across varying spatial scales, and can incorporating volumetric water content (VWC) measurements enhance the accuracy of flow models and their application in urban flood management?

The results show that VWC can significantly influence contingent runoff; however, it is not the sole determining factor. At the hillslope scale, three physically similar areas were analysed. Despite their similarities, different runoff behaviours are observed. In particular, the area in Lystrup demonstrates a statistically significant relationship between VWC and runoff generation. In contrast, this relationship is less clear in the other two locations, suggesting that while contingent runoff is present across all areas, the specific conditions under which it occurs vary locally. For Elmelundsvej and Lystrup, it is observed that VWC must exceed a certain critical VWC threshold of 0.2 and 0.30 [m^3/m^3], respectively, before contingent runoff can occur. However, contingent runoff does not always occur when the critical threshold is reached.

At the urban subcatchment scale, runoff is found to be primarily driven by rainfall rather than VWC. Although there are indications that VWC may have some influence, this can not be statistically confirmed. In this part of the analysis, a baseflow separation is applied to isolate the runoff signal. While this processing affects the raw data, it is considered not to alter the overall conclusions.

At the hydrological scale, using data from the Grejs Å catchment, Vejle, it is both evident and statistically supported that VWC affects streamflow. In Vejle, runoff is influenced not only by high VWC values but also by rainfall intensity and changes in soil moisture. This suggests that the soil in the area generally has a high infiltration capacity but becomes saturated during prolonged rainfall events, leading to increased runoff. In Vejle, an increased runoff ratio is observed when the VWC descend 0.15 or exceeds 0.33 [m^3/m^3], revealing that both very dry and wet conditions can generate additional runoff.

Across all three scales, there is a general tendency for long-duration winter precipitation to generate the largest runoff volumes, primarily due to elevated soil moisture levels. However, extreme events such as the critical flow event in Vejle in September 2024 can still produce substantial flow volumes despite lower initial soil moisture conditions.

Following the analysis, three simple flow models are developed to assess whether

incorporating VWC or the drought index (DI) as model parameters can improve model performance. All three models are capable of predicting overall flow patterns, however, they consistently struggle to capture the highest peak flows. If these models are to be used for applications such as flood forecasting or risk management, a flow band can be included to account for the underestimation of peak events.

For the Extended Time-Area Model and the Linear Reservoir Model, performance improves significantly when either VWC or DI is incorporated. The model using DI yields the best overall performance in terms of statistical fit, while the model incorporating VWC is more effective at predicting peak flows. This suggests that while DI captures broader moisture trends well, VWC better reflects the short-term soil saturation conditions that drive peak flow.

In summary, it can be concluded that VWC does influence contingent runoff. However, it is not the only controlling factor. Runoff is the result of a complex interaction of multiple variables, including rainfall intensity, previous conditions, and soil properties.

Reflection 16

From the data analysis performed in this thesis, a clear contribution from green areas is found in some of the project locations, while it is less noticeable at the urban subcatchment scale, especially. This is most likely because the contribution from impervious surfaces during rainfall events is superior to the contribution from the green areas. However, when water volumes from multiple urban subcatchments are combined and discharged to the same recipient or treatment plant, the cumulative contribution from green areas may become significant and potentially lead to capacity issues. Therefore, it may be valuable to expand the analysis to estimate the additional load from contingent runoff in urban areas, e.g. using a *hydrological mass balance analysis*. If a substantial volume of such runoff is identified, it could warrant a reassessment of the design and capacity of existing water management systems.

This thesis found that simple flow models generally improved with the inclusion of volumetric water content (VWC) and drought index (DI) data. Therefore, it is beneficial for catchment areas similar to Vejle, where flooding is a concern, to explore the potential of incorporating VWC or DI as parameters. Simple models are selected in this thesis due to their fast simulation times and ease of implementation, making them suitable for use by municipalities and local utility companies. However, for flood warning purposes, more complex models, such as neural network models, may offer improved predictive capabilities. In Vejle, there is a need to forecast flow or water levels in Grejs Å at least 12 hours in advance to effectively prepare for critical events. While neural network models typically use precipitation as the primary input, the availability of VWC data in Vejle presents an opportunity to test its effectiveness in enhancing model performance. Figure 16.1 compares two neural network models: one using only rainfall as input, and the other using both rainfall and VWC data.

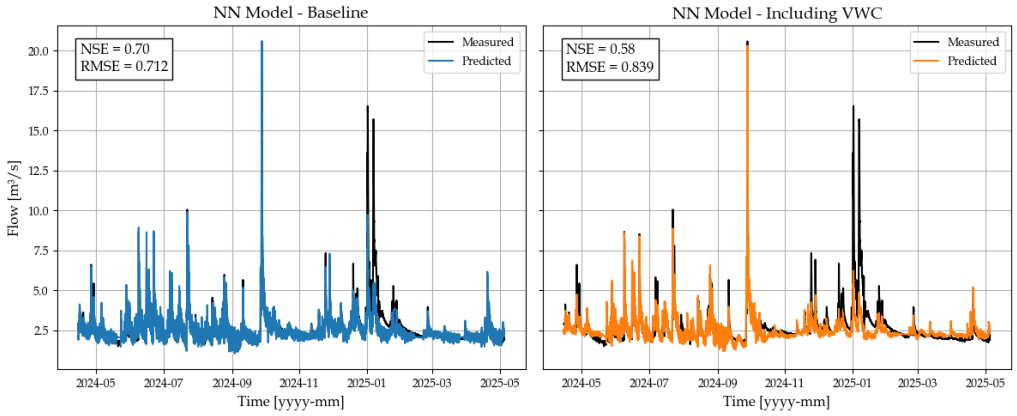

Figure 16.1. Neural network models using only precipitation as input (Baseline- blue line) and using both VWC and precipitation as input (Including VWC - orange line). The NSE and RMSE are shown in the top left corner of the subplots.

It can be seen that including the VWC does not improve model performance based on the RMSE and NSE metrics. However, it is observed that the model incorporating VWC exhibits reduced noise around the baseflow. Since it is a machine learning model, it is difficult to pinpoint the exact cause of this behaviour, but it presents an interesting opportunity for further investigation in future flow modelling studies. The models shown in Figure 16.1 predict each data point using the preceding 14 days of precipitation and 7 days of VWC data. By adjusting these time windows, a better performance of the models could likely be achieved.

Since the VWC is not forecasted, the model will have to predict based on the most recent available VWC data or alternatively, the latest DI data. Notably, there is a possibility that DMI will begin forecasting the drought index in the future, as all input parameters required for its calculation are already part of DMI's forecasting system. This will make the DI an even more valuable input for flood forecasting applications.

Bibliography

[Aarhus Kommune et al., 2017] Aarhus Kommune, Vand, A., Universitet, K., and A/S, E. (2017). AARHUSMETODEN TIL KLIMATILPASNING AF DEN EKSISTERENDE BY. https://www.aarhusvand.dk/media/cibgdc0v/drejebog-klimatilpasning-af-den-eksisterende-by.pdf.

[Basset et al., 2023] Basset, C., Abou Najm, M., Ghezzehei, T., Hao, X., and Daccache, A. (2023). How does soil structure affect water infiltration? a meta-data systematic review. Soil and Tillage Research, 226.

[Bleam, 2017] Bleam, W. (2017). Chapter 2 - chemical hydrology. In Soil and Environmental Chemistry (Second Edition), pages 39–85. Academic Press, second edition edition.

[Coolidge, 2020] Coolidge, F. L. (2020). A Gentle Introduction. SAGE Publications, Inc, 4th edition. ISBN: 9781071939000.

[Dinno, 2015] Dinno, A. (2015). Nonparametric pairwise multiple comparisons in independent groups using dunn's test. The Stata Journal, 15(1):292–300.

[DMI, 2024] DMI (2024). Vejret i Danmark bliver varmere, vådere og vildere. https://www.dmi.dk/klima-atlas/om-klimaatlas/vejretidanmarkblivervarmerevaadereogvildere. Last visited: 03-06-2025.

[DMI, 2025] DMI (2025). Alvorlig tørke på vej? https://www.dmi.dk/nyheder/alvorlig-toerke-paa-vej. Last visited: 03-06-2025.

[DMI, 2025] DMI (2025). Andet år i træk med ekstremt meget nedbør. https://www.dmi.dk/nyheder/2024/andet-aar-i-traek-med-ekstremt-meget-nedboer. Last visited: 03-06-2025.

[DMI, 2025] DMI (2025). Vejrarkiv. https://www.dmi.dk/vejrarkiv.

[Eckhardt, 2005] Eckhardt, K. (2005). How to construct recursive digital filters for baseflow separation. Hydrological Processes: An International Journal, 19(2):507–515.

[Gnann et al., 2025] Gnann, S., Baldwin, J. W., Cuthbert, M. O., Gleeson, T., Schwanghart, W., and Wagener, T. (2025). The influence of topography on the global terrestrial water cycle. Reviews of Geophysics, 63.

[Ladson, 2013] Ladson, T. (2013). A standard approach to baseflow separation using the lyne and hollick filter. Australian Journal of Water Resources, 17:25–34.

[Li et al., 2025] Li, X., Liu, Y., Zhang, J., Wang, Y., Li, Y., and Zheng, X. (2025). Landscape pattern and surface runoff in urban agglomerations: A case study from the guangdong–hong kong–macao greater bay area. Frontiers in Earth Science, 13:1542985.

[Linacre, 1977] Linacre, E. T. (1977). A simple formula for estimating evaporation rates in various climates, using temperature data alone. Agricultural Meteorology, 18(6):409–424.

[Liu et al., 2019] Liu, Y., Cui, Z., Huang, Z., López-Vicente, M., and Wu, G.-L. (2019). Influence of soil moisture and plant roots on the soil infiltration capacity at different stages in arid grasslands of china. CATENA, 182(2).

[Loll and Moldrup, 2000a] Loll, P. and Moldrup, P. (2000a). Soil Characterization and Polluted Soil Assessment. Chapter 3.

[Loll and Moldrup, 2000b] Loll, P. and Moldrup, P. (2000b). Soil Characterization and Polluted Soil Assessment. Chapter 2.

[Loll and Moldrup, 2000c] Loll, P. and Moldrup, P. (2000c). Soil Characterization and Polluted Soil Assessment. Chapter 1.

[Lyne and Hollick, 1979] Lyne, V. and Hollick, M. (1979). Stochastic time-variable rainfall-runoff modelling. In Institute of Engineers Australia National Conference, volume 79, pages 89–93. Institute of Engineers Australia Barton, Australia.

[Miljøstyrelsen, 2025] Miljøstyrelsen (2025). Vejle klimasikrer og skaber nyt byrum. `https://klimatilpasning.dk/kommuner-og-forsyning/loesninger/eksempler-paa-klimatilpasning/region-syddanmark/vejle-klimasikrer-og-skaber-nyt-byrum`. Last visited: 03-06-2025.

[Nielsen, 2019] Nielsen, K. T. (2019). Monitoring of rainfall-runoff from urban pervious areas. Technical report, Aalborg Universitetsforlag.

[Nielsen et al., 2020a] Nielsen, K. T., Nielsen, J. E., Uggerby, M., and Rasmussen, M. R. (2020a). Modeling of subsurface throughflow in urban pervious areas. Journal of Hydrologic Engineering, 25(12).

[Nielsen et al., 2020b] Nielsen, K. T., Uggerby, M., and Rasmussen, M. R. (2020b). Afstrømning fra byens ubefæstede områder. Technical report, Aalborg Universitet.

[Novafos, 2025] Novafos (2025). Novafos Borgerkort. `https://webgis.novafos.dk/portal/apps/experiencebuilder/experience/?id=0427851a06bb40d4a7b487c9634d3557`. Last visited: 02-06-2025.

[Novafos, 2025] Novafos (2025). Novafos/Om os. `https://novafos.dk/om-os`. Last visited: 03-06-2025.

[Reid, 2014] Reid, H. M. (2014). Introduction to Statistics: Fundamental Concepts and Procedures of Data Analysis. SAGE Publications, Inc. ISBN: 9781071878927.

[Ritter and Muñoz-Carpena, 2013] Ritter, A. and Muñoz-Carpena, R. (2013). Performance evaluation of hydrological models: Statistical significance for reducing subjectivity in goodness-of-fit assessments. Journal of Hydrology, 480:33–45.

[Robinson and Ward, 2017a] Robinson, M. and Ward, R. C. (2017a). Hydrology : Principles and Processes. IWA Publishing. EBOOK ISBN: 9781780407296.

[Robinson and Ward, 2017b] Robinson, M. and Ward, R. C. (2017b). Hydrology : Principles and Processes. IWA Publishing. EBOOK ISBN: 9781780407296.

[Scalgo, 2024] Scalgo (2024). Scalgo Live. https://scalgo.com/live/denmark. Last visited: 07/01-2024.

[Scalgo Live, 2025] Scalgo Live (2025). Top soil in the catchment area of Grejs Å, Vejle. https://scalgo.com/live/denmark. Last visited: 03-06-2025.

[Schaarup-Jensen, 1985] Schaarup-Jensen, K. (1985). Lineære reservoirer - forlæsningsnoter. Technical report, Aalborg university (I5/AUC).

[Thorndahl et al., 2024] Thorndahl, S., Lerer, S., Nielsen, J. E., and Nielsen, K. T. (2024). Monitering og modellering af situationsafhængig afstrømning. https://www.danva.dk/media/10681/abstracts-2024-dvk.pdf.

[Winther et al., 2011] Winther, L., Linde, J. J., Jensen, H. T., Mathiasen, L. L., and Johansen, N. B. (2011). Afløbsteknik. Polyteknisk Forlag, 6 edition.

[Wong, 2011] Wong, T. S. (2011). Overland Flow and Surface Runoff. Nova Science Publishers. ISBN: 9781613247419.

[World Meterological Organization, 2025] World Meterological Organization (2025). Precipitation. https://community.wmo.int/en/activity-areas/aviation/hazards/precipitation? Last visited: 03-06-2025.

Appendix
Presentation of Location and Data

Hillslope Scale A

This appendix provides essential information regarding the available data from the hillslope scale areas Ejby Mølle, Elmelundsvej and Lystrup.

A.1 Ejby Mølle

The measurement stations in Ejby Mølle consist of:

Table A.1. Overview of the measurement stations and soil texture at Ejby Mølle, Odense. The soil texture has been determined using the top soil map in Scalgo Live [Scalgo, 2024].

Sensor No.	Name	Soil Texture	Source
Water Level Sensors			
1	Målebrønd - EM tryk 1	-	Dryp
2	Målebrønd - EM tryk 2	-	Dryp
Rain Gauges			
-	5417 Ejby Mølle Renseanlæg	-	SVK
Volumetic Water Content Sensors (VWC)			
1	971-Nord	Fine clay with sand	Dryp
2	34d-Midt	Fine clay with sand	Dryp
3	C64-Syd	Fine clay with sand	Dryp

Figure A.1 illustrates the data series from the rain gauge, the two water level sensors, and the three VWC sensors. The lighter colours in the VWC data periods indicate breaks in the data series.

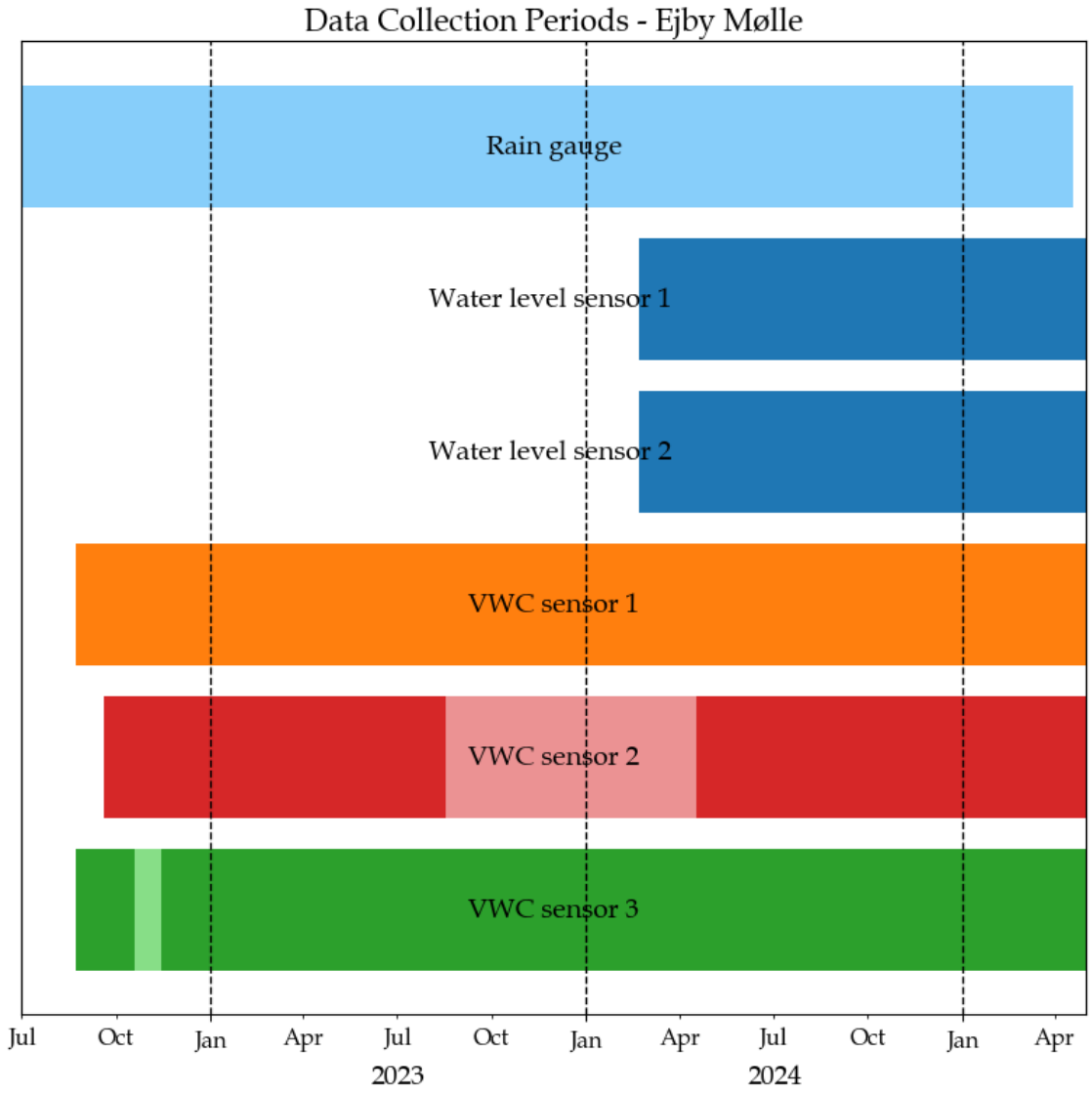

Figure A.1. Overview of the data periods for each of the measuring stations in Ejby Mølle, Odense. Data disturbances in the VWC sensors are illustrated with lighter colours.

The precipitation data ends earlier than the other sensors, which is due to the absence of rainfall during the latter half of April. Additionally, both Sensors 2 and 3 exhibit data gaps, whereas Sensor 1 provides a continuous time series. The limiting data for the analysis is the water level data. The water level is converted into a flow using a Q/H curve, presented in Appendix F.

Figure A.2 illustrates the data series in each of the VWC sensors. The dashed line indicates breaks in the data series.

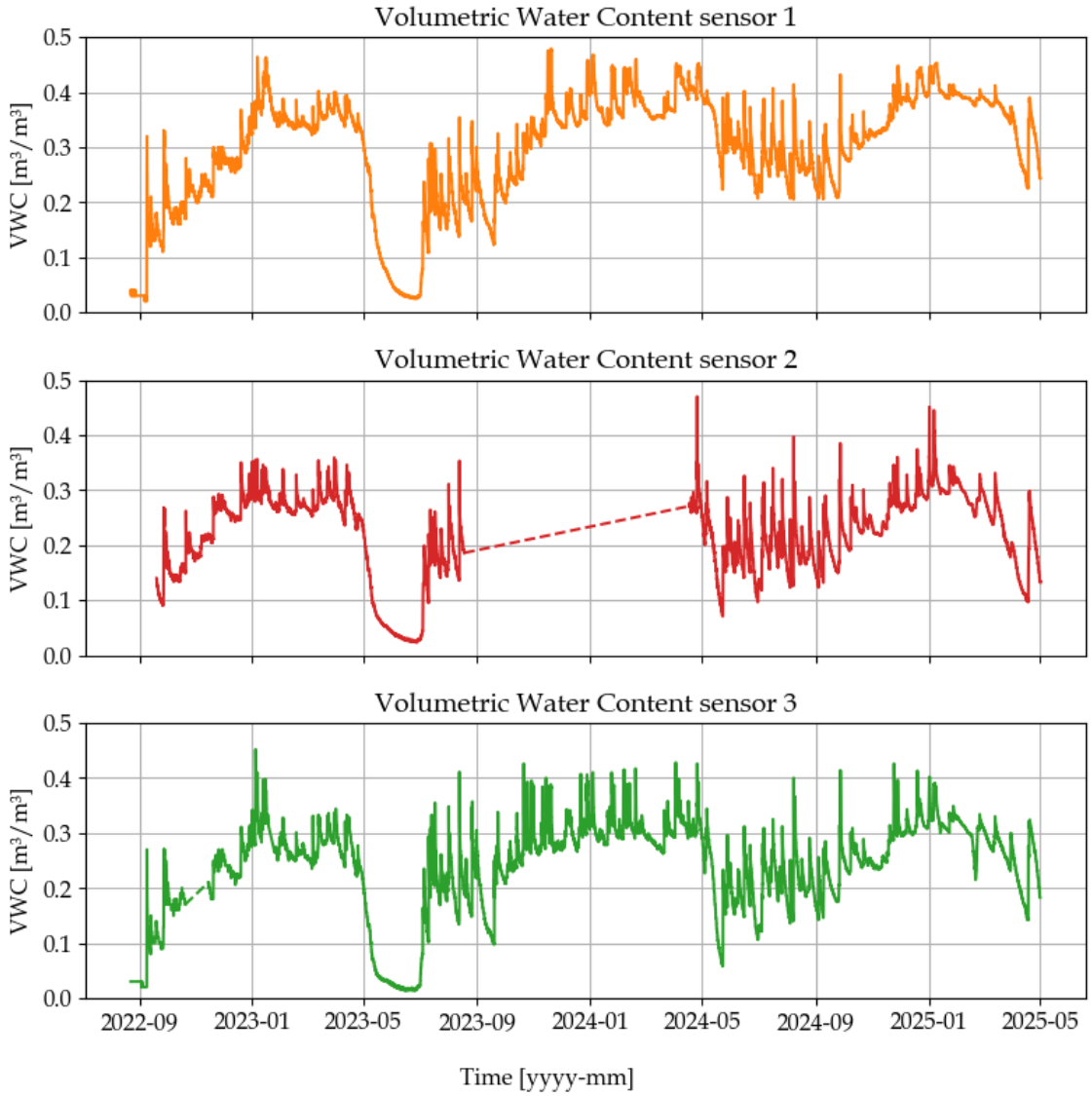

Figure A.2. VWC [m^3/m^3] measurements from Sensor 1, 2 and 3 at Ejby Mølle, Odense. Data disturbances in the VWC sensors are illustrated with a dashed line.

It can be seen that VWC Sensor 1 generally captures the widest range of VWC, ranging from approximately 0.05 to 0.50 m^3/m^3. Furthermore, the aforementioned data gaps in Sensors 2 and 3 are visible.

A.2 Elmelundsvej

The measurement stations in Elmelundsvej consist of:

Table A.2. Overview of the measurement stations at Elmelundsvej, Odense. The soil texture has been determined using the top soil map in Scalgo Live [Scalgo, 2024].

Sensor No.	Name	Soil Texture	Source
Water Level Sensors			
1	Målebrønd - 520-tryk1	-	Dryp
2	Målebrønd - 74E1-tryk2	-	Dryp
Rain Gauges			
-	5422 Bolbro Højdebeholder	-	SVK
Volumetic Water Content Sensors (VWC)			
1	Syd	Fine clay with sand	Dryp
2	Øst	Coarse clay with sand	Dryp
3	Nord	Coarse clay with sand	Dryp

The two figures below shows the land use change at Elmelundsvej, from a maintained lawn (Figure A.3) to a deliberately wild, natural landscape (Figure A.4)

Figure A.3. Elmelundsvej, Odense, March 2023. [Google Maps, 2024]

Figure A.4. Elmelundsvej, Odense, September 2024. [Google Maps, 2024]

Figure A.5 illustrates the data series from the rain gauge, the two water level sensors, and each of the VWC sensors. The lighter colours in the VWC data periods indicate breaks in the data series.

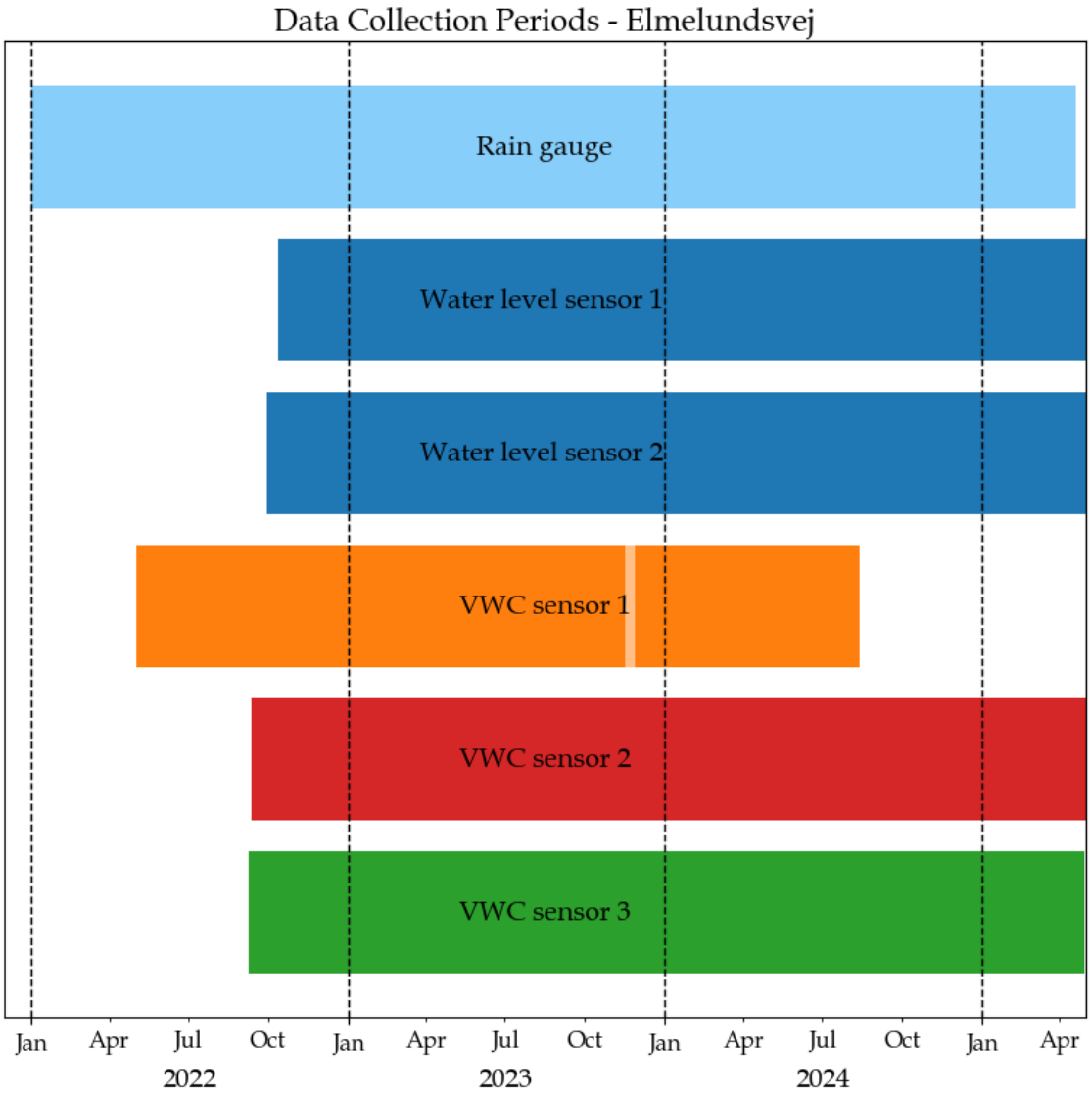

Figure A.5. Overview of the data periods for each of the measuring stations in Elmelundsvej, Odense. Data disturbances in the VWC sensors are illustrated with lighter colours.

The precipitation data ends earlier than the other sensors, which is due to the absence of rainfall during the latter half of April. Additionally, Sensor 1 exhibits a small data gap and a shorter time series, whereas Sensors 2 and 3 provide continuous time series. The limiting data for the analysis is the water level data, which is converted into a flow using a Q/H curve, presented in Appendix F.

Figure A.6 illustrates the data series in each of the VWC sensors. The dashed line indicates breaks in the data series.

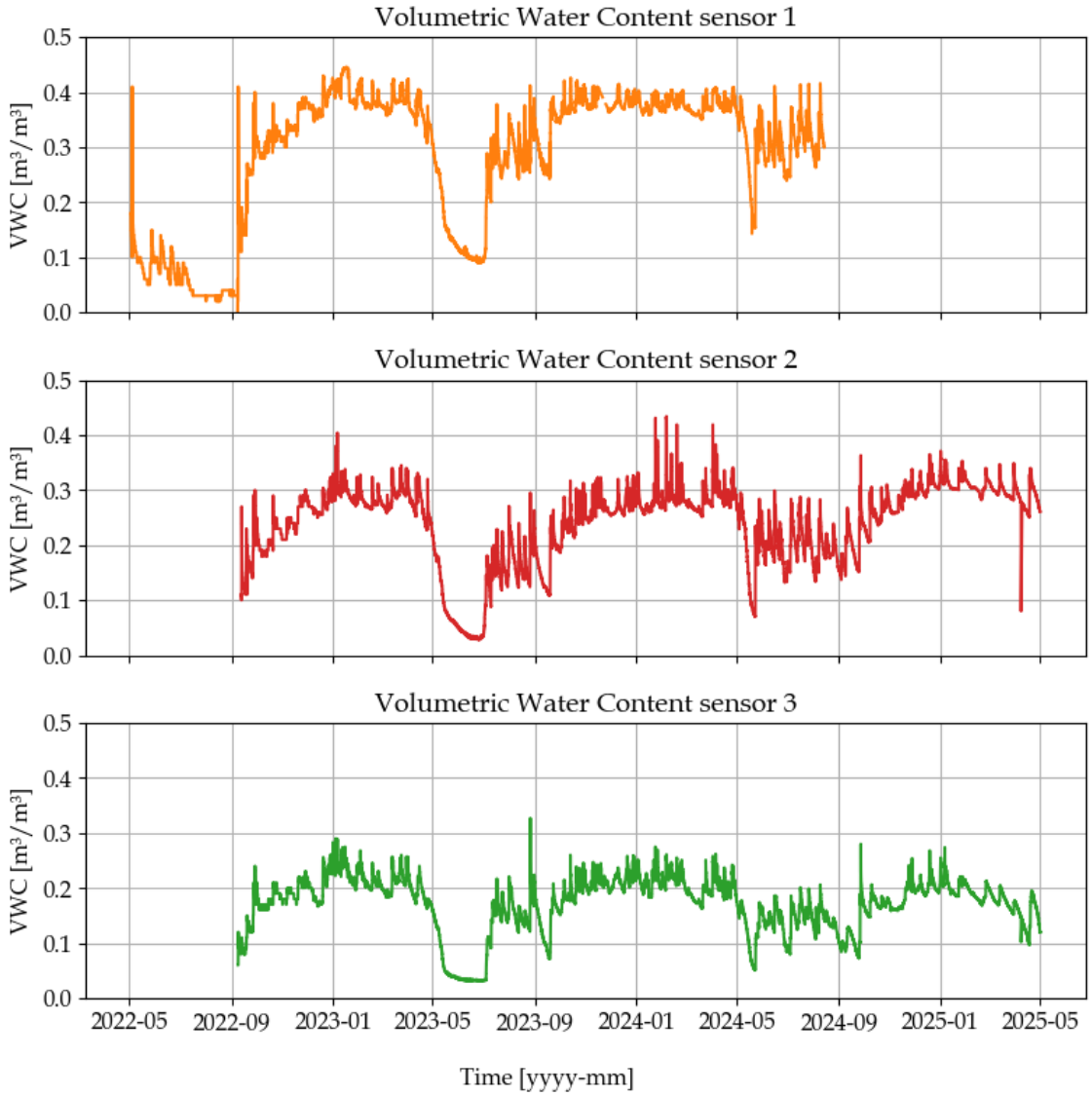

Figure A.6. VWC [m^3/m^3] measurements from sensors 1, 2, and 3 at Elmelundsvej, Odense. Data disturbances in the VWC sensors are illustrated with a dashed line.

It can be seen that VWC Sensor 1 generally captures the widest range of VWC, ranging from approximately 0.05 to 0.40 m^3/m^3, while Sensor 3 captures the narrowest range of VWC, ranging from 0.05 to 0.30 m^3/m^3. Furthermore, the aforementioned data gap in Sensor 1 is visible.

A.3 Lystrup

Figure A.7 shows the land use of the project area in Lystrup.

Figure A.7. Photograph of the project location in Lystrup. [Google Maps, 2024]

The measurement stations in Lystrup consist of:

Table A.3. Overview of the measurement stations in Lystrup. The soil texture has been determined using the top soil map in Scalgo Live [Scalgo, 2024].

Sensor No.	**Name**	**Soil Texture**	**Source**
Water Level Sensors			
-	V-overløb - Venstre	-	Dryp
Rain Gauges			
-	5180 Egå renseanlæg	-	SVK
Volumetic Water Content Sensors (VWC)			
1	Lystrup øverst 10 cm dybde	Fine clay with sand	Dryp
2	Lystrup øverst 20 cm dybde	Fine clay with sand	Dryp
3	Lystrup nederst 20 cm dybde	Fine clay with sand	Dryp

Figure A.8 illustrates the data series from the rain gauge, Q/H estimated flow, and each of the VWC sensors. The lighter colours in the VWC data periods indicate breaks in the data series.

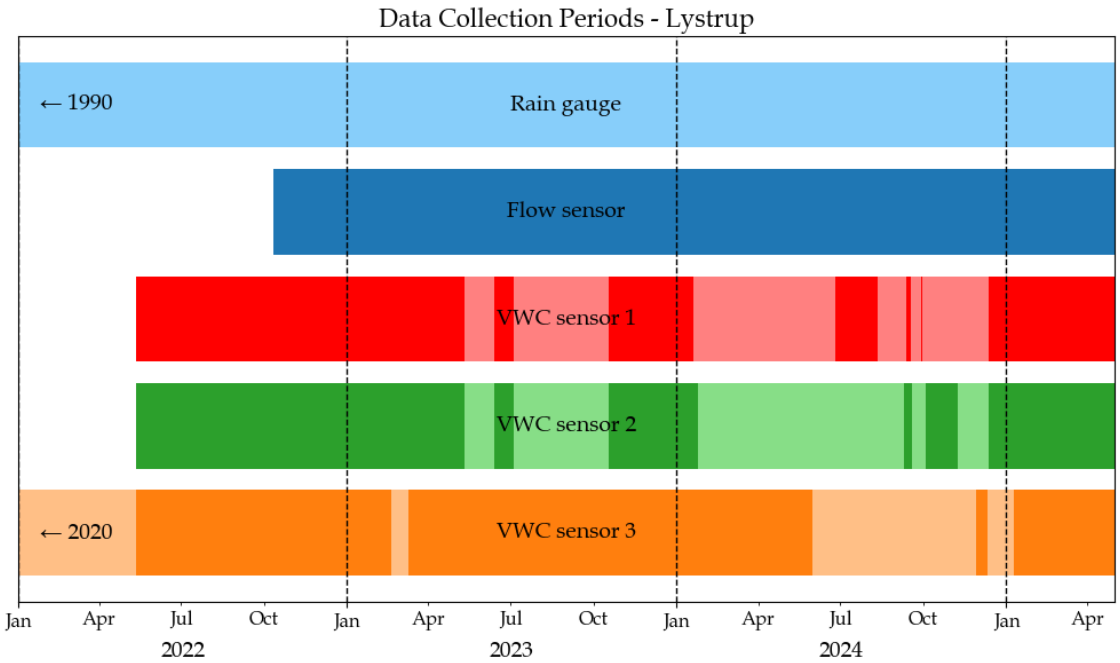

Figure A.8. Overview of the data periods for each of the measuring stations in Lystrup. Data disturbances in the VWC sensors are illustrated with lighter colours.

It is evident that all three sensors exhibit data gaps, while Sensor 1 and 2 contains shorter time series. The limiting data for the analysis is the flow data.

Figure A.9 illustrates the data series in each of the VWC sensors. The dashed line indicate breaks in the data series.

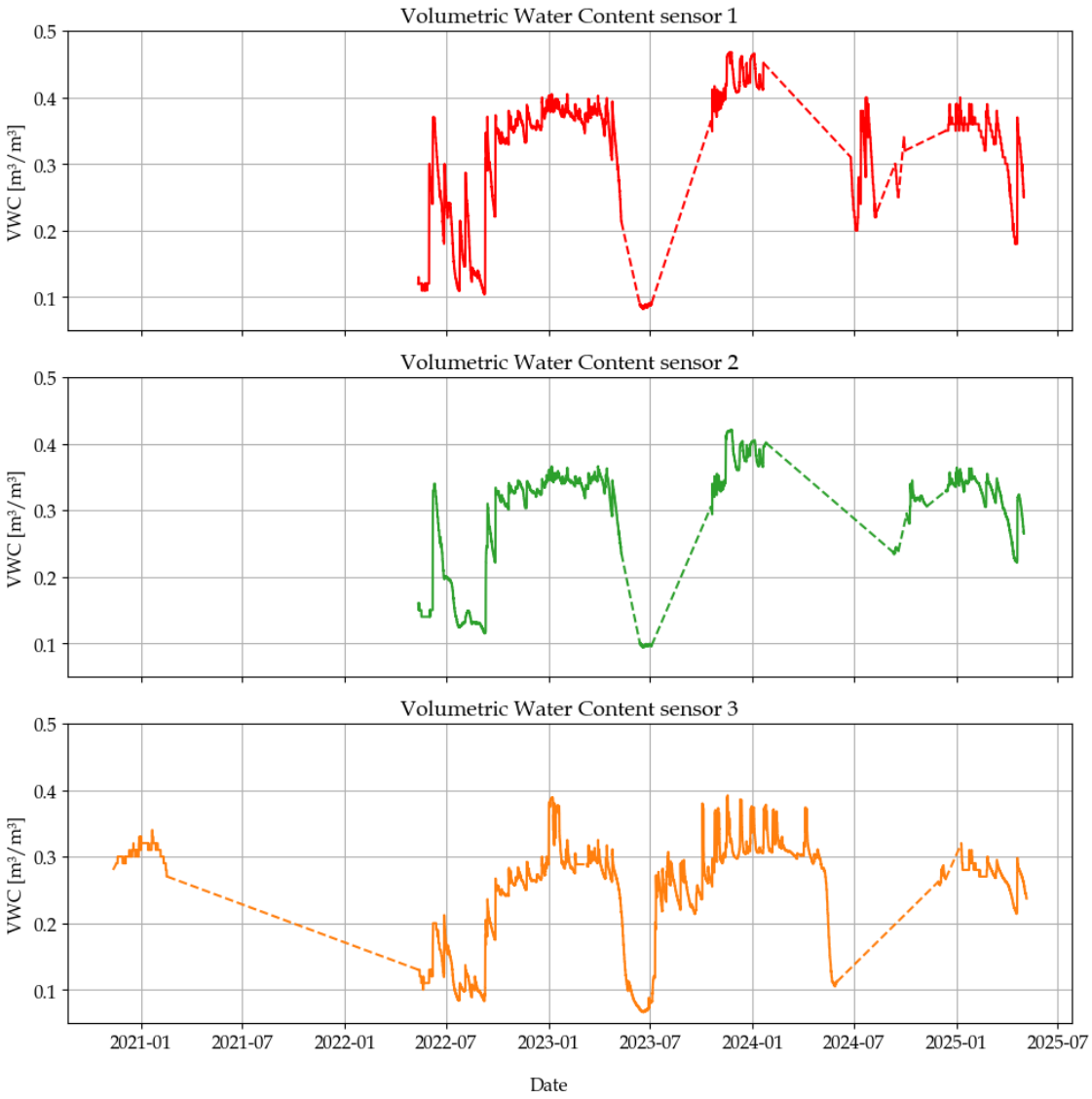

Figure A.9. VWC [m^3/m^3] measurements from sensor 1, 2 and 3 at Lystrup. Data disturbances in the VWC sensors are illustrated with a dashed line.

It can be seen that VWC Sensor 1 generally captures the widest range of VWC, ranging from approximately 0.10 to 0.45 m^3/m^3, while Sensors 2 and 3 capture slightly narrower ranges of VWC, ranging from 0.01 to 0.40 m^3/m^3. The aforementioned data gaps in all three sensors are visible, however, Sensor 3 contains the most continuous time series.

Urban Subcatchment Scale B

This appendix provides essential information regarding the available data from the urban subcatchment-scale areas Christianshusvej and Rungstedvej.

B.1 Christianshusvej

The measurement stations in Christianshusvej consist of:

Table B.1. Overview of the measurement stations at Christianshusvej, Hørsholm. The soil texture has been determined using the top soil map in Scalgo Live [Scalgo, 2024].

Sensor No.	Name	Soil Texture	Source
Flow sensors			
-	Målebrønd - Pipeflow-est-lvl1	-	Danova
Rain Gauges			
-	5622 Usserød Renseanlæg	-	SVK
Volumetic Water Content Sensors (VWC)			
1	- 10 cm	Fine clay with sand	Dryp
2	- 20 cm	Fine clay with sand	Dryp
3	- 25 cm	Fine clay with sand	Dryp
4	- 40 cm	Fine clay with sand	Dryp
5	Plæne midt	Fine clay with sand	Dryp
6	Skråning Syd	Fine clay with sand	Dryp

Figure B.1 illustrates the data series from the rain gauge, the two water level sensors, and the 6 VWC sensors. The lighter colours in the VWC data periods indicate breaks in the data series.

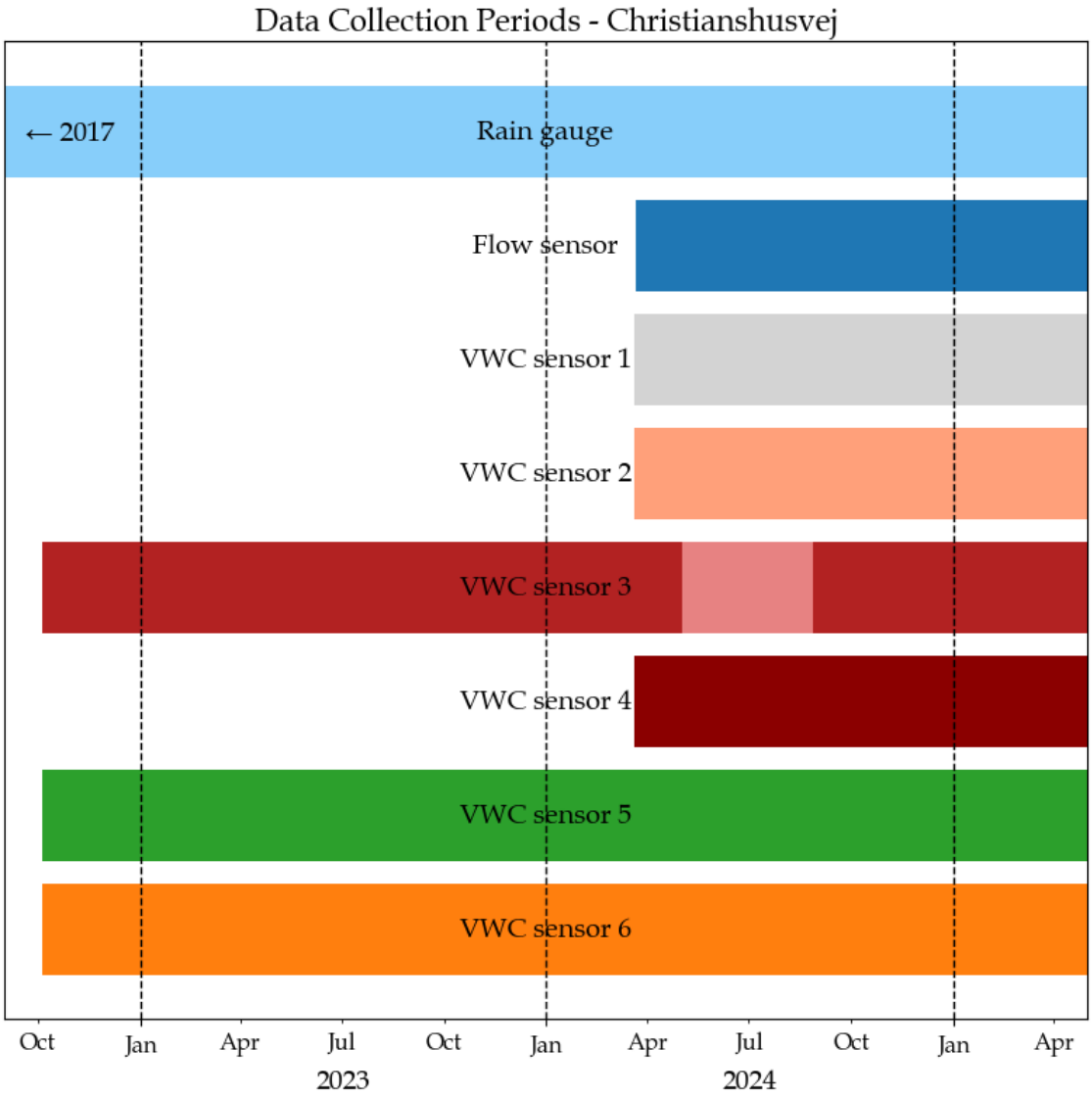

Figure B.1. Overview of the data periods for each of the measuring stations at Christianshusvej, Hørsholm. Data disturbances in the VWC sensors are illustrated with lighter colours.

It is evident that Sensor 3 exhibit a data gap, while Sensors 1, 2, 4, and the flow sensor dontains short time series. The limiting data for the analysis is the water level data.

Figure B.2 illustrates the data series in each of the VWC sensors. The dashed line indicate breaks in the data series.
It can be seen that Sensor 5 generally captures the widest range of VWC, ranging from approximately 0.01 to 0.40 m^3/m^3, while Sensor 6 capture the narrowest ranges of VWC, ranging from 0.15 to 0.35 m^3/m^3. The aforementioned data gap in Sensor 3 are visible.

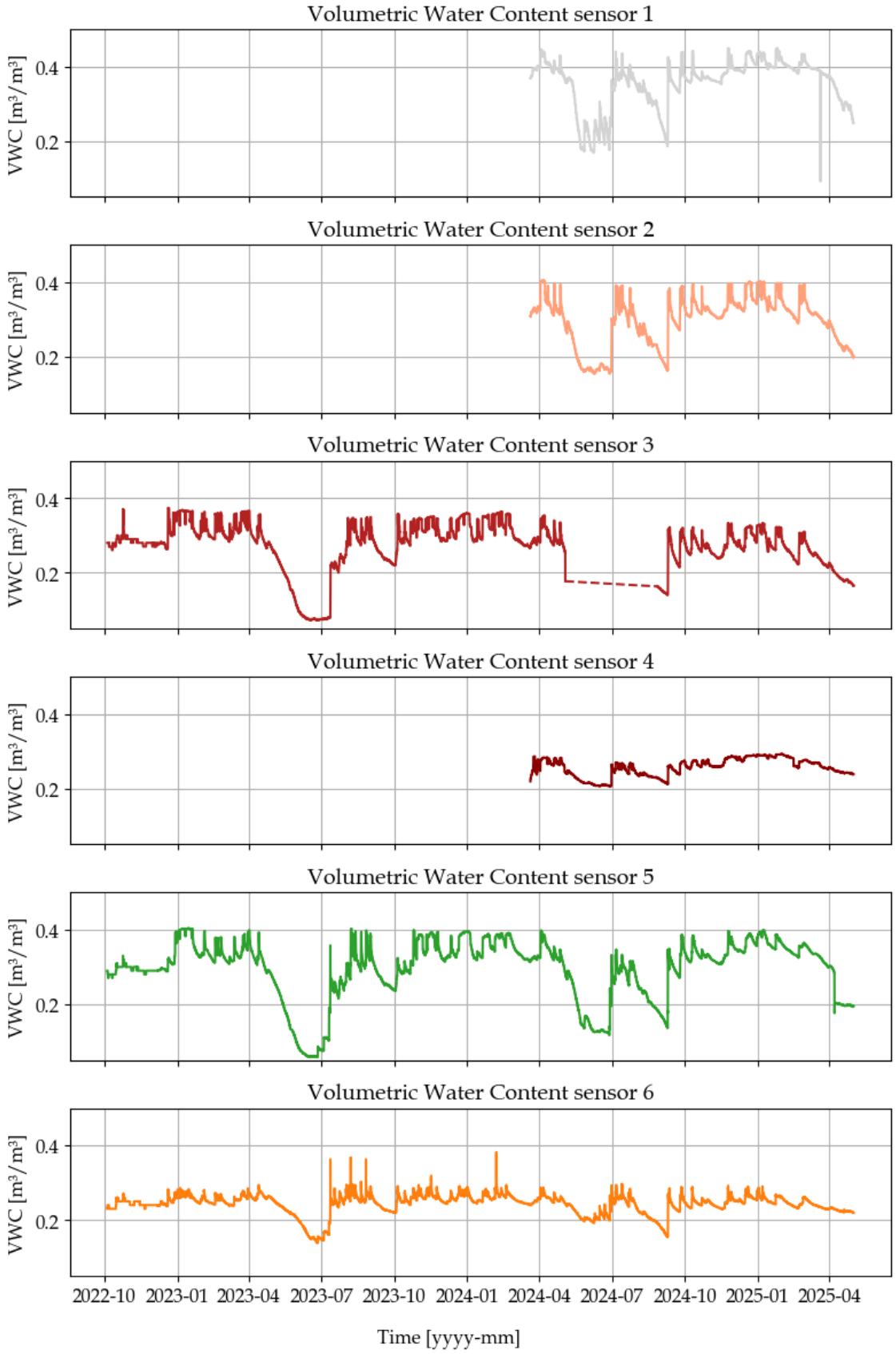

Figure B.2. VWC [m^3/m^3] measurements from Sensors 1, 2, 3, 4, 5 and 6 at Christianshusvej, Hørsholm. Data disturbances in the VWC sensors are illustrated with a dashed line.

Figure B.3 shows the land cover for the catchment area at Christianshusvej, and Table B.2 presents the percentage and total area for each land cover.

Figure B.3. Land cover in the catchment area at Christianshusvej, Hørsholm.

Table B.2. Values of land cover in Christianshusvej [Scalgo Live, 2025].

Land cover	**Area [Ha]**	**Cover [%]**
Natural land cover		
High vegetation	3.18	30
Low vegetation	2.41	23
Bare land	1.01	10
Water	0.01	0
Artificial land cover		
Buildings	1.58	15
Other impervious surfaces	1.4	13
Paved road	0.95	9

The degree of imperviousness is calculated by dividing the total artificial land cover by the total catchment area.

$$\beta = \frac{3.93\text{Ha}}{10.54\text{Ha}} = 37\% \tag{B.1}$$

B.2 Rungstedvej

The measurement stations in Rungstedvej consist of:

Table B.3. Overview of the measurement stations at Rungstedvej, Hørsholm. The soil texture has been determined using the top soil map in Scalgo Live [Scalgo, 2024].

Sensor No.	Name	Soil Texture	Source
Flow sensors			
-	2. 1970000 flow	-	Danova
Rain Gauges			
-	5623 Bukkeballevej pumpestation	-	SVK
Volumetic Water Content Sensors (VWC)			
1	Have Stolbjergsvej 15	Fine clay with sand	Dryp
2	Ane's bror	Fine clay with sand	Dryp
3	Borsøvej 34	Fine clay with sand	Dryp

Figure B.4 illustrates the data series from the rain gauge, the two water level sensors, and the 3 VWC sensors. The lighter colours in the VWC data periods indicate breaks in the data series.

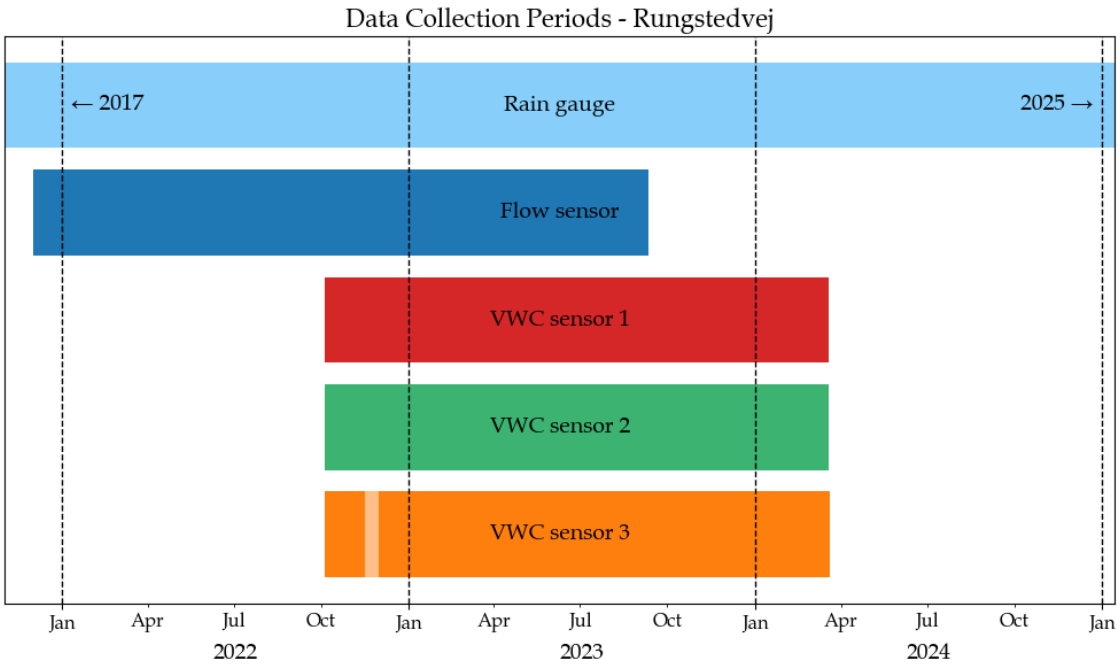

Figure B.4. Overview of the data periods for each of the measuring stations at Rungstedvej, Hørsholm. Data disturbances in the VWC sensors are illustrated with lighter colours.

It is evident that Sensor 3 exhibit a minor data gap. The limiting data for the analysis is the water level data.

Figure B.5 illustrates the data series in each of the VWC sensors. The dashed line indicate breaks in the data series.

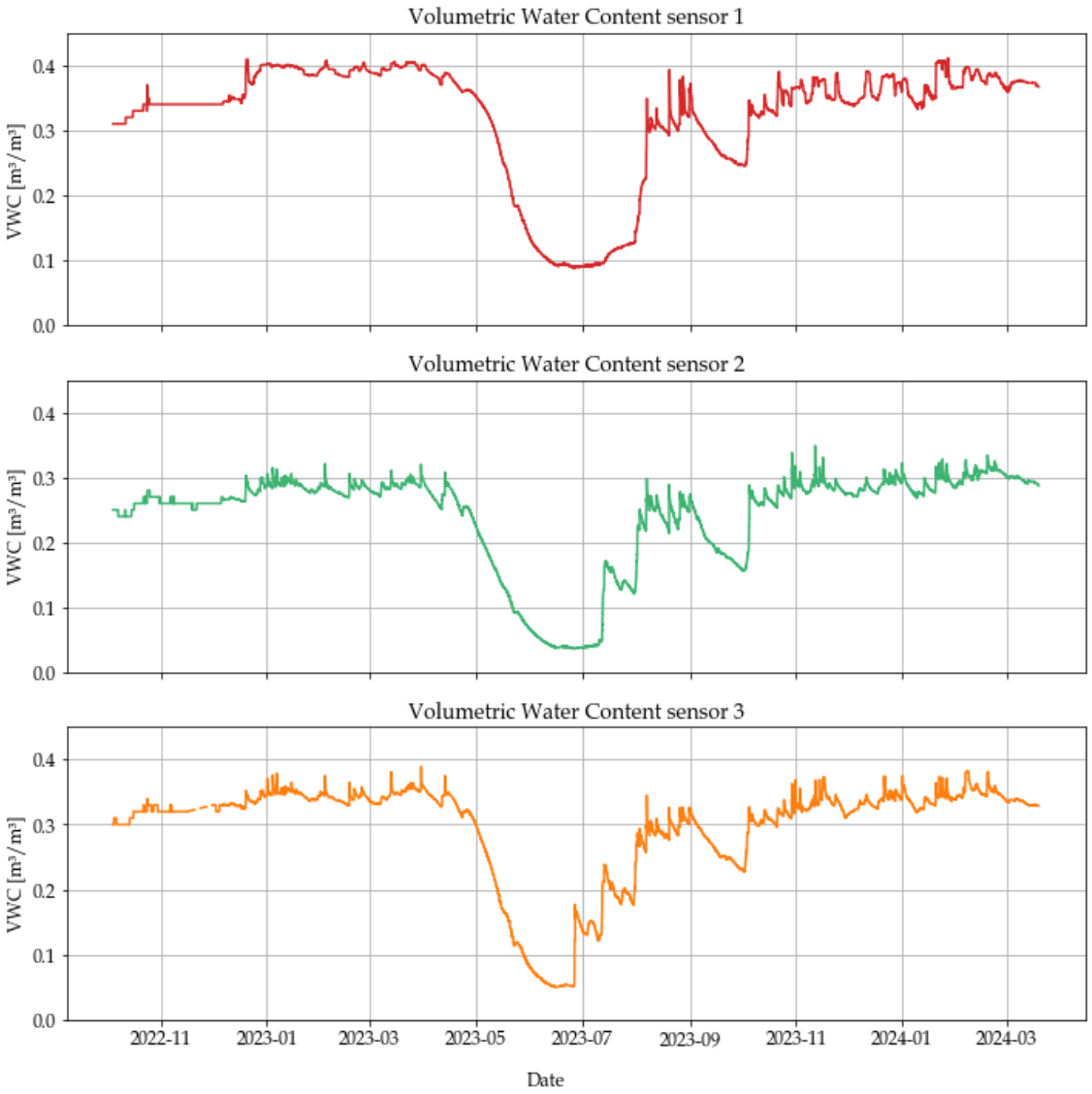

Figure B.5. VWC [m^3/m^3] measurements from sensor 1, 2, and 3 at Rungstedvej, Hørsholm. Data disturbances in the VWC sensors are illustrated with a dashed line.

It can be seen that all three sensors covers the same range, however, Sensor 2 generally measures lower VWC (0.05-0.30 m^3/m^3), while Sensor 1 measures higher VWC (0.10-0.40 m^3/m^3).

Figure B.6 shows the land cover of the catchment area at Rungstedvej, and Table B.4 presents the total area and percentage.

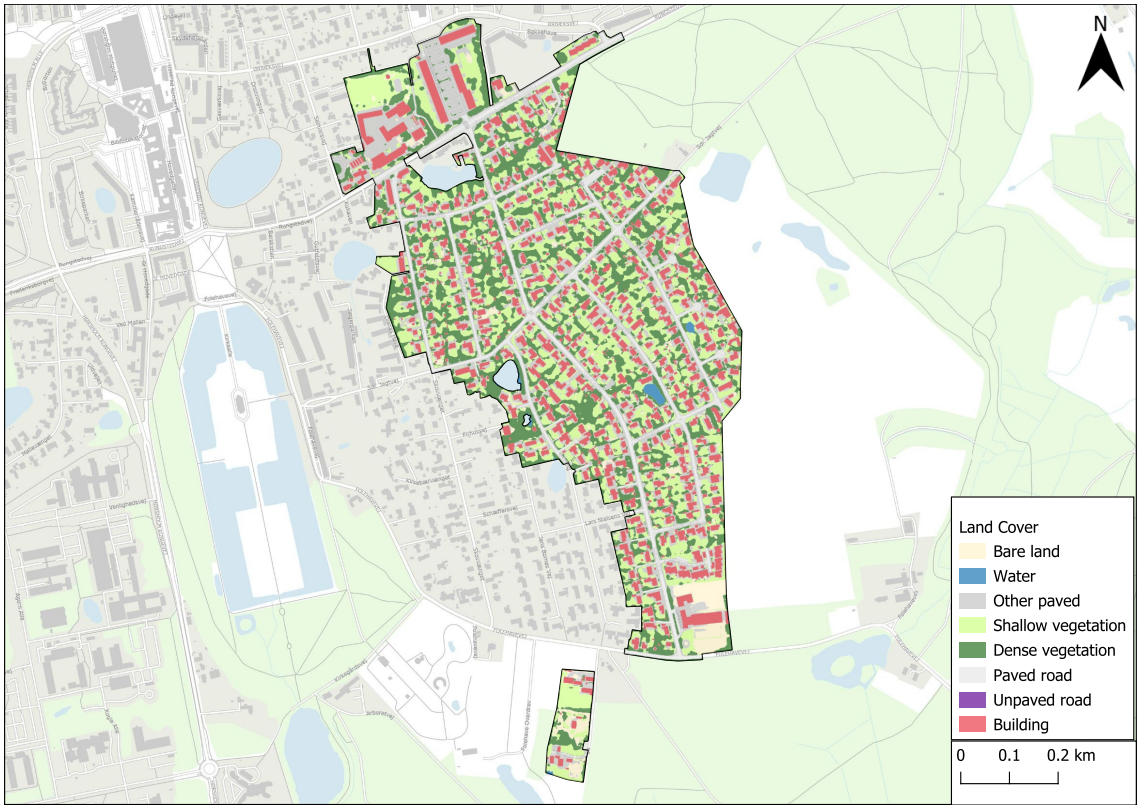

Figure B.6. Land cover in the catchment area at Rungstedvej, Hørsholm.

Table B.4. Values of land cover in Rungstedvej [Scalgo Live, 2025].

Land cover	**Area [Ha]**	**Cover [%]**
Natural land cover		
High vegetation	13.77	24
Low vegetation	13.91	25
Bare land	1.94	3
Water	0.16	0
Artificial land cover		
Buildings	10.07	18
Other impervious surfaces	11.92	21
Paved road	4.76	8

The degree of imperviousness is calculated by dividing the total artificial land cover by the total catchment area.

$$\beta = \frac{26.75\text{Ha}}{56.54\text{Ha}} = 47\% \tag{B.2}$$

Hydrological Scale C

This appendix provides essential information regarding the available data from the catchment area of Grejs Å within the large-scale project area, which directs water through the city of Vejle into Vejle Fjord. A comprehensive understanding of the processes and key influencing factors in the catchment area is necessary, as Vejle city faces a high risk of urban flooding during specific events.

C.1 Soil Characterisation and Land Cover

Given the large size of Grejs Å catchment area, the soil structure is anticipated to play a significant role in determining the extent of contingent runoff from the area. To illustrate this Figure C.1 and Table C.1 have been created to represent the distribution of key soil types within the topsoil of the catchment area. The topsoil refers to the upper 0-30 cm layer of soil at the surface, and it is assumed that potential subsurface interflow may occur within this depth.

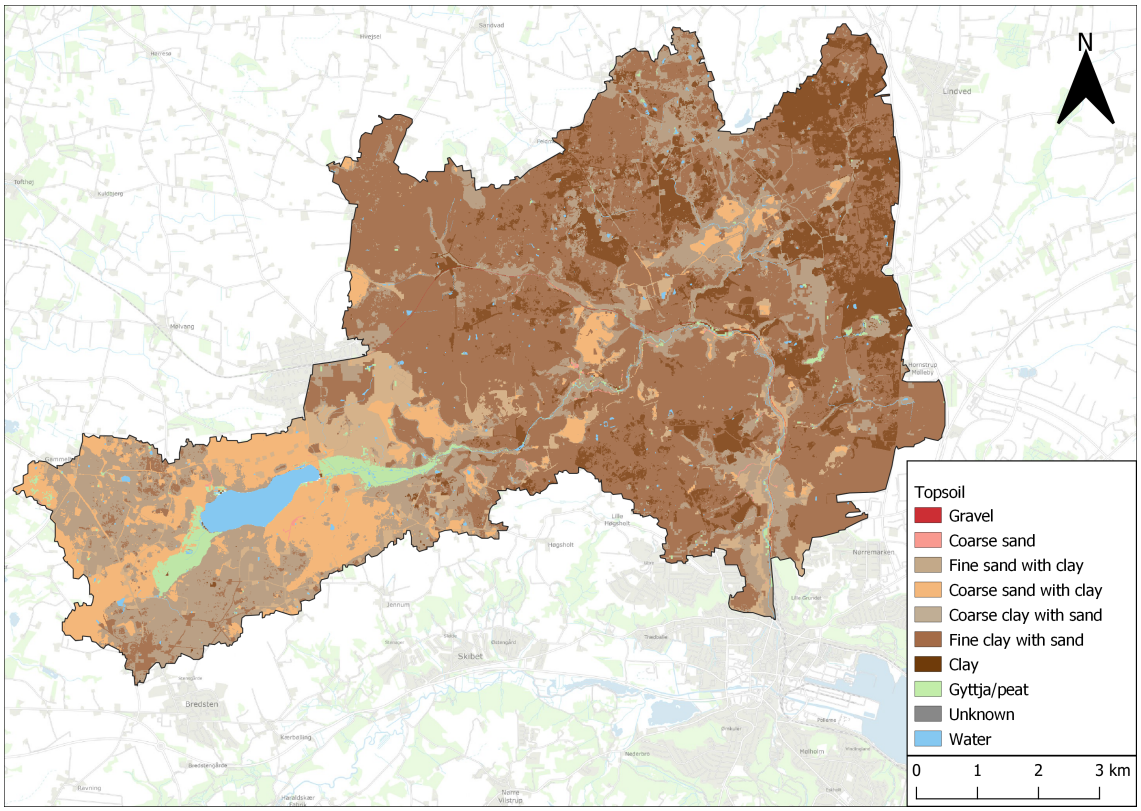

Figure C.1. Overview of the topsoil (0-30 cm) in Grejs Å catchment area [Scalgo Live, 2025].

Table C.1. Values of soil types in the top soil of Grejs Å catchment area [Scalgo Live, 2025].

Soil texture	**Area [km^2]**	[%]
Coarse sand with clay	111,43	33
Coarse clay with sand	110,84	33
Fine clay with sand	54,25	16
Clay	18,07	5
Fine sand with clay	16,42	5
Coarse sand	12,64	4
Gyttja/peat	8,58	3
Water	5,32	2
Unknown	8,13 ha	0
Gravel	6,48 ha	0
Fine sand	2,03 ha	0

From Figure C.1 and Table C.1, it is evident that the Grejs Å catchment area is predominantly composed of coarse sand with clay and coarse clay with sand, which generally results in limited water storage capacity in the soil column.

Additionally, land cover influences the areas contributing to contingent runoff. Areas with vegetation reduce runoff by absorbing water through the root system, while areas with heavy machinery can become compacted, increasing their contribution to contingent runoff. The land cover of Grejs Å catchment area is illustrated in Table C.2.

Table C.2. Values of land cover in Grejs Å catchment area [Scalgo Live, 2025].

Land cover	**Area [km^2]**	**Cover [%]**
Natural land cover		
Fields	149,26	44
High vegetation	90,26	27
Low vegetation	56,55	17
Bare soil	18,76	6
Unpaved road	0,50	0
Railway	6,48	0
Water	5,32	2
Artificial land cover		
Buildings	6,15	2
Other impervious surfaces	5,56	2
Paved road	5,29	2

It is evident that the land cover in Grejs Å catchment area is dominated by natural areas with vegetation, with 44% covered by fields, 27% by high vegetation, and 17% by low vegetation.

C.2 Measurement Stations in the Catchment Area

To study the contingent runoff from the catchment area, eight volumetric water content (VWC) sensors and two flow stations have been installed. The VWC data is retrieved from DRYP's database, while the flow data is obtained from Vandportalen.dk. Additionally, two SVK rain gauges, placed in the catchment area, are used to account for precipitation. An overview of the flow station, rain gauges, and VWC sensors is provided in Table C.3.

Table C.3. Overview of the measurement stations in Grejs Å catchment area.

Sensor No.	**Name**	**Soil Texture**	**Source**
Flow Sensors			
-	St. 32.22 (Water Level and flow)	-	Vandportalen
Rain Gauges			
1	5230 Jelling	-	SVK
2	5235 Vejle Centralrenseanlæg	-	SVK
Volumetic Water Content Sensors (VWC)			
1	Meltas Skråning	Clay	Dryp
2	Tør Rigkær	Coarse clay with sand	Dryp
3	Våd Rigkær	Coarse clay with sand	Dryp
4	Grejs Skov	Coarse clay with sand	Dryp
5	Skoven	Clay	Dryp
6	Mark-kant	Fine clay with sand	Dryp
7	Græs 1	Fine clay with sand	Dryp
8	Græs 2	Fine clay with sand	Dryp

It is informed that both flow and water level are measured at St. 32.22. was only installed in 2024, whereas the water level measurement dates back to 2013. Hence why the Q/H estimated flow from the water level measurement will be utilised for the analysis.

Figure C.2 illustrates the data series from the rain gauge, Q/H estimated flow, and each of the VWC sensors. The lighter colours in the VWC data periods indicate breaks in the data series.

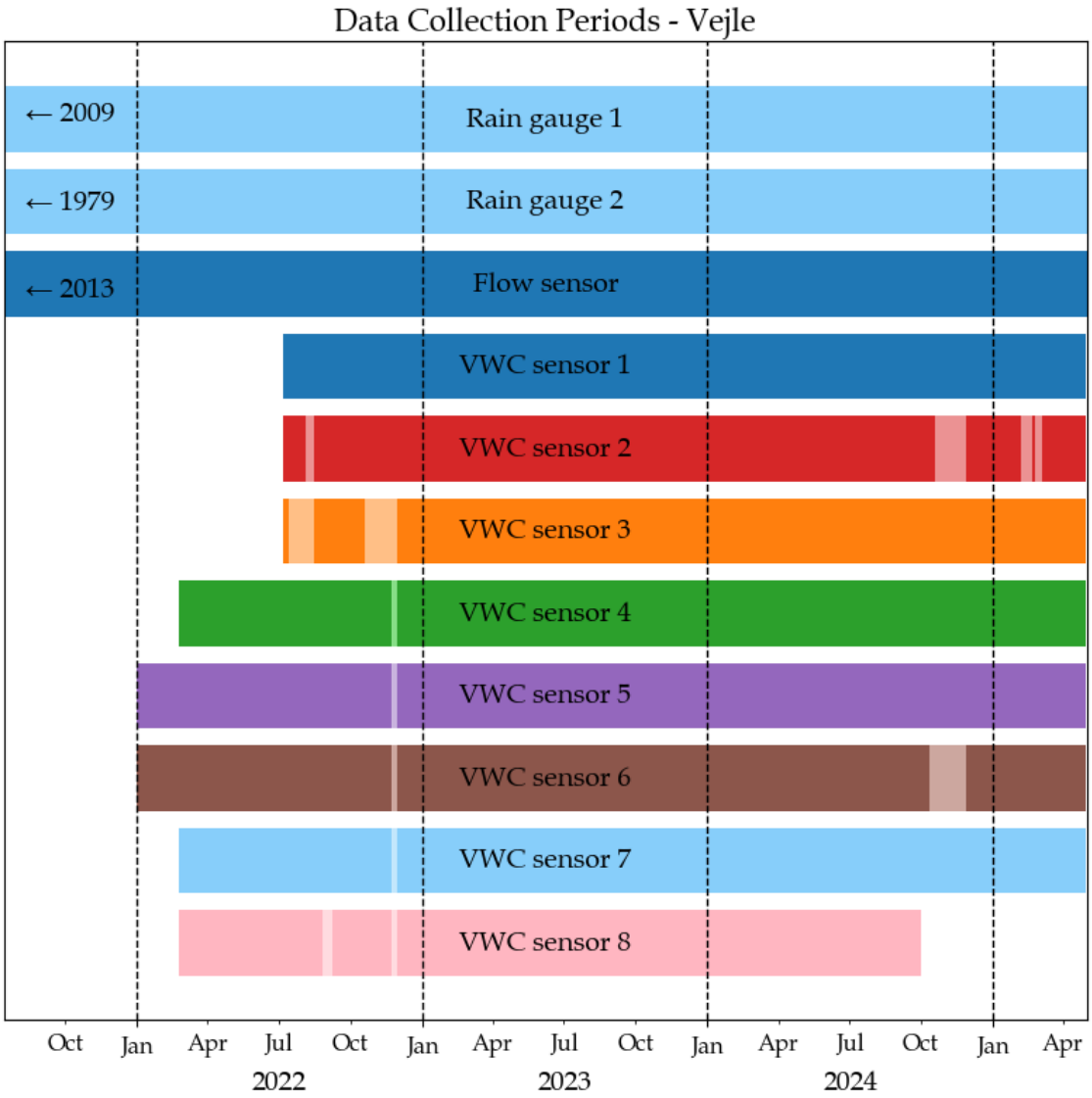

Figure C.2. Overview of the data periods for each of the measuring stations in Vejle. Data disturbances in the VWC sensors are illustrated with lighter colours.

It is evident that all but Sensor 1 exhibit data gaps, and that Sensor 8 contains a shorter time series.

Figure C.3 illustrates the data series in VWC sensors 1, 2, 3, and 4. The dashed line indicates breaks in the data series.

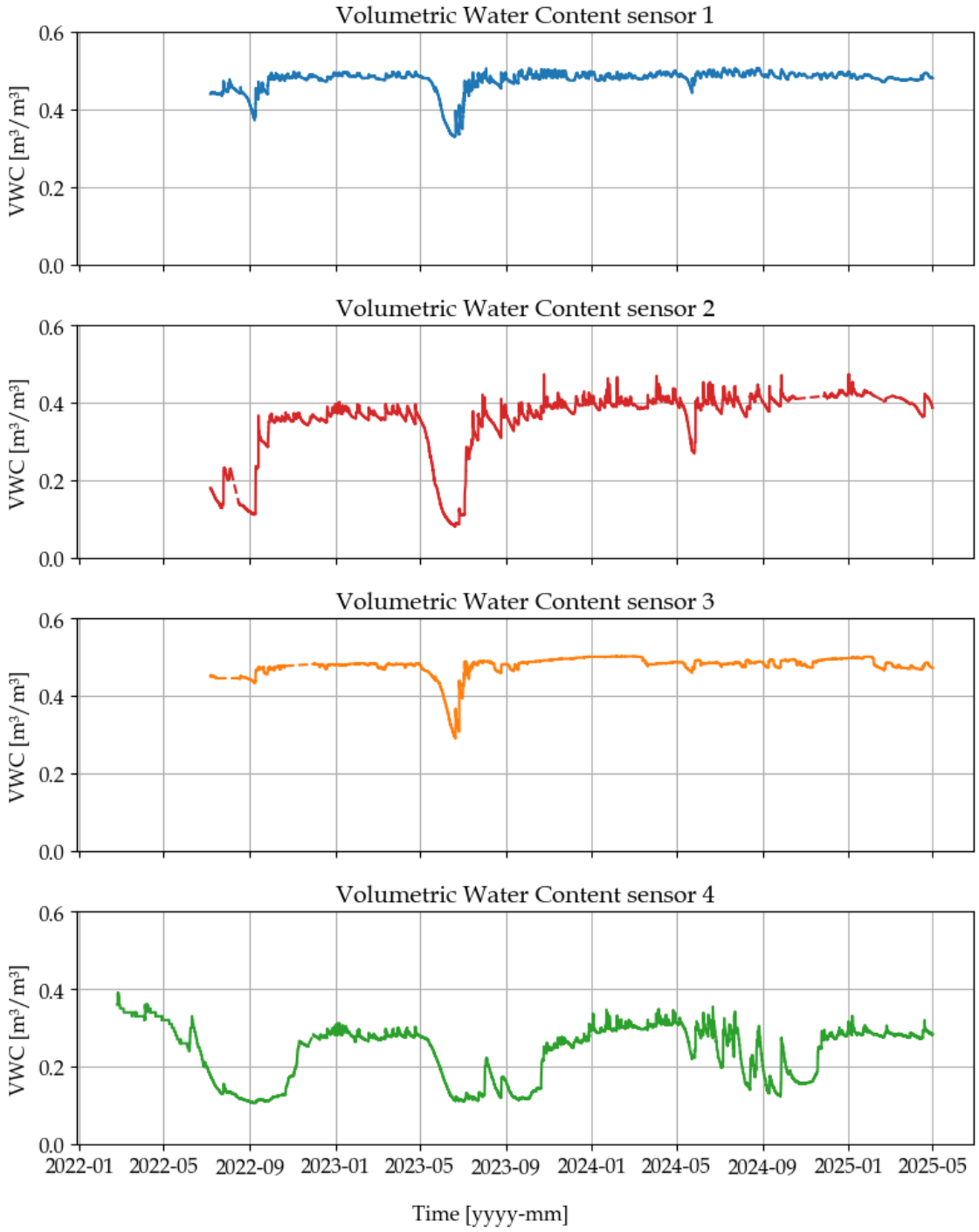

Figure C.3. VWC [m^3/m^3] measurements from sensor 1, 2, 3 and 4 in Vejle. Data disturbances in the VWC sensors are illustrated with a dashed line.

Figure C.4 illustrates the data series in VWC sensors 5, 6, 7, and 8. The dashed line indicates breaks in the data series.

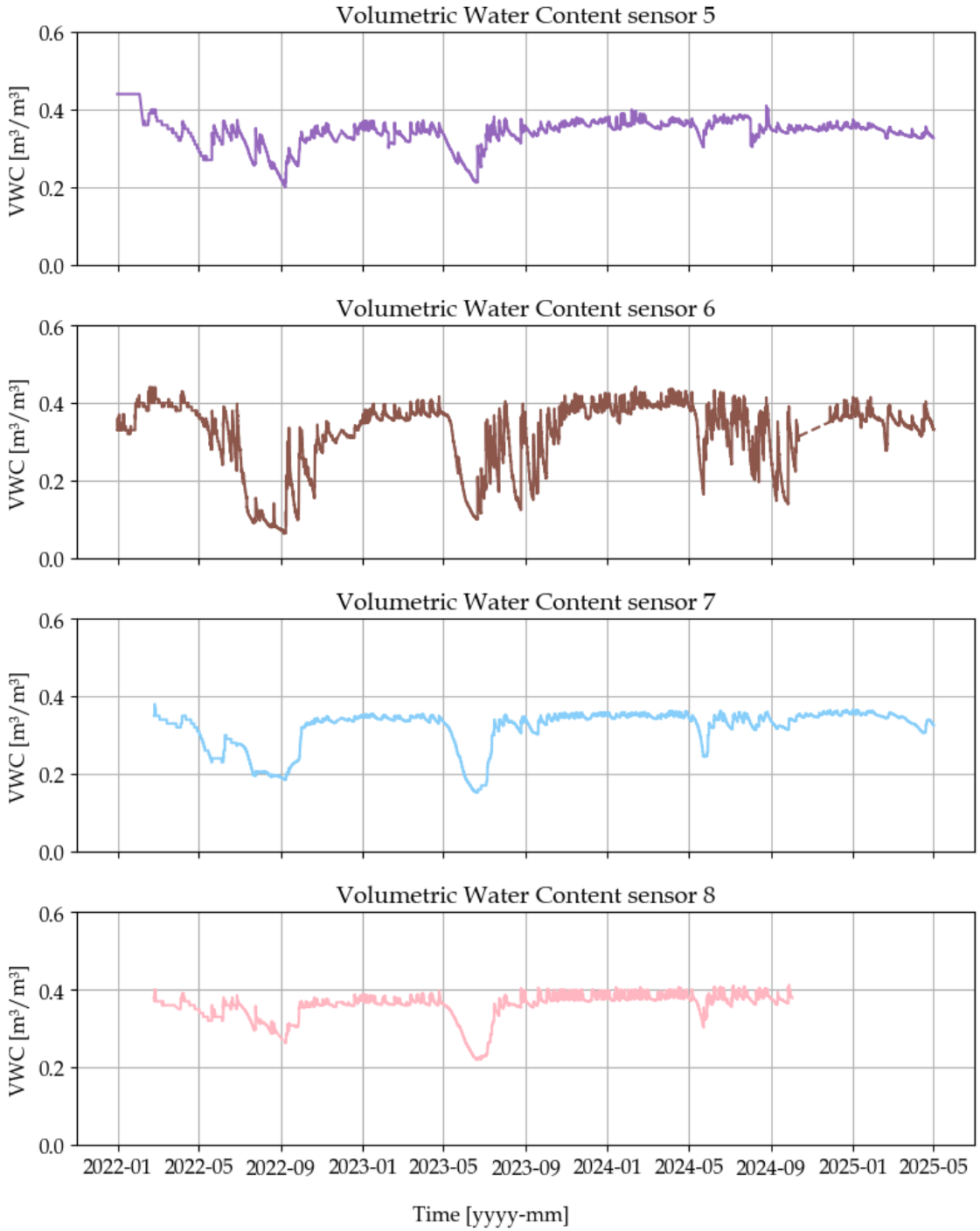

Figure C.4. VWC [m^3/m^3] measurements from sensor 5, 6, 7 and 8 in Vejle. Data disturbances in the VWC sensors are illustrated with a dashed line.

It can be seen that VWC Sensors 2 and 6 generally captures the widest ranges of VWC, ranging from approximately 0.10 to 0.40 m^3/m^3, whereas Sensor 6 contains more variable VWC data, while the generally highest VWC is measured in Sensor 1 ($\approx$ 0.45 m^3/m^3). The aforementioned data gaps are also visible.

Analysis of VWC Sensors D

This appendix will present some additional results of the *statistical analysis*, including Spearman's correlations for choosing the optimal VWC sensor (section D.1), the optimal VWC metric for runoff prediction (section D.2), the optimal sensor depth (section D.3), and density plots for VWC data (section D.4).

D.1 Determination of the Optimal VWC Sensor for Runoff Prediction

At all project locations, multiple sensors have been installed. These sensors vary in length, VWC measurements, and continuity. Therefore, a Spearman's correlation analysis is conducted to determine which of the VWC sensors best represents runoff at each location.

Hillslope Scale

Table D.1. Spearman's correlation for sensors at hillslope scale ($\alpha_{adjusted} = 0.0166$).

Sensor No.	**1**	**2**	**3**
Ejby Mølle, Odense			
ρ	0.123	0.110	0.025
p-value	$1.54{\cdot}10^{-1}$	$1.11{\cdot}10^{-1}$	$7.43{\cdot}10^{-1}$
Elmelundsvej, Odense			
ρ	0.129	0.054	0.199
p-value	$2.91{\cdot}10^{-2}$	$3.59{\cdot}10^{-1}$	$7.11{\cdot}10^{-4}$
Lystrup			
ρ	0.700	0.584	0.765
p-value	$1.24{\cdot}10^{-34}$	$4.33{\cdot}10^{-22}$	$1.04{\cdot}10^{-44}$

In Table D.1, the Spearman's coefficients and p-values are presented for Ejby Mølle, Elmelundsvej (both located in Odense), and Lystrup. At Ejby Mølle, Sensor 1 exhibits the highest Spearman's coefficient among the three sensors, indicating the strongest correlation between VWC and runoff. However, its p-value is above the adjusted significance level ($\alpha_{adjustet}$). However, since the primary objective is to determine which sensor best represents the VWC-runoff relationship, correlation strength is prioritised over the statistical significance. Additionally, the relatively small sample size at Ejby Mølle (n = 151) may

introduce statistical uncertainties, potentially affecting the p-value and reinforcing the need to consider effect size in the analysis. Therefore, given Sensor 1's stronger correlation, it is deemed the most representative sensor for capturing the VWC-runoff relationship at this location.
At Elmelundsvej, the p-value for all three sensors is below the significance level ($\alpha_{adjusted}$). Therefore, Sensor 3 is selected for the *VWC and runoff analysis*, as it has the highest Spearman's coefficient (ρ) and a long, continuous time series. Similarly, at Lystrup, the p-values for all three sensors are below the significance level ($\alpha_{adjusted}$). Hence, Sensor 3 is chosen, as it has the highest Spearman's coefficient (ρ) and a long, continuous time series.

Urban Subcatchment Scale

Table D.2. Spearman's correlation for sensors at urban subcatchment scale ($\alpha_{adjusted} = 0.0166$).

Christianshusvej, Hørsholm			
Sensor No.	**3**	**5**	**6**
ρ	0.533	0.306	0.553
p-value	$8.93{\cdot}10^{-10}$	$4.89{\cdot}10^{-8}$	$8.69{\cdot}10^{-26}$
Rungstedvej, Hørsholm			
Sensor No.	**1**	**2**	**3**
ρ	0.142	0.318	0.298
p-value	$3.43{\cdot}10^{-2}$	$1.24{\cdot}10^{-6}$	$5.86{\cdot}10^{-6}$

In Table D.2, the Spearman's coefficients and p-values are presented for Christianshusvej and Rungstedvej, both located in Hørsholm. At Christianshusvej, the p-values for all three sensors are below the significance level ($\alpha_{adjusted}$). Sensor 6 is selected for the *VWC and runoff analysis*, as it has the highest Spearman's coefficient (ρ). At Rungstedvej, the p-values for all three sensors are below the significance level ($\alpha_{adjusted}$). Hence, Sensor 2 is chosen, as it has the highest Spearman's coefficient (ρ).

Hydrological Scale

Table D.3. Spearman's correlation for sensors at Vejle ($\alpha_{adjusted} = 6.3{\cdot}10^{-3}$).

Sensor	**1**	**2**	**3**	**4**	**5**	**6**	**7**	**8**
Vejle								
ρ	0.545	0.596	0.263	0.391	0.563	0.595	0.546	0.597
p-value	$2.71{\cdot}10^{-46}$	$3.77{\cdot}10^{-57}$	$1.25{\cdot}10^{-10}$	$9.45{\cdot}10^{-23}$	$5.9{\cdot}10^{-50}$	$4.37{\cdot}10^{-57}$	$1.37{\cdot}10^{-46}$	$1.5{\cdot}10^{-57}$

In Table D.2, the Spearman's coefficients and p-values for Vejle are presented. It is evident that the p-values for all eight sensors are below the significance level ($\alpha_{adjusted}$). Although Sensors 8 and 2 have the highest Spearman's coefficient, Sensor 2 is located relatively

far from the flow measurement station 32.22 and Sensor 8 only has data until October 2024. Therefore, Sensor 6 is selected for the *VWC and runoff analysis*, as it has a high Spearman's coefficient (ρ) and a long, continuous time series.

D.2 Determination of the Optimal VWC Metric for Runoff Prediction

To determine which VWC metric best predicts runoff generation, a Spearman's correlation is performed on the minimum, median, mean, and maximum VWC for all project locations. It is evident that the maximum VWC has the highest spearman's coefficient across all six areas, with p-values below the significance level ($\alpha_{adjusted}$) (cf. Table D.4, Table D.5, and Table D.6). Therefore, the maximum VWC is used in the runoff analysis in Part I.

Hillslope Scale

Table D.4. Spearman's correlation for the optimal VWC metric at Hillslope Scale ($\alpha_{adjusted} = 0.0125$).

	Minimum	**Median**	**Mean**	**Max**
Ejby Mølle, Odense				
ρ	-0.076	-0.029	-0.011	0.110
p-value	$3.24{\cdot}10^{-1}$	$7.11{\cdot}10^{-1}$	$8.85{\cdot}10^{-1}$	$1.54{\cdot}10^{-1}$
Elmelundsvej, Odense				
ρ	-0.006	0.137	0.131	0.251
p-value	$8.99{\cdot}10^{-1}$	$6.76{\cdot}10^{-3}$	$9.71{\cdot}10^{-3}$	$5.796{\cdot}10^{-7}$
Lystrup				
ρ	0.605	0.657	0.661	0.671
p-value	$5.27{\cdot}10^{-39}$	$5.28{\cdot}10^{-48}$	$9.11{\cdot}10^{-49}$	$1.11{\cdot}10^{-50}$

Urban Subcatchment Scale

Table D.5. Spearman's correlation for the optimal VWC metric at Urban Subcatchment Scale ($\alpha_{adjusted} = 0.0125$).

	Minimum	**Median**	**Mean**	**Max**
Christianshusvej, Hørsholm				
ρ	0.185	0.419	0.407	0.552
p-value	$1.16{\cdot}10^{-3}$	$1.99{\cdot}10^{-14}$	$1.16{\cdot}10^{-13}$	$7.76{\cdot}10^{-26}$
Rungstedvej, Hørsholm				
ρ	0.050	0.217	0.212	0.318
p-value	$4.58{\cdot}10^{-1}$	$1.14{\cdot}10^{-3}$	$1.43{\cdot}10^{-3}$	$1.24{\cdot}10^{-6}$

Hydrological Scale

Table D.6. Spearman's correlation for the optimal VWC metric at Hydrological Scale ($\alpha_{adjusted} = 0.0125$).

	Minimum	**Median**	**Mean**	**Max**
Vejle				
ρ	0.340	0.452	0.455	0.604
p-value	$1.01{\cdot}10^{-21}$	$7.70{\cdot}10^{-39}$	$1.96{\cdot}10^{-39}$	$2.40{\cdot}10^{-75}$

D.3 Determination of the Optimal VWC Sensor Depth

To determine the optimal sensor depth for predicting runoff generation, a Spearman's correlation analysis is performed on Sensors 1–4 at Christianshusvej, Hørsholm, as these sensors are installed at different depths (-10, -20, -25, and -40 cm, respectively) within the same borehole. The p-values for Sensors 1-3 are below the significance level ($\alpha_{adjusted}$), with Sensor 3 (-25 cm) exhibiting the highest Spearman's coefficient. However, Sensor 3 is the only sensor with a prolonged data gap (May-September 2024) in VWC measurements, which is expected to impact its reliability in predicting runoff. Therefore, Sensor 1 (-10 cm) is deemed the optimal depth, as it has the second highest Spearman's coefficient and a continuous time series.

Table D.7. Spearman's correlation for sensor depth, Christanshusvej, Hørsholm ($\alpha_{adjusted} = 0.0125$).

Sensor No.	**1**	**2**	**3**	**4**
Christianshusvej, Hørsholm				
ρ	0.509	0.469	0.533	0.173
p-value	$6.42{\cdot}10^{-9}$	$1.28{\cdot}10^{-7}$	$8.93{\cdot}10^{-10}$	$6.51{\cdot}10^{-2}$

D.4 Density Distribution Functions for VWC Sensors

To understand variations in VWC between the sensors at the six different project locations, probability density functions (PDFs) are generated for all VWC sensors at each location.

Hillslope Scale

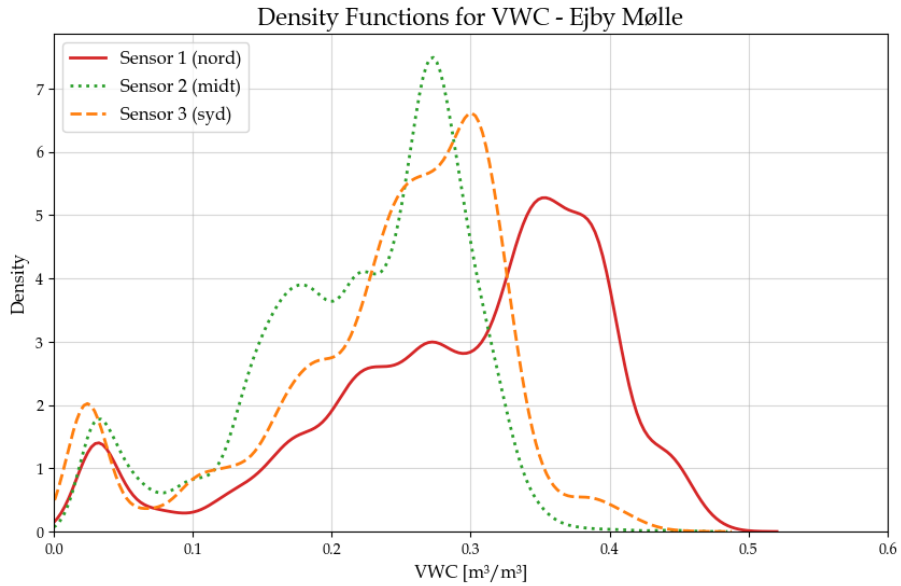

Figure D.1. PDF's of VWC for the three sensors at Ejby Mølle, Odense.

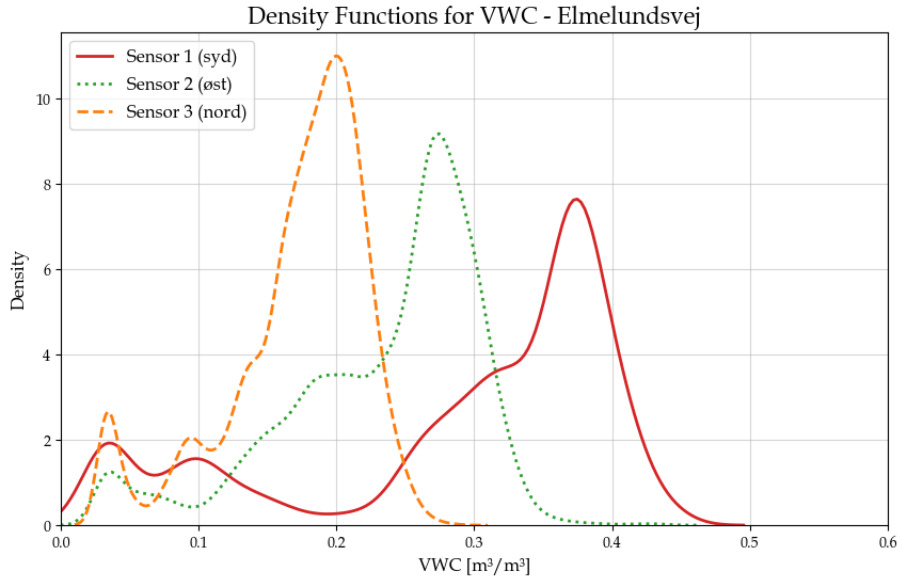

Figure D.2. PDF's of VWC for the three sensors at Elmelundsvej, Odense.

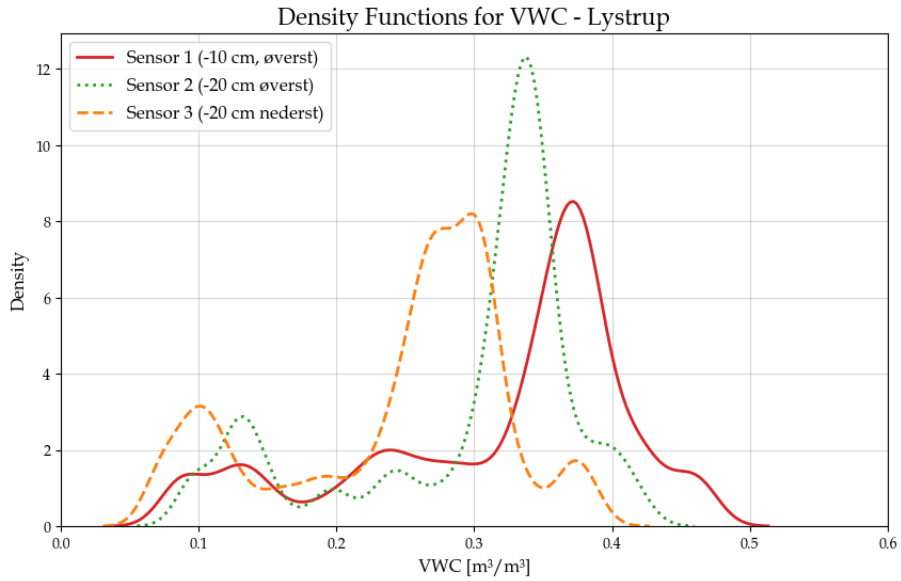

Figure D.3. PDF's of VWC for the three sensors at Lystrup.

Urban Subcatchment Scale

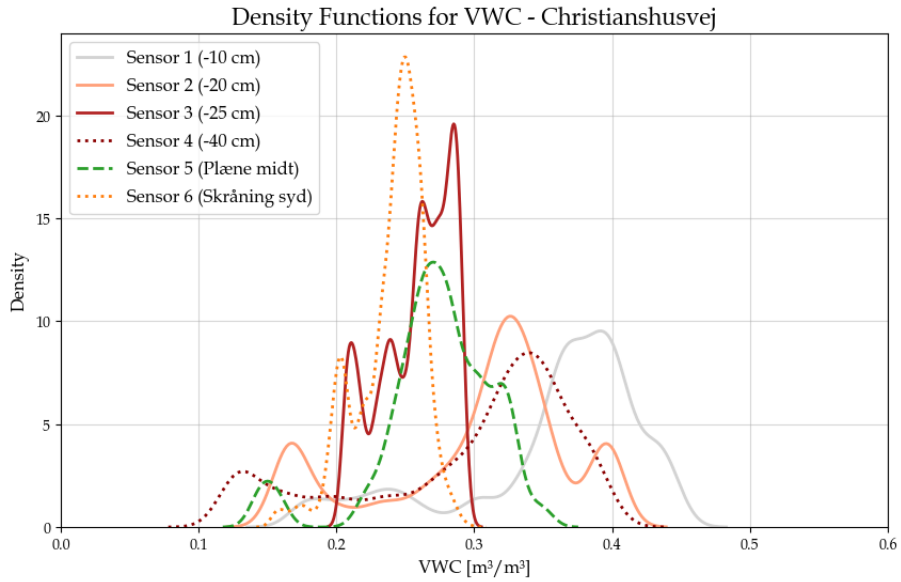

Figure D.4. PDF's of VWC for the six sensors at Christianshusvej, Hørsholm.

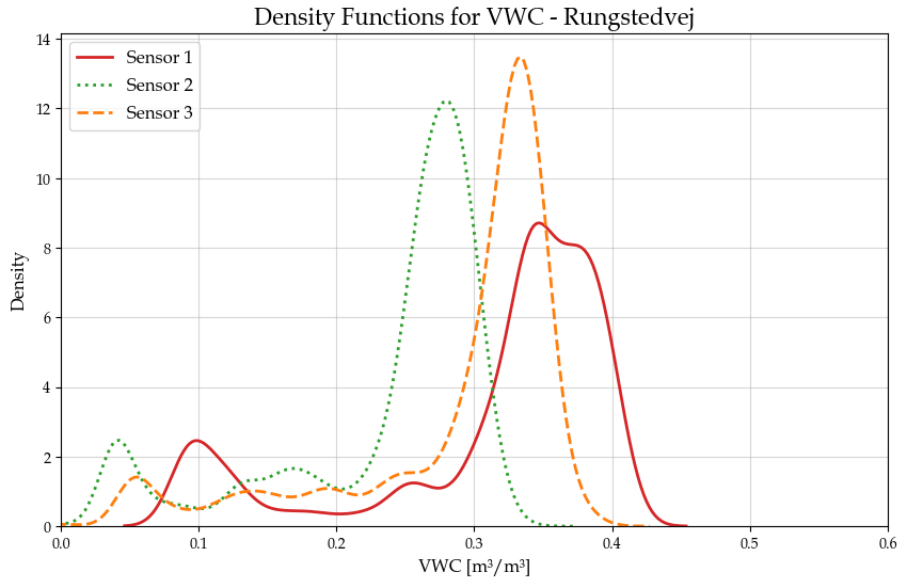

Figure D.5. PDF's of VWC for the three sensors at Rungstedvej, Hørsholm.

Hydrological Scale

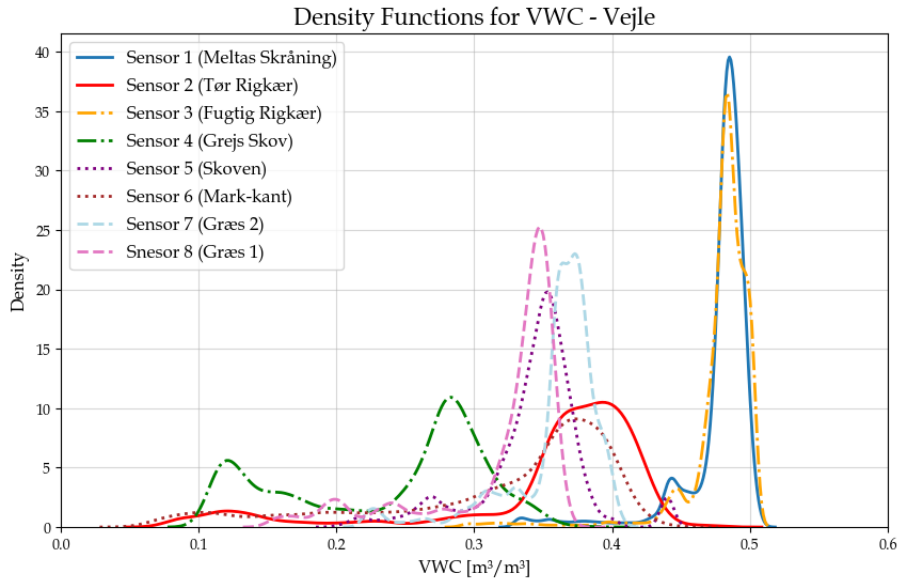

Figure D.6. PDF's of VWC for the eight sensors in Vejle.

Appendix
Location Analysis of Runoff

Cross-Correlation Analysis E

This appendix presents the results of the *cross-correlation analysis*, which is used to estimate the time delay between rainfall and runoff. The analysis is an essential step in determining the appropriate resampling period for each of the project locations.

E.1 Hillslope Scale

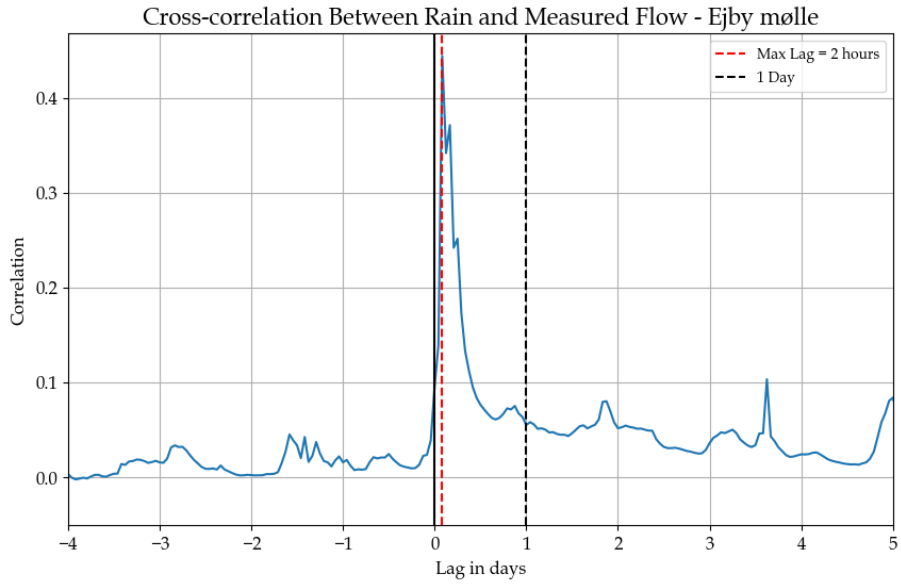

Figure E.1. *Cross-correlation analysis* between rainfall and direct runoff at Ejby Mølle, Odense.

At Ejby Mølle, the highest correlation is observed with a lag time of 2 hours. To ensure that the full runoff response from the rain event is captured, the data points are resampled over a 1-day period.

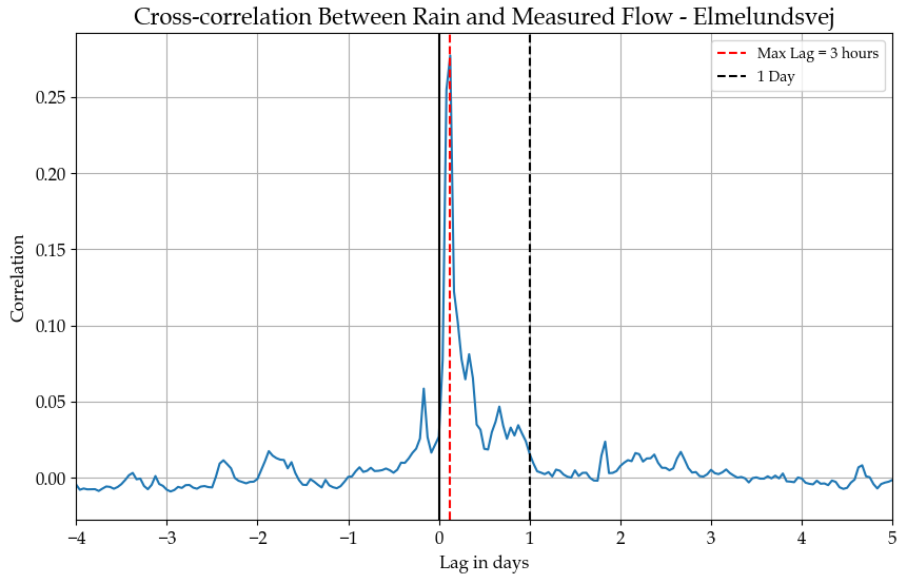

Figure E.2. *Cross-correlation analysis* between rainfall and direct runoff at Elmelundsvej, Odense.

At Elmelundsvej, the highest correlation is observed with a lag time of 3 hours. To ensure that the full runoff response from the rain event is captured, the data points are resampled over a 1-day period.

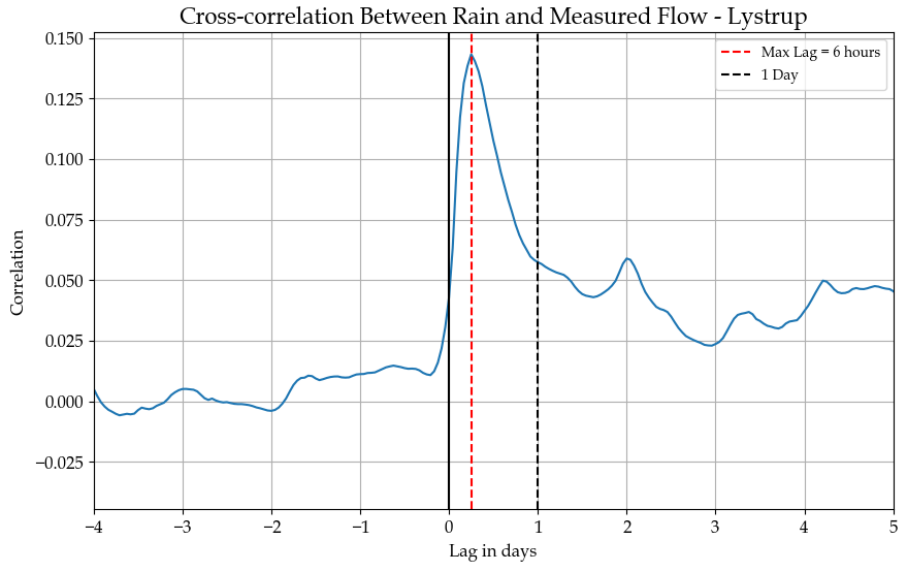

Figure E.3. *Cross-correlation analysis* between rainfall and direct runoff at Lystrup.

At Lystrup, the highest correlation is observed with a lag time of 6 hours. To ensure that the full runoff response from the rain event is captured, the data points are resampled over a 1-day period.

E.2 Urban Subcatchment Scale

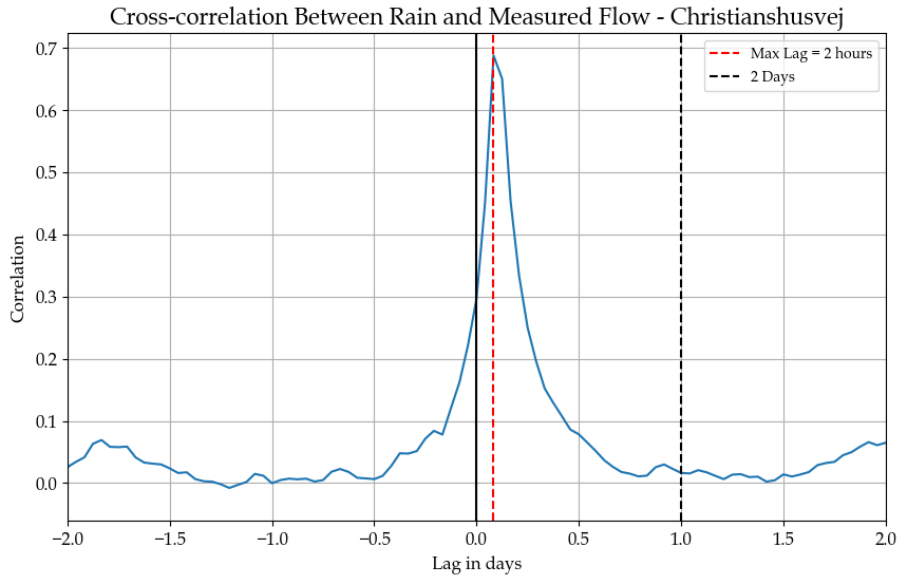

Figure E.4. *Cross-correlation analysis* between rainfall and measured pipe flow at Christianshusvej, Hørsholm.

At Christianshusvej, the highest correlation is observed with a lag time of 0 hours, indicating an immediate runoff response. To ensure that the full runoff response from the rain event is captured, the data points are resampled over a 1-day period.

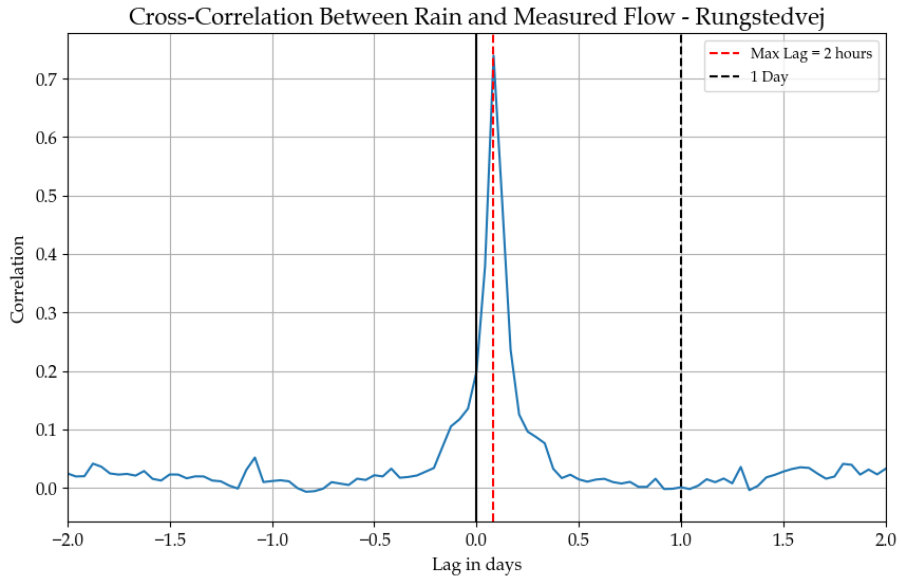

Figure E.5. *Cross-correlation analysis* between rainfall and measured pipe flow at Rungstedvej, Hørsholm.

At Rungstedvej, the highest correlation is observed with a lag time of 2 hours. To ensure that the full runoff response from the rain event is captured, the data points are resampled

over a 1-day period.

E.3 Hydrological Scale

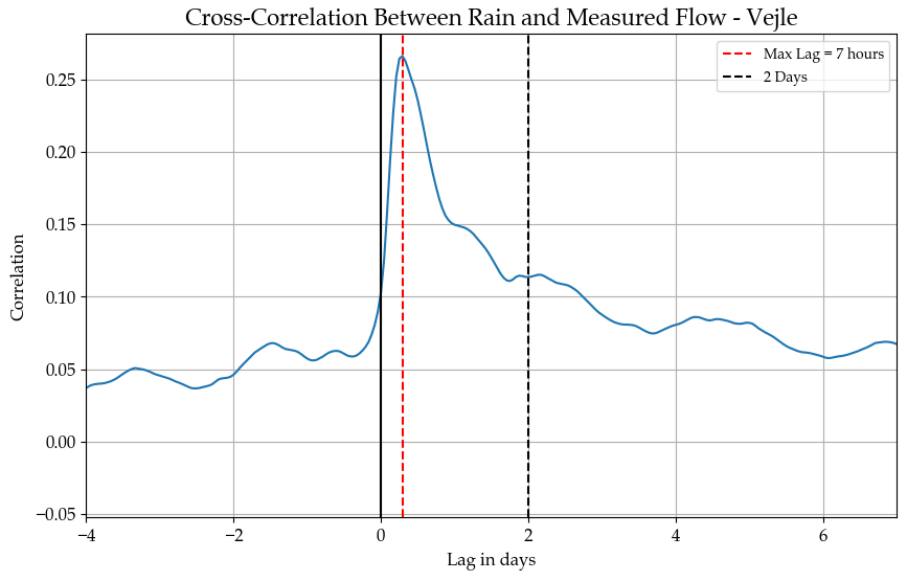

Figure E.6. *Cross-correlation analysis* between rainfall and Q/H estimated flow in Grejs Å at station 32.22, Vejle.

In Vejle, the highest correlation is observed with a lag time of 7 hours, although the peak is less distinct than in the urban subcatchment scale. To ensure that the full runoff response from the rain event is captured, the data points are resampled over a 2-day period.

Q/H Curve F

F.1 Hillslope Scale

At Ejby Mølle and Elmelundsvej, flow is not measured directly, however, the water level in the well is measured. To find the flow, a Q/H curve is made. The Q/H curve is calculated using known values for the outflow at different water levels.

Ejby Mølle
Two pressure sensors measure the water level in Ejby Mølle. Both sensors are located in the well and should, in principle, measure the same water level. The Measurements are shown in Figure F.1.

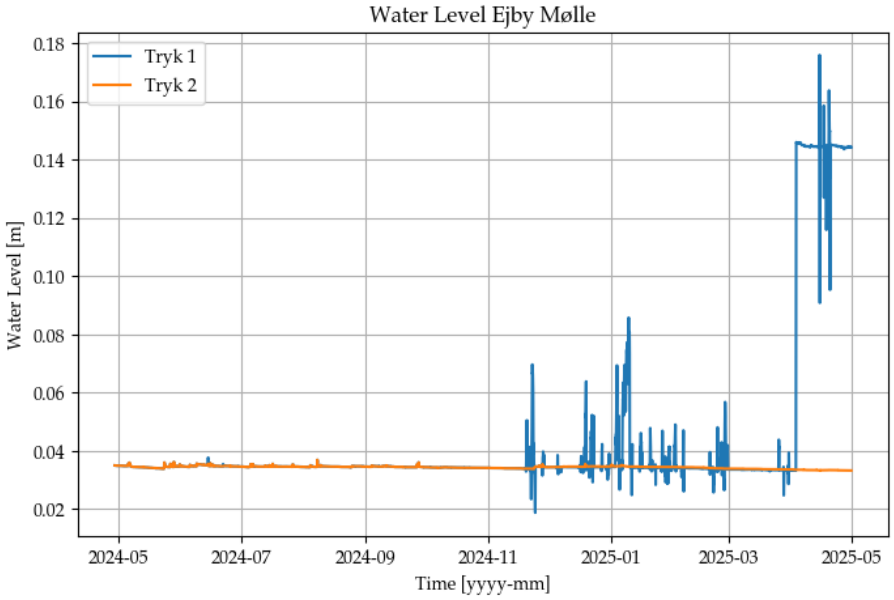

Figure F.1. Water level [m] for Ejby Mølle, Odense.

The Q/H curve is made using the sensor Tryk 1. After November 2024, the sensor Tryk 1 is showing values that are varying outside the interval that the Q/H curve is based upon. The inconsistent measurements are likely due to grease or moisture in the measurement equipment. Therefore, the data for the sensor Tryk 2 is used. There is a constant difference between the two sensors, which is added to the water level measured by Tryk 2. The Mean difference found between the two flow sensors is 0.00132 m. The Q/H curve is shown in Figure F.2.

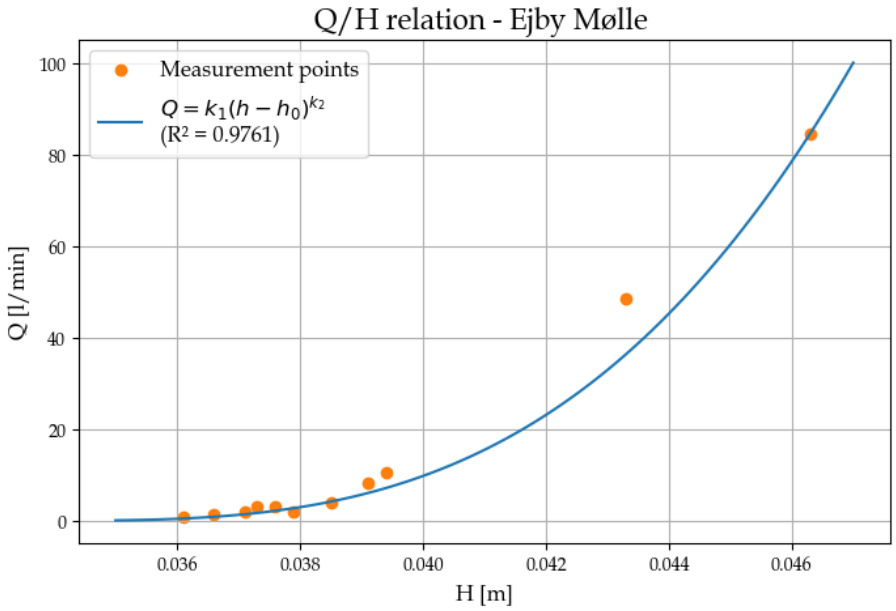

Figure F.2. Q/H curve for Ejby Mølle, Odense.

Elmelundsvej

Two sensors measure the water level at Elmelundsvej. Both sensors are located in the well. The Q/H curve is made using the sensor Tryk 2. The Q/H curve is shown in Figure F.3.

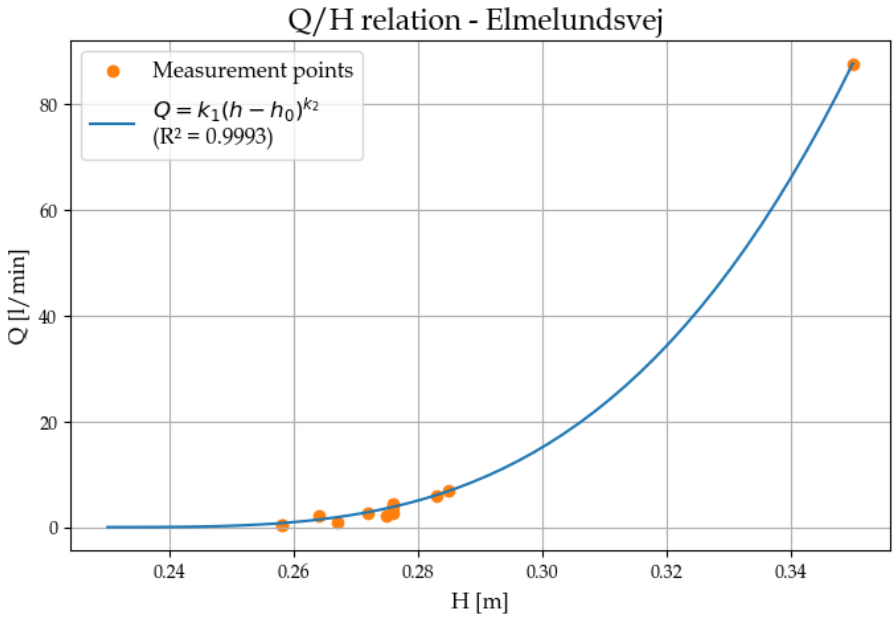

Figure F.3. Q/H curve for Elmelundsvej, Odense.

Baseflow Analysis G

Baseflow analysis is not performed on the hill slope scale catchments, as it is expected that all the flow is direct runoff.

The total flow in Grejs Å consists of a direct runoff caused by rainfall or snow melt and a baseflow. The baseflow is defined as the portion of the flow that is not direct runoff hence it is the flow discharged from the groundwater storage [Eckhardt, 2005]. The total stream flow is defined as: [Eckhardt, 2005]

$$Q_k = f_k + b_k \tag{G.1}$$

Where:

Q	Total stream flow	$[m^3/s]$
f	Direct runoff	$[m^3/s]$
b	Baseflow	$[m^3/s]$
k	Time step	$[-]$

A hydrograph typically consists of two components: a quick response from direct runoff and a slower response from the baseflow. *Lyne and Hollick, 1979* introduces a method for base flow separation in which the hydrograph is analyzed in the frequency domain. By assuming that the baseflow corresponds to the low-frequency components and the runoff is the high frequencies, it is possible to separate these flows by applying either a low-pass filter or a high-pass filter [Lyne and Hollick, 1979].

The Lyne Hollick method uses a first-order recursive high-pass filter. Recursive processing means that the filter reuses its previous output in the calculation. The filter is defined by the equation:

$$f_k = \begin{cases} \alpha \cdot f_{k-1} + \frac{1+\alpha}{2}(Q_k - Q_{k-1}) & \text{for } f_k > 0 \\ 0 & \text{otherwise} \end{cases} \tag{G.2}$$

α	Filter parameter	$[-]$

A higher filter parameter results in a greater portion of the flow being classified as direct runoff, while a lower filter parameter allows more flow to be considered baseflow.
The literature has historically recommended a filter parameter value of 0.925; hence, this value is applied in calculating the baseflow. [Ladson, 2013]

The filter equation, as presented in Equation G.2 is a forward-facing filter. However, it is common practice to apply the filter multiple times to improve the accuracy of baseflow separation. In the Lyne-Hollick method, this involves first applying a forward filter, followed by a backwards filter to minimise lag effects.

Ladson, 2013 suggests in their study that the number of passes should depend on the time step of the streamflow data. Since the flow data used in this analysis is recorded at an hourly scale, applying nine passes, alternating between forward and backward filtering (i.e., forward, backward, forward, etc.) is recommended [Ladson, 2013].

G.1 Sensitivity Analysis of the Alpha Parameter

Since the actual baseflow is unknown, it is not possible to calibrate the filter parameter precisely. Therefore, the impact of different filter parameters on the runoff analysis is investigated. Figure G.1 and G.4 present the results of the runoff analysis scenarios. The baseflow separation is performed using four different filter parameters, ranging from 0.9 to 0.98, as these values are considered likely [Ladson, 2013].

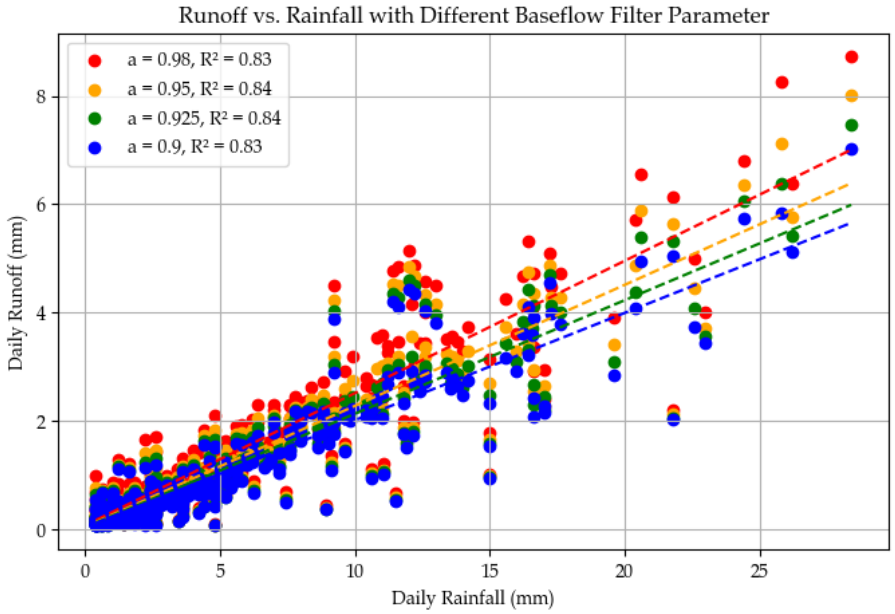

Figure G.1. Baseflow filter parameters influence on the runoff analysis at Rungstedvej, Hørsholm.

For each runoff analysis, a trendline is made and an R^2 is calculated to better be able to disguise what the difference is between the four runoff scenarios, and not to choose where the R^2 is best. The equations for each trendline are shown in Table G.1.

Table G.1. Trendline equations

α	**Equation**	R^2
0.980	$y = 0.040x + 0.013$	0.83
0.950	$y = 0.037x + 0.008$	0.84
0.925	$y = 0.035x + 0.007$	0.84
0.900	$y = 0.033x + 0.006$	0.83

From the equations, the R^2, and Figure G.1, it is found that the filter parameter influences the runoff, but its primary effect is on the scale rather than the degree of scatter. The slope of the trendlines indicates that the difference between the four runoff scenarios becomes more pronounced at higher daily rainfall values. The interception indicates that there is not a big change in the overall flow level.

To further understand the impact of excluding baseflow, the runoff analysis was conducted using data without baseflow separation, where the runoff data still includes baseflow, presented in Figure G.2. The results from this analysis are then compared to those from the analysis excluding baseflow, which uses an alpha value of 0.925.

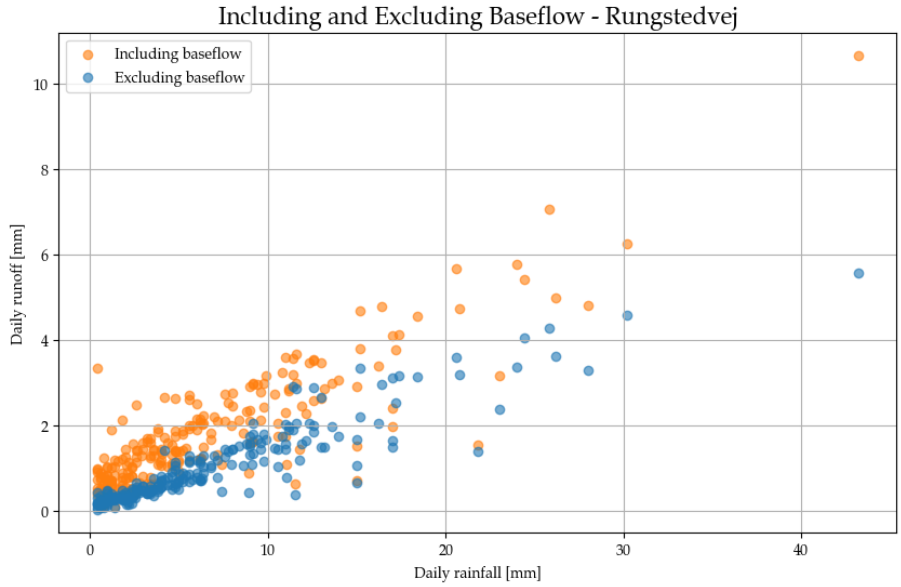

Figure G.2. Runoff analysis for Rungstedvej, Hørsholm, including baseflow and excluding baseflow where a baseflow separation is performed with a $\alpha = 0.925$.

To fully understand the impact of baseflow on the runoff analysis, including VWC, both the runoff with and without baseflow separation are presented in Figure G.3. The left figure is the figure form the analysis, where the baseflow is sustracted, hence excluding baseflow. The right figure illustrates the runoff analysis were the baseflow is included.

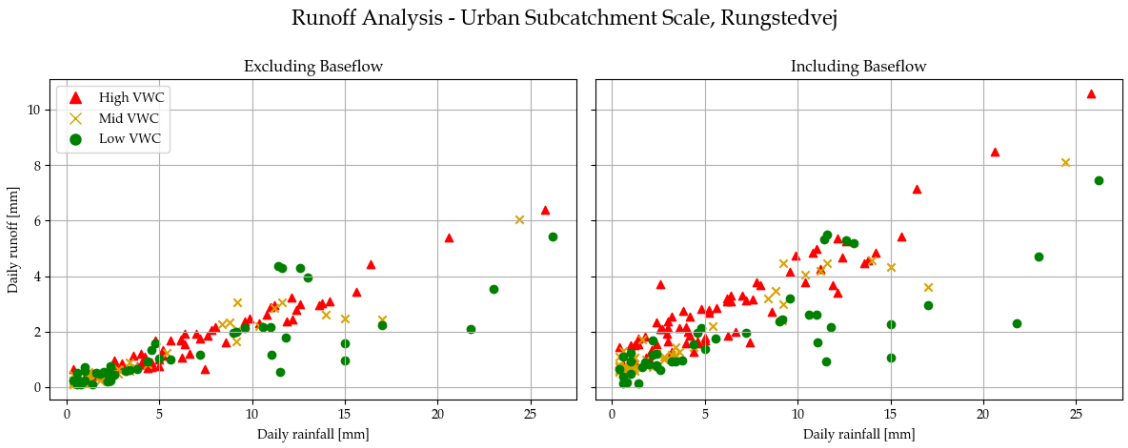

Figure G.3. Runoff analysis for Rungstedvej, Hørsholm, colours by VWC. Left Figure excludes the baseflow (with $\alpha = 0.925$) and the right includes the baseflow.

Figure G.3 indicates that there is no significant difference in the overall pattern. One noticeable difference is that when the baseflow is excluded, four green points with low water content lie above the general trend. This pattern is not observed in the analysis that includes baseflow.

The same overall trends and conclusions are made for the data for Christianshusvej.

The impact of the filter parameter in Vejle is investigated as well. The same method is used as for the Urban subcatchment scale.

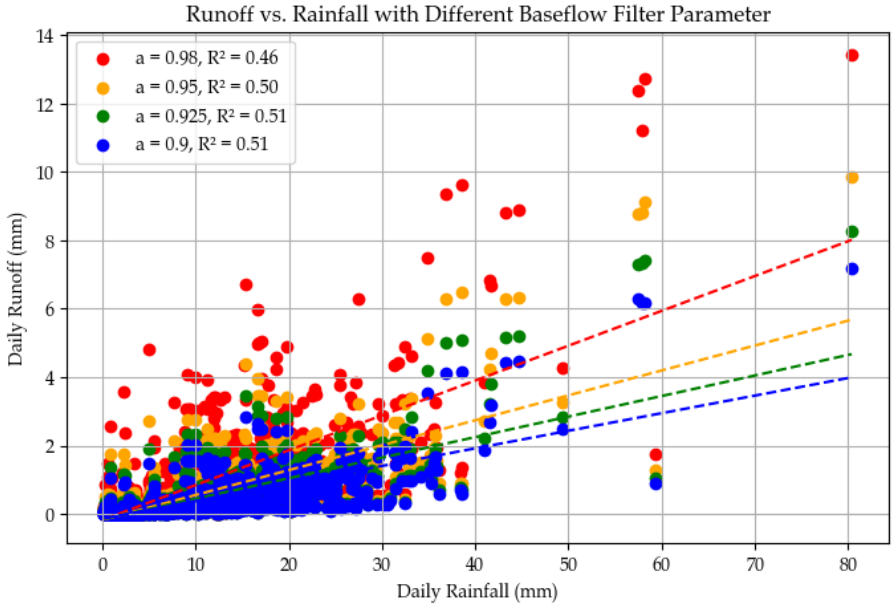

Figure G.4. Baseflow filter parameter influence on the runoff analysis in Vejle.

Table G.2. Trendline equations for Vejle

α	**Equation**	R^2
0.980	$y = 0.102x - 0.168$	0.46
0.950	$y = 0.073x - 0.170$	0.50
0.925	$y = 0.06x - 0.151$	0.84
0.900	$y = 0.051x - 0.134$	0.83

For Vejle, the general trend indicates that the filter parameter primarily affects the overall scale of the runoff rather than the degree of scatter. However, it is observed that at the highest alpha value, there is slightly more scatter in the lower runoff values.

To further examine the impact of excluding baseflow, the runoff analysis was also conducted using data without baseflow separation, where the runoff data still includes baseflow. The results from this analysis are then compared to those from the analysis excluding baseflow, using an alpha value of 0.925.

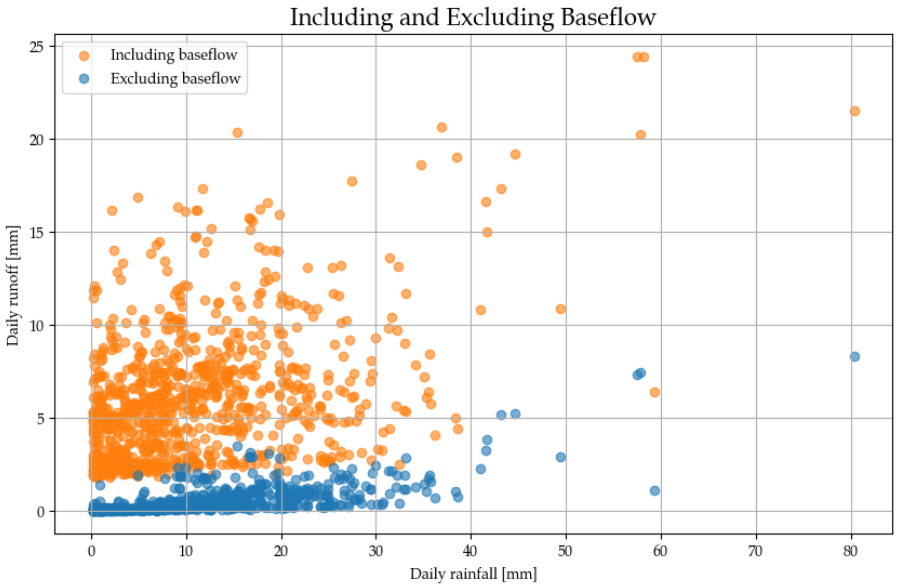

Figure G.5. Runoff analysis for Vejle, including and excluding baseflow.

Figure G.5 clearly shows that baseflow separation significantly impacts the flow. However, separating the baseflow is essential to accurately analyse the runoff generated by rainfall. If the baseflow were to be included in the analysis, it would have been an analysis of the general flow in the stream, and not of the contingent runoff. It can additionally be observed that there in general is no stream flow below 2, making even the smaller rainfalls result in a significant flow.

G.2 Urban Subcatchment Scale

The two flows in Hørsholm (Christianshusvej and Rungstedvej) are both measured in the sewer system. Baseflow separation is typically used for streams, but to analyse only the flow expected to result from rainfall, it is also applied at these two urban sub-catchments. For Christianshusvej, which has a separate sewer system, baseflow separation is performed to exclude potential infiltration and non-direct runoff. In the combined sewer system at Rungstedvej, baseflow separation is used to subtract wastewater as well.

Christianshusvej

Figure G.6 illustrates the total flow at Christianshusvej, Hørsholm, along with its separation into baseflow and direct runoff.

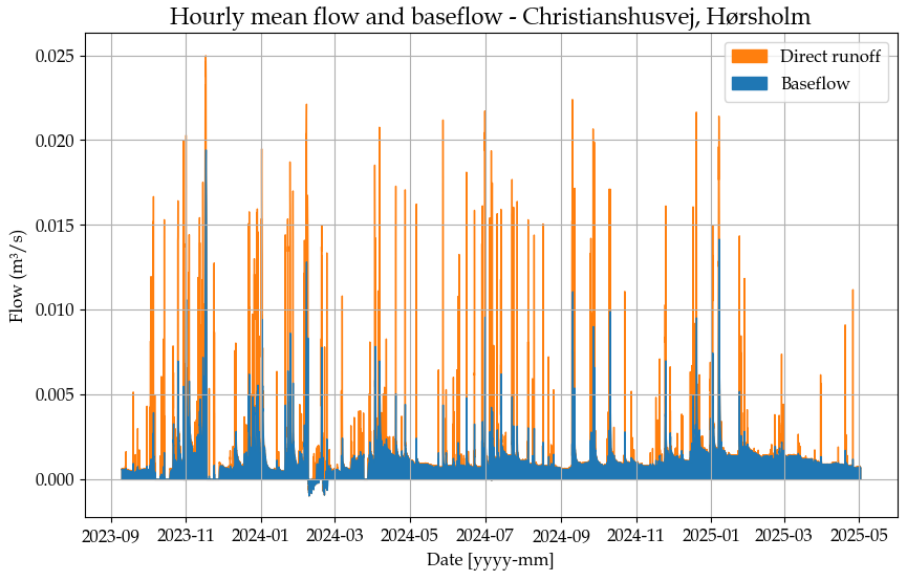

Figure G.6. Baseflow analysis of the flow measured at Christianshusvej, Hørsholm.

Figure G.7 presents the direct runoff applied in the analysis.

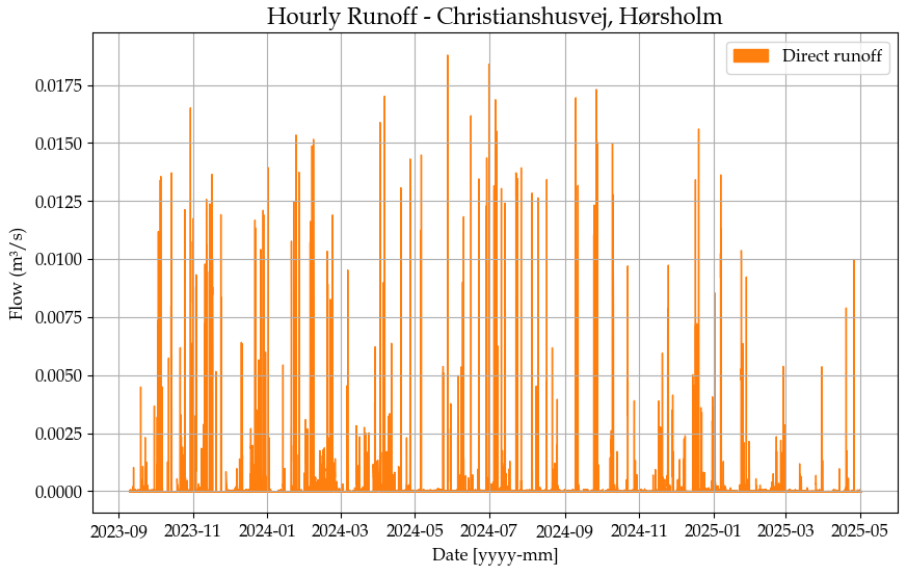

Figure G.7. The direct runoff for Christianshusvej, Hørsholm.

Rungstedvej

Figure G.8 illustrates the total flow at Rungstedvej, Hørsholm, along with its separation into baseflow and direct runoff.

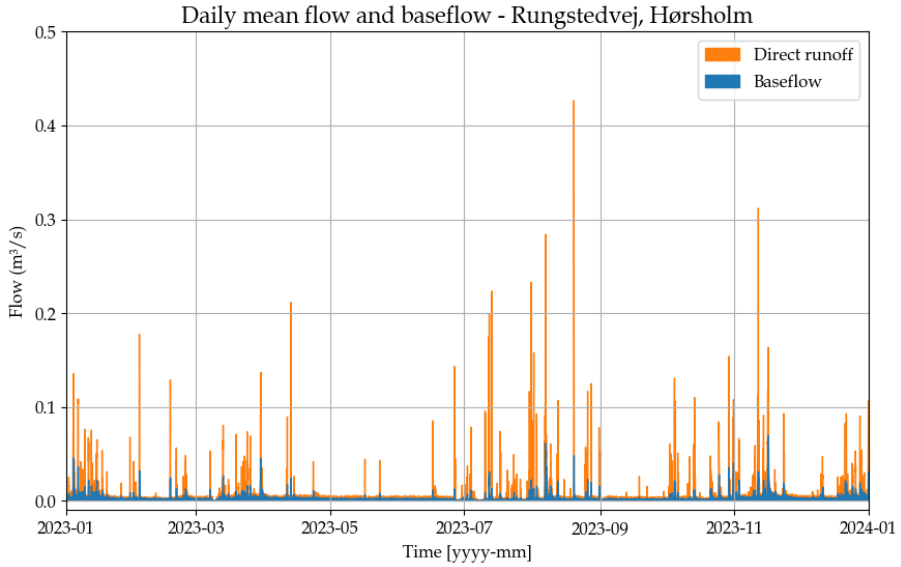

Figure G.8. Baseflow separation for Rungstedvej, Hørsholm

Figure G.9 presents the direct runoff applied in the analysis.

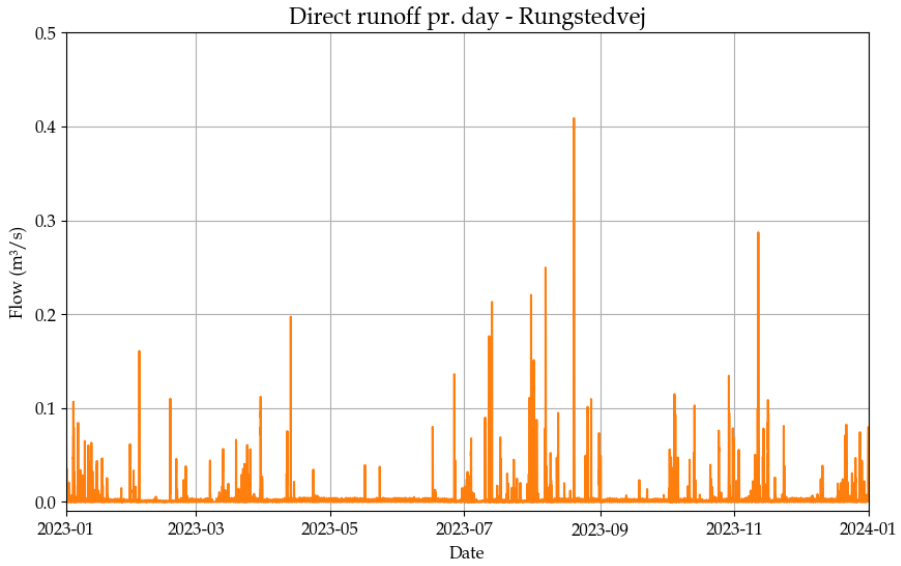

Figure G.9. Direct runoff for Rungstedvej, Hørsholm.

G.3 Hydrological Scale

Figure G.10 illustrates the mean daily flow in Grejs Å, along with its separation into baseflow and direct runoff.

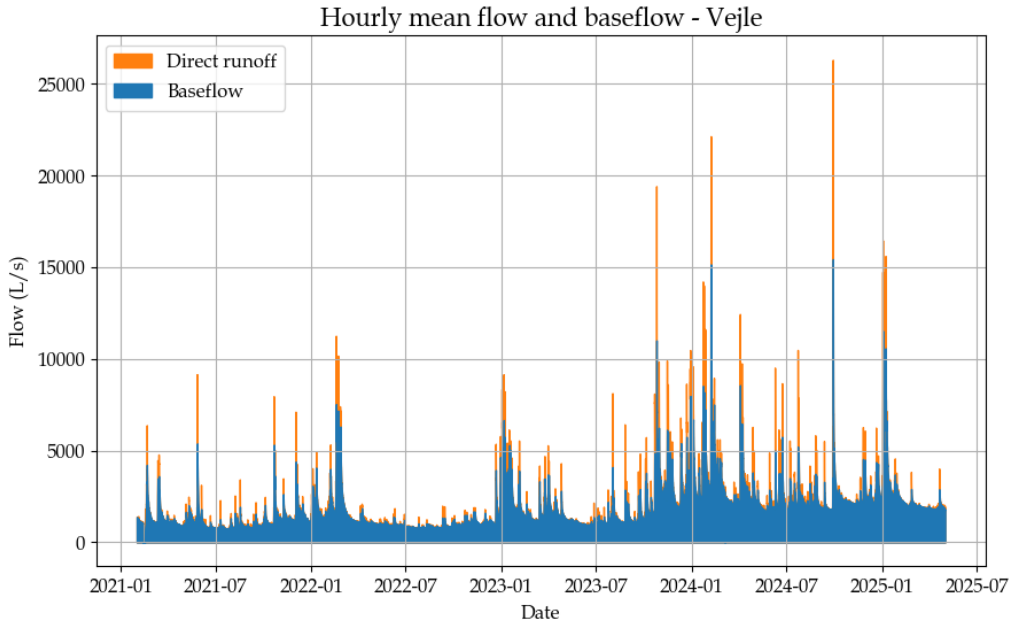

Figure G.10. Baseflow analysis of the flow in Grejs Å.

Figure G.11 presents the direct runoff applied in the analysis.

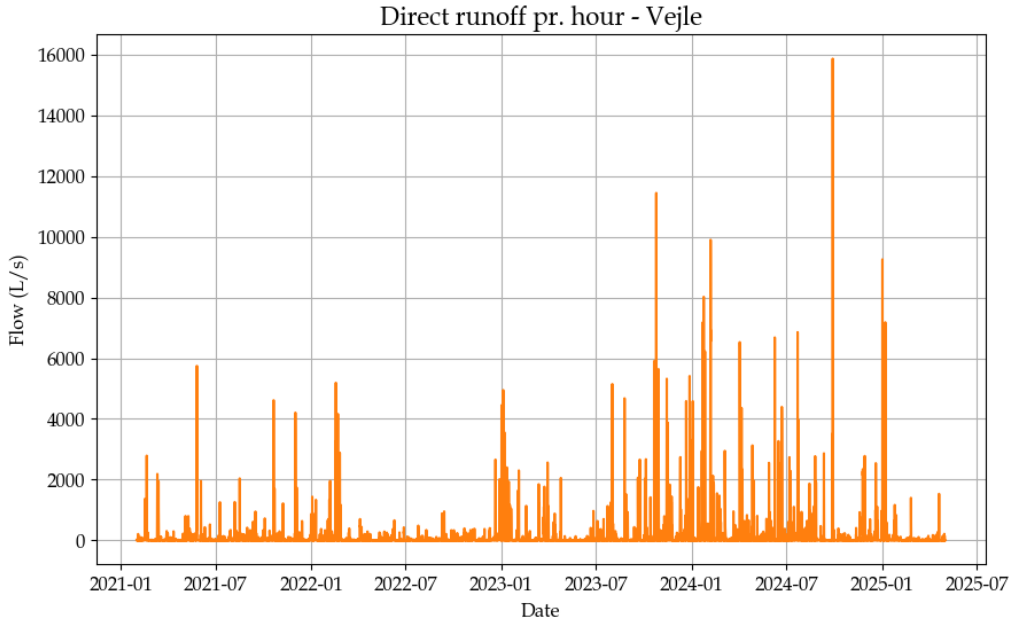

Figure G.11. Direct runoff for Grejs Å.

To better understand the baseflow on a daily scale is the flow in Grejs Å plotted for nine days.

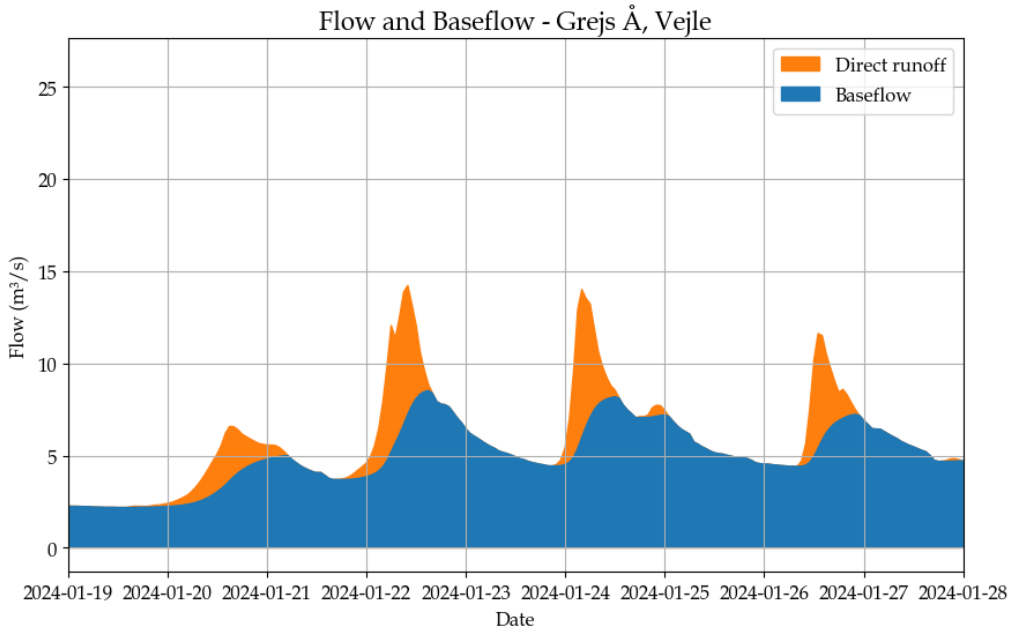

Figure G.12. Runoff separation of the flow in Grejs Å over a nine-day period.

VWC and Runoff Analysis H

This appendix provides additional information and visualisation about the classification of the volumetric water content (section H.1), the data points removed due to freezing conditions (section H.2) and a separation of the original scatter plot into wet and dry period (section H.3).

H.1 Classification of Volumetric Water Content

As described in chapter 5, the VWC values are divided into three categories based on quartiles: High VWC (top 25% of values), Mid VWC (middle 50%), and Low VWC (bottom 25% of values). Since each VWC sensor has its own range of measurements, the bin intervals differ between sensors. To provide a better visualisation of how values are classified, the VWC measurements are plotted using their designated colour coding, where red represents high values, yellow represents mid-range values, and green represents low values. Figure H.1 through H.6 displays the VWC measurements colour-coded according to their respective bin classifications.

Hillslope Scale

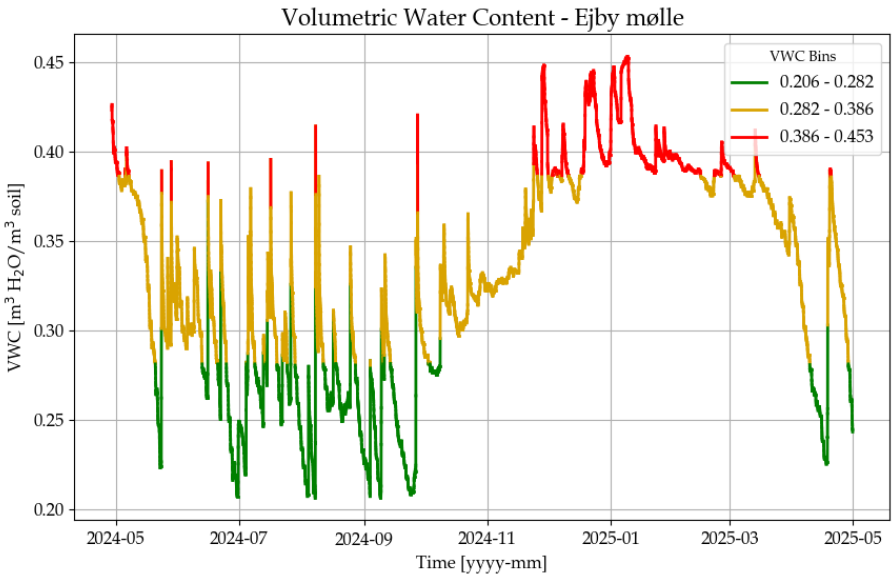

Figure H.1. Volumetric water content classified into high (red), mid (yellow), and low (green) bins for Ejby Mølle, Odense.

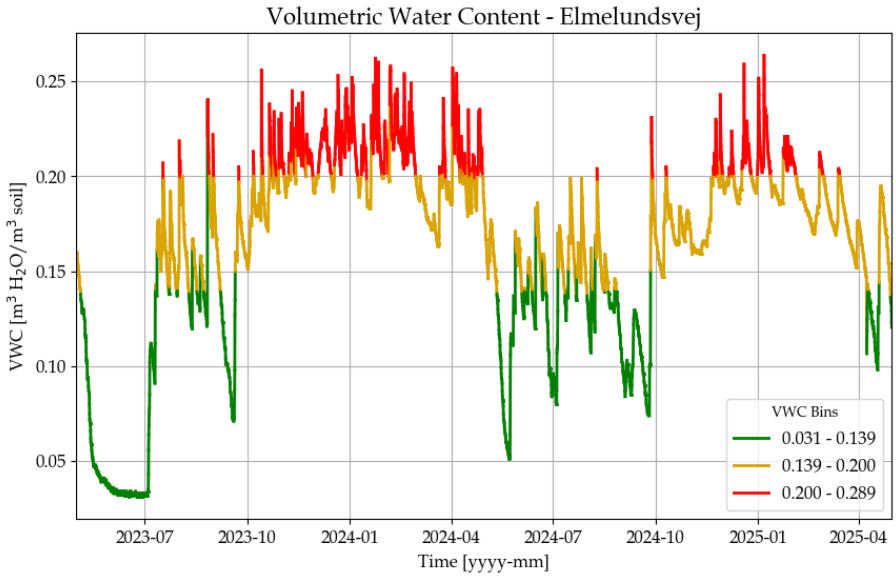

Figure H.2. Volumetric water content classified into high (red), mid (yellow), and low (green) bins for Elmelundsvej, Odense.

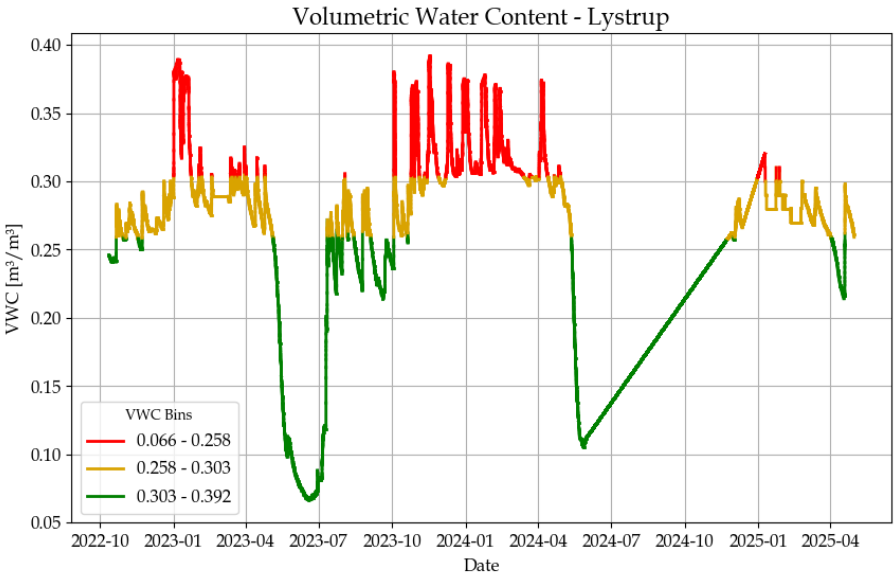

Figure H.3. Volumetric water content classified into high (red), mid (yellow), and low (green) bins for Lystrup.

Urban Subcatchment Scale

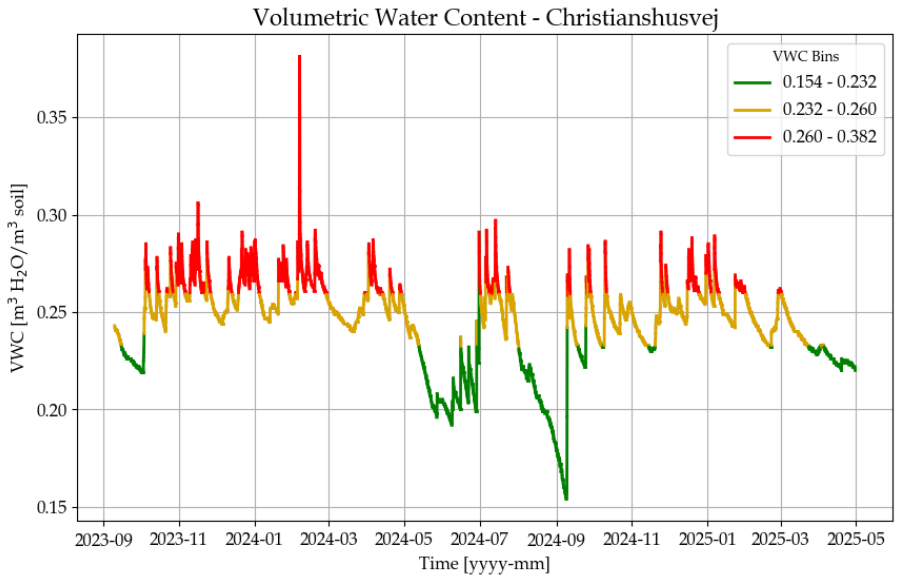

Figure H.4. Volumetric water content classified into high (red), mid (yellow) and low (green) bins for Christianshusvej, Hørsholm.

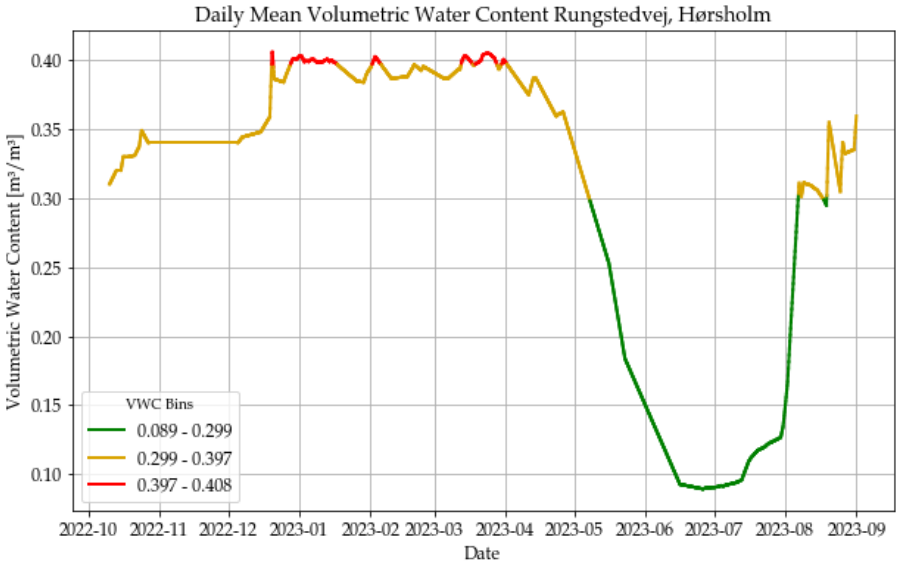

Figure H.5. Volumetric water content classified into high (red), mid (yellow) and low (green) bins for Rungstedvej, Hørsholm.

Hydrological Scale

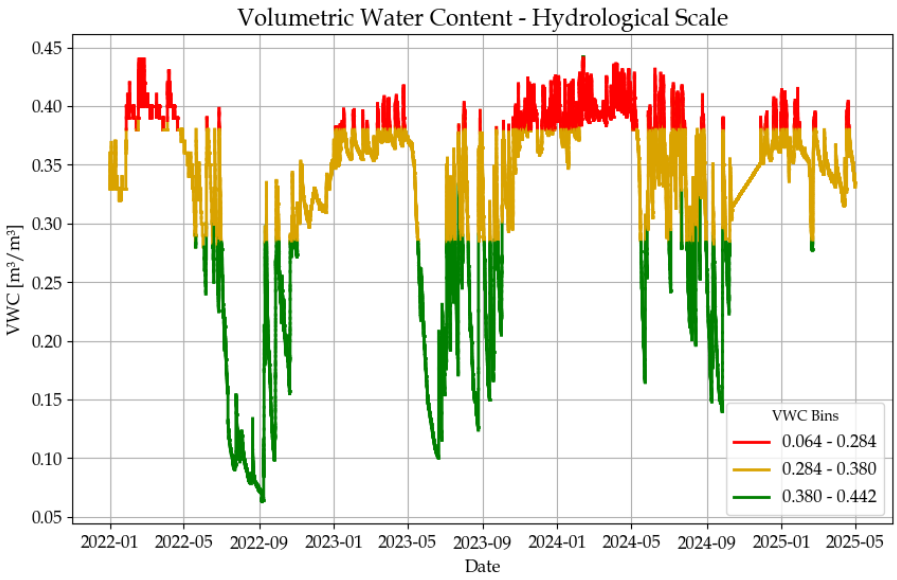

Figure H.6. Volumetric water content classified into high (red), mid (yellow) and low (green) bins for Vejle.

H.2 Visualisation of Runoff Values at Sub-zero Temperatures

As described in chapter 5, data points where the temperature drops below 0 degrees are removed before the analysis, due to the unique conditions during snowfall and frozen grounds. To provide a better visualisation of which values are removed, these points are illustrated with a blue colour in Figure H.7 through H.12. On the figures, the markings indicate the time series that are plotted in the event analysis.

Hillslope Scale

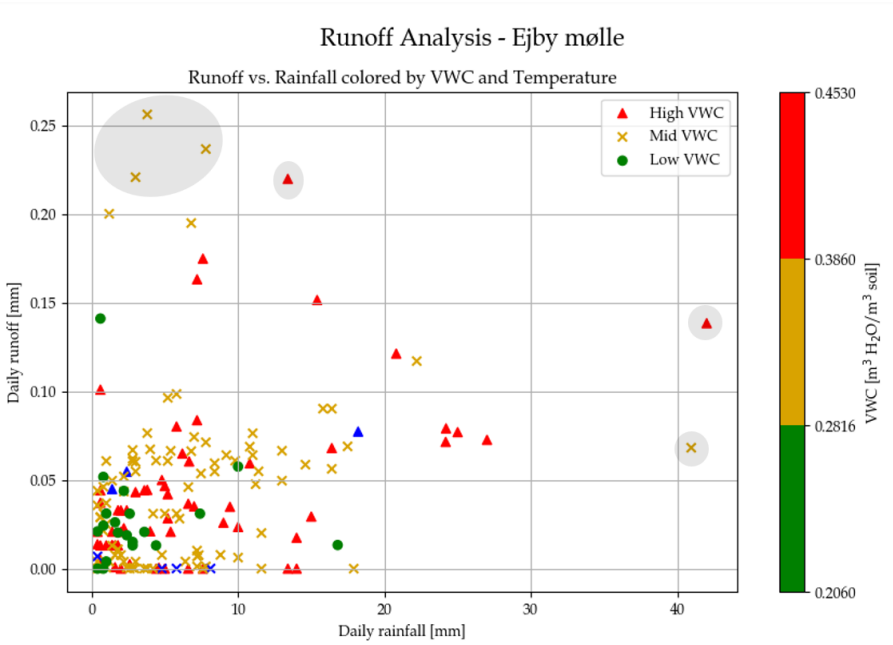

Figure H.7. Comparison between runoff [mm/day] and rainfall [mm/day] classified into high (red triangle), mid (yellow cross), and low (green circle) VWC [m^3/m^3] for Ejby Mølle, Odense. Days with temperatures below 0 are coloured dark blue. Grey circles indicate the events analysed in Figure 6.1.

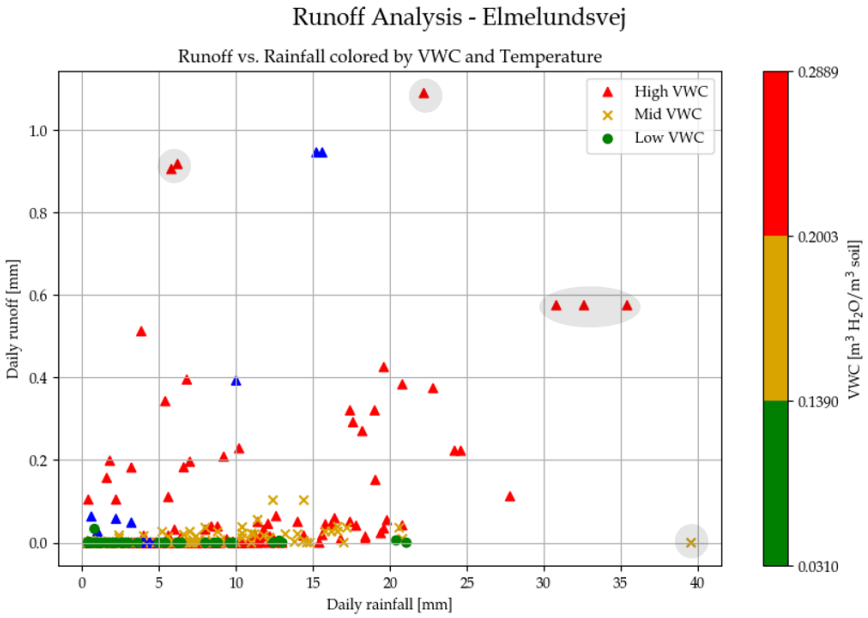

Figure H.8. Comparison between runoff [mm/day] and rainfall [mm/day] classified into high (red triangle), mid (yellow cross), and low (green circle) VWC [m^3/m^3] for Elmelundsvej, Odense. Days with temperatures below 0 are coloured dark blue. Grey circles indicate the events analysed in Figure 6.5.

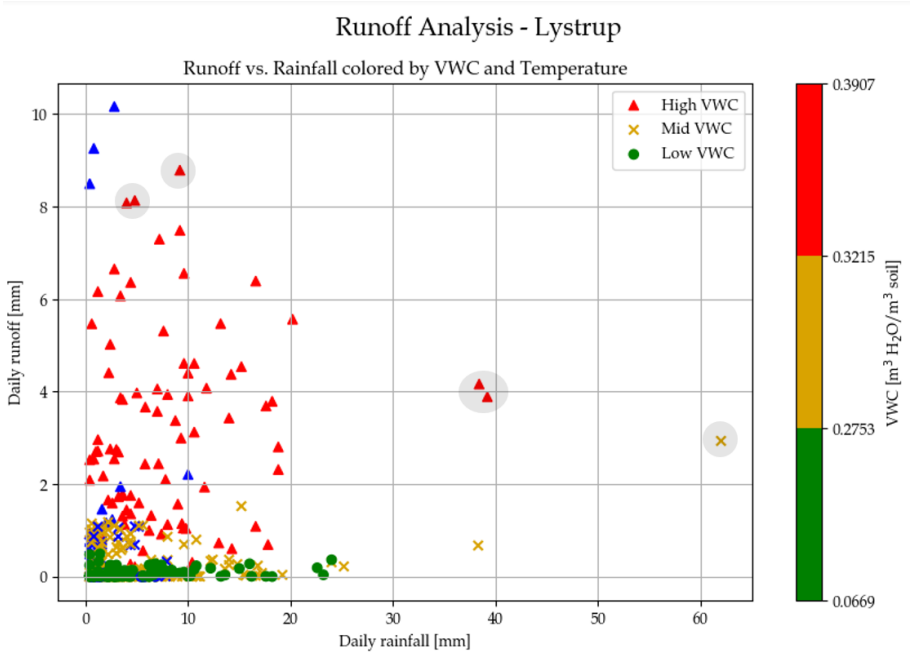

Figure H.9. Comparison between runoff [mm/day] and rainfall [mm/day] classified into high (red triangle), mid (yellow cross), and low (green circle) VWC [m^3/m^3] for Lystrup. Days with temperatures below 0 are coloured dark blue. Grey circles indicate the events analysed in Figure Figure 6.9

Urban Subcatchment Scale

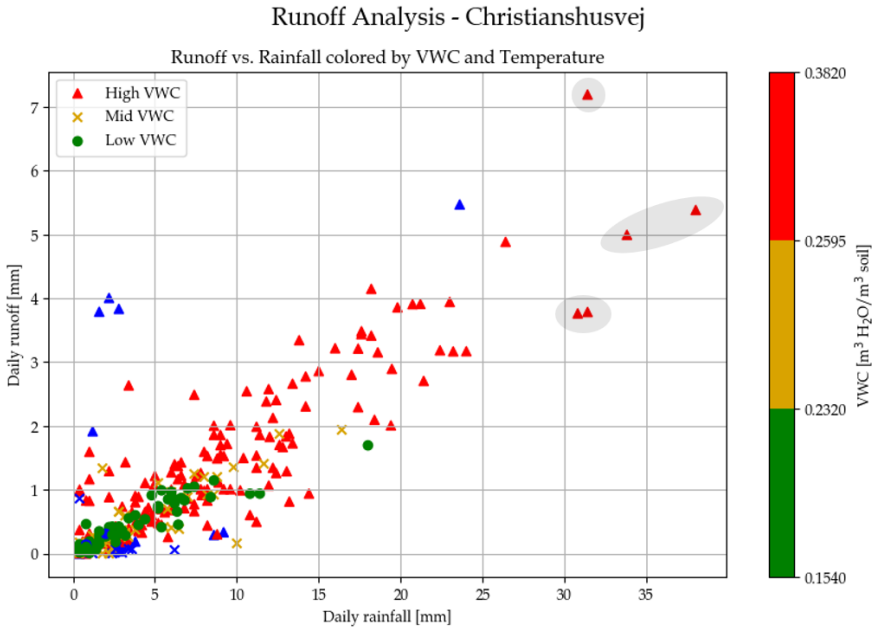

Figure H.10. Comparison between runoff [mm/day] and rainfall [mm/day] classified into high (red triangle), mid (yellow cross) and low (green circle) VWC [m^3/m^3] for Christianshusvej, Hørsholm. Days with temperatures below 0 are coloured dark blue. Grey circles indicate the events analysed in Figure 7.1

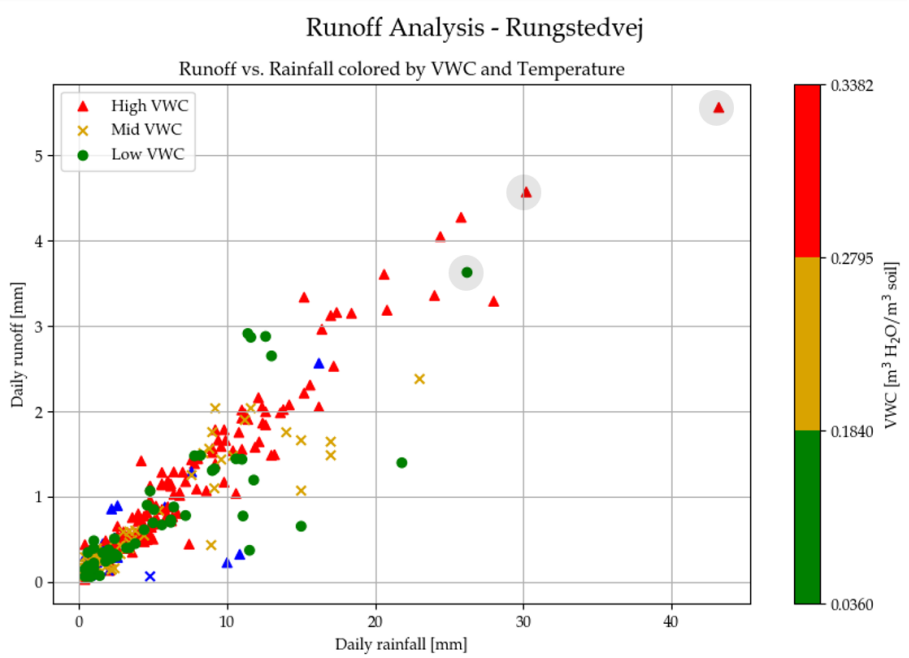

Figure H.11. Comparison between runoff [mm/day] and rainfall [mm/day] classified into high (red triangle), mid (yellow cross) and low (green circle) VWC [m^3/m^3] for Rungstedvej, Hørsholm. Days with temperatures below 0 are coloured dark blue. Grey circles indicate the events analysed in Figure 7.5

Hydrological Scale

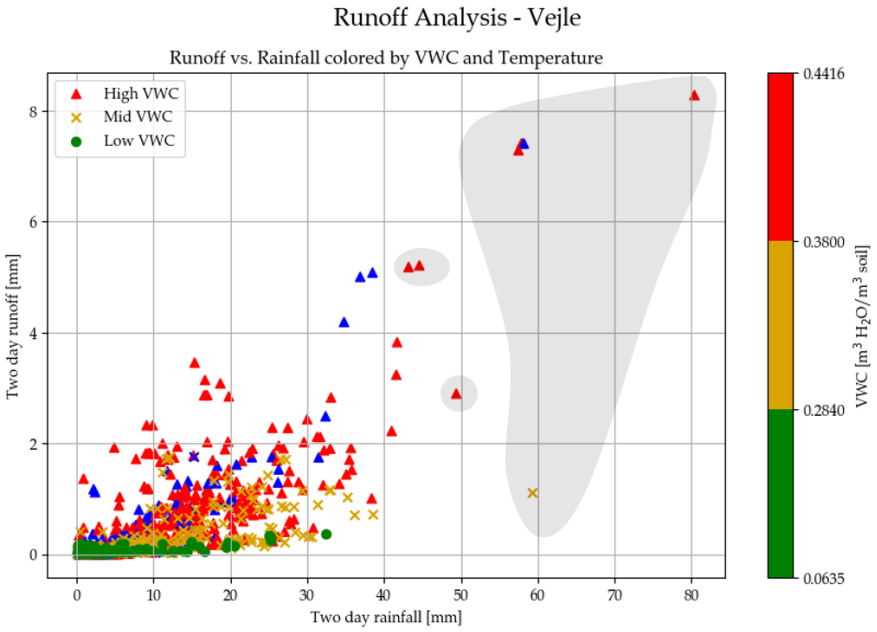

Figure H.12. Comparison between runoff [mm/day] and rainfall [mm/day] classified into high (red triangle), mid (yellow cross), and low (green circle) VWC [m^3/m^3] for Vejle. Days with temperatures below 0 are coloured dark blue. Grey circles indicate the events analysed in Figure 8.1

H.3 Runoff Trends in Wet and Dry Periods

The original scatter plot is separated into wet and dry periods to better illustrate the distribution of data points. This is visualised for each of the areas in Figure H.13 through H.18.

Hillslope Scale

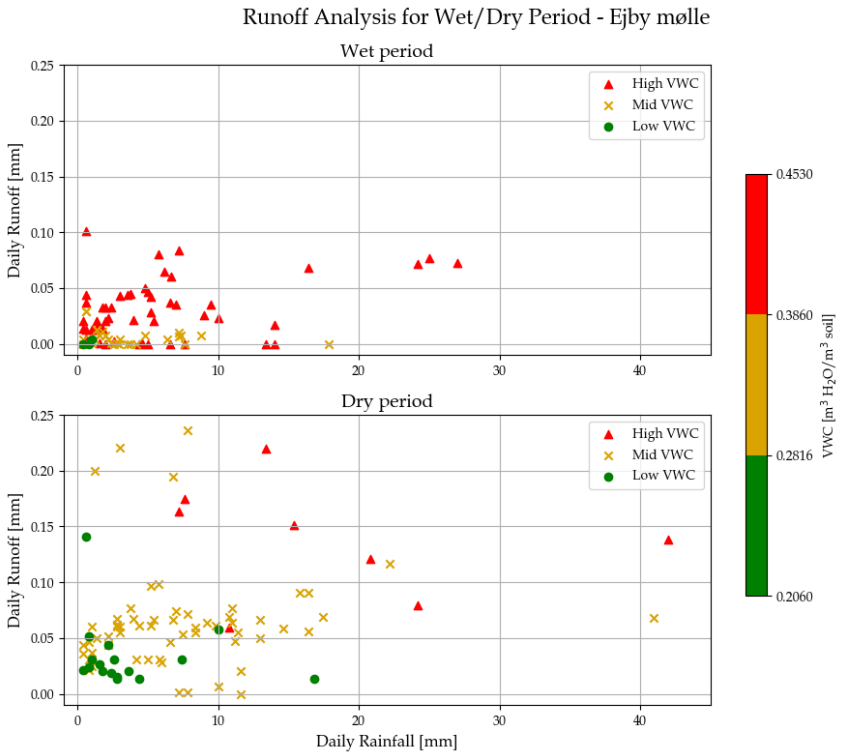

Figure H.13. Runoff analysis divided into two sub-plots one for the wet period and one for the dry period at Ejby Mølle, Odense.

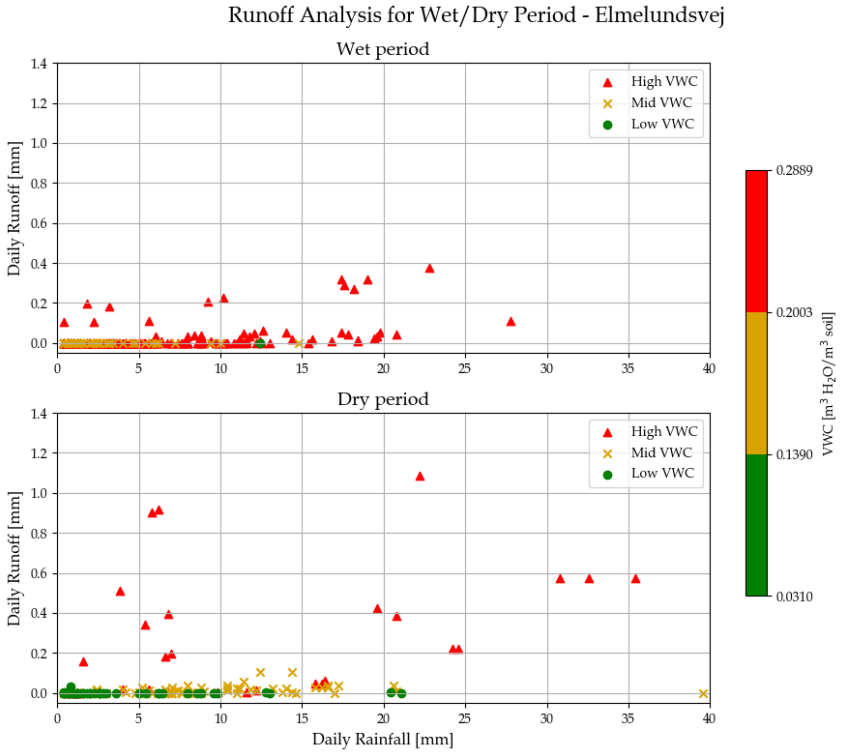

Figure H.14. Runoff analysis divided into two sub-plots one for the wet period and one for the dry period at Elmelundsvej, Odense.

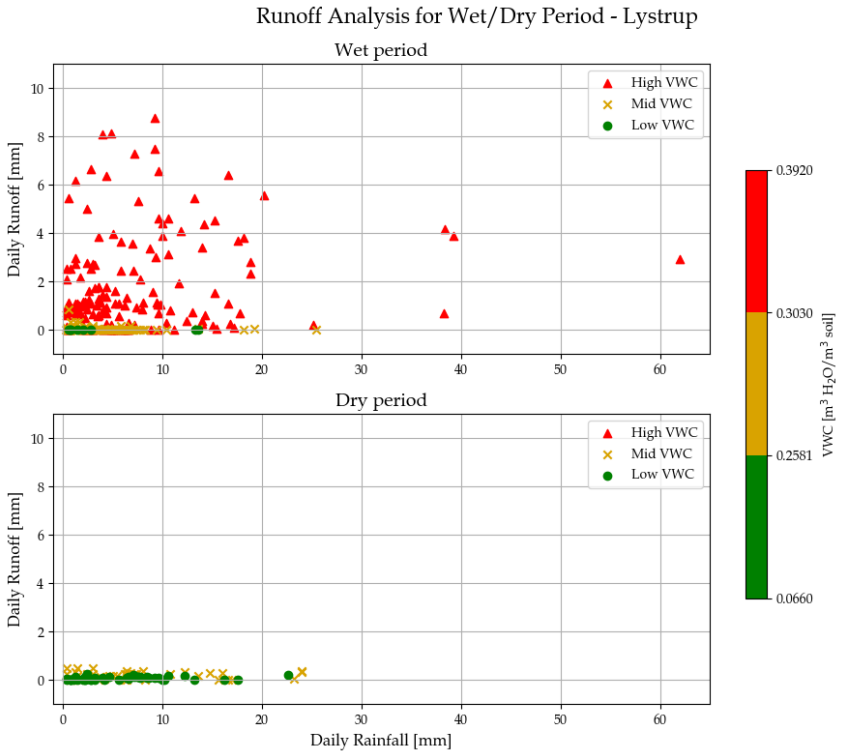

Figure H.15. Runoff analysis divided into two sub-plots one for the wet period and one for the dry period at Lystrup.

Urban Subcatchment Scale

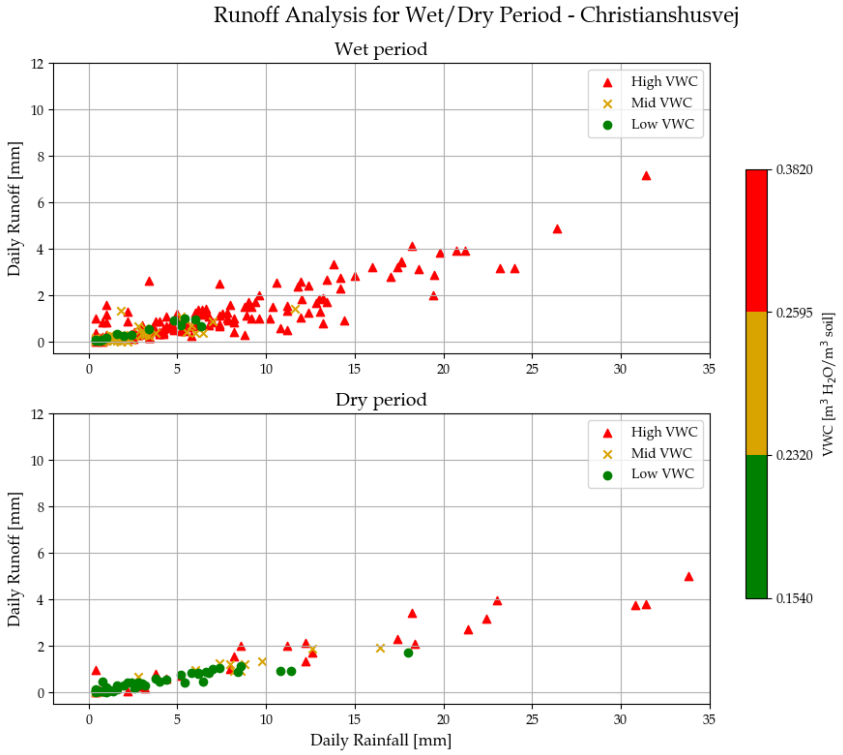

Figure H.16. Runoff analysis divided into two sub-plots one for the wet period and one for the dry period at Christianshusvej, Hørsholm.

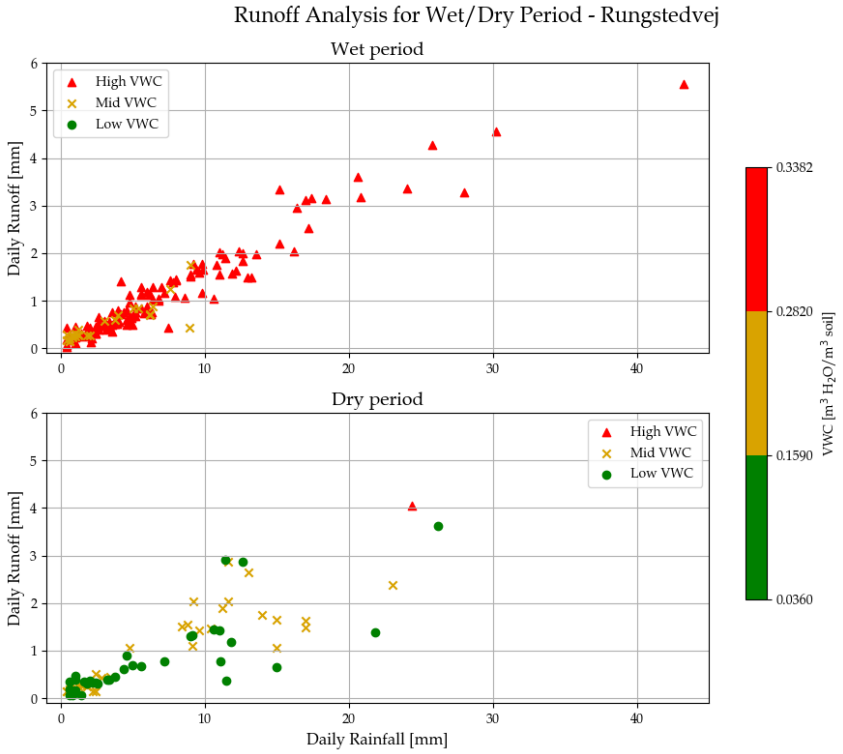

Figure H.17. Runoff analysis divided into two sub-plots one for the wet period and one for the dry period at Rungstedvej, Hørsholm.

Hydrological Scale

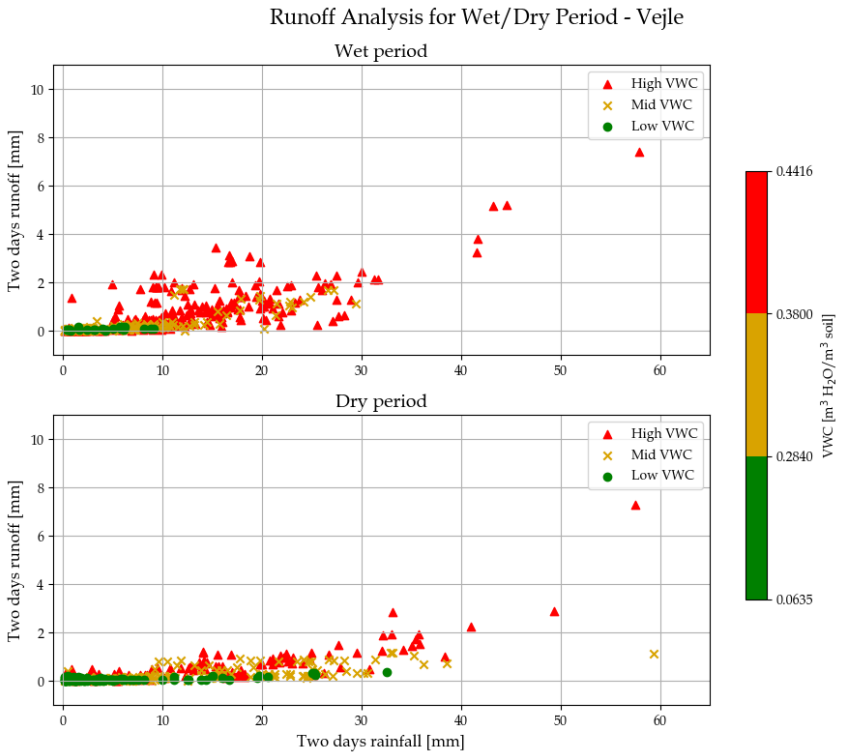

Figure H.18. Runoff analysis divided into two sub-plots one for the wet period and one for the dry period at Vejle.

Statistical Analysis of Runoff

I

This appendix will present some additional results of the *statistical analysis*, including frequency histograms for runoff data (section I.1), boxplots for runoff values within the three VWC classifications (section I.2), Dunn's test results from the three VWC classifications (section I.3) and Dunn's test results from the runoff ratio plots (section I.4).

I.1 Frequency Histogram

As described in chapter 5, the runoff data distribution is investigated, visually by histograms and statistically with the Kolmogorov-Smirnov Test, for normal distribution. In all cases, the data follows a non-normal distribution, hence why non-parametric tests are performed in the analysis. The histograms with Kolmogorov-Smirnov Test for all locations are illustrated in Figure I.1 through I.6.

Hillslope Scale

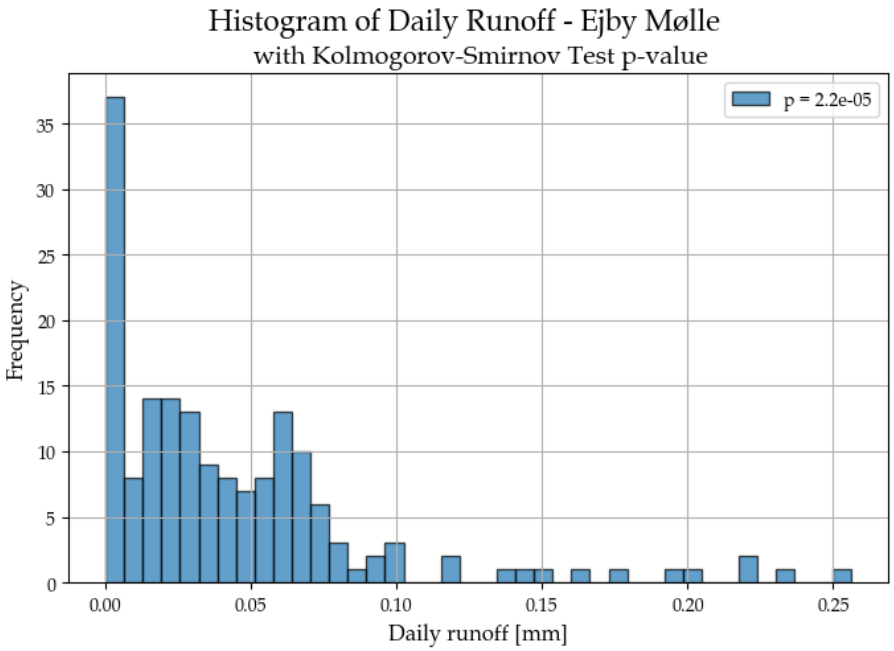

Figure I.1. Frequency histogram with Kolmogorov-Smirnov Test for Ejby Mølle, Odense.

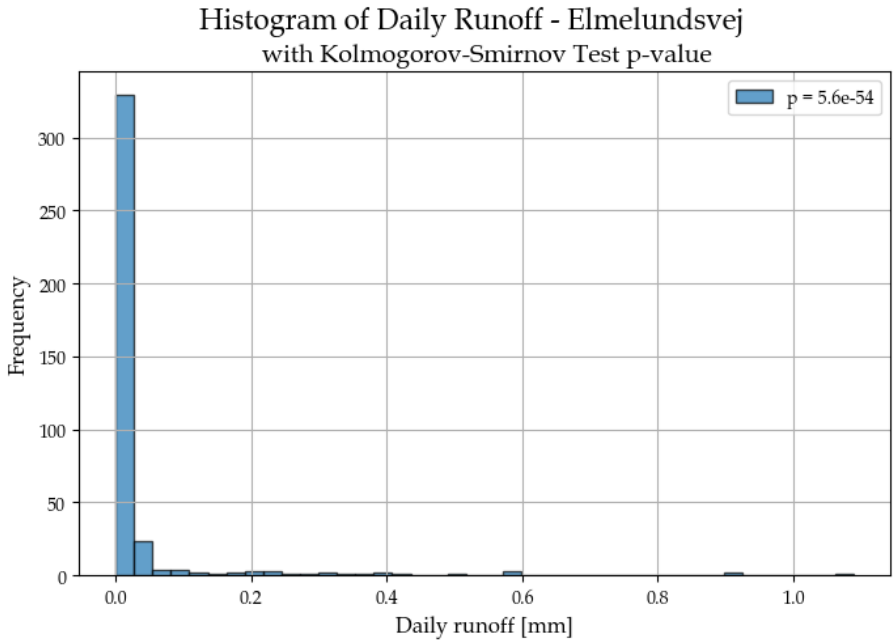

Figure I.2. Frequency histogram with Kolmogorov-Smirnov Test for Elmelundsvej, Odense.

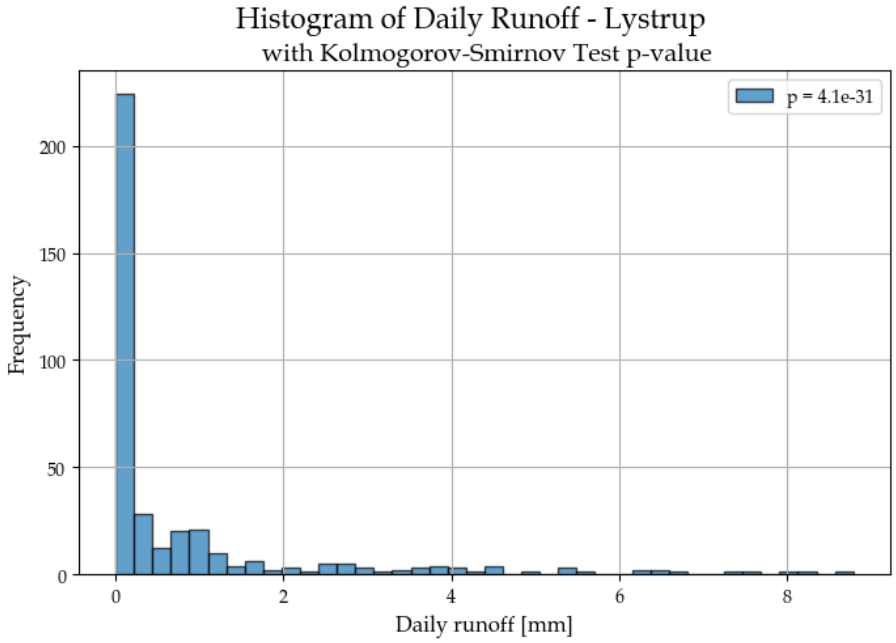

Figure I.3. Frequency histogram with Kolmogorov-Smirnov Test for Lystrup.

Urban Subcatchment Scale

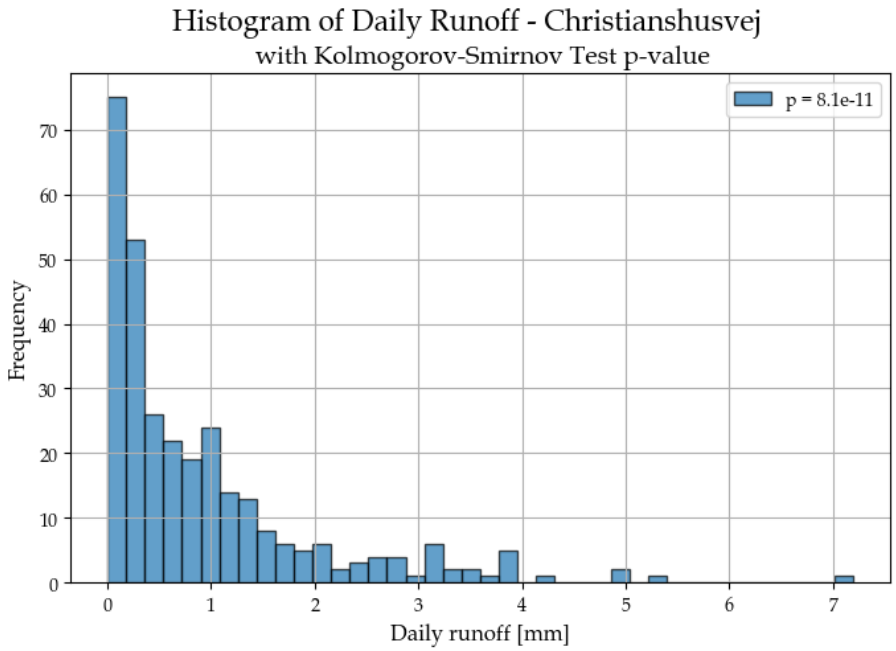

Figure I.4. Frequency histogram with Kolmogorov-Smirnov Test for Christianshusvej, Hørsholm.

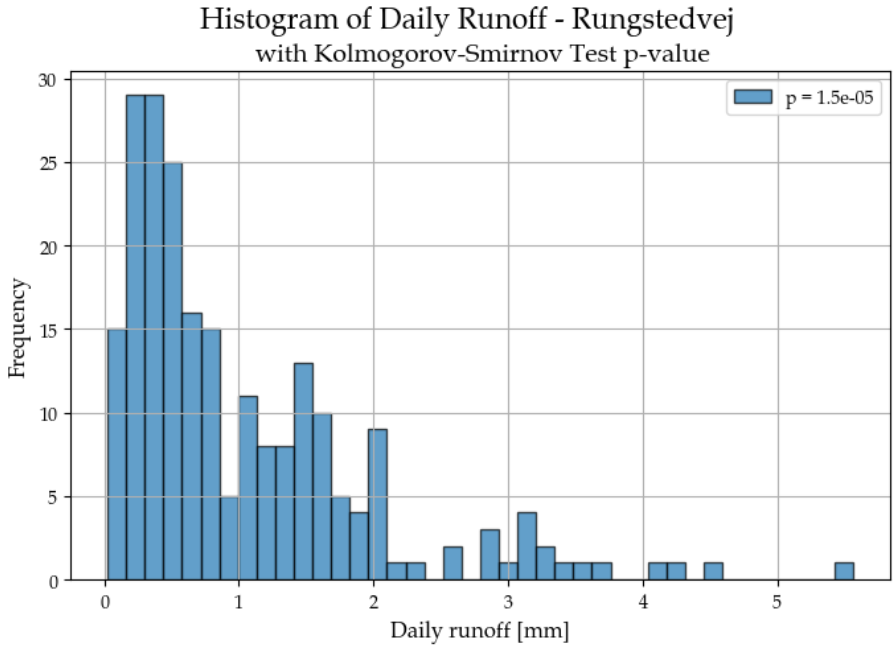

Figure I.5. Frequency histogram with Kolmogorov-Smirnov Test for Rungstedvej, Hørsholm.

Hydrological Scale

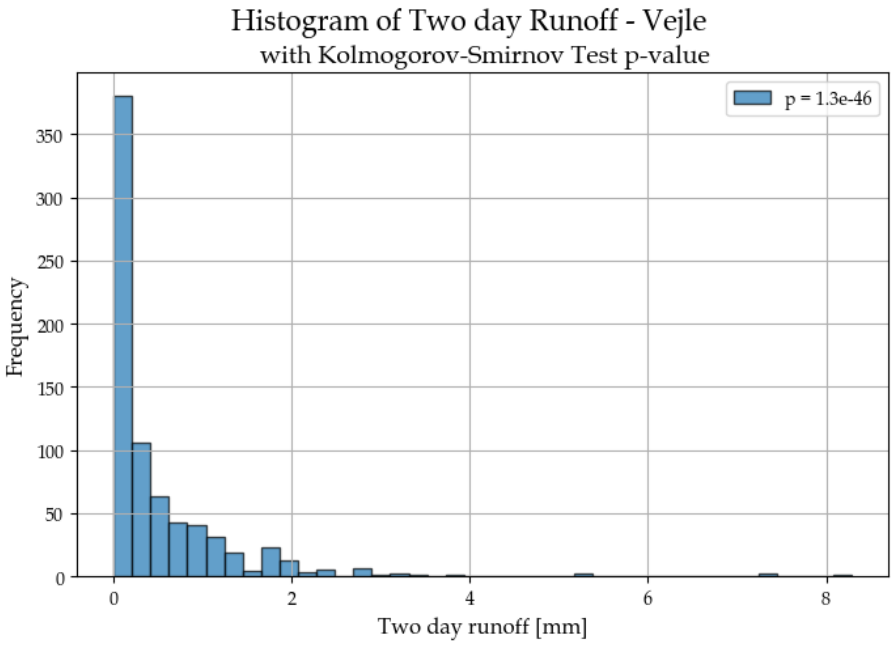

Figure I.6. Frequency histogram with Kolmogorov-Smirnov Test for Vejle.

I.2 Boxplots

Boxplots illustrating the runoff at high, mid, and low VWC for the six project locations are presented below.

Hillslope Scale

Ejby Mølle

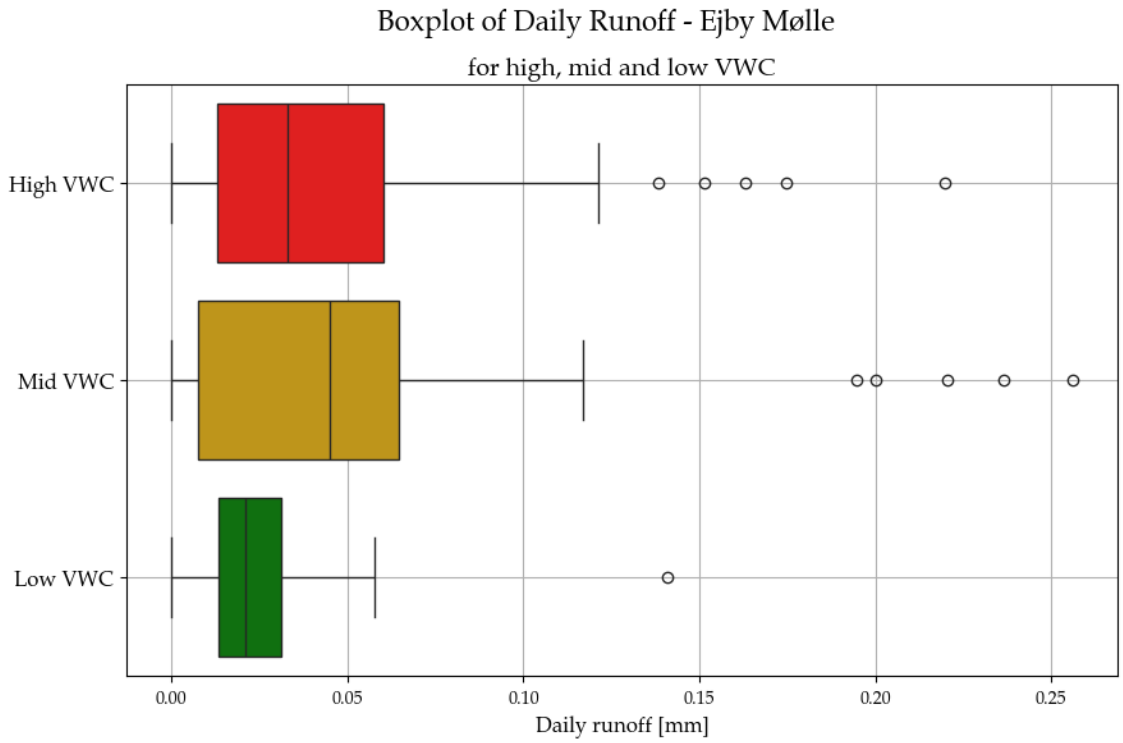

Figure I.7. Boxplot for runoff at high, mid, and low VWC at Ejby Mølle, Odense.

Figure I.7 shows that the high VWC bin exhibits the greatest spread in runoff values, as indicated by longer whiskers. This suggests slightly higher variability in runoff under high VWC compared to mid VWC conditions. However, the mid VWC bin exhibits both a large spread, wider IQR, higher median, and higher runoff outliers compared to the high VWC bin. Thus, extreme runoff events can occur under both mid and high VWC conditions. In contrast, the low VWC group has a much narrower spread and only one outlier, suggesting more consistent runoff values.

Elmelundsvej

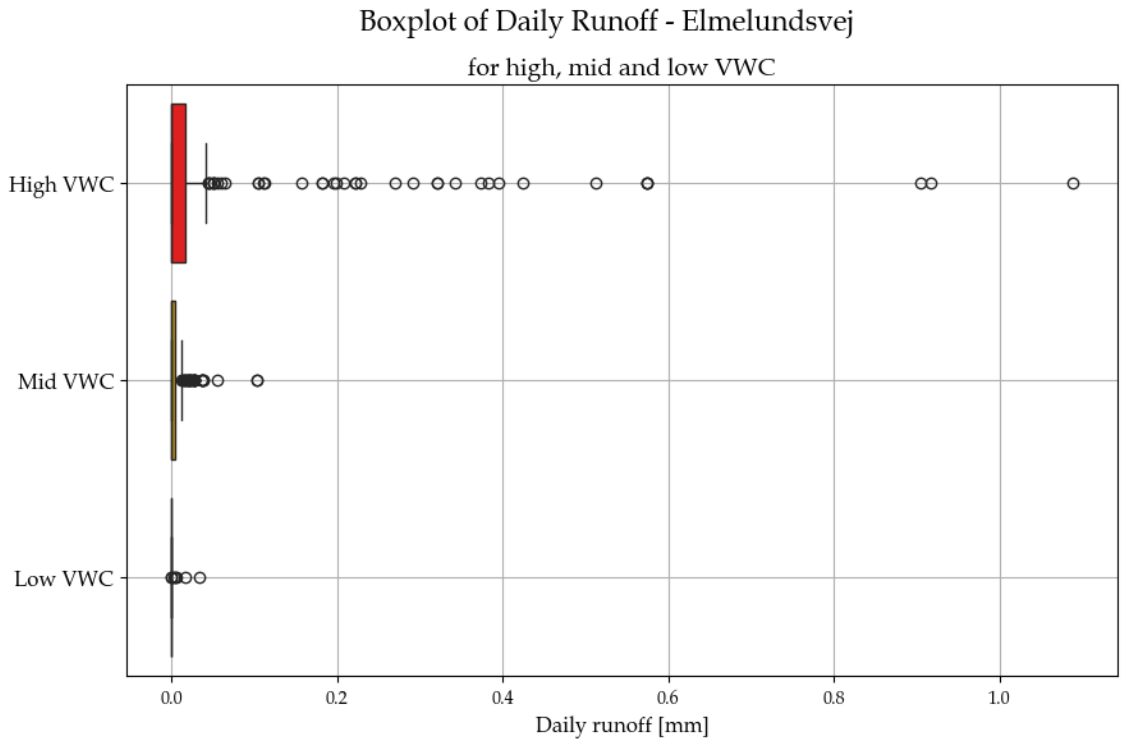

Figure I.8. Boxplot for runoff at high, mid, and low VWC at Elmelundsvej, Odense.

The boxplot in Figure I.8 shows that the high VWC group exhibits the greatest spread in runoff values, as evidenced by its slightly wider IQR and longer whiskers. This suggests higher variability in runoff under high VWC conditions, which is likely due to elevated saturation levels and larger variations in both rainfall duration and intensity. In contrast, the mid and low VWC group displays much narrower distributions, indicating more consistent runoff values, likely due to the soil's high infiltration capacity, which typically results in more uniform and lower runoff response. All three VWC categories contain multiple outliers, suggesting that runoff events not only occur under high VWC conditions but are also influenced by both rainfall intensity and the system's hydraulic memory (e.g. effects of prior drought). However, the high VWC group notably exhibit a right-skewed distribution, indicating a higher risk of extreme runoff events when the soil's VWC conditions are classified as high.

Lystrup

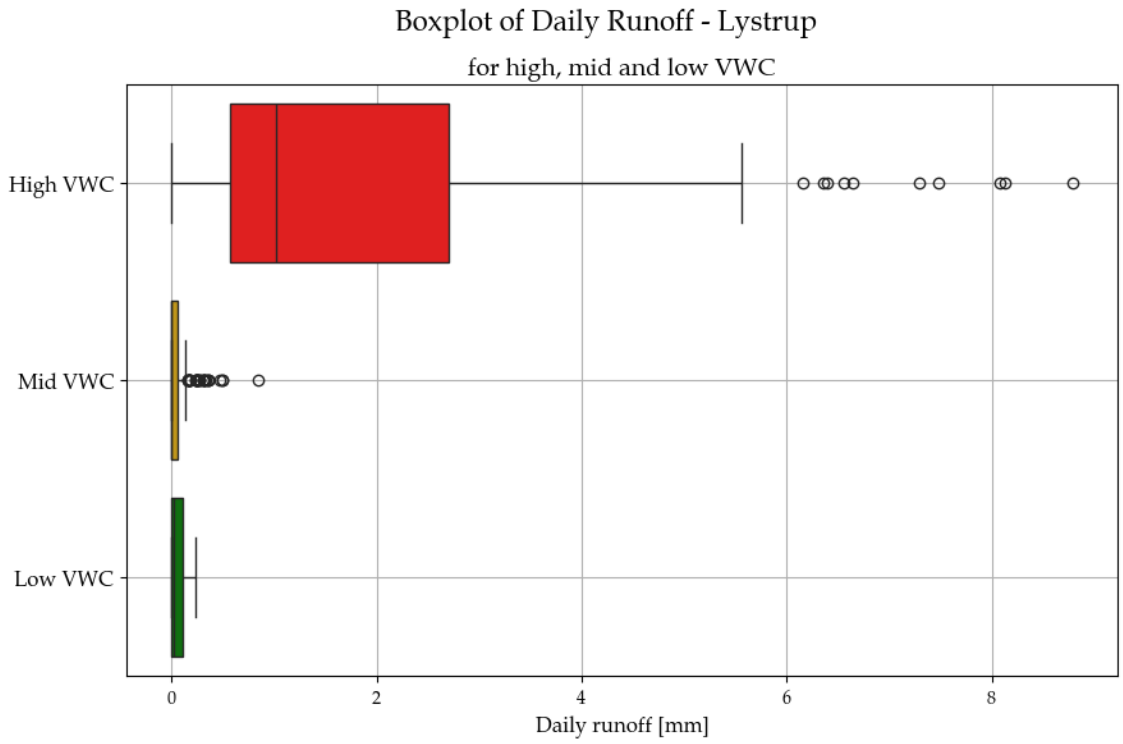

Figure I.9. Boxplot for runoff at high, mid, and low VWC at Lystrup.

The boxplot shows that the high VWC group exhibits the greatest spread in runoff values, as evidenced by its wider IQR and longer whiskers, suggesting greater variability in runoff under high VWC conditions. In contrast, the mid and low VWC groups display much narrower distributions, indicating more consistent and generally lower runoff values. The median daily runoff in the high bin is significantly higher, indicating generally higher runoff generation within this group.
Moreover, multiple outliers are present within the high and mid VWC categories, suggesting that significant runoff events not only occur under high VWC conditions, but are also influenced by both rainfall intensity and the system's hydraulic memory (e.g. effects of prior drought).
Overall, the high VWC group notably exhibit a right-skewed distribution, indicating a higher risk of extreme runoff events when the soil's VWC conditions are classified as high. In contrast, the mid and low bins show more symmetrical distributions centred around lower runoff values, indicating a lower runoff sensitivity under these conditions.

Urban Subcatchment Scale

Christianshusvej

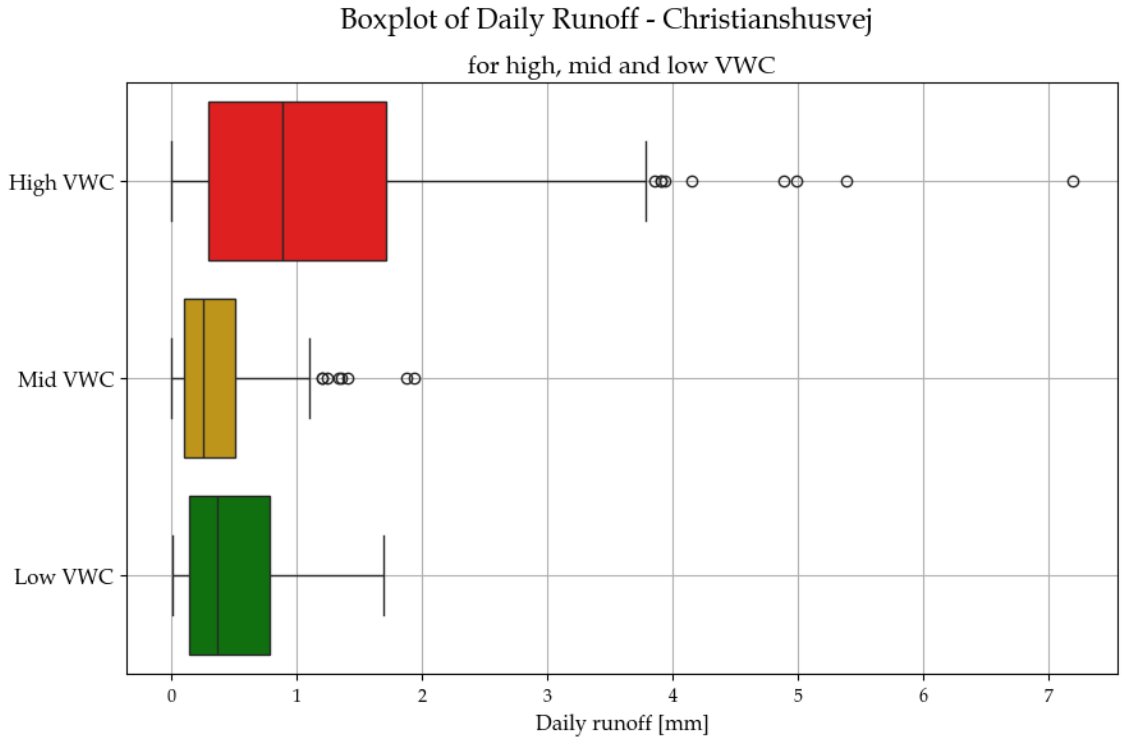

Figure I.10. Boxplot for runoff at high, mid, and low VWC at Christianshusvej, Hørsholm.

The boxplot in Figure I.10 shows that the high VWC group exhibits both the highest median runoff and the greatest variability, as indicated by its wider IQR and longer whiskers. This suggests that runoff under high VWC conditions is more variable and prone to higher runoff volumes. In contrast, the mid and low VWC groups show much narrower spreads (especially the mid VWC group), indicating more consistent and generally lower runoff values. Multiple outliers are present in both the high and mid groups, with the most extreme values (up to $\approx$ 8 mm) occurring in the high VWC bin.
Overall, the high VWC group exhibit a clear right-skewed distribution, indicating a greater likelihood of extreme runoff events when VWC are classified as high. In contrast, the mid and low groups show more symmetrical distributions centred around lower runoff values, suggesting lower runoff sensitivity under these conditions. Thus, the boxplot analysis supports the other analyses, indicating that high runoff generation is associated with high VWC conditions. However, as previously noted, the high VWC group comprises 58.82 % of all data points, which may introduce some uncertainty due to the unequal distribution of observations.

Rungstedvej

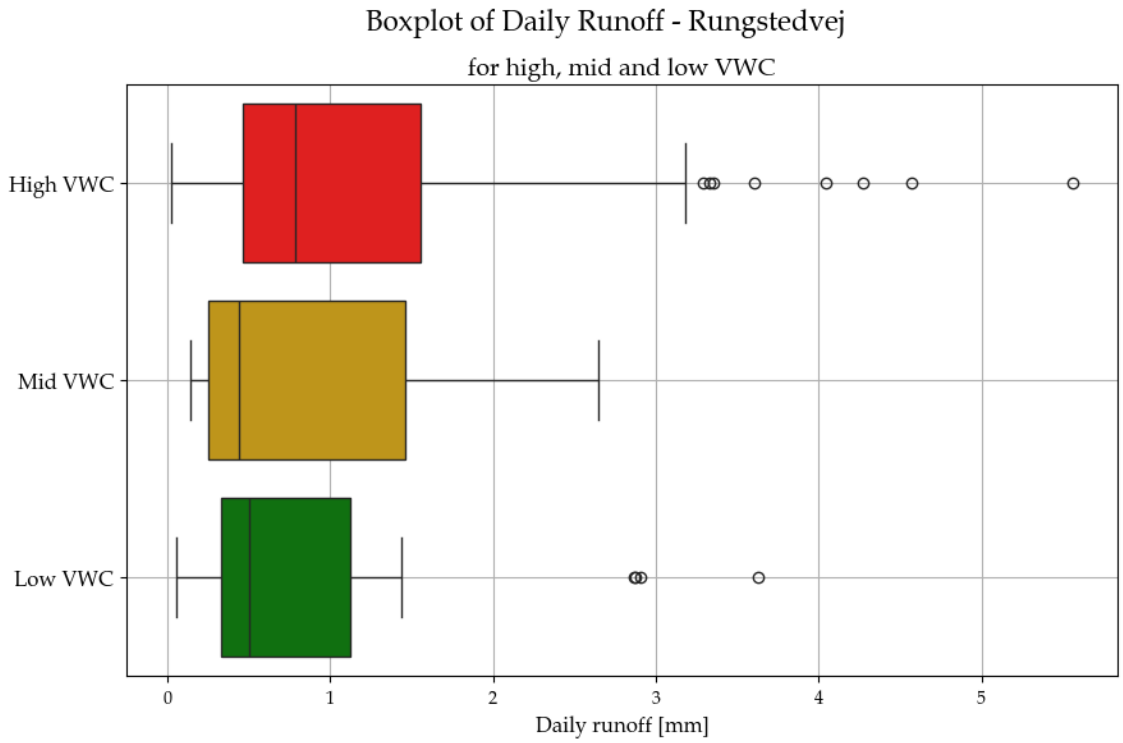

Figure I.11. Boxplot for runoff at high, mid, and low VWC at Rungstedvej, Hørsholm.

A boxplot illustrating the runoff at high, mid, and low VWC is presented in Figure I.11, from where it is evident that the high VWC group exhibits the greatest spread in runoff values, as evidenced by its longer whiskers. This suggests higher variability in runoff under high VWC conditions. In contrast, the low and mid VWC groups display narrower spreads, indicating more consistent and generally lower runoff values. Multiple outliers are present in the high and low groups, with the most extreme values (up to ≈ 5.50 mm) occurring in the high VWC bin.

Overall, the high VWC group exhibit a clear right-skewed distribution, indicating a greater likelihood of extreme runoff events when VWC are classified as high. In contrast, the mid and low groups show more symmetrical distributions centred around lower runoff values, suggesting lower runoff sensitivity under these conditions. Thus, the boxplot analysis indicates that higher runoff generation is associated with high VWC conditions. However, as previously noted, the high VWC group comprises 52.05% of all data points, which may introduce some uncertainty due to the unequal distribution of observations.

Hydrological Scale

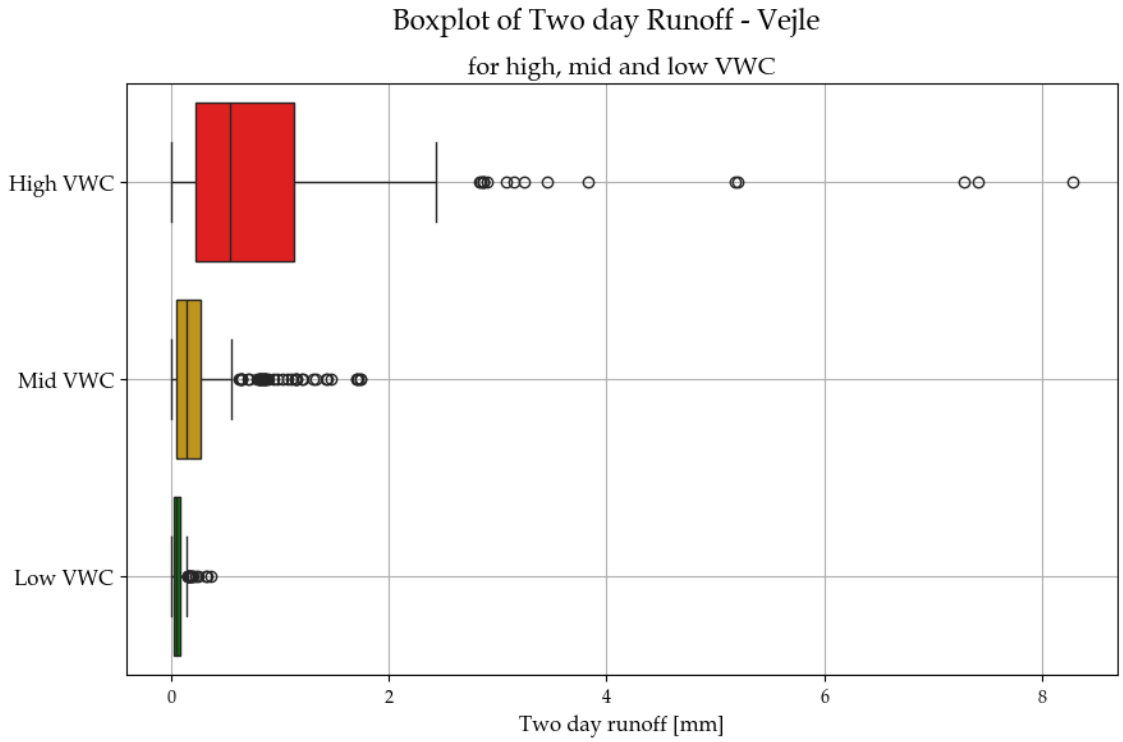

Figure I.12. Boxplot for runoff at high, mid, and low VWC at Vejle.

The boxplot shows that the high VWC group exhibits the greatest spread in runoff values, as evidenced by its wider IQR and longer whiskers, suggesting greater variability in runoff under high VWC conditions. In contrast, the mid and low VWC groups display much narrower distributions, indicating more consistent and generally lower runoff values. The median two-day runoff in the high VWC bin is also significantly higher, indicating generally higher runoff generation when VWC conditions in the soil are classified as high.
Moreover, multiple outliers are present across all three categories. The highest outliers (up to ≈ 8 mm) occur in the high VWC bin, while the mid VWC bin contains the greatest number of outliers. This suggests that significant runoff events not only occur under high VWC conditions, but are also influenced by both rainfall intensity and the system's hydraulic memory (e.g. effects of prior drought).
Overall, the high VWC group notably exhibit a right-skewed distribution, indicating a higher risk of extreme runoff events when the soil's VWC conditions are classified as high. In contrast, the mid and low bins show more symmetrical distributions centred around lower runoff values, indicating a lower runoff sensitivity under these conditions.

I.3 Dunn's Test for Boxplot

To see which of the three VWC groups: high, mid and low, differ from each other, a Dunn's test is performed for each of the areas where a difference was found using the Kruskal-Wallis test.

Table I.1. Dunn's test for runoff at high, mid and low VWC bin in the boxplot for Elmelundsvej, Odense ($\alpha_{adjusted} = 0.0166$).

High VWC : Mid VWC	**High VWC : Low VWC**	**Mid VWC : Low VWC**
$p = 6.97 \cdot 10^{-2}$	$p = 1.52 \cdot 10^{-4}$	$p = 1.26 \cdot 10^{-2}$

Table I.2. Dunn's test for runoff at high, mid and low VWC bin in the boxplot for Lystrup ($\alpha_{adjusted} = 0.0166$).

High VWC : Mid VWC	**High VWC : Low VWC**	**Mid VWC : Low VWC**
$p = 6.68 \cdot 10^{-38}$	$p = 2.57 \cdot 10^{-14}$	$p = 0.139$

Table I.3. Dunn's test for runoff at high, mid and low VWC bin in the boxplot for Christianshusvej, Hørsholm ($\alpha_{adjusted} = 0.0166$).

High VWC : Mid VWC	**High VWC : Low VWC**	**Mid VWC = Low VWC**
$p = 8.4 \cdot 10^{-10}$	$p = 2.62 \cdot 10^{-6}$	$p = 3.63 \cdot 10^{-1}$

Table I.4. Dunn's test for runoff at high, mid and low VWC bin in the boxplot for Rungstedvej, Hørsholm ($\alpha_{adjusted} = 0.0166$).

High VWC : Mid VWC	**High VWC : Low VWC**	**Mid VWC : Low VWC**
$p = 5.43 \cdot 10^{-3}$	$p = 2.65 \cdot 10^{-2}$	$p = 0.83$

Table I.5. Dunn's test for runoff at high, mid and low VWC bin in the boxplot for Vejle ($\alpha_{adjusted} = 0.0166$).

High VWC : Mid VWC	**High VWC : Low VWC**	**Mid VWC : Low VWC**
$p = 1.26 \cdot 10^{-24}$	$p = 3.14 \cdot 10^{-41}$	$p = 1.03 \cdot 10^{-8}$

I.4 Dunn's Test for Runoff Ratio Analysis

Dunn's test is performed on the binned VWC in the runoff ratio plots for each location. The test is only performed in case the Kruskal-Wallis test indicates that a significant difference exists, which includes Ejby Mølle (Figure 6.4), Elmelundsvej (Figure 6.8), Lystrup (Figure 6.12), Christianshusvej (Figure 7.4) and Vejle (Figure 8.4). The results of the Dunn's test for each of these locations are illustrated in Figure I.13 through I.17.

Hillslope Scale

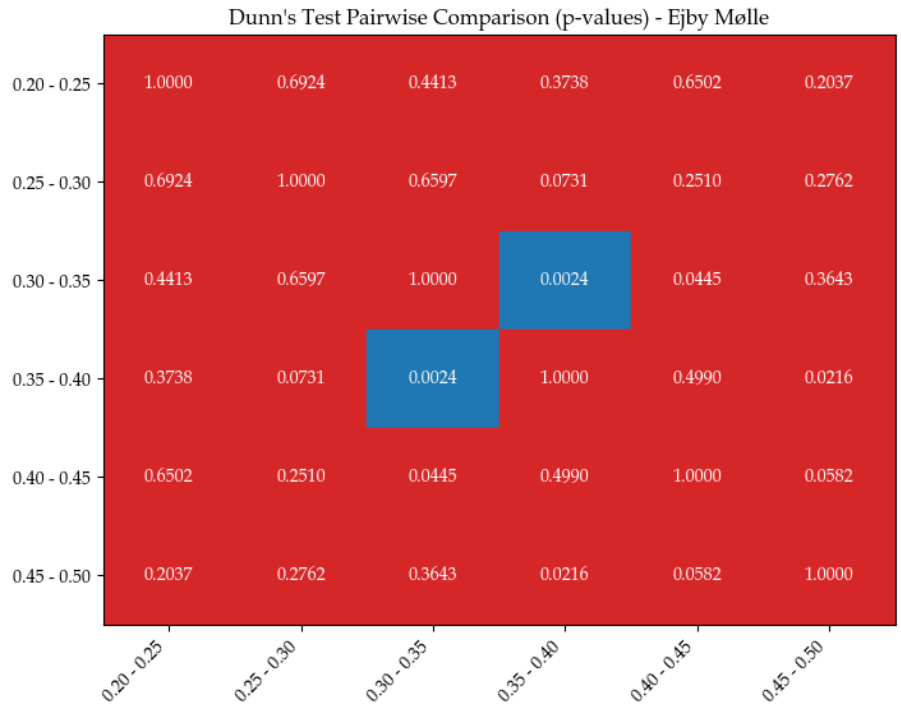

Figure I.13. Dunn's test for Ejby Mølle, Odense. The blue coloured squares indicate a significant difference between the medians of the compared groups ($\alpha_{adjusted} = 0.0083$).

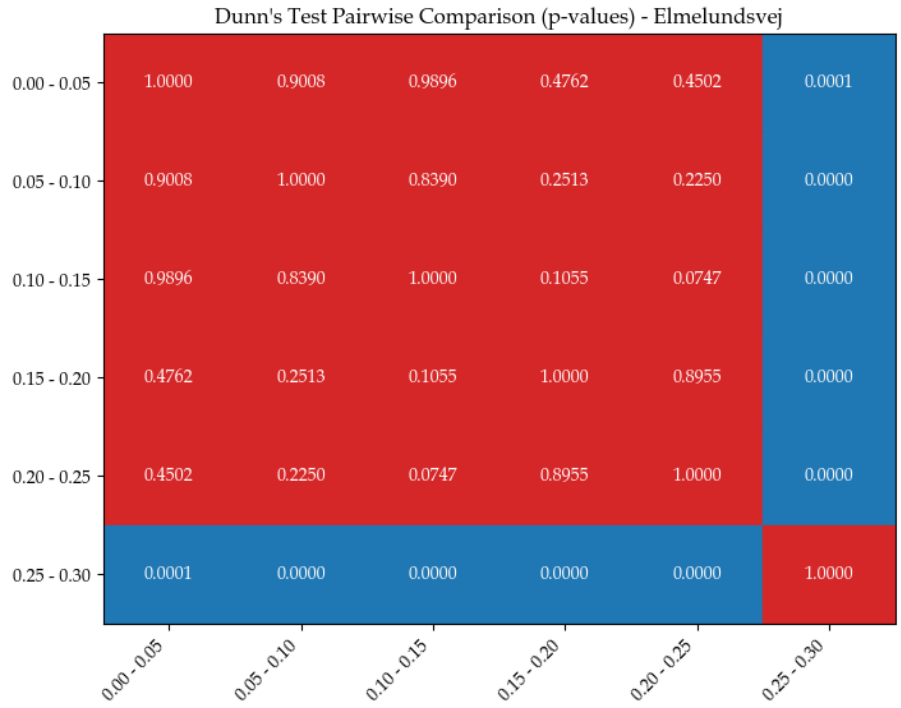

Figure I.14. Dunn's test for Elmelundsvej, Odense. The blue coloured squares indicate a significant difference between the medians of the compared groups ($\alpha_{adjusted} = 0.002$).

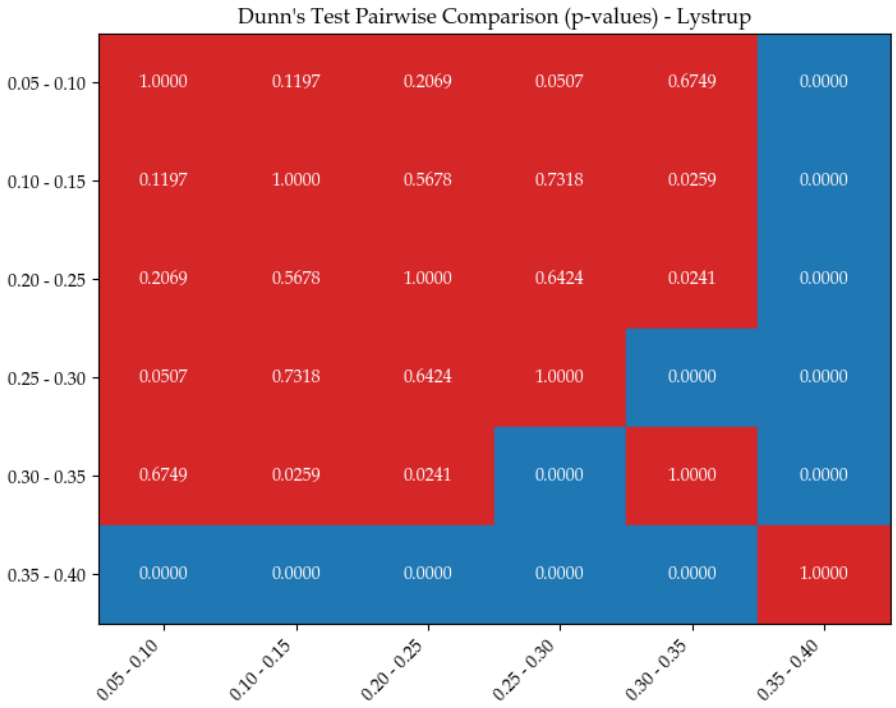

Figure I.15. Dunn's test for Lystrup. The blue coloured squares indicate a significant difference between the medians of the compared groups ($\alpha_{adjusted} = 0.002$).

Urban Subcatchment Scale

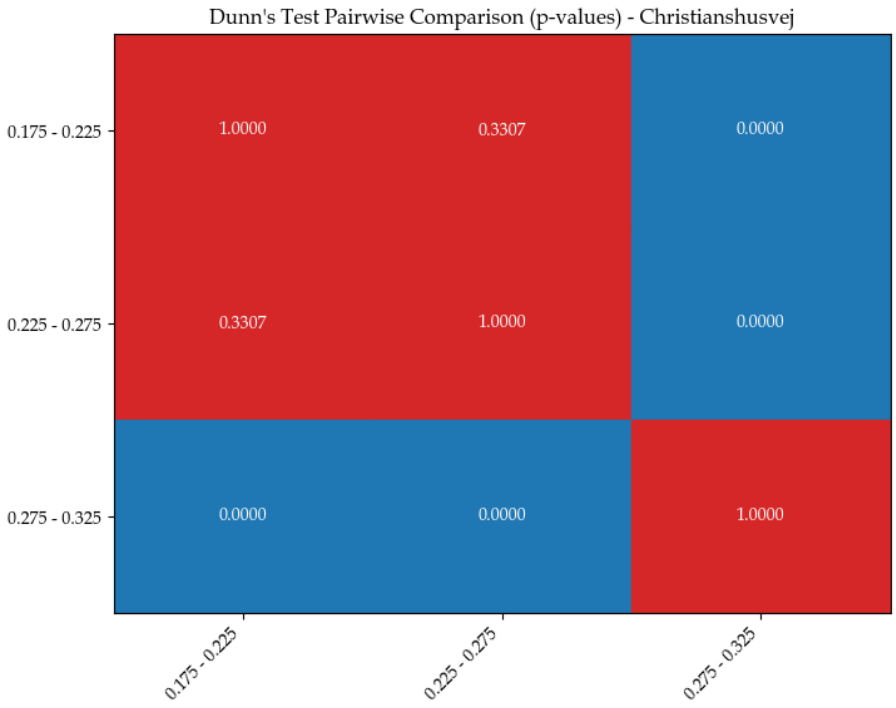

Figure I.16. Dunn's test for Christianshusvej, Hørsholm. The blue coloured squares indicate a significant difference between the medians of the compared groups ($\alpha_{adjusted} = 0.0166$).

Hydrological Scale

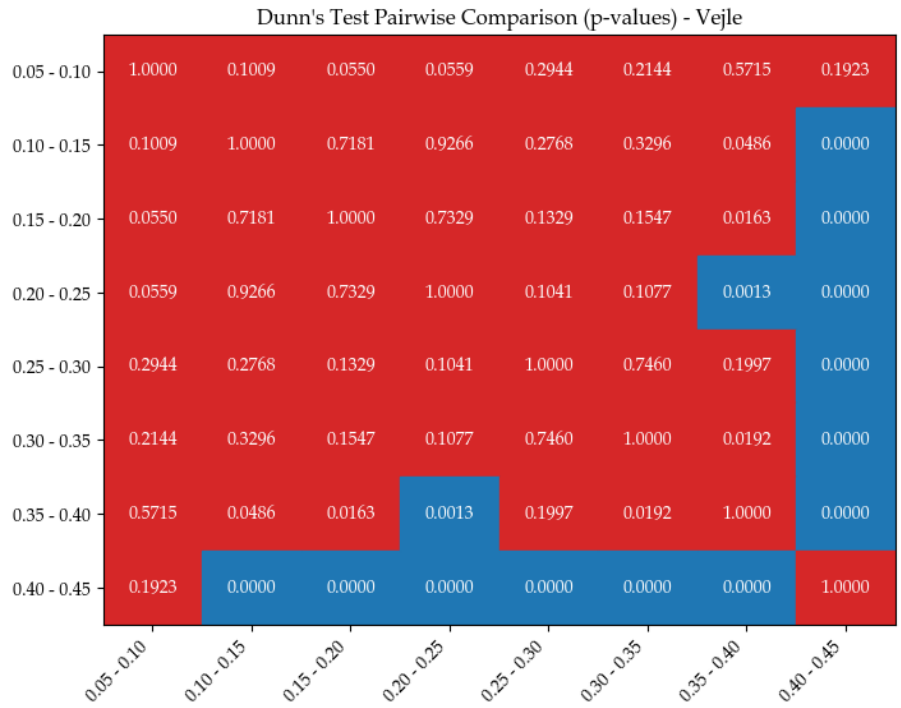

Figure I.17. Dunn's test for Vejle. The blue coloured squares indicate a significant difference between the medians of the compared groups ($\alpha_{adjusted} = 0.0017$).

Slope J

The slope is calculated in QGIS and is based on the DHM terrain model. The mean slope of the six areas is calculated using the same method.

The tool used is the GDAL DEM processing (gdaldem slope) command. The GDAL uses the finite difference method, which estimates the rate of elevation change in both the east-west and north-south directions. The rate of change is calculated using a moving 3x3 window, which results in each cell's slope being based on the surrounding eight cells. The output is calculated in both percent and degrees.

Table J.1. Slope of the catchment areas in percent and degrees.

	Mean slope ± SD [%]	**Mean slope ± SD [°]**
Ejby Mølle	11.50 ± 10.12	6.56 ± 5.78
Elmelundsvej	17.60 ± 4.56	9.98 ± 2.61
Lystrup	9.18 ± 4.97	5.42 ± 2.84
Christianshusvej	13.76 ± 24.74	7.07 ± 10.68
Rungstedvej	11.42 ± 15.93	6.52 ± 9.05
Vejle	19.30 ± 67.11	10.92 ± 33.86

Appendix
Implementation of VWC and DI in Flow Modelling

Potential Evaporation Rate

K

The water inflow to the Linear Reservoir Model and Extended Time-Area Model is calculated as precipitation minus the potential evaporation rate.
Potential evaporation rate is estimated by a simplified version of the Penman formula developed by [Linacre, 1977], which assumes that the area contains well-watered vegetation.

$$E_t = \frac{500\frac{T+0.006h}{100-A} + 15(T - T_d)}{80 - T} \tag{K.1}$$

Where:

h	Elevation	[m]
A	Latitude	[−]
T	Mean temperature	[°C]
T_d	Mean dew point	[°C]
E_t	Potential evaporation	[mm/day]

The calculation is based on latitude, elevation, temperature, and dew point data from Billund, the nearest location to Vejle with available meteorological observations. Temperature and dew point are recorded with a frequency of 10 minutes, from which daily mean values are derived and used in Equation K.1. Figure K.1 shows the calculated daily mean temperature and dew point.

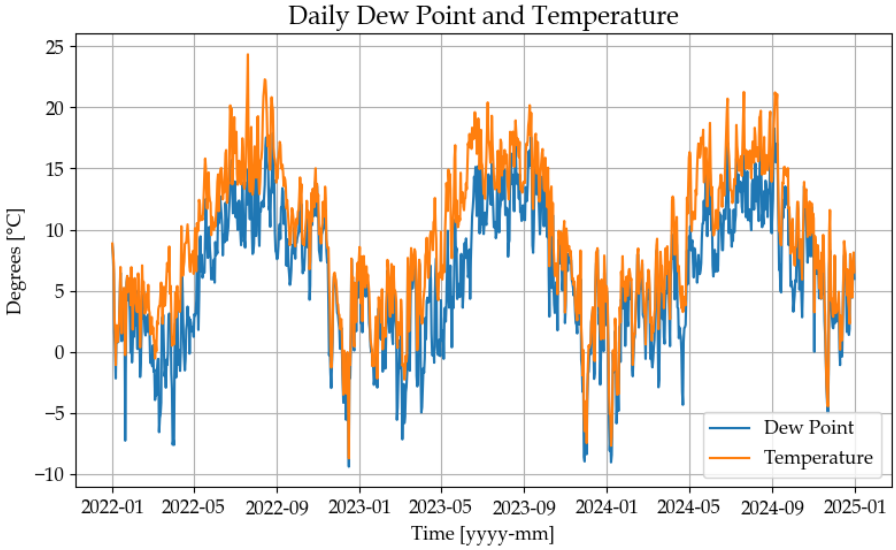

Figure K.1. Daily temperature and dew point.

Based on Equation K.1 and the data illustrated in Figure K.1, the estimated potential evaporation is presented in Figure K.2.

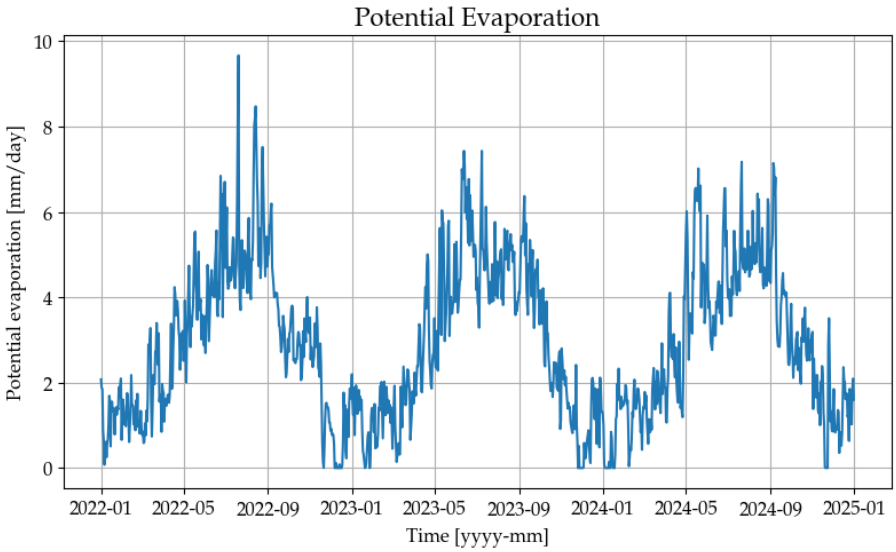

Figure K.2. Estimated daily potential evaporation in the catchment area of Grejs Å, Vejle.

Extended Time-Area Model L

L.1 Calibration of Extended Time-Area Models

Three Extended Time-Area Models are developed: a baseline model, one that includes VWC as a parameter, and one that includes DI as a parameter. All models are calibrated to yield the lowest RMSE value.

Baseline
Figure L.1 illustrates the calibrated model. The first plot shows the precipitation input, while the second plot displays the fast flow and baseflow. These flows are combined and presented as the total flow in the third plot, alongside the observed flow for comparison. The fourth plot shows the error between the modelled and observed flow and the NSE and RMSE values.

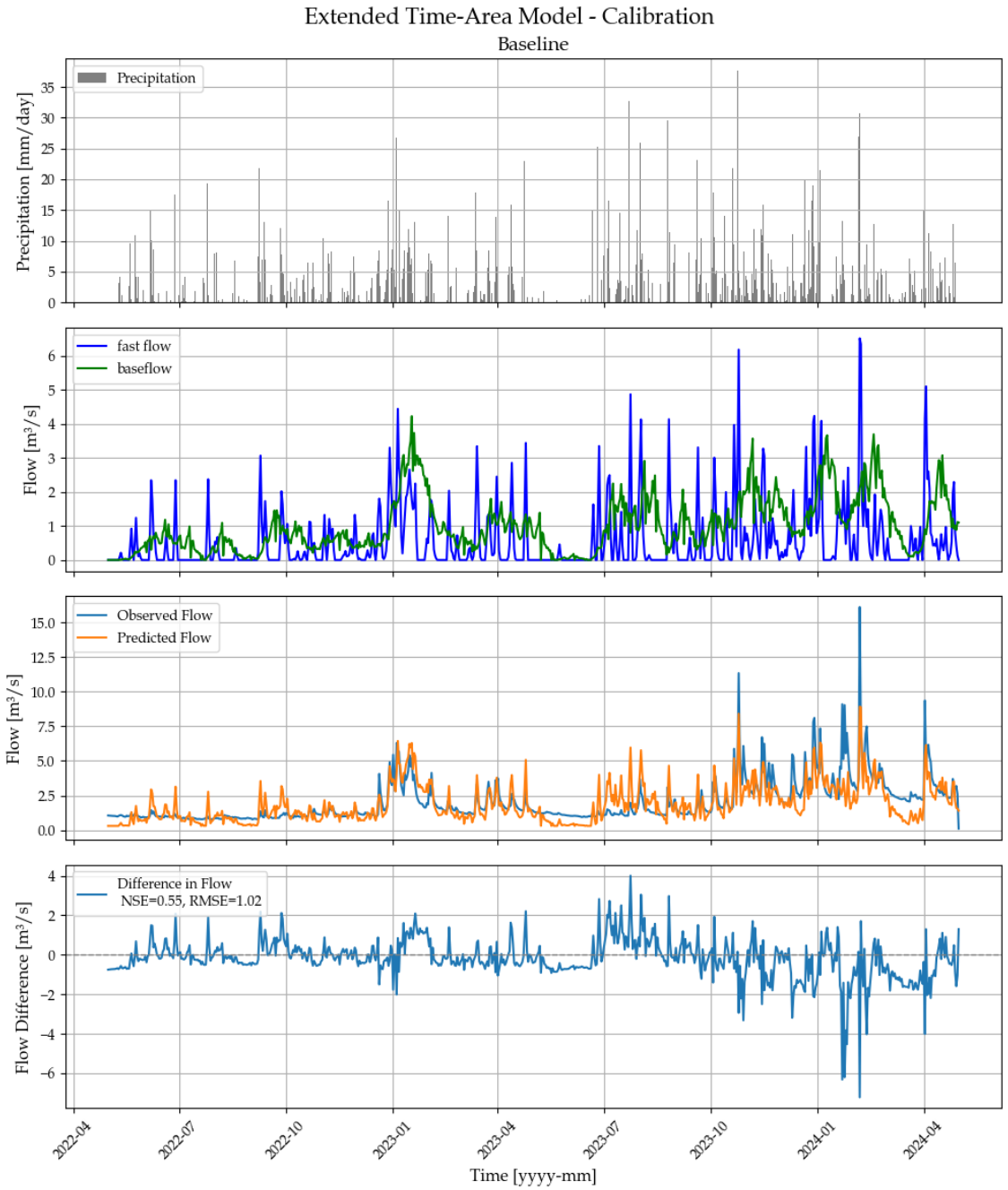

Figure L.1. Overview of 1. precipitation, 2. estimated flow (fast flow, baseflow), 3. observed flow compared with predicted calibrated baseline flow, and 4. flow differences.

Including VWC

Figure L.2 illustrates the calibrated model with the VWC as a parameter. The first plot shows the precipitation input, while the second plot displays the fast flow and baseflow. These flows are combined and presented as the total flow in the third plot, alongside the observed flow for comparison. The fourth plot shows the error between the modelled and observed flow, the VWC, and the NSE and RMSE values.

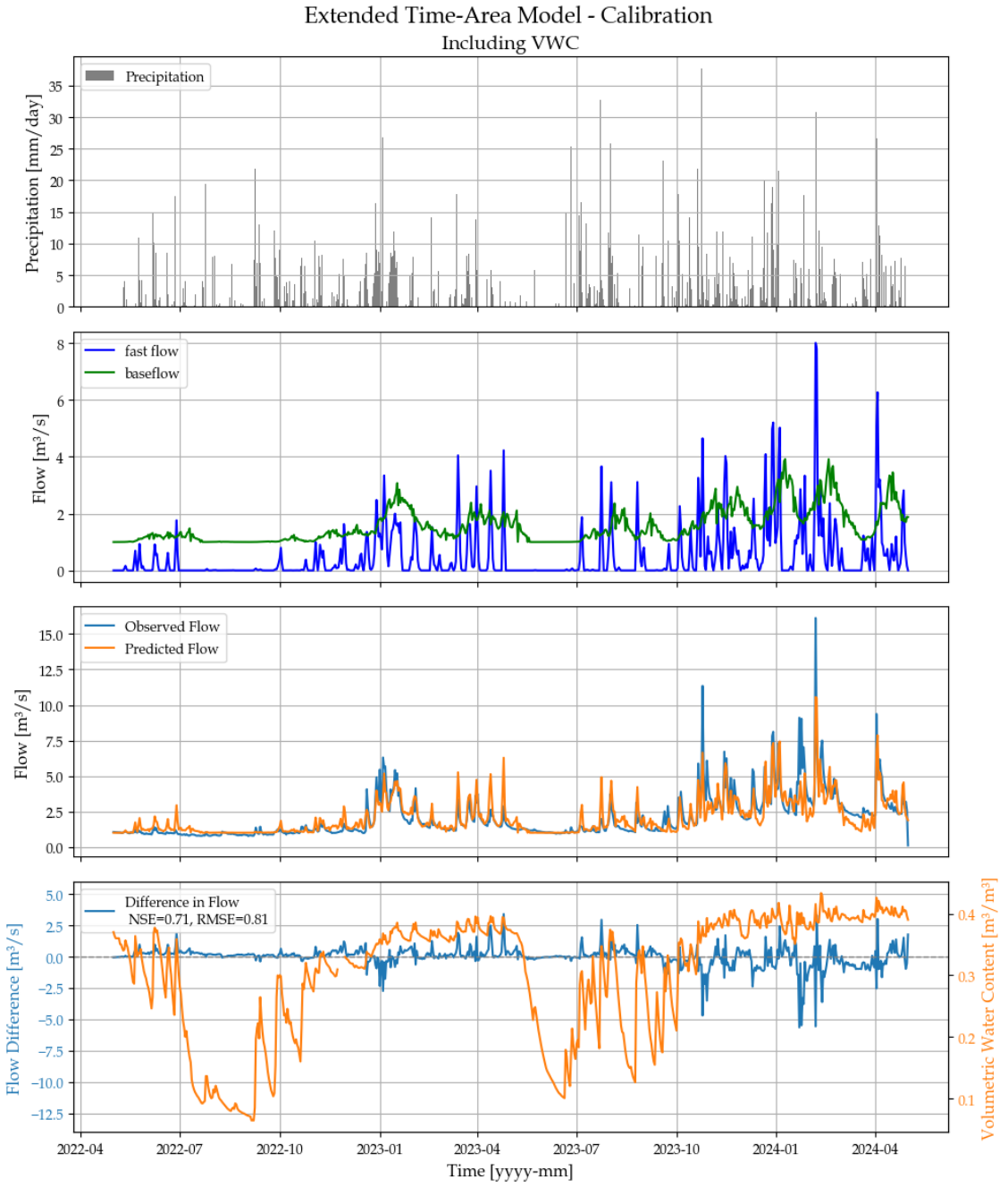

Figure L.2. Overview of 1. precipitation, 2. estimated flow (fast flow, baseflow), 3. observed flow compared with predicted calibrated flow including VWC, and 4. flow differences. The NSE and RMSE for the calibration are shown.

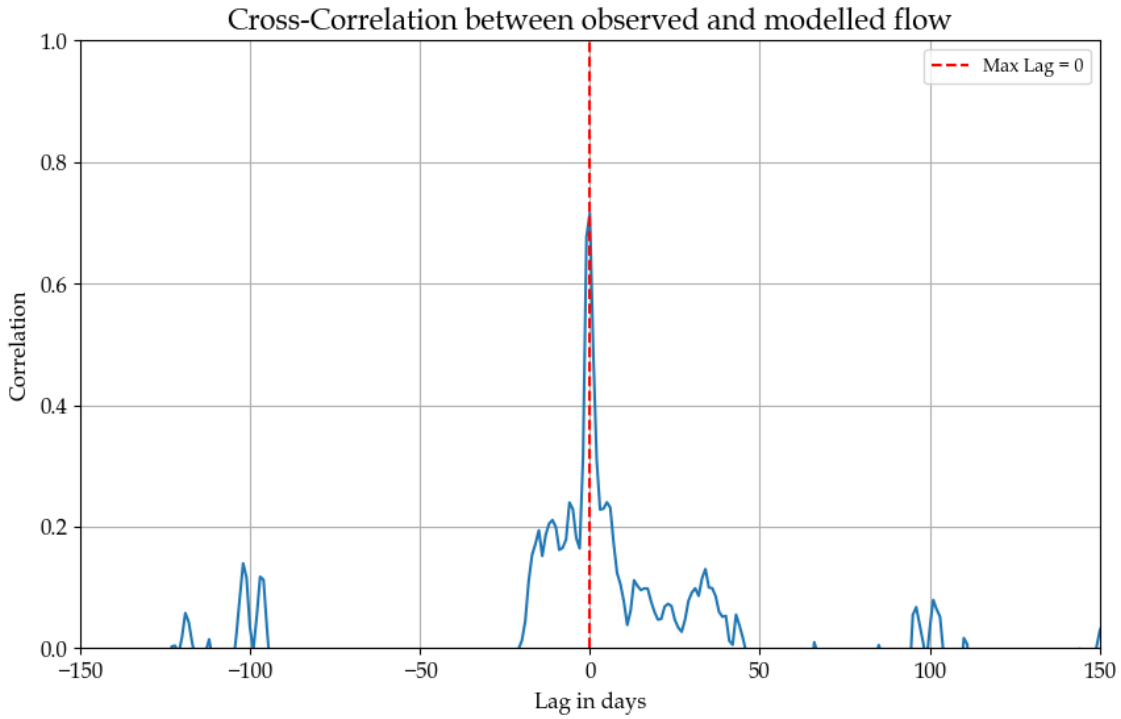

Figure L.3. Cross-correlation between the observed flow and the modelled for the Extended Time-Area Model including VWC.

Including DI

Figure L.4 illustrates the calibrated model with the DI as a parameter. The first plot shows the precipitation input, while the second plot displays the fast flow and baseflow. These flows are combined and presented as the total flow in the third plot, alongside the observed flow for comparison. The fourth plot shows the error between the modelled and observed flow, the VWC, and the NSE and RMSE values.

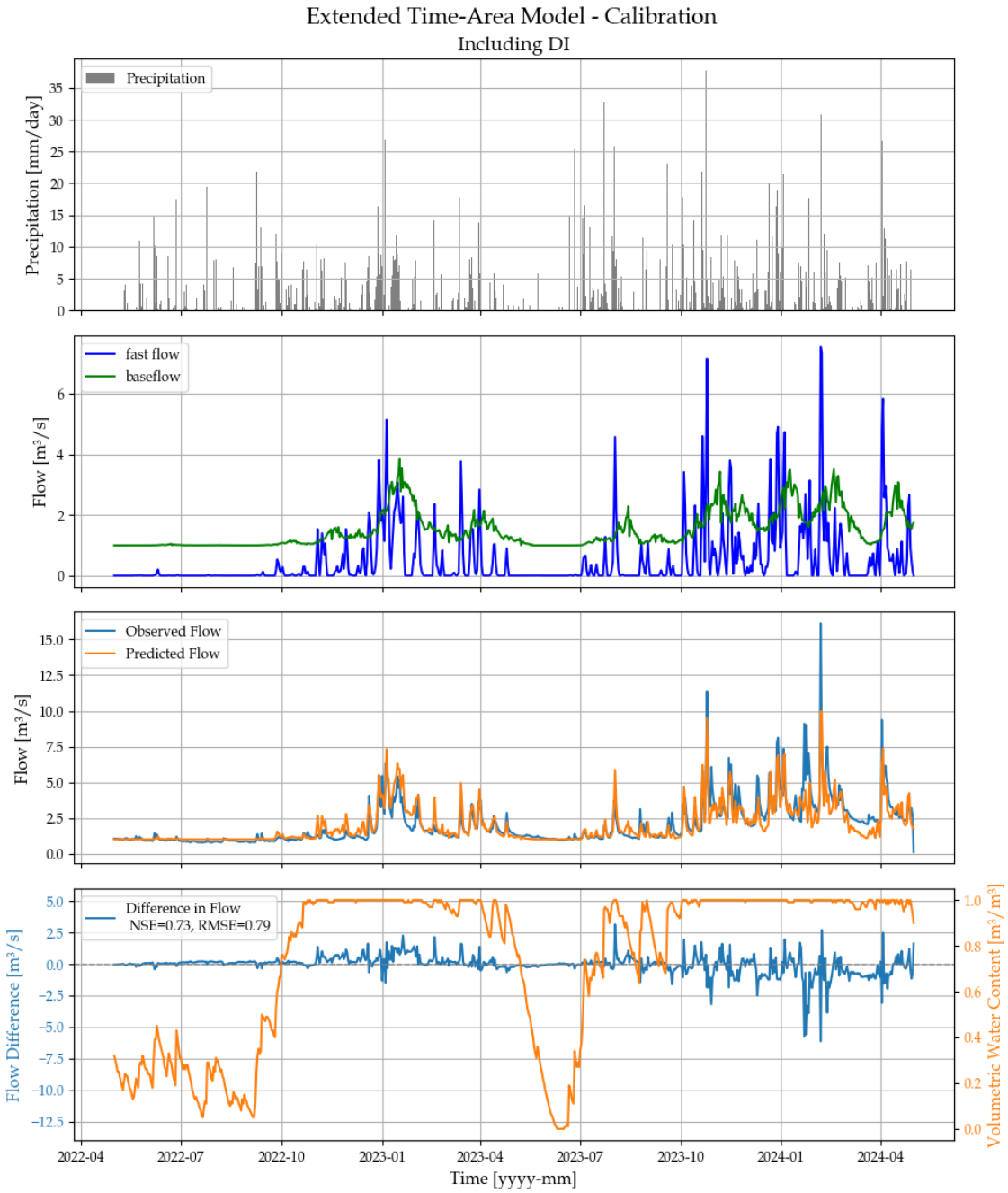

Figure L.4. Overview of 1. precipitation, 2. estimated flow (fast flow, baseflow), 3. observed flow compared with predicted calibrated flow including DI, and 4. flow differences. The NSE and RMSE for the calibration are shown.

L.2 Validation of the Extended Time-Area Models

In the following, the validation period for the three models is plotted.

Baseline

Figure L.5. Overview of 1. precipitation, 2. estimated flow (fast flow, baseflow), 3. observed flow compared with predicted validated baseline flow, and 4. flow differences. The NSE and RMSE for the calibration are shown.

Including VWC

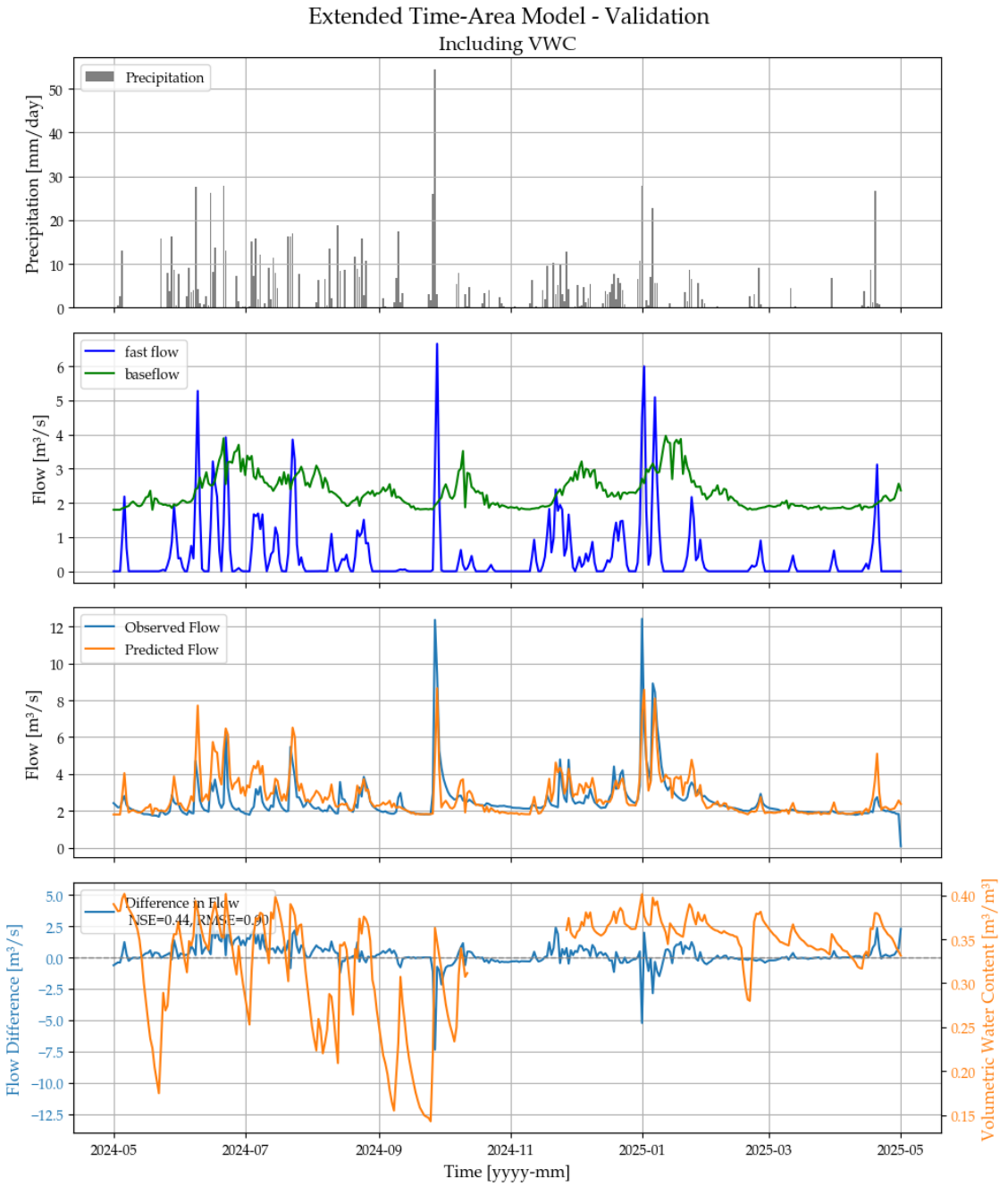

Figure L.6. Overview of 1. precipitation, 2. estimated flow (fast flow, baseflow), 3. observed flow compared with predicted validated flow including VWC, and 4. flow differences. The NSE and RMSE for the calibration are shown.

Including DI

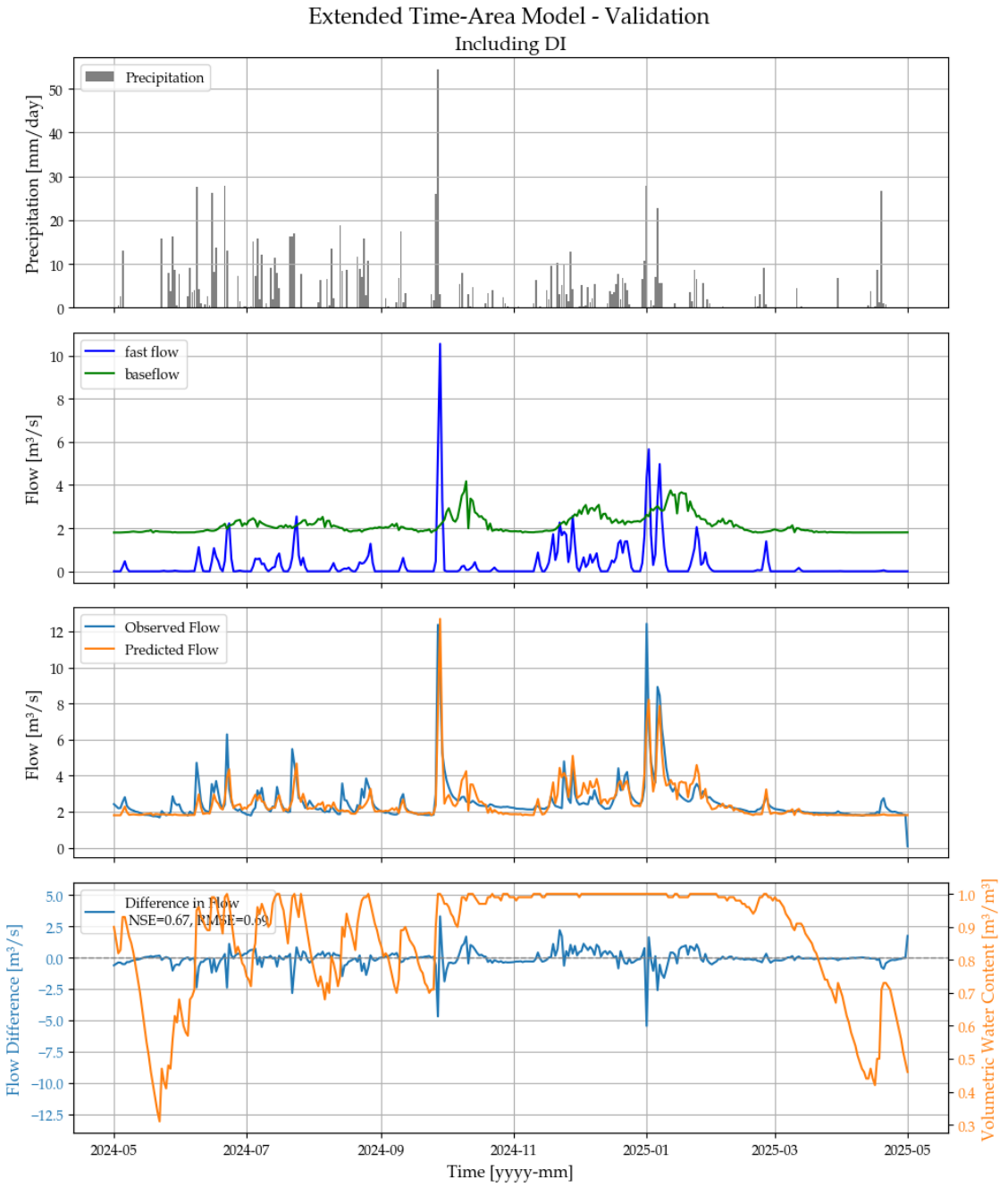

Figure L.7. Overview of 1. precipitation, 2. estimated flow (fast flow, baseflow), 3. observed flow compared with predicted validated flow including DI, and 4. flow differences. The NSE and RMSE for the calibration are shown.

Linear Reservoir Model M

M.1 Calibration of the Linear Reservoir Models

Three linear reservoir models are developed: a baseline model, one that includes VWC as a parameter, and one that includes DI as a parameter. All models are calibrated to yield the lowest RMSE value.

Baseline
Figure M.1 illustrates the calibrated model. The first plot shows the precipitation input, while the second plot displays the outflow from the two reservoirs. These outflows are combined and presented as the total flow in the third plot, alongside the observed flow for comparison. The fourth plot shows the error between the modelled and observed flow and the NSE and RMSE values.

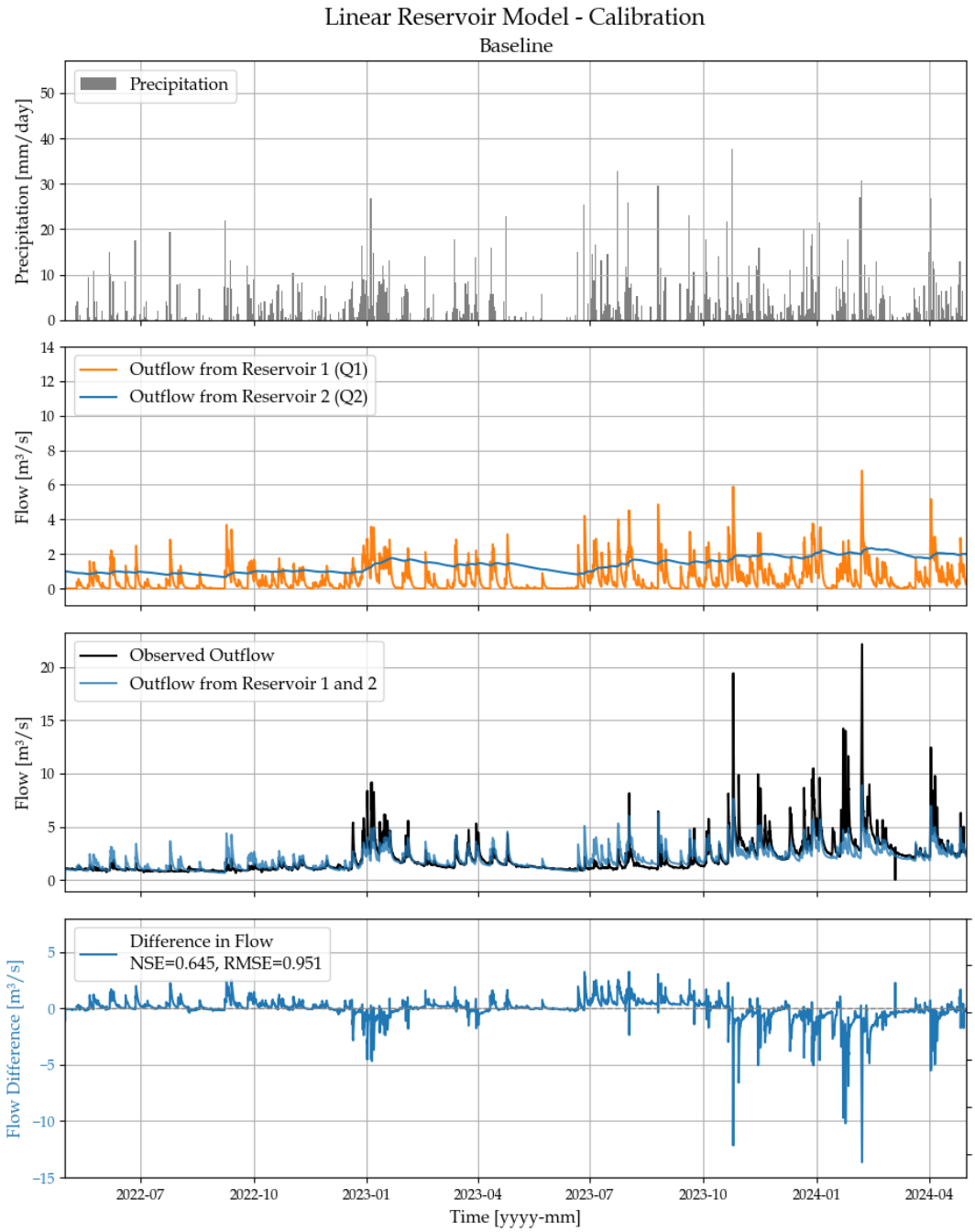

Figure M.1. Overview of 1. precipitation, 2. estimated flow (fast flow, baseflow), 3. observed flow compared with predicted calibrated baseline flow, and 4. flow differences. The NSE and RMSE for the calibration are shown.

Including VWC

Figure M.2 illustrates the calibrated model with the VWC as a parameter. The first plot shows the precipitation input, while the second plot displays the outflow from the two reservoirs. These outflows are combined and presented as the total flow in the third plot, alongside the observed flow for comparison. The fourth plot shows the error between the modelled and observed flow, the VWC, and the NSE and RMSE values.

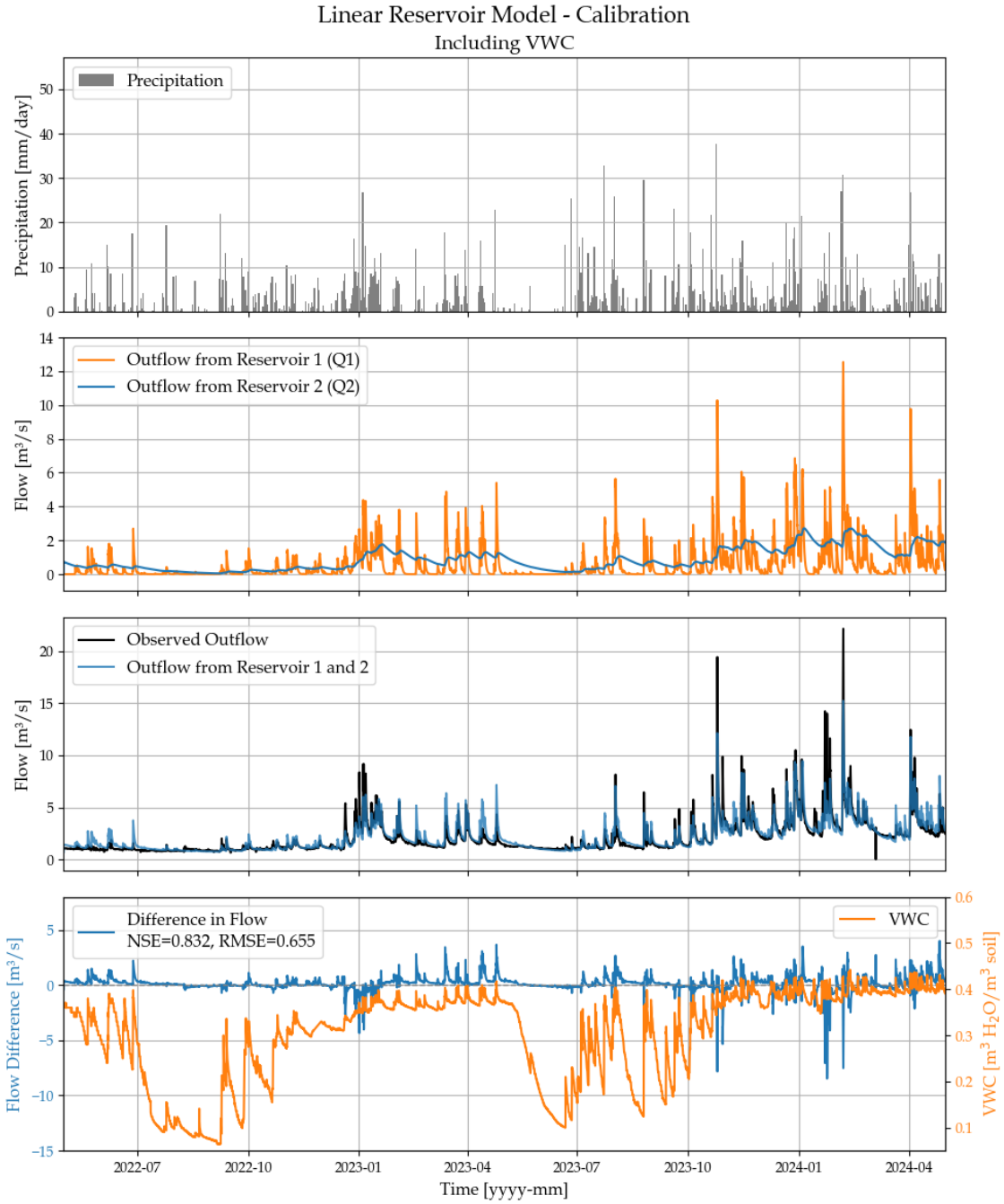

Figure M.2. Overview of 1. precipitation, 2. estimated flow (fast flow, baseflow), 3. observed flow compared with predicted calibrated flow including VWC, and 4. flow differences. The NSE and RMSE for the calibration are shown.

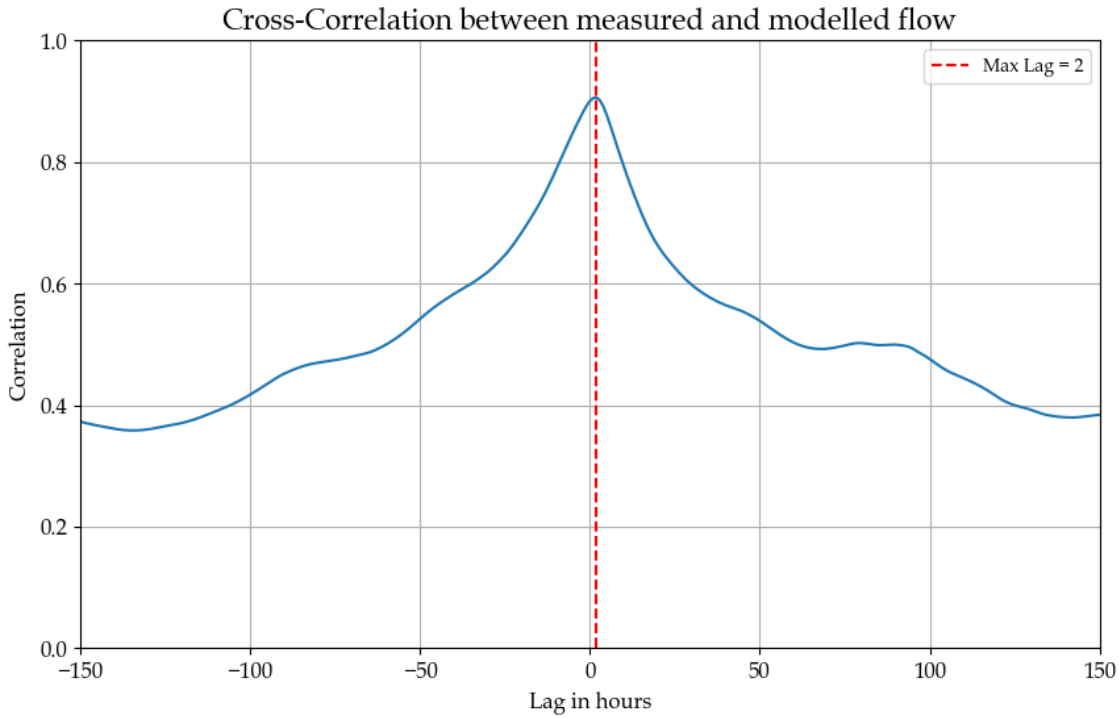

Figure M.3. Cross-correlation between the observed flow and the modelled for the Linear Reservoir Model including VWC.

Including DI

Figure M.4 illustrates the calibrated model with the DI as a parameter. The first plot shows the precipitation input, while the second plot displays the fast flow and baseflow. These flows are combined and presented as the total flow in the third plot, alongside the observed flow for comparison. The fourth plot shows the error between the modelled and observed flow, the VWC, and the NSE and RMSE values.

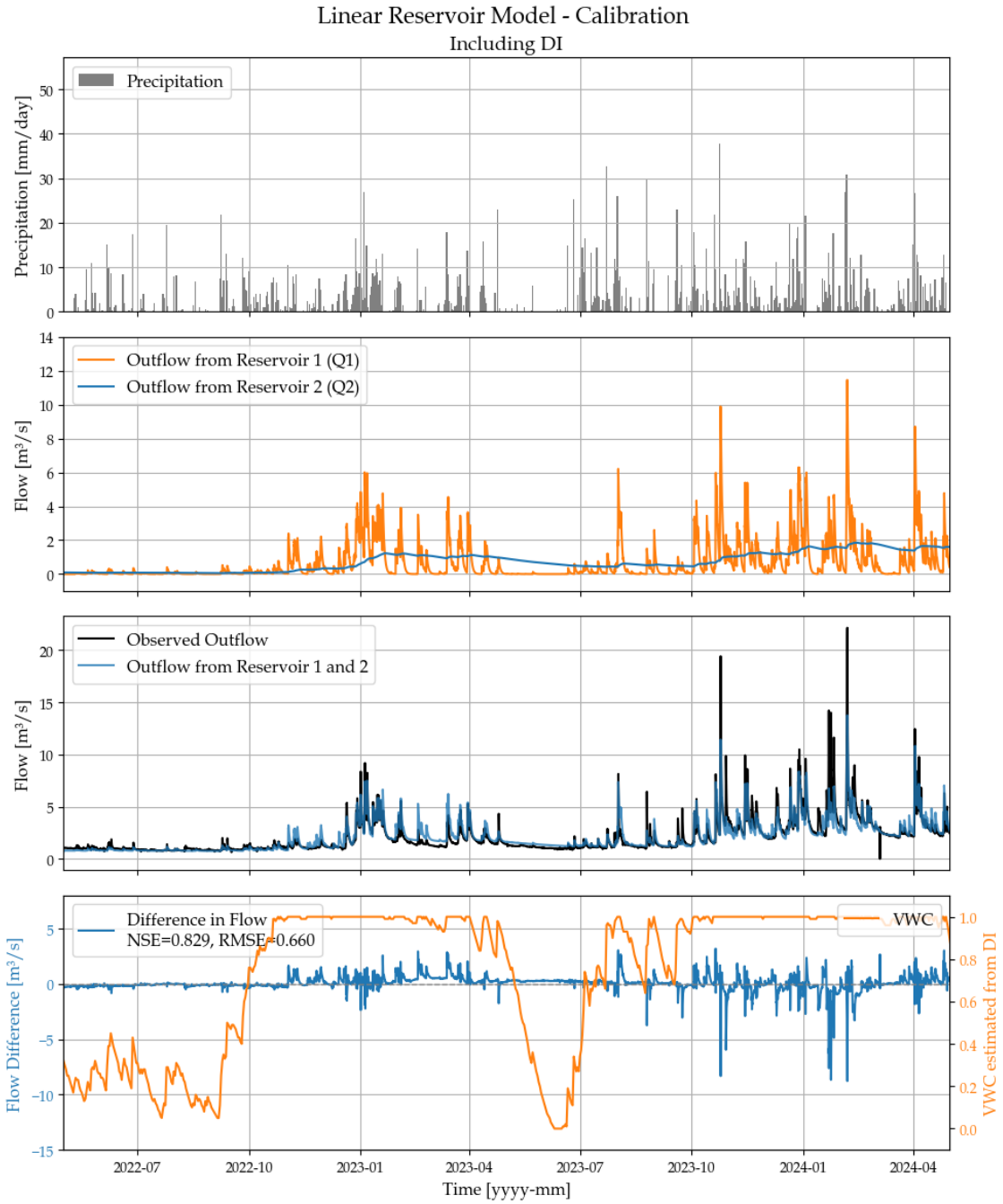

Figure M.4. Overview of 1. precipitation, 2. estimated flow (fast flow, baseflow), 3. observed flow compared with predicted calibrated flow including DI, and 4. flow differences. The NSE and RMSE for the calibration are shown.

M.2 Validation of the Linear Reservoir Models

In the following is plotted the validation period for the three models.

Baseline

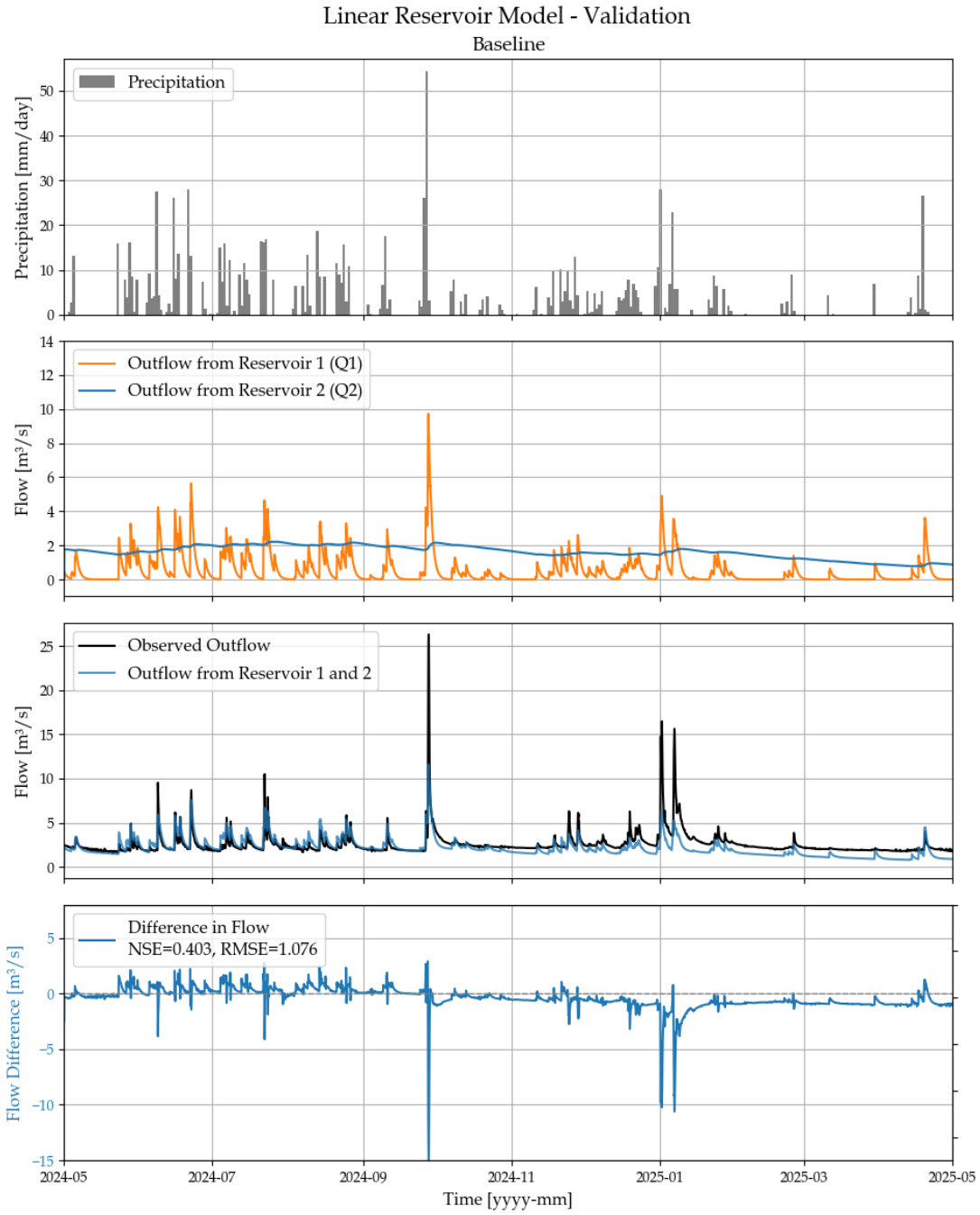

Figure M.5. Overview of 1. precipitation, 2. estimated flow (fast flow, baseflow), 3. observed flow compared with predicted validated baseline flow, and 4. flow differences. The NSE and RMSE for the calibration are shown.

Including VWC

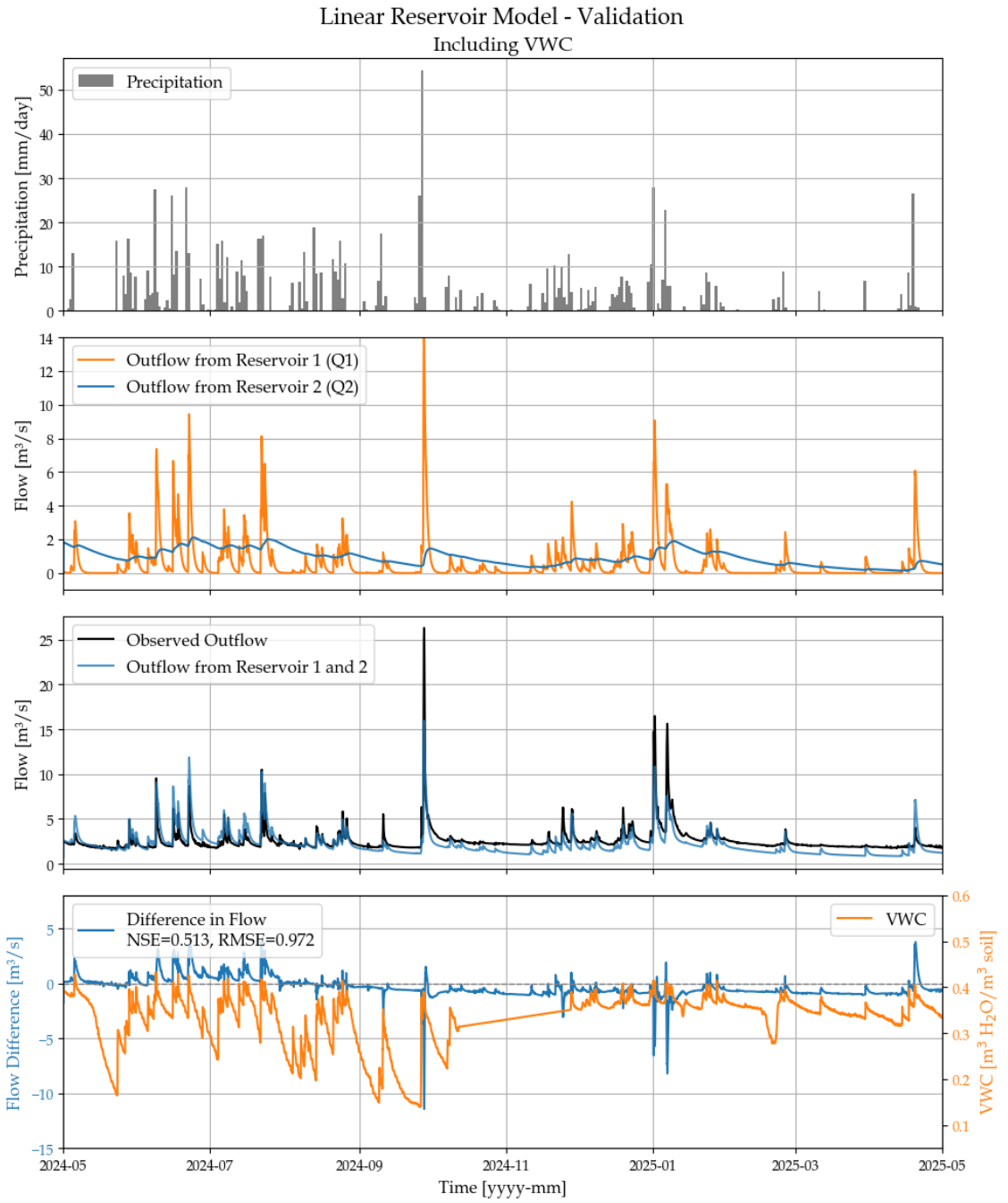

Figure M.6. Overview of 1. precipitation, 2. estimated flow (fast flow, baseflow), 3. observed flow compared with predicted validated flow including VWC, and 4. flow differences. The NSE and RMSE for the calibration are shown.

Including DI

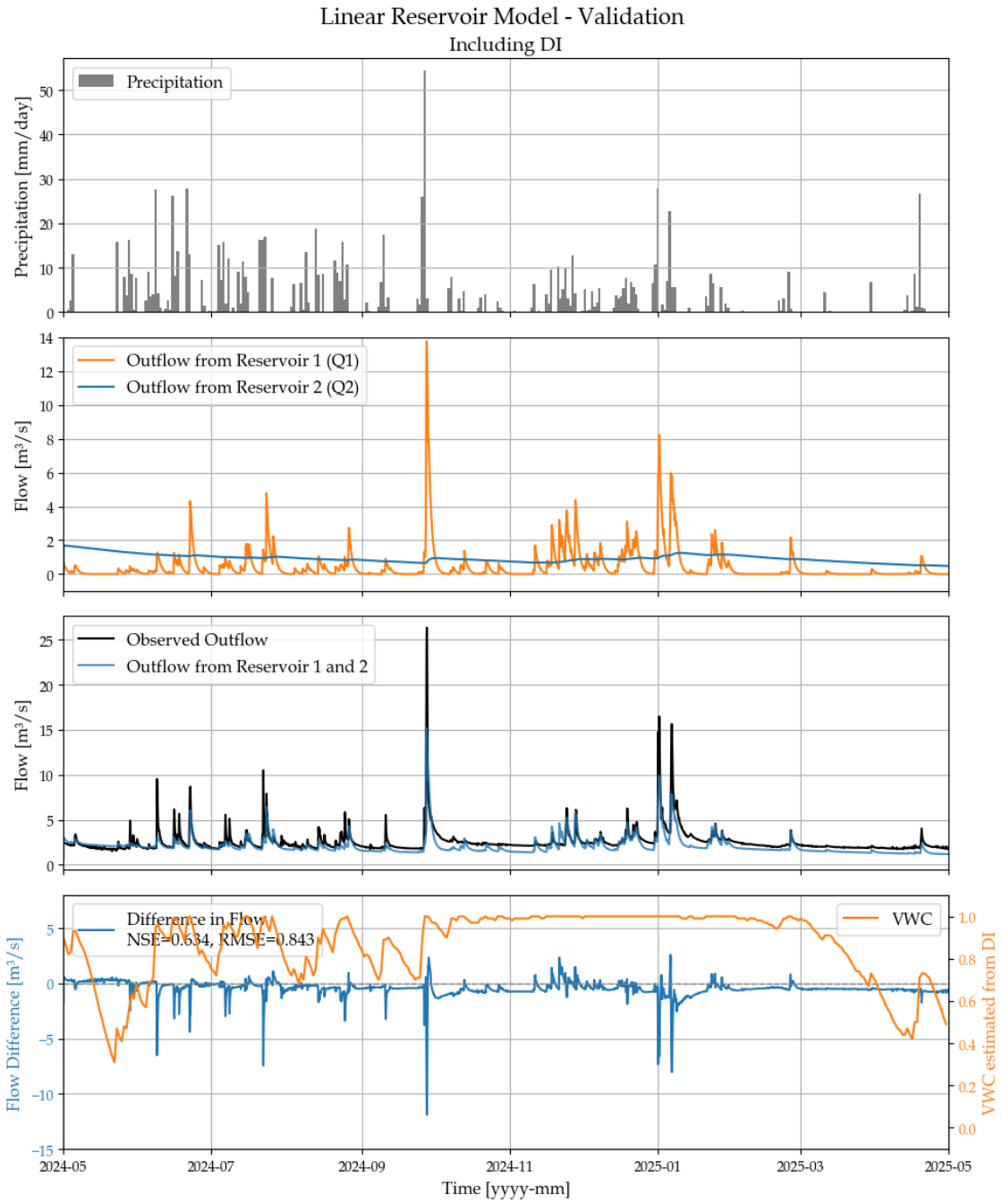

Figure M.7. Overview of 1. precipitation, 2. estimated flow (fast flow, baseflow), 3. observed flow compared with predicted validated flow including DI, and 4. flow differences. The NSE and RMSE for the calibration are shown.

M.3 Evaluation of Model Accuracy for Predicting Peak Flow Events

Event Selection

Vejle is significantly affected by flooding caused by cloudbursts, snow melts, prolonged rainfall, high water levels in Vejle Fjord, and storm surges. The extent of the flood risk in Vejle has led to the city being designated as one of the 10 areas in Denmark with a high flood risk, according to the EU Floods Directive.
During the validation period alone (01-05-2024 - 01-05-2025), two critical flow events hit Vejle city centre. These were caused by heavy rain events that led Grejs Å to overflow its banks. On the 27th of September 2024, 58 mm of rain fell in the Vejle catchment, corresponding to a return period of 11.5 years. This amount was on top of the 30 mm that fell on the day before, putting Vejle city centre in a critical flood situation. Another critical flow event happened at the beginning of 2025, where a mixture of rain and snow melt increased the flow in Grejs Å to a critical level. The flow in Grejs Å during these two events is displayed in Figure M.8.

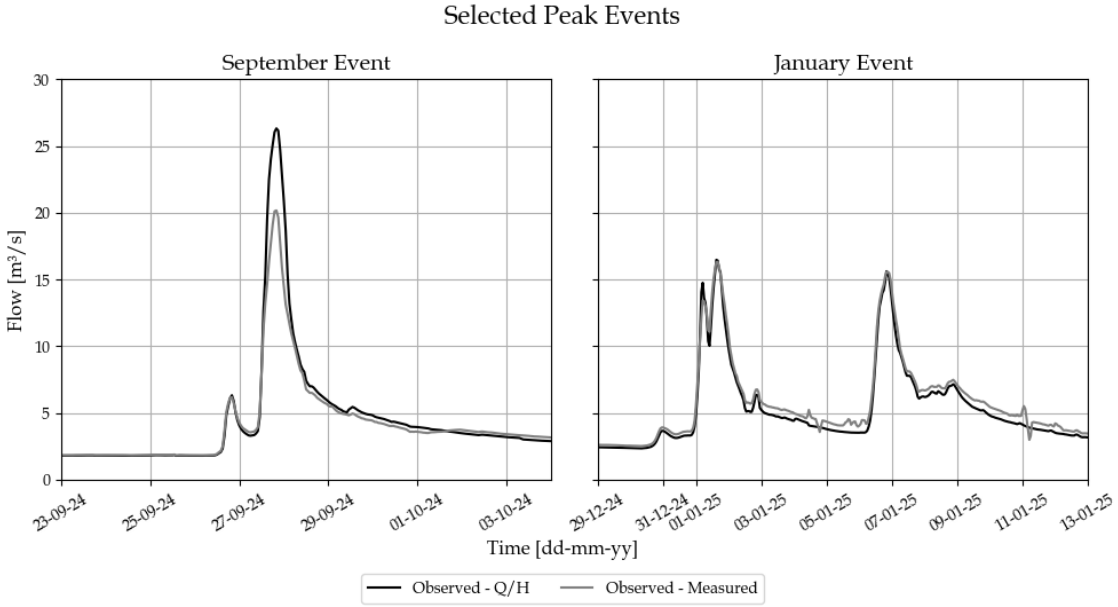

Figure M.8. Q/H estimated and measured flow during the September and January events in Vejle catchment.

Several methods are implemented to try and model these critical events sufficiently. This includes an alteration of the rain input where the rainfall is calculated by identifying the minimum and maximum 10-minute intensity within each hour and assuming this intensity persists throughout the entire hour. Using these inputs, a flow envelope is constructed, intended to bracket the estimated flow. Furthermore, different calibration periods up until the critical events are used to identify the optimal calibration period for real-time flow modelling. These methods used for modelling the peak events are performed on the model,

including VWC. The reason for this is that VWC represents actual, local measurements, unlike the DI, which is based on a nationwide model. However, if the drought index is forecasted in the future, it will be logical to use the forecasted precipitation and drought index concurrently for real-time flow modelling purposes.

Capturing Peak Flow Through Rainfall Range Modelling

The full time series on the flow envelope using minimum and maximum precipitation input can be seen in Figure M.9.

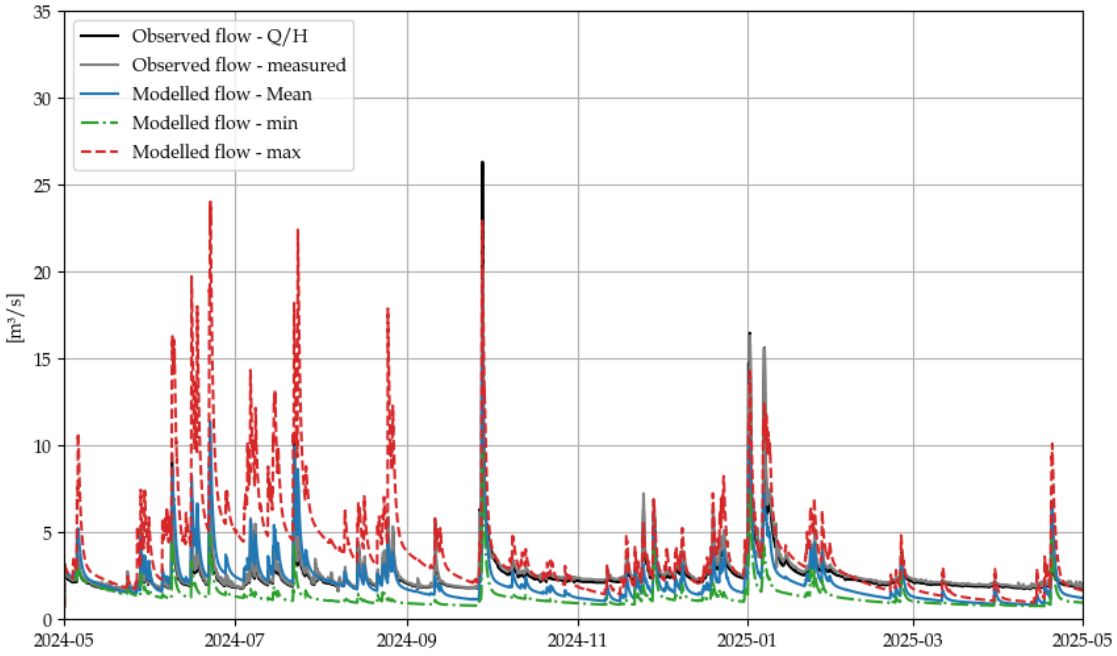

Figure M.9. Full time series showing the minimum, mean, and maximum modelled flow using modified rain inputs compared to the observed flow.